Durham E-Theses

The petrology and geochemistry of the Carrock Fell gabbro-granophyre complex, Cumbria.

Hunter, R H.

How to cite:

Hunter, R H. (1980) *The petrology and geochemistry of the Carrock Fell gabbro-granophyre complex, Cumbria.*, Durham theses, Durham University. Available at Durham E-Theses Online: http://etheses.dur.ac.uk/1022/

Use policy

The full-text may be used and/or reproduced, and given to third parties in any format or medium, without prior permission or charge, for personal research or study, educational, or not-for-profit purposes provided that:

- a full bibliographic reference is made to the original source
- a link is made to the metadata record in Durham E-Theses
- the full-text is not changed in any way

The full-text must not be sold in any format or medium without the formal permission of the copyright holders.

Please consult the full Durham E-Theses policy for further details.

Academic Support Office, Durham University, University Office, Old Elvet, Durham DH1 3HP
e-mail: e-theses.admin@dur.ac.uk Tel: +44 0191 334 6107
http://etheses.dur.ac.uk

Durham University
SCIENCE
30 OCT 1980
SECTION
Library

THE PETROLOGY AND GEOCHEMISTRY OF THE CARROCK FELL GABBRO-GRANOPHYRE COMPLEX, CUMBRIA.

R.H.HUNTER BSc.

The copyright of this thesis rests with the author. No quotation from it should be published without his prior written consent and information derived from it should be acknowledged.

A thesis submitted for the degree of Doctor of Philosophy at the University of Durham

SEPTEMBER 1980

ABSTRACT

The Carrock Fell igneous complex is a multiple dyke-like intrusion composed of two Units; Unit A, gabbros of Llanvirnian age, and Unit B, a gabbro-granophyre suite of Caradoc-Ashgill age.

The Unit A gabbros show chemical and petrological affinities to the Eycott Volcanic Group, and are believed to be cogenetic. They were intruded late in the evolution of the lavas, after an early phase of intra-volcanic tectonism. The Unit is divided into three subunits, A1, A2 and A3, composed of plagioclase-augite-ilmenite gabbros. In addition, subunits A2 and A3 contain hypersthene and inverted-pigeonite respectively. The suite shows a limited range of cryptic variation. Low liquidus temperatures and the stabilisation of late magmatic reaction products as primary phases, are features of the gabbros.

Unit B is divided into five subunits, B1 to B5, composed of gabbro, ferrogabbro, ferrodiorite, ferrogranophyre and granophyre respectively. Subunit B1 is the former diabase, and subunit B5 the Carrock Fell and Rae Crags granophyres. Subunits B2 to B4 are the rocks originally described as hybrids. Members of the suite are related by high-level fractional crystallisation of an evolved tholeiitic parent, of low Mg-basalt or ferrobasaltic composition. Plagioclase and Ca-rich pyroxene were liquidus phases throughout, with Fe-Ti oxides + apatite, amphibole and zircon in addition, in Subunits B2, B3 and B4 respectively.

The Unit B suite shows initial iron-enrichment followed by strong residual silica-enrichment. It shows LREE enrichment, and the granophyres of B5 show a negative europium anomaly.

Subunits B2, B3 and B4, represent injections of fractionated magmas, that have crystallised and fractionated further, in situ, within an asymmetric thermal gradient. This has led to a regular cryptic,incompatible element and modal variation, laterally within each sub-vertical sheet. Systematic changes in crystal morphology and growth of hydrous-phases occur, with the development of pegmatitic facies. Fractionation within the subunits has been enhanced by rapid crystallisation, which has produced strong zonation in plagioclase, plus a variety of undercooled textures in pyroxenes and apatites. The order of emplacement of the five subunits is the reverse of their order in the fractionation sequence.

The Unit B suite forms part of the last widespread igneous event, at c.420 ma, related to subduction before continent-continent collision closed the Iapetus Ocean in the late Silurian. It possibly represents a continental extension of a back-arc tectonic regime.

The role of silicate liquid immiscibility in the Unit B magma and in tholeiitic magmas in general is discussed, and it is concluded that most tholeiitic melts should intersect a stable liquid miscibility gap in their late stages of fractionation. A model of silicate liquid immiscibility-controlled crystallisation is described that accounts for the observed major and trace element distribution between iron-rich and silica-rich associations.

LIST OF CONTENTS

	Page
Abstract	i
List of Contents	iii
List of figures	vi
List of plates	viii
List of tables	x
Acknowledgements	xi
Copyright	xiii
CHAPTER ONE: INTRODUCTION	
1.1 Geographical setting	1
1.2 Geological setting and background	2
1.3 Aims of the project	7
1.4 Layout of thesis and nomenclature	9
1.5 Maps and sampling	13
CHAPTER TWO: FIELD RELATIONSHIPS	
2.1 Unit A	22
2.2 Unit B	24
2.2.1 Subunit B1	24
2.2.2 Subunit B2	24
2.2.3 Subunit B3	25
2.2.4 Subunit B4	26
2.2.5 Subunit B5	27
2.2.6 Order of emplacement	28
CHAPTER THREE: THE PETROGRAPHY, MINERALOGY AND GEOCHEMISTRY OF UNIT A	
3.1 Petrography of Unit A	30
3.2 Petrography of the Eycott Volcanic Group	34
3.3 Mineral chemistry	37
3.3.1 Plagioclase	37
3.3.2 Pyroxene	37
3.3.3 Fe-Ti oxides	39
3.3.4 Biotite	39
3.3.5 Amphibole	40
3.4 Crystallisation and mineral stability in Unit A	40
3.5 The geochemistry of Unit A	45

Page

CHAPTER FOUR: THE PETROGRAPHY AND MINERAL CHEMISTRY OF UNIT B

4.1 Petrography 64

4.1.1 Plagioclase 65
4.1.2 Pyroxene 65
4.1.3 Amphibole 66
4.1.4 Iron-Titanium oxides 67
4.1.5 Apatite 68
4.1.6 Zircon 68
4.1.7 Quartz and Alkali felspar 68
4.1.8 Accessory phases 69
4.1.9 Hydrothermal alteration 69
4.1.10 Variations in texture 70

4.1.10.1 Crystal growth rate dependant textures 70
4.1.10.2 Pegmatitic facies 74
4.1.10.3 Plagioclase rich segregations 76
4.1.10.4 Xenoliths, hybrid and contact features 76

4.2 Mineral Chemistry 77

4.2.1 Plagioclase 78
4.2.2 Pyroxene 79
4.2.3 Plagioclase-Pyroxene relationships 91
4.2.4 Amphibole 92
4.2.5 Iron-Titanium oxides 98

CHAPTER FIVE : THE GEOCHEMISTRY OF THE UNIT B ROCKS

5.1 Introduction 144
5.2 Major element variation 148
5.3 Trace element variation 153
5.4 Summary 157

CHAPTER SIX: THE EMPLACEMENT AND FRACTIONATION OF UNIT B

6.1 Evidence for in-situ fractionation 171
6.2 The emplacement of Unit B 175
6.3 Mechanism of fractionation in Unit B 178
6.4 The water content of Unit B magma 182
6.5 The fractionation of the Unit B magma 184
6.6 The role of silicate liquid immiscibility (SLI) in the evolution of tholeiitic rocks 187

Page

CHAPTER SEVEN: SUMMARY AND CONCLUSIONS

7.1 Unit A, summary of conclusions 211
7.2 Unit A and the Eycott Volcanic Group 212
7.3 The Eycott Volcanic Group 214
7.4 Unit B, summary of conclusions 216
7.5 Unit B and the c.420 Ma event 219

LIST OF REFERENCES 225

APPENDIX ONE 242
Sampling

APPENDIX TWO 252
Mineral data

APPENDIX THREE 298
Whole-rock data

LIST OF FIGURES

		Page
1.1	Map of the Caldbeck Fells	16
1.2	Regional geology of the Lake District	18
1.3	Geological map of the complex, from Eastwood et al (1968)	20
1.4	Field relations in the Further Gill Sike area	21
3.1	Unit A, Plagioclase core compositions: Or-Ab-An	49
3.2	Unit A, Pyroxene compositions: Di-Hd-Fs-En	51
3.3	Unit A, Biotite compositions: Ann-Si-Ea-Ph	53
3.4	Unit A, Amphibole compositions: Ca-Fe-Mg	53
3.5	Unit A, plagioclase-pyroxene relationships	55
3.6a	Unit A, major element variation v. MgO	57
3.6b	Unit A, trace element variation v. MgO	57
3.7	Unit A, AFM plot	59
4.1	Unit B, Plagioclase core compositions: Or-Ab-An	103
4.2	Unit B, Normative whole rock felsic components : Ab-Or-SiO_2-H_2O	105
4.3	Unit B, Pyroxene compositions: Di-Hd-Fs-En	107
4.4 A-K	Unit B, Pyroxene compositions: Di-Hd-Fs-En	109-10
4.5	Pseudobinary phase relations across parts of the pyroxene quadrilateral	112
4.6	Variation in minor pyroxene components	114
4.7a	Si v Al for pyroxenes. Unit B.	116
4.7b	Al v Ti for pyroxenes. Unit B.	116
4.8	Sketches of sector zoned pyroxenes. Subunit B1	118
4.9	Plagioclase-pyroxene relationships in Unit B	120
4.10	Al^{IV} v A site occupancy for Unit B amphiboles	122
4.11	Unit B, Amphiboles Classification diagrams of Leake (1978)	124
4.12	Unit B, Amphibole compositions: Ca-Mg-(Fe+Mn)	126
4.13	Si v (Ca+Na+K), Unit B amphiboles	128
4.14	Unit B, Ilmenite-magnetite analyses: Fe_2O_3-FeO-TiO_2	130
4.15	Compositions coexisting Fe-Ti oxides projected onto fO_2-temperature plane	132
5.1	Unit B, Harker variation plots. Major elements	160
5.2a	Unit B, A.F.M plot	162
5.2b	A.F.M plot for tholeiitic suites	162
5.3	Unit B, Harker variation plots. Trace elements	164

		Page
5.4a	Unit B, Sr v Rb	166
5.4b	Unit B, Sr v Ba	166
5.5a	Unit B, Chondrite normalised REE patterns	168
5.5b	Chondrite normalised REE patterns for tholeiitic suites	168
5.6	Unit B. Sm_N v $(Ce/Yb)_N$	170
6.1	Modal variation histograms, Unit B	201
6.2a	Unit B, Zr v MgO	203
6.2b	Unit B, Zr v CaO	203
6.3	Sketch diagrammatic representation of the proposed sequence of intrusion. Unit B.	205
6.4	Change in Wt%H_2O with degree of crystallisation	207
6.5	Distribution coefficients for major elements between iron-rich and silica-rich conjugate melts	209
7.1	(Zr/Y) v Zr for Eycott Volcanic Group	222
7.2	Unit A. Chondrite normalised REE pattern	224
A1.1	The six sample traverses.	250-1

LIST OF PLATES

		Page
1.1	Carrock Fell from the east	xiv
1.2	Geological map of the eastern part of the Carrock Fell complex	folded inside back cover
2.1	Pegmatitic ferrogabbro showing spotting caused by hydrothermal alteration	29
2.2	Felsitic back vein in hybridised granophyre	29
3.1	Photomicrograph : Plagioclase-ilmenite gabbro, subunit A.1	60
3.2	Photomicrograph : Plagioclase- ilmenite- biotite - pyroxene gabbro, subunit A1	60
3.3	Photomicrograph : Plagioclase gabbro, subunit A1	61
3.4	Photomicrograph : Laminated two-pyroxene gabbro, subunit A2	61
3.5	Photomicrograph : Augite showing repeated twinning, subunit A1	62
3.6	Photomicrograph : Inverted pigeonite, subunit A3	62
3.7	Photomicrograph : Plagioclase rich vein cutting hornfelsed lava xenolith. Subunit A1	63
3.8	Photomicrograph : Hornfelsed xenolith of porphyritic Eycott lava	63
4.1	Photomicrograph : Ferrogabbro, subunit B2	133
4.2	Photomicrograph : Apatite-oxide rich ferrogabbro subunit B2	133
4.3	Photomicrograph : Ferrodiorite, subunit B3	134
4.4	Photomicrograph : Laminated ferrodiorite, subunit B3	134
4.5	Photomicrograph : Ferrogranophyre, subunit B4	135
4.6	Photomicrograph : Porphyritic granophyre, subunit B5	135
4.7a	Photomicrograph : Elongate, skeletal, subophitic ferroaugite, subunit B3	136
4.7b	Photomicrograph : Elongate, skeletal, subophitic ferrohedenbergite, subunit B5	136
4.8	Photomicrograph : Augite with inclusions in core region, subunit B2	137
4.9	Photomicrograph : Amphibole rim to pyroxene, subunit B3	137
4.10a	Photomicrograph : Branching augite, subunit B2	138
4.10b	Photomicrograph : Corkscrew augite, subunit B2	138
4.11	Photomicrograph : Subskeletal apatite, subunit B2	139

		Page
4.12	Photomicrograph : Sector zoned augite, subunit B1	139
4.13	Photomicrograph : Pegmatitic granophyric ferrodiorite, subunit B3	140
4.14	Photomicrograph : Elongate ferroaugite in pegmatitic ferrodiorite, subunit B3	140
4.15	Photomicrograph : Zircon in pegmatitic ferrodiorite subunit B3	141
4.16	Photomicrograph : Allanite mantled by epidote in pegmatitic ferrodiorite subunit B3	142
4.17	Photomicrograph : Resorbed ilmenite in pegmatitic ferrogabbro, subunit B2	142
4.18a.b.	Dendritic mafic phase in pegmatitic ferrodiorite, subunit B3	143
6.1a.b	Photomicrographs: Iron-rich immiscible globules in tholeiitic basalt - Giants Causeway.	210

LIST OF TABLES

		Page
1.1	Subunits of Unit A, with former names, and principal rock types	11
1.2	Subunits of Unit B with former names, and principal rock types	12
3.1	Modes of samples from Unit A	31
3.2	Summary of Eycott lava petrography	35
4.1	Average analyses of non-prism and prism sectors from sector zoned pyroxenes in subunit B1	89
4.2	Minimum and maximum cases for Fe_2O_3 recalculation for Unit B amphiboles	94
5.1	Residual porosity calculations for subunit B4	147
5.2	Comparison of bulk-rock compositions from Unit B with liquid composition from Eastern Iceland Tholeiites	150
5.3	MgO-FeO data for pyroxenes from Unit B, together with FM ratios for coexisting lavas	152
6.1	Modal analyses from Unit B	172
A.1.1.	Sample numbers, descriptions and map reference	243-8
A.2.1	Optimum analysing conditions and standards	254
A.2.2	Phases analysed from each specimen	255-7
A.2.3	Electron microprobe data	258-97
A.3.1	Detection limit and upper limit of standardisation for trace element analysis	302
A.3.2	Whole-rock XRF data	303-18
A.3.2	INAA data	329
A.3.3	C.I.P.W Norms	321-34

ACKNOWLEDGEMENTS

The work for this thesis was done while the author was under the tenureship of an N.E.R.C. research studentship, which is gratefully acknowledged.

I thank Prof. G.M. Brown, former Head of the Department of Geological Sciences, and Prof. M.H.P. Bott, present Head, for making available the research facilities of the Department.

To Prof. G.M. Brown and Dr. C.H. Emeleus, go my sincerest thanks, for their help and time, as supervisors during this project.

Dr. J.G. Holland and Mr. R. Hardy gave instruction and advice on X-Ray fluorescence analysis, Dr. B. Beddoe-Stevens gave instruction on electron microprobe analysis, Messrs. G. Randall and L. MacGregor produced thin sections, and Mr. G. Dresser has aided in photographic work; to all these people go my thanks for their generous help and time.

I thank Dr. D.L. Hamilton, Dr. I. Freestone and Dr. D. Manning for their help during an unfruitful period spent at the experimental laboratory at Manchester, in September, 1978.

I would like to take this opportunity to thank all the people who, during my past years at Durham, have given me generous advice, help and hinderance on matters academic, and non-academic, but particularly :

J. Anstee, B. Beddoe-Stevens, P. Betten, G.M. Biggar, C.C. Bristol, G.M. Brown, S. Caunt, C.H. Emeleus, R.M. Forster,

I. Freestone, D.M. Hirst, J.G. Holland, A.P. Jones, J.A. Pearce, R. Powell, R. Phillips, A.R. Westerman, I. Williamson, J.R. Wilson, and last, but not least, all the 'chaps and chapesses' of D.U.S.A.

My thanks must also go to Mr. & Mrs. Waites of Amber cottage, Mosedale for their kind hospitality, and to Mrs. M. Bell, Miss K. Anderson and Mrs. L. Mines for their very efficient typing.

To my Mother and Father and to Miss J. Stockell go my sincere thanks for their moral support.

STATEMENT OF COPYRIGHT

The copyright of this thesis rests with the author. No quotation from it should be published without the author's prior written consent, and information derived from it should be acknowledged.

PLATE 1.1 Carrock Fell from the east. The summit is hidden behind Pike summit. The gulley to the left of centre is Further Gill Sike, with the Unit A gabbros to the left and the Carrock Fell granophyre (subunit B5) forming the cliffs to the right.

CHAPTER ONE

INTRODUCTION

Durham University SCIENCE 30 OCT 1980 SECTION Library

1.1 GEOGRAPHICAL SETTING

Carrock Fell, at 660 metres O.D., forms the most northerly significant hill within the boundary of the Lake District National Park. It lies between the mountains of Skiddaw and Blencathra to the south, and the rolling Caldbeck Fells to the north and west. The Fell itself, (Plate 1.1 and figure 1.1) forms the exposed part of the Carrock Fell igneous complex, which is bounded to the north by Carrock Beck, to the west by Roughten Gill, to the south by Grainsgill Beck and the River Caldew, and to the east by the road from Mosedale to Hesket Newmarket. The area to the west of Brandy Gill is very poorly exposed with only a few in-situ outcrops in Arm O'Grain and the Roughten Gill areas. East of Brandy Gill exposure is limited but increases towards the eastern end of the Fell, where, in the steep 250 m. scarp overlooking the marshy valley of Mosedale, exposure is good.

The summit of Carrock Fell forms the site of a five-acre, Iron-age earthworks and Hill fort. This, according to Collingwood (1938), was a stronghold of the Brigantian Celtic tribe, and was rased by the Romans in their conquest of Northern England. Only grazing sheep, walkers, geologists and hang-glider pilots frequent the bleak, windswept summit today.

The area has had a long history of copper, lead and barytes mining, with more recent interest in tungsten. The main mines were situated (fig. 1.1), in Roughten Gill, Dry Gill, Brandy Gill and at Carrock End. Only the Carrock

Wolfram mine, at the junction of Brandy Gill and Grainsgill beck is still, if sporadically, operational at present.

1.2. GEOLOGICAL SETTING AND BACKGROUND

The regional geology of the Lake District is shown in figure 1.2, and is described in detail in 'The Geology of the Lake District' (Ed. F. Moseley, 1978). The geology of the area around Cockermouth and Caldbeck in the north of the Lake District, is described in a Geological Survey Memoir. (Eastwood et al, 1968).

The lower Ordovician Skiddaw Slates Group forms a broad E-W trending anticline. To the north of this anticline the slates are interbedded with, and pass upwards into, the Eycott Volcanic Group of Llanvirnian age (Downie and Soper, 1972). The Eycott Volcanic Group is a succession of tuffs and, characteristically, porphyritic lavas, outcropping intermittently over an area of 50 km^2, from Binsey Hill in the west to the Cross Fell Inlier in the east. The lavas reach a maximum exposed thickness of 2500 m. on Binsey Hill. The Eycott volcanic group is overlain, unconformably, to the north and east by Carboniferous rocks.

The Carrock Fell igneous complex is a multiple intrusion, dyke-like in form, extending for approximately 7 km. on a line W.10^{o}N, and varying from 1.5 to 2.5 km. from north to south. It is intruded along the southern contact of the Eycott Volcanic Group with the Skiddaw Slates.

Ward (1876) recognised three main rock types in the intrusion, hypersthenite, diorite and spherulitic felsite, and considered that the existence of parallel banding and

metamorphosed xenoliths of lava within the complex, suggested an origin by metamorphism of Borrowdale Volcanic rocks.

Trechmann (1882) recognised that the dominant pyroxene in the so called hypersthenite, was diallage rather than hypersthene, and the rock was therefore more correctly termed a gabbro.

Teall (1885; 1888) considered the spherulitic felsite to be a typical granophyre in the sense of Rosenbuch, and that it passed by 'insensible gradations' into the Gabbro.

Groom (1889) describes a thin tachylitic vein associated with the gabbro (a very thin dyke, in fact) and confirmed the apparently continuous transition from the gabbro to the granophyre.

Harker (1894; 1895), in his classic study of the complex, described the rocks under the major headings gabbro, diabase and granophyre, and gave petrographic descriptions of the major types. He noted the increasing basicity of the gabbro from the centre to the margin of the intrusion, which he explained in terms of the Soret principle. Basic elements concentrated in the cooler portions of the magma chamber (the margins), during the progressive crystallisation of the magma. It was also suggested that the gabbro and granophyre were formed by magmas, which were themselves 'partial magmas' derived by differentiation from a common source. He ascribed the, apparent, continual gradation from granophyre to gabbro, to incorporation of re-fused, ultrabasic gabbro into the granophyre magma.

Whilst the application of the physical mechanisms

which Harker held responsible for the observed variations leave much to be desired in the light of present knowledge, it must be noted that these publications (Harker op cit), form a landmark in the geological literature, in that they offered, for the first time, suggestions as to the physical and chemical mechanisms of in-situ differentiation of igneous intrusions.

The intrusion received little further attention until the years between the two world-wars, when Eastwood and his co-workers from the Geological Survey, surveyed the area on a Six-Inch to the Mile scale. The One-Inch geological map of the area (sheet 23), was published in 1959, but the Geological Survey Memoir did not appear until 1968. The Memoir (Eastwood et al, 1968) contains a detailed account of the field relationships and petrography of the Carrock Fell complex, and figure 1.3 is from the memoir. (fig. 10, page 80).

The main divisions, gabbro, diabase and granophyre, were retained by Eastwood et al (op cit). The gabbro was divided into six main types, from north to south; the Southern Melagabbro, Southern Leucogabbro, Buck Kirk Gabbro, Central Leucogabbro, Fluxion gabbro and Northern Melagabbro, respectively. It was suggested that as the uniform colour belts in the gabbro, apparently, maintained their identities over considerable distances, and had gradational but fairly rapid transitions with one another, that the field relationships - "seem to preclude successive injections of magma separated by long intervals of time. It remains, however, possible that a stratified mush was injected, and that crystallisation of

the inter-crystal liquid was well advanced when one or more later waves of magma (with crystals) arrived, the whole complex still being hot. Such a mechanism might account for the leucogabbro bands.". It is not clear to the author exactly what is meant by a 'stratified mush', but Eastwood et al (op cit) conclude "There are thus two hypotheses for the gabbro :
(1) that they were produced by recrystallisation and metasomatism of lavas, either in-situ or with limited movement;
(2) that they resulted from the completion of crystallisation of a mush of crystals and liquid - that is, a magma in the original sense of the term - in which some layering of minerals had already been produced before intrusion. Neither is entirely satisfactory and a combination of the two seems nearest the truth in the present state of knowledge."

The granophyre was interpreted as representing a low melting faction of sialic material, intrusive at its present level, produced by heat from the basic magma at depth. It was noted that at the southern margin of the granophyre, separate injections of melagranophyre, enriched in hedenbergite, occurred. They supported Harker's hybrid interpretation for the rocks between the gabbro and granophyre, stating that "there is plain evidence in the pegmati tic belt between the northern melagabbro and the mela granophyre, of recrystallisation of the gabbro and mingling with the granophyre".

It is generally accepted that the diabase and granopyre are younger than the gabbro, but their relative ages are uncertain, (Skillen, 1973). Harker (op cit) favoured the order gabbro-granophyre-diabase, Eastwood et al (op cit), however, suggested that the diabase predates the granophyre,

on the basis of felsitic veins cutting the diabase. Skillen (op cit) however, favoured Harker's original interpretation, suggesting that the hydrothermal alteration of the diabase was caused by the Skiddaw granite, rather than the granophyre as suggested by Eastwood and his co-workers.

The age of the complex: Harker (1902) suggested, on petrological affinities, that the complex possibly formed part of the Tertiary province of the British Isles. Green (1917) proposed an Ordovician age, however, on the supposed pre-Bala age of the folding in the Skiddaw Grits. Eastwood et al (1968) noted that the gabbros were intruded after the main folding of the Skiddaw slates, but that the rocks were affected by the metamorphism and mineralisation associated with the emplacement of the Skiddaw Granite, and bracketed the age as post-Caledonian folding, but pre-Carboniferous. Firman (1978) however, brackets the age more concisely, as younger than the lowest Eycott volcanics, but older than the Lower Devonian Skiddaw Granite.

Both Fitton (1971) and Soper (1974) note the petrological and chemical similarities of the Gabbros to the Eycott Volcanic Group and suggest a cogenetic origin, and therefore, a Llanvirnian age.

Absolute ages have been determined by Brown et al (1964) and Rundle (1979). K-Ar whole-rock, biotite, and hornblende ages range from 356 $\pm$ 20 ma. (Brown et al, op cit) to 468 $\pm$ 10 ma. (Rundle, op cit). The later ages are ascribed to later re-crystallisation or argon loss, and the preferred date for the gabbros, is now 468 $\pm$ 10 ma., contemporareous with the Eycott Volcanic Group.

Rb-Sr whole-rock isotopic determinations for the granophyre of Carrock Fell and Rae Crags, (Rundle, 1979) gives an age of 416 ± 20 ma., with an initial $Sr^{87/86}$ ratio of 0.70708 ± 0.0016, and thus supports a significantly younger age for the granophyres than that of the gabbro.

The Harestones Felsite, a fine grained acidic rock associated with the down faulted block of Caradocian Drygill Shales, gives a Rb-Sr whole-rock age of 419 ± 4 ma., and an initial $Sr^{87/86}$ ratio of 0.70799 ± 0.00029. (Rundle, op cit).

The Gabbros, as was noted by Eastwood et al (1968), show the effects of metamorphism and mineralisation from the Skiddaw granite. The granite and the mineralisation have been dated, by the K-Ar method (Shepherd et al, 1976), at 392 ± 4 ma. and 385 ± 4 ma. respectively.

1.3. AIMS OF THE PROJECT

The initial aim of the project was to study the gabbro-granophyre contact zone in detail, as part of an investigation of acid-basic hybridisation in general. This required a detailed re-survey of the field relationships along and across the contact zone, with particular attention being paid to small scale variations. Three partial and three complete sample traverses were collected across the contact zone (see Appendix One). Sample spacing depended on the scale of the variation, and on the availability of continuous outcrop. Other occasional samples were collected as required within the contact zone, and throughout the complex in order to assess the type and variability of the rocks exhibited within the complex as a whole.

The re-survey showed that the contact zone is more complex than had been described previously. It consists of a number of sub-vertical, sub parallel sheets, of variable width, with contacts diffuse on a centimetre scale. A detailed survey of the literature on hybrid rocks suggested that many of the features observed in the contact zone superficially resemble features common to supposed hybrid rocks in general. The rocks are blotchy and inhomogeneous on a centimetre scale. (see Pl. 2.1), although not so on any larger scale, with variations within individual sheets apparently gradational on an outcrop scale. Pegmatitic facies are developed within the sheets, although they have a systematic spatial arrangement, occurring on the northern margins of each individual sheet. No evidence for assimilated or reacted xenoliths of gabbroic material exist within the contact zone, nor does any evidence exist for back-veining or net-veining.

A preliminary petrographic and chemical investigation, indicated a number of features pertinent to the hybrid interpretation of the suite. Firstly, the ilmenite-apatite gabbro along the southern-margin of the so-called hybrid zone is, in fact, quite distinct from the northern melagabbro of Eastwood et al (1968). Secondly, within each sheet, there is a systematic change in petrographic, mineralogical and chemical characteristics. And, finally, the whole suite of so-called hybrid rocks exhibits continal variation into the granophyre, and shows a remarkable similarity to fractionated gabbroic rocks from other tholeiitic intrusions. These features do not discount an origin by hybridisation.

Recent dating has, however, shown that the main gabbroic suite is significantly older than the granophyre (see above). This precludes mixing of coeval, contrasted magma compositions, as the Northern Melagabbro was undoubtedly solid, and cold, when the granophyre was intruded. For the granophyre to melt the mafic gabbro, it would require substantial superheat. However, petrographic observation provides convincing evidence that the later magmas may have been locally supercooled on intrusion, which would have removed any superheat that the melt might have possessed. Also, the blotchy nature of the so-called hybrid rocks, which in hand specimen resembles mechanical breakdown of the gabbro by the granophyre, (see for example Pl. 2.1) is, in fact, a function of small-scale, selective, inhomogeneous hydrothermal alteration.

Thus, it became apparent after the preliminary survey, that the evidence does not support an origin by hybridisation, but that the suite of rocks may be related by fractional crystallisation. It was felt that the detailed mapping and sampling of the suite as a whole, had provided an excellent opportunity to study the differentiation of an evolved tholeiitic magma, and this forms the main theme of this thesis

1.4. LAYOUT OF THESIS AND NOMENCLATURE

The diabase has been shown, on petrological and geochemical affinities, to represent the higher temperature fraction of the more evolved ferrogabbro-granophyre suite, previously interpreted as being of hybrid origin. These rocks form Unit B, for the purpose of description, and have been divided into five subunits on the basis of their occurrence

as discrete mappable sheets, and their mineralogy. The subunits are listed in table 1.2, together with the principal rock types, and the names under which the rocks were described by Eastwood et al (1968). The field relations, petrography, mineral chemistry and geochemistry, together with their interpretation, forms the bulk of this thesis (Chapters 2, 4, 5 and 6).

A study of the Carrock Fell complex would, however, not be complete without covering the gabbro suite. These rocks form Unit A. This unit has been divided into three subunits on the basis of field occurrence and mineralogy. These subunits, together with the principal rock types, and the former names (Eastwood et al, 1968), are shown in table 1.1. The field occurrence, petrography, mineralogy, and geochemistry of Unit A are described, in much less detail than for Unit B, with emphasis on description rather than interpretation, in Chapters 2 and 3. The Unit A gabbros are compared with the Eycott Volcanic Group.

During the study of the Unit B evolved tholeiitic suite, the author became interested in the role of silicate liquid immiscibility in the evolution of tholeiitic magmas in general, and this subject forms the basis of section 6.6.

A brief summary of the main conclusions concerning the evolution of the Carrock Fell igneous complex, and a brief discussion of its place in Lake District geology, is given in Chapter Seven.

The terms gabbro, diorite and granophyre used in this thesis are synonymous with subunits B1 and B2, subunit B3, and subunits B4 and B5, respectively and reflect the plagioclase

TABLE 1.1 :

Former Units and Names (Eastwood etal, 1968)	New Units and Subunits (This study)	Principal Rock Types
GABBROS	UNIT A	
Northern Melagabbro	A1	Pl-Aug-Ilm Gabbros
Central Leucogabbro	A1	Pl Gabbros
Southern Leucogabbro	A1	Pl-(Aug-Ilm) Gabbros
Southern Melagabbro	A1	Pl-Aug-Ilm-Bi Gabbros
Fluxion Gabbro	A2	Pl-Aug-Hy-Ilm Laminated gabbros
Buck Kirk Gabbro	A3	Pl-Aug-In.pig-Ilm-Qz Gabbros

Pl. Plagioclase; Aug. Augite; Hy. Hypersthene; In Pig. Inverted Pigeonite;
Ilm. Ilmenite (Subordinate titanomagnetite); Bi. Biotite; Qz. Quartz

TABLE 1.2 :

Former Units and Names (Eastwood etal, 1968)	New Units and Subunits (This study)	Principal Rock Types
	UNIT B	
Diabase	B1	Pl-Aug-Gabbros
Northern Melagabbro (in part) Gabbro Pegmatite	B2	Pl-Aug-Mt-Ilm-Ap Ferrogabbros Peg-Grph Ferrogabbros
Basic Granophyre (in part) Coarse Pegmatite	B3	Pl-Feaug-FeEd-Mt-Ilm Ferrodiorites Peg-Grph Ferrodiorites
Basic Granophyre Melagranophyre	B4	Pl-FeHd-Mt-(Zr) Ferrogranophyres + plagioferrogranophyres
Granophyre Rae Crags Carrock Fell	B5	Pl-Fe h d-Mt-(Zr)Porphyritic granophyres

Pl. Plagioclase; Aug. Augite; Feaug. Ferroaugite; Fehd. Ferrohedenbergite;
FeEd. ferroedenite; Mt. Titanomagnetite; Ilm.Ilmenite; Zr. Zircon;
Peg.Pegmatitic; Grph. Granophyric
B2 + B3 occasionally laminated.

core compositions within each subunit. A modal classification based on Strekeisen (1976), was not possible because no distinction could be made, modally, between intergrown quartz and alkali-felspar. The term granophyre, or granophyric, implies that the quartz and alkali felspar in the rock are intergrown micrographically. It must be noted, however, that in subunit B4, the granophyric intergrowths may form as little as 25 modal%.

The prefix 'ferro' is used for the gabbros, diorites and granophyres of subunits B2, B3 and B4 respectively. The term ferro simply implies that the rock contains modally abundant oxide or Fe-rich mafic phases, and does not imply a preferred oxidation state for the iron in the rock.

Some of the rocks of subunit B4 would, because of their modal abundance of plagioclase, be termed trondhjemites in the classification of Strekeisen (op cit). The term plagio-ferrogranophyre is preferred, however, as trondhjemite can have genetic implications, and the K_2O content is rather too high for them to be trondhjemites in the ophiolitic sense of the term (Coleman and Peterman, 1975).

It must be emphasised here that the whole suite of Unit B rocks shows continuous gradation, and that taken out of their field context, some rocks would be classified differently.

1.5. MAPS AND SAMPLING

Plate 1.2 and figure 1.4, show a geological map of the eastern part of the Carrock Fell complex, and a more detailed map of the Further Gill Sike region, respectively.

Field relationships in the western part of the complex,

west of Brandy Gill, are entirely conjectural, because of the lack of exposure. Also metamorphism and mineralisation associated with the emplacement of the Skiddaw Granite, has affected the rocks to a very great extent. The field relationships in this area are described in Eastwood et al (1968) and Skillen (1973), and the map of the former authors was shown in figure 1.3. What outcrops there are, confirm that features in the gabbros are similar to those described from the better exposed, eastern part of the complex.

Sample localities are shown in plate 1.2 and figure A1.1, and a complete list of samples, with very brief descriptions and eight-figure map references, is given in Appendix one. No samples have been collected from west of, or from within Brandy Gill, for reasons stated above.

126 samples have been either sectioned for petrographic or electron microprobe work, or prepared for whole-rock analysis. Additional samples from the collections of the Department of Geological Sciences at Durham University, and the Geological Survey, together with analyses of rocks from Eastwood et al (1968), Fitton (1971) and R.N. Thompson (written comm. 1978), have been used in this study. (see Appendix one).

FIGURE 1.1

The principal hills, streams and settlements of the Caldbeck Fells region, Cumbria, showing the location of Carrock Fell.

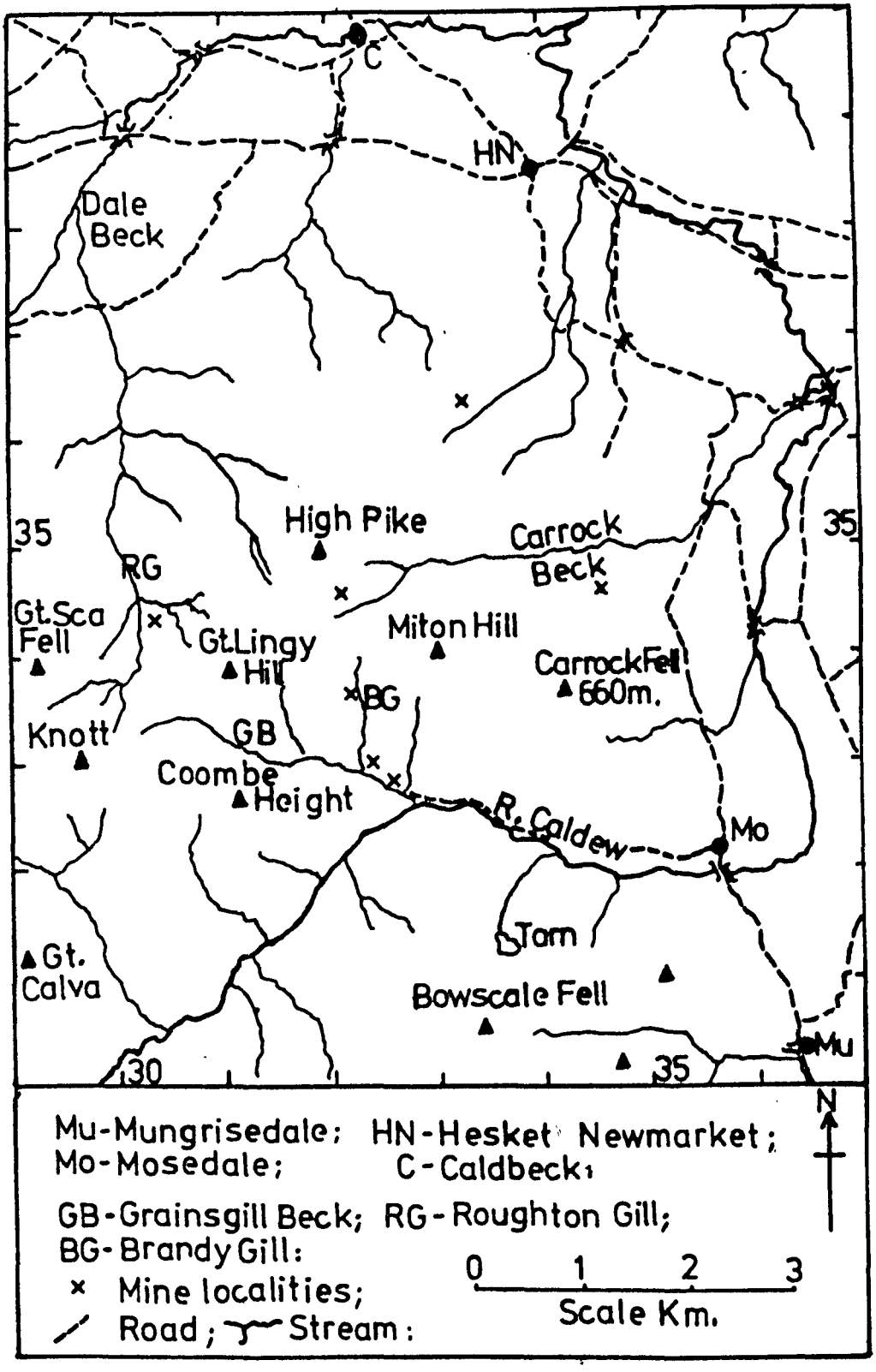
C
HN
Dale Beck
35
High Pike
Carrock Beck
35
RG
Gt.Sca Fell
Gt.Lingy Hill
Miton Hill
Carrock Fell 660m.
BG
Knott
GB
Coombe Height
R. Caldew
Mo
Tom
Gt. Calva
Bowscale Fell
Mu
30
35
Mu-Mungrisedale; HN-Hesket Newmarket;
Mo-Mosedale; C-Caldbeck;
GB-Grainsgill Beck; RG-Roughton Gill;
BG-Brandy Gill:
× Mine localities;
Road; Stream:
N
0 1 2 3
Scale Km.

FIGURE 1.2

Regional geology of the Lake District, showing the location of the Carrock Fell intrusion.

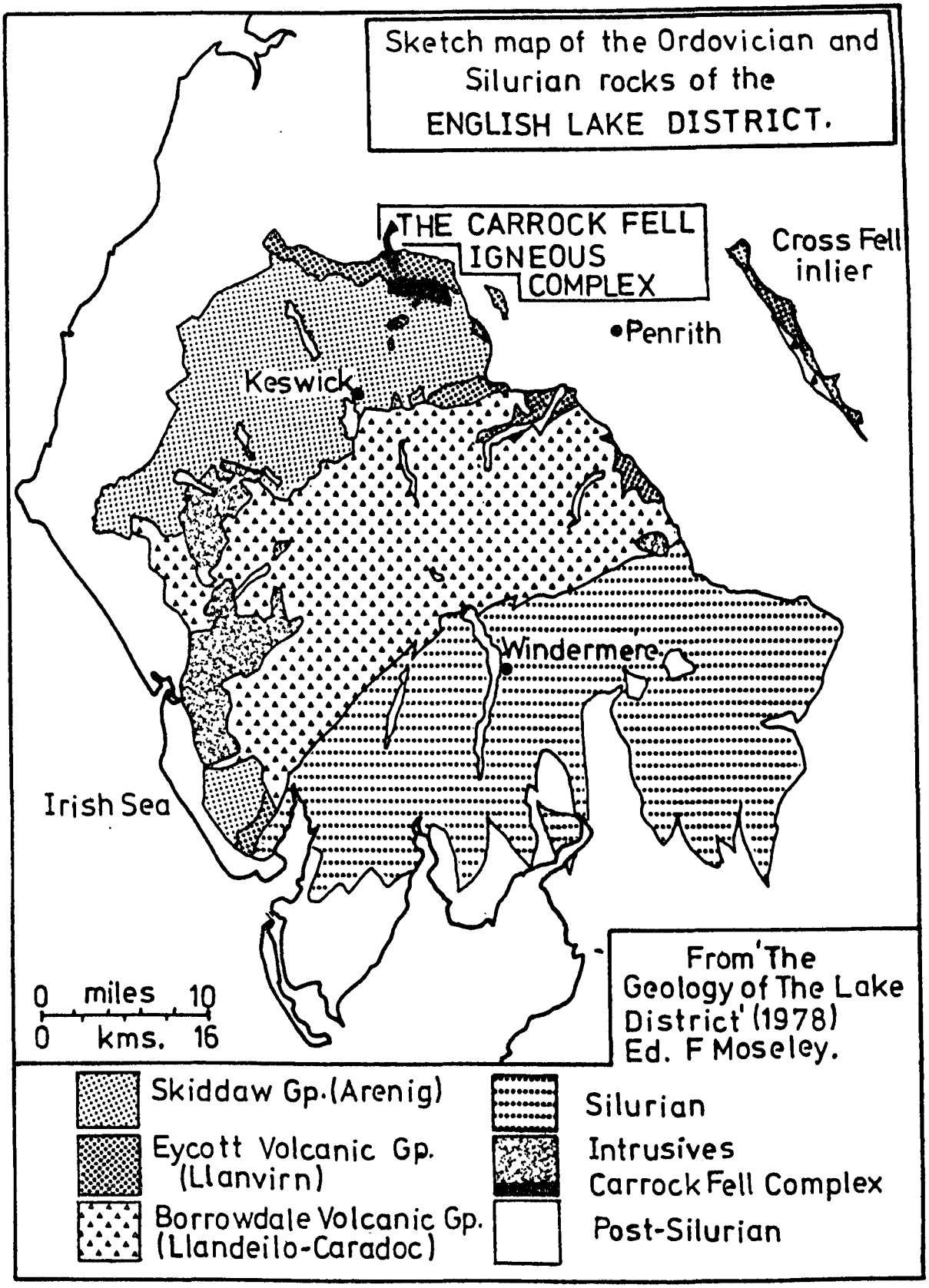
Sketch map of the Ordovician and Silurian rocks of the ENGLISH LAKE DISTRICT.
THE CARROCK FELL IGNEOUS COMPLEX
Cross Fell inlier
Penrith
Keswick
Windermere
Irish Sea
0 miles 10
0 kms. 16
From 'The Geology of The Lake District' (1978) Ed. F Moseley.
Skiddaw Gp. (Arenig)
Eycott Volcanic Gp. (Llanvirn)
Borrowdale Volcanic Gp. (Llandeilo-Caradoc)
Silurian
Intrusives Carrock Fell Complex
Post-Silurian

FIGURE 1.3

Geological Map of the Carrock Fell complex, from Eastwood et al (1968, figure 10, p.80).

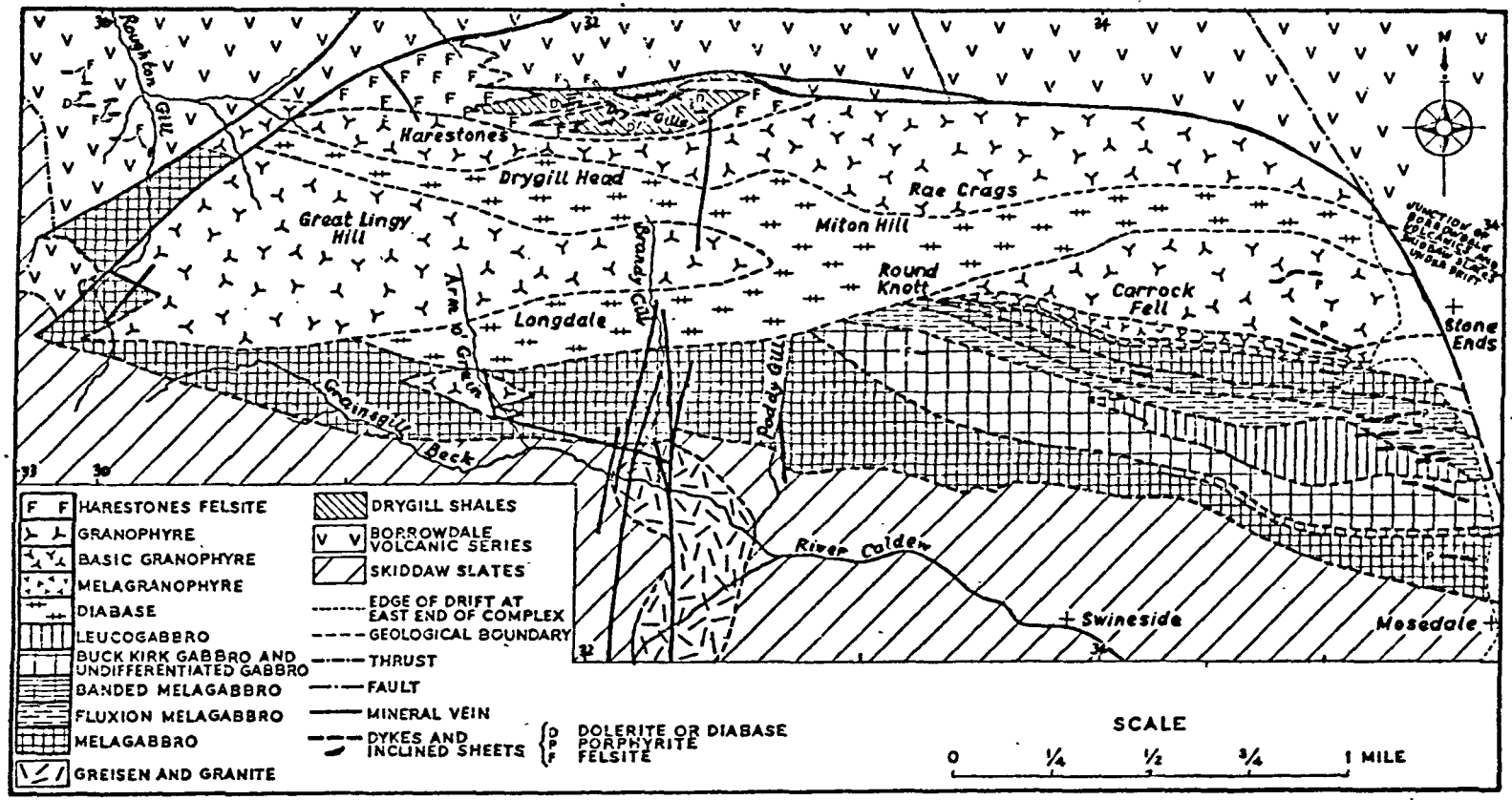
Roughton Gill
Harestones
Drygill Head
Great Lingy Hill
Rae Crags
Miton Hill
Round Knott
Carrock Fell
Stone Ends
Arm o' Green
Longdale
Grainsgill Beck
Roaring Gill
River Caldew
Swineside
Mosedale
N
HARESTONES FELSITE
GRANOPHYRE
BASIC GRANOPHYRE
MELAGRANOPHYRE
DIABASE
LEUCOGABBRO
BUCK KIRK GABBRO AND UNDIFFERENTIATED GABBRO
BANDED MELAGABBRO
FLUXION MELAGABBRO
MELAGABBRO
GREISEN AND GRANITE
DRYGILL SHALES
BORROWDALE VOLCANIC SERIES
SKIDDAW SLATES
EDGE OF DRIFT AT EAST END OF COMPLEX
GEOLOGICAL BOUNDARY
THRUST
FAULT
MINERAL VEIN
DYKES AND INCLINED SHEETS
D DOLERITE OR DIABASE
P PORPHYRITE
F FELSITE
SCALE
0 1/4 1/2 3/4 1 MILE

Figure 1.4

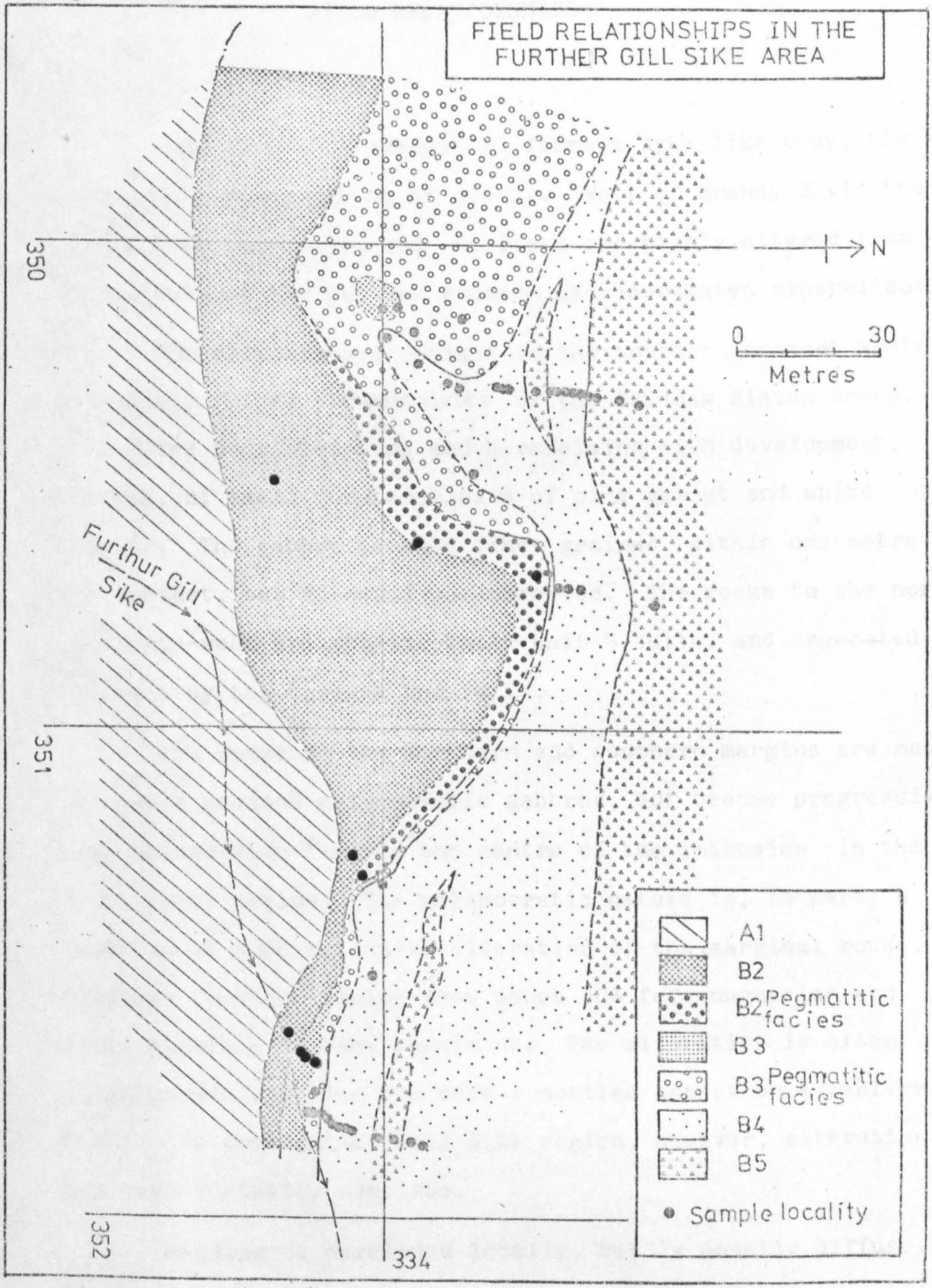
FIELD RELATIONSHIPS IN THE FURTHER GILL SIKE AREA
N
0
30
Metres
350
351
352
334
Furthur Gill Sike
A1
B2
B2 Pegmatitic facies
B3
B3 Pegmatitic facies
B4
B5
Sample locality

CHAPTER TWO

FIELD RELATIONSHIPS

2.1. UNIT A.

The gabbro of subunit A1 forms a dyke like body, six km. in length and one km. at its widest. West of Brandy Gill the exposure is very poor, and the rocks are highly altered from the effects of the Skiddaw granite and associated mineralisation.

The only exposed contact is the southern contact against the highly folded Kirkstile slates of the Skiddaw Slates Group. The slates show bleaching and hornfelsing with development, locally, of small porphyroblasts of pink garnet and white felspar. The gabbro becomes finer grained within one metre of the contact, but no chill was observed. The rocks to the north and north-west are cut by the later Unit B suite, and truncated to the east by the Carrock End fault.

The rocks on the northern and southern margins are medium to coarse grained melanocratic gabbros, but become progressively more leucocratic towards the centre of the intrusion in the White Crags region. The melanocratic nature is, in part, a function of more extensive alteration of the marginal rocks, although fresher samples show about 30% ferromagnesian and oxide minerals in hand specimens. The alteration is often inhomogeneous, giving the rock a mottled aspect on a centimetre scale. In the Further Gill Sike region, however, alteration has been virtually complete.

Banding is developed locally, but is usually diffuse. Individual bands vary from 1 cm. to 1 m. in width. The attitude of the banding is vertical or dipping steeply to the north,

and has a trend parallel to the length of the intrusion. The bands reflect differing proportions of interstitial mafic and oxide phases. Lamination is widely developed, and has the same strike direction and dip as the banding.

Subunits A2 and A3, form narrow sheets up to 150 m. wide, extending from the eastern margin for 2.5 km. to the west, where they are truncated by Unit B1. The contacts with subunit A1 are diffuse over 1-5 m, and are vertical or at a steep angle to the south.

Subunit A2, the fluxion gabbro of Eastwood et al. (1968), is strongly laminated. The lamination is vertical, and strikes parallel to the margins of the intrusion.

Subunit A3, the Buck Kirk gabbro of Eastwood et al. (op.cit), is finer grained, more compact and well jointed than subunit A1, which is coarser grained and more massive.

A prominent feature of the gabbros, particularly along the southern, and to a lesser extent, the northern margin of the intrusion, is the occurrence of large, hornfelsed, xenolithic screens of Eycott Volcanic Group lavas. They form the bulk of the outcrop in the Snailshell Crag and Black Crag regions on the eastern margin, and in the gabbros north of Swineside. The xenoliths have been equilibrated with the gabbros to varying degrees. Some are only slightly hornfelsed, others show signs of being digested by the gabbros, and are cut by felspathic veins. Biotite is developed in the gabbros in association with the xenoliths, and clots of pink quartzofelspathic pegmatite are abundant in the xenolithic gabbro. In the central region of the intrusion, the xenoliths are much less common and rarely

exceed 10 cm. in size.

Throughout the Unit, thin veins of acidic material occur, often along early joint planes.

2.2. UNIT B

2.2.1. Subunit B1 : Formerly the Diabase of Harker (1894) and Eastwood et al. (1968), B1 forms a poorly-exposed sheet that extends from the eastern margin, north of Scurth, to Round Knott and Miton Hill, where it bifurcates. The southern limb outcrops in Brandy Gill and Arm O'Grain, the northern limb, on Drygill Head. Outcrop is virtually non-existent west of Brandy Gill and the rocks are affected by the metamorphism and mineralisation from the Skiddaw granite.

In the eastern part of the complex, the rocks are hard, grey, compact, microgabbros and gabbros. Nowhere is a contact seen with the subunit B5 granophyres, or Unit A, but it can usually be located to within 2 m. Banding, of a very diffuse nature, can be seen on Round Knott (MR. 3343, 3375). Small cognate xenoliths, rarely exceeding 2 cm. in size, occur in the gabbro north of Carrock Fell summit. (MR 3415, 3394).

2.2.2. Subunit B2 : The B2 ferro gabbros form a sheet, 20-50 m. in width, extending for 2 km. along the southern margin of Unit B, from south of Round Knott, to the lower reaches of Further Gill Sike. The ferrogabbros are dark in colour, primarily a function of their altered nature, and occasionally laminated parallel to the margin of the sheet.

A pegmatitic facies is developed on the northern margin, along the complete length of the exposed sheet. Tabular

plagioclase prisms, and pyroxene crystals, set in a ground mass of pink quartz and alkali felspar can be seen in hand specimens. The alteration is inhomogeneous and gives the rock a conspicuous spotted appearance. (Pl.2.1)

The northern margin cuts the subunit B4 ferrogranophyres south of Carrock Fell and Pike summits, but the contacts are very diffuse. In the Further Gill Sike region, the northern margin is against both the pegmatitic facies and finer grained ferrodiorites of subunit B3, again the contact is diffuse. The southern contact against the gabbro of Unit A is unexposed.

Thin leucocratic schlieren and segregations up to 5 cm. in width occur in the laminated ferrogabbro from south of Carrock Fell summit. They only occur in loose blocks, and their exact location is unestablished.

2.2.3. Subunit B3 : The ferrodiorites of subunit B3 are only exposed in the Further Gill Sike region. They form the lowest exposed slabs in the stream bed, (MR 3517, 3337) and extend as a thin sheet up to the cliffs at the head of the sike. The width of the sheet varies from 5 m. in the slabs in the stream, to 2 m. in the cliffs below the path, 50 m. above, (MR 3513, 3340). Above the cliffs at the head of the Sike, the pegmatitic facies widens to 50 m., but does not extend higher than the sheepfold, 200 m. above (MR 3477, 3342). The finer grained ferrodiorite is well laminated, and outcrops as a thin sheet in the slabs in the stream bed. There is a sharp contact with the pegmatitic facies in the stream bed, but 10 m. above, the change is gradational. The dark finer grained type disappears and the pegmatitic facies is in contact with the pegmatitic facies of B2 in the cliff below the path, 50 m. above.

(MR 3513, 3340). The contact here is subhorizontal. The darker variety occurs locally at the southern end of the cliffs at the head of Further Gill Sike (MR 3501, 3340). The pegmatitic facies widens out here, and has a diffuse sub-horizontal contact with B3, running along the top of the cliffs. The contact with B2 further south is unexposed. The pegmatitic facies shows its most spectacular development above the cliffs. Plagioclase up to 2 cm, and ferromagnesian crystals up to 8 cm. in length occur, set in a coarse, quartzofelpathic matrix. A mafic phase also develops dendritic morphology with individual forms up to 20 cm. in length occurring. (Pl. 4.18.). The pegmatite above the cliffs does not outcrop but the limit of its sub-surface outcrop is indicated by the occurrence of near in-situ blocks.

2.2.4. Subunit B4 : The ferrogranophyre of B4 extends from Round Knott to the lower regions of Further Gill Sike, in a continuous sheet 50-100 m. wide. The southern margin is diffuse against B2 south of Carrock Fell and Pike summit. In the Further Gill Sike region, the southern contact against B3 is exposed in the northern bank of the stream (MR 3518, 3338), and is diffuse over 1-2 cm. Along the southern part of the sheet, the rocks are medium to fine grained and dark in colour. They become pinker and finer grained towards the northern contact. The contact against the B5 granophyre at the northern end of the cliffs at the head of the sike, is very sharp, and slightly chilled in places (MR 3503, 3344). 30 m. south of Carrock Fell summit the contact is sharp, but not chilled. Screens of hornfelsed B5 granophyre occur in the Further Gill Sike region. No pegmatitic facies of B4 occurs.

2.2.5. Subunit B5 : Four granophyre masses are exposed. The Great Lingy Hill and Arm O'grain exposures are highly altered by the Skiddaw granite metamorphism and mineralisation. The Rae Crags granophyre is only exposed along its southern margin against subunit B1. The contact is not exposed. The granophyre near the contact is darker than the Carrock Fell granophyre, contains small acicular mafic crystals, and appears to be somewhat hybridised.

The Carrock Fell granophyre forms the largest exposed mass of B5. Along the southern contact against B4 in the Further Gill Sike region, and as far west as Pike summit, the granophyre is grey in colour. Further north, extending from Central Scurth to Round Knott, the granophyre is pink-grey in colour. A band extending from north of Carrock Fell summit, eastwards to Northern Scurth, is a darker, reddish colour with prominent small phenocrysts of felspar. These three types may represent three different sheet like injections as they form subparallel bands, but have not been shown as such in plate 1.2

The southern margin is very slightly hornfelsed, as are the stoped blocks in B4 in the Further Gill Sike area. Near the northern contact with subunit B1 in the Northern Scurth region (MR 3515,3388), and south of Round Knott (MR 3345, 3372), marginal modifications of the granophyre occur. At the aforementioned locality, the granophyre is darker, and contains a small acicular mafic phase. The granophyre shows continuous gradation from pink to dark grey and is very inhomogeneous on a 10 cm. scale. Thin 2 cm. wide veins of pink felsitic material cut both the normal and dark varieties. Similar gradational relationships occur south of Routh Knott, but here the veins

brecciate the granophyre, (Pl.2.2.) and resemble back veining phenomena. The patchiness in the granophyre is attributed to hybridisation of the granophyre by the emplacement of subunit B1. In addition, local melting of the granophyre may have occurred to produce the felsitic veins.

Small (< 20 cm) hybridised xenoliths of B4 and B5 granophyre occur in the bottom of the cliffs at the head of Further Gill Sike, 10 m. south of the thin sheet of granophyre in B4 (MR 3503, 3343) and also 20 m. below this (MR 3505, 3342). The matrix appears to be either ferrodioritic or a dark ferrogranophyre.

2.2.6. Order of emplacement

The observed field relationships, described above, would favour the order B5, B4, B3, B2, B1. Although the contacts, when exposed, between subunits B2 to B4 are diffuse, each of the subunits seems to be truncated on the southern margin. The slight chill of B4 against B5, and the slight hornfelsing of B5, would suggest that the granophyre was emplaced prior to subunit B4. The apparent cross-cutting relationships of B1, and the observed hybridisation of the B5 granophyre, would suggest that subunit B1 was the last subunit to be emplaced.

PLATE 2.1 Subunit B2 pegmatitic, granophyric ferrogabbro. The spotting is caused by hydrothermal alteration (From traverse six MR.3403, 3358).

PLATE 2.2 Felsitic back-vein brecciating darkened, hybridised granophyre. South of Round Knott (MR 3345. 3370).

CHAPTER THREE

THE PETROGRAPHY, MINERALOGY AND GEOCHEMISTRY OF UNIT A.

3.1. PETROGRAPHY OF UNIT A

The modal proportions of the primary mineral phases in Unit A are shown in table 3.1, from which it can be seen that plagioclase is the dominant phase throughout, and that in subunit A1, the proportion of opaque oxides and Ca-rich pyroxene, decreases from the margins towards the centre of the intrusion. This variation is also apparent in Plates 3.1, 3.2, and 3.3, which are ilmenite and biotite rich gabbro from the northern and southern margins, and a leucocratic plagioclase-rich gabbro from the centre of Unit A respectively. Plate 3.4 is a laminated, two-pyroxene, ilmenite gabbro from subunit A2.

Plagioclase forms euhedral laths, up to 5 mm. in length. Commonly the crystals have an unzoned core-region, mantled by strongly normally, and oscillatory, zoned overgrowths. Smaller, unzoned crystals, rarely exceeding 2 mm. in length, often occur enclosed in ophitic pyroxene. Their size corresponds roughly to that of the unzoned cores of the larger plagioclase crystals described above. The zoned overgrowths in subunit A3, contain small (< 0.2 mm.) inclusions of Ca-rich and Ca-poor pyroxene. The plagioclase in the pegmatitic segregations of the gabbro are larger, up to 7 mm. in length, and show very marked marginal zonation.

Pale-mauve calcium-rich clinopyroxene occurs as ophitic plates, up to 8 mm. in size. Twinning on (100) is common, and is occasionally repeated. (Pl. 3.5). 'Herringbone' cleavage, on (001), is also a common feature. Patchy, or complete, replacement by a pale-green variety of Ca-rich pyroxene, occurs

TABLE 3.1 :

		PL	Ca+ Px	Ca- Px	Fe-Ti Ox	Bi	Am	Qtz/ Ksp	
A1	20798	60	10		30				NORTH
	88	52	30		15	1	2		
	136	65	26		6	1	2		
	170	85	5		2			8	APPROX. CENTRE
	46	73	17		5			5	
	E16181	60	24		8	1	1	6	
	158	66	20		6			8	
	150	52	18		20	4	1	5	
	E17389	51	20		12	10	2	5	SOUTH
A2	E 16192	55	22		10	2		1	
	E23545	60	27		9	1		3	
	117	50	16	17	10	3	1	3	
A3	152	63	17	6	6	3	1	4	

MODES OF SAMPLES FROM UNIT A. (PRIMARY PHASES)

A1 FROM TOP TO BOTTOM IS A ROUGH TRAVERSE FROM NORTH TO SOUTH

Modes calculated by point counting method, 500-1000 points per thin section - CORRECTED TO Wt% MODES.

SOME MODES ARE APPROXIMATE ONLY BECAUSE OF ALTERATION EFFECTS.

throughout subunit A1. Small, secondary, biotite inclusions occur within the pale-green pyroxene. In rocks with abundant primary biotite, the pale-green pyroxene forms discrete grains, up to 2 mm. in length, in addition to its occurrence as a reaction product from the pale-mauve variety. These discrete grains show no biotite inclusions, and appear to be primary.

In subunits A2 and A3, the Ca-rich pyroxene forms smaller, pale-green, interstitial grains rather than ophitic plates, with a single (100) twin, and good (001) cleavage.

Calcium-poor pyroxene only occurs in subunits A2 and A3, hypersthene in A2, and both hypersthene and inverted-pigeonite in A3, although the hypersthene in the latter only occurs as inclusions in the plagioclase rims. The faintly pleochroic hypersthene in A2 is interstitial, and has very thin lamellae of Ca-rich pyroxene exsolved along (100) cleavage planes. The inverted-pigeonite in subunit A3, can occur in large grains up to 7 mm. in diameter. The exsolution history in a single grain, can be quite complex, and is well illustrated in plate 3.6. A central core region of hypersthene, which may be uninverted, grades outwards into a zone of inverted-pigeonite, (host hypersthene, with blebby exsolution of Ca-rich pyroxene). This is, in turn, mantled by further inverted-pigeonite, with host hypersthene containing thin oriented rods of Ca-rich pyroxene exsolved in herringbone fashion, prior to inversion to hypersthene, on (001) cleavage planes. No post-inversion exsolution of Ca-rich pyroxene, on (100) can be seen in thin section.

Both ilmenite and titanomagnetite occur in subunits A1 and A3, but the former is the much more abundant. In the melanocratic gabbros from the northern and southern margins,

the oxides form subhedral to rounded grains, up to 3 mm. in size, often in chains of up to seven or eight grains in length (Pl. 3.1). Towards the centre of the intrusion, the oxides are interstitial or subpoi kilitic towards plagioclase. (Pl. 3.3). In subunit A2 ilmenite is the only oxide phase, and occurs as rod-like crystals, parallel to the lamination.

The magnetite is invariably oxidised, leaving a trellis pattern of pre-oxidation exsolution lamellae of ilmenite, in a grey or brown, semi-opaque material.

Biotite occurs throughout Unit A in small amounts, as discrete interstitial flakes, or as reactions to opaque oxides. In specimens located near to xenolithic screens of Eycott lavas, and particularly along the southern margin, biotite is particularly abundant (Pl. 3.2), occasionally forming up to 10 modal %.

Green-straw yellow pleochroic amphibole, apatite and zircon form small, interstitial, accessory phases.

Quartz as discrete, irregular grains, and intergrown micrographically with alkali-felspar, occurs throughout the unit but is most abundant in the pegmatitic segregations and leucocratic gabbros, where it forms 'pools' between the plagioclase crystals. Much of the quartz, however, may be of secondary, hydrothermal origin.

The mineralogical banding that occurs locally throughout Unit A, reflects differences in interstitial pyroxene and opaque oxides. Some of the leucocratic bands are almost pure plagioclase.

The screens of xenolithic Eycott type lava are cut by thin, gabbroic veins. An example is shown in Plate 3.7. This vein is composed of small (< 2mm.) elongate, zoned plagioclase laths, subophitic Ca-rich pyroxene, sub-skeletal Fe-Ti oxides, mostly ilmenite, occasional small prisms of apatite, interstitial biotite, and quartz.

All of Unit A is affected, to some degree, by hydrothermal alteration. The alteration is irregular and often selective. Plagioclase is replaced by sericite, or occasionally chlorite. Pyroxene is pseudomorphed by either a pale-brown to ochre, or a blue-green fibrous amphibole, probably anthophyllite and actinolitic hornblende respectively. Chlorite also locally replaces pyroxene. Titanomagnetite is oxidised to sphene, haematite or leucoxene. Quartz and perthitic alkali-felspar, tend to increase in abundance in more altered samples. Associations of calcite, prehnite, epidote and secondary, subskeletal, apatite grow interstitially or form thin, cross cutting veins.

3.2. PETROGRAPHY OF THE EYCOTT VOLCANIC GROUP

Data from Eastwood et al. (1968), and Fitton (1971), summarising the petrography of the Eycott Volcanic Group lavas are given in table 3.2, and summarised below, for comparison with the gabbros.

Eastwood et al. (op cit) identified chlorite and serpentine pseudomorphs after olivine in the more basic lavas, although Fitton (op cit) found no evidence for the latter phase. In view of the percentage of quartz in the mesostasis of the lavas, it would seem unlikely that much, if any, olivine

TABLE 3.2 : SUMMARY OF EYCOTT LAVA PETROGRAPHY

	PHENOCRYST						GROUNDMASS					
LAVA TYPE	Ol	Pl	AUG	Hy	Pig	Mt/Il	Pl	Aug	Mt/Il	Qz/Ksp	Gl	Chl
		(1)	(1)	(1)	(1)	(2)		(3)				(4)
Olivine basalt(5)	x	x	x				x	x	x	x	x	x
Basalt							x	x	x	x	x	x
Basaltic andesite												
Eycott type (6)		x	x	x	x	x	x	x	x		x	x
Berrier type (7)		x	x	x		x	x	x	x	x	x	x
Aphyric							x	x	x	x	x	x

Data from Eastwood etal (1968), Fitton (1971).

Notes (1) often glomeroporphyritic
(2) only in lavas with >55 Wt% SiO_2
(3) often ophitic
(4) may be pseudomorphing Hy or Pig.
(5) no olivine. cf. Fitton (1971)
(6) macroporphyritic
(7) microporphyritic

KEY
Ol . olivine
Pl . plagioclase
Aug . augite
Hy . hypersthene
Pig . pigeonite
Mt/Il . magnetite or ilmenite
Qz/Ksp . quartz-alkali feldspar
Gl . glass
Chl . chlorite

crystallised in the lavas.

Plagioclase is the dominant phenocryst phase with large crystals, up to 3 cm. in size, showing oscillatory zoning. They often occur in glomeroporphyritic clots. Hypersthene and augite are very subordinate, and occur as small phenocrysts or glomeroporphyritic aggregates. Fe-Ti oxides, both ilmenite and titanomagnetite, occur as ground-mass phases in the more basic types, but are found as microphenocrysts in rocks with bulk-rock SiO_2 contents of greater than 55%.

There is an obvious similarity of the petrography of the Eycott lavas and the Unit A gabbros, particularly in the dominance of plagioclase, and subordinate nature of pyroxene and Fe-Ti oxide. Obviously features related to the slower cooling of the gabbros are not present in the lavas, such as the inversion of pigeonite, and the late magmatic and sub-solidus hydrothermal effects.

Despite the minor differences related to contrasting physio-chemical conditions of crystallisation in the gabbro magma chamber, and the extrusive lavas, the similarities support Fitton (1971), who suggests that the gabbros and Eycott lavas are genetically related.

Xenoliths and screens of Eycott lava are common in Unit A. The thermal metamorphic effect of the gabbros on the lavas is quite marked, with hornfelsing and re-crystallisation in the ground mass. Relict textures are occasionally preserved, noteably the porphyritic and glomeroporphyritic plagioclases and pyroxenes, also, flow banding is sometimes preserved. The relict porphyritic plagioclases, however, show clouding and

occasionally sieve texture. The groundmass becomes much coarser and granular, with recrystallisation of plagioclase, pyroxene and opaques, and development of biotite.

3.3. MINERAL CHEMISTRY

The chemistry of each group of primary phases is described briefly in this section, but discussion of conclusions drawn from this section, and the petrography, is deferred until section 3.4.

All the mineral analyses were obtained by electron-microprobe analsis. The analytical and correction procedures are given in Appendix Two , together with the tabulated mineralogical data.

3.3.1. Plagioclase :

Analyses of core compositions of plagioclases from Unit A are shown in figure 3.1, in terms of the end member components orthoclase-albite-anorthite. The marginal rocks of subunit A1 have plagioclase compositions of An_{74-73}. The unzoned core compositions in both A2 and A3 are An_{62-64}, while the compositions between An_{58-52} are from the cores of continuously zoned plagioclase crystals, or are compositions immediately adjacent to the unzoned core. The dashed line shows the extent of marginal zonation, which reaches An_{28} accompanied by slight potassium enrichment.

3.3.2. Pyroxenes :

The compositions of subunit A1 Ca-rich pyroxenes, plotted in terms of their principal end-member components, are shown in figure 3.2a, also shown is the compositional range of Eycott

Volcanic Group phenocryst augites from Fitton (1971). The pale-mauve pyroxenes are augitic and range in composition from $Wo_{40}En_{40}Fs_{19}$ to $Wo_{42}En_{26}Fs_{32}$, from the margin to the interior of the intrusion. Individual pale-mauve augites also show normal zonation. The coexisting pale-green pyroxenes are unzoned, and plot nearer the Di-Hd join into the salite field. As well as being enriched in Ca relative to the pale-mauve type, they are also relatively enriched in Si, and depleted in Al and Ti. Consistent tie-lines cannot be drawn between coexisting pyroxenes, suggesting varying degrees of equilibrium between the pale mauve and pale green varieties. There is a continuum of compositions in some specimens, from one type to the other.

There is considerable scatter in the minor element data as a result of the alteration, however, in general, both Al and Ti decrease with decreasing Mg/Mg+Fe, and Mn increases. Na is low and shows no systematic variation.

The variation in principal end-member components of the subunit A2 and A3 Ca-rich and Ca-poor pyroxenes, is shown in figure 3.2.b. The Ca-rich pyroxenes are pale-green augites and correspond to the mid to late stages of fractionation of subunit A1. They show virtually no zonation.

The Ca-poor pyroxenes are hypersthene in subunit A2, hypersthene in the inclusions in the plagioclase crystals, and interstitial inverted pigeonites in subunit A3. The Wo contents are very low compared to the Skaergaard trend and the hypersthene-inverted pigeonite transition, expressed Wo-free, occurs at En_{50}, compared to En_{70} in the Skaergaard intrusion. The minor element chemistry of the Ca-poor pyroxenes shows

only slight variation with fractionation. The distribution of minor elements between Ca-rich and Ca-poor pyroxenes follows similar patterns to other intrusions, with Ti, Al and Na preferentially partitioned into the Ca rich phase, and Mn into the Ca-poor phase.

3.3.3. Fe-Ti oxides :

No satisfactory analyses could be obtained from the titanomagnetites, due to their oxidised and resorbed nature. Ilmenites are homogeneous, even in altered rocks. The Fe_2O_3 in the analysis has been re-calculated by the method of Carmichael (1967). The haematite content of most of the ilmenites lies between 2.0 and 0.5%, indicating that the ilmenites are virtually pure. The ilmenites of subunit A2, which has the least altered samples, have haematite contents of 5.2%, and probably reflect magmatic values. Calculations of fO_2 and temperature, however, cannot be made, as no titanomagnetites exist in subunit A2. The $ilmenite_{95}$ - $haematite_5$ composition, in fO_2-temperature space (Eugster and Wones, 1962; Buddington and Lindsley, 1964) lies near the Ni-NiO buffer assemblage in the likely temperature range of these rocks.

3.3.4. Biotites :

The chemistry of the biotites, in terms of the four end-members phlogopite-eastonite-siderophyllite-annite, is shown in figure 3.3. The analyses cluster near the annite-phlogopite join, within the 'biotite' field. Some of the biotites show limited $Mg \rightleftharpoons Fe^{2+}$ zonation (ie 17389). Also plotted in figure 3.3., are analyses of other igneous biotites

from the Ardnamurchan cone sheets (Walsh, 1975) and the Palisades sill. (Walker et al, 1973). The Unit A biotites are fairly similar to those from the Ardnamurchan gabbros, but have a slightly increased siderophyllite component. They also compare favourably with biotites from the middle ranges of fractionation of the Palisades sill.

3.3.5. Amphiboles :

Amphibole is not a common primary phase in Unit A. Using the recalculation and classification of Leake (1978), most of the amphiboles from Unit A are magnesio-hornblendes. (the calculation of Fe^{3+} and the classification of amphiboles is discussed more fully in chapter 4).

The compositions of the amphiboles, in terms of Ca-Mg-Fe, are plotted in figure 3.4, with all Fe as FeO, together with co-existing pyroxene analyses. Although there is a general decrease in Mg/Mg+Fe with fractionation in the amphiboles, the tie line orientations show that the variation is irregular, suggesting that the amphiboles are a product of later stage reactions, rather than fractional crystallisation.

3.4. CRYSTALLISATION AND MINERAL STABILITY IN UNIT A.

Plagioclase and pyroxene crystallised cotectically during the early cooling history of the Unit A magma. Figure 3.5, shows the core compositions of coexisting plagioclases and Ca-rich pyroxenes, in terms of An% and Mg/Mg+Fe respectively. There is a systematic decrease in the An content and Mg number, in the respective phases, with fractionation. The trend is parallel to the earlier parts of the trends from the Skaergaard

intrusion (Wager and Brown, 1968) and the Palisades sill (Walker et al, 1973). In contrast to these intrusions, however, ilmenite is an important early crystallising phase in Unit A, as indicated by its abundance and textural relations. The crystallisation of ilmenite and plagioclase is favoured by high $aSiO_2$ (Carmichael et al, 1974), according to the reaction :

$$2FeTiO_3 + 2CaAl_2Si_2O_8 \rightleftharpoons 2CaTiAl_2O_6 + Fe_2SiO_4 + 3SiO_2$$

ilmenite in plagioclase in pyroxene in olivine

High $aSiO_2$ drives the reaction to the left. This is supported by the lack of olivine, and also, the generally limited substitution of Ti and Al in pyroxene in this Unit.

The limited crystallisation of magnetite suggests that the fO_2 during crystallisation was fairly low. This conclusion is supported by the limited solution of haematite in the ilmenites of Unit A. Substantial Fe-enrichment in the magma, however, was prevented by the continued crystallisation of ilmenite.

The pyroxene crystallisation in Unit A is typical of tholeiitic rocks, in that Ca-poor pyroxene crystallised in addition to Ca-rich pyroxenes. There are, however, certain differences between the pyroxene trends in this Unit, and, say the Skaergaard trend. Figure 3.2 shows the Ca-rich pyroxenes to be enriched in the Wo component, relative to the Skaergaard trend. Similarly, the Ca-poor pyroxenes in subunits A2 and A3, are Wo-poor, with respect to the Skaergaard trend. The hypersthene-pigeonite transition, expressed Wo free, occurs at En_{72} in the Skaergaard (Nwe, 1976), and in most slowly cooled plutons occurs between En_{72} and En_{65} (Campbell and Nolan, 1974). The Palisades, however, has a more Fe-rich transition, at En_{60} (Walker et al, 1973).

In subunit A3, the transition occurs at En_{50}. It is clear from the blebby nature of the exsolution in the inverted-pigeonites of subunit A3, that the inversion curve from monoclinic to orthorhombic symmetry, was fairly near the solidus curve. If it is assumed that the structural inversion curve (Brown, 1957) remains constant with respect to temperature and composition, then the liquidus-solidus curves must be suppressed to a lower temperature in the Palisades sill and Unit A, than for other intrusions, thus, expanding the compositional range of the orthopyroxene stability field and causing the transition to pigeonite to occur at a lower temperature.

While the higher and lower Wo contents for the Ca-rich and Ca-poor pyroxenes respectively, in Unit A compared to Skaergaard, are, to a certain extent, a feature of late stage re-equilibration (see below), the low En value at which the hypersthene-pigeonite transition occurs, suggests that liquidus temperatures were lower in Unit A than in other intrusions.

As noted above, the hypershene-pigeonite transition in the Palisades Sill occurs at En_{60}, which is lower than in most tholeiitic intrusions. The Palisades Sill also shows the effects of reactions in the late-magmatic stage, to a greater extent than other major tholeiitic intrustions (Walker et al, 1973), with stabilisation of pale-green Ca-rich pyroxene, biotite and amphibole. It is perhaps significant, therefore, that Unit A shows an even more Fe-rich hypersthene-pigeonite transition, as the effects of late-magmatic reaction are very well developed in this Unit.

Petrographic and chemical evidence suggests that the pale-green augites and salites in Unit A, have formed by reaction from the pale-mauve augites. A similar relationship has been proposed, for coexisting pale-mauve and pale-green ferroaugites and ferrosalites respectively, from the Palisades Sill (Walker et al, 1973) and the Dufek intrusion (Himmelberg and Ford, 1976). During the reaction process, Al and Ti are lost from the pyroxene, and, presumably, taken up into the small amount of biotite that forms in the pale-green pyroxene. In was noted above that rocks in which biotite is modally abundant, the pale-green pyroxene formed discrete grains and appeared to be primary. The biotite in these rocks forms a discrete phase which often shows Mg $\rightleftharpoons$ Fe zonation, and, thus, is also likely to be primary. This suggests that temperatures were low enough in the late magma, for pale-green Ca-rich pyroxene to crystallise in equilibrium with biotite. The biotite also forms reaction rims to ilmenite, showing that ilmenite was no longer a stable phase in the late stage magma.

An equation may be written that relates the reaction of ilmenite and pale-mauve pyroxene, with late stage magma, to the production of pale-green pyroxene and biotite. The equation shows the relationships of components within phases, and expressed Mg and Fe free is :

$$4TiO_2 + 2CaTiAl_2O_6 + 14SiO_2 + 4H_2O + 2K_2O \rightleftharpoons$$

IN ILMENITE IN PYROXENE IN MELT

$$Ca_2Si_2O_6 + 2K_2 Ti_3 [Si_6Al_2O_{20}] (OH)_4$$

IN PYROXENE IN BIOTITE

The biotite is most abundant along the southern margin, and adjacent to xenoliths. This suggests that there may have been selective leaching of K_2O and dehydration of the country rocks and xenoliths, although no chemical data are available to support this argument.

The amphibole shows irregular variations which are consistent with it forming as a reaction product, rather than by fractional crystallisation.

The petrographic and mineral chemical observations, indicate that late-stage reactions were a prominent feature of the crystallisation in the Unit A magma, but also, that magma conditions were such that the reaction products subsequently became stable primary phases. This lends support to the contention that liquidus temperatures were low, compared to other slowly cooled intrusions, the conclusion drawn from the Fe-rich hypersthene-pigeonite transition.

The lower liquidus temperatures, and stabilisation of biotite and amphibole, presumably results from the increased volatiles, principally water, in the magma. At the margins of the intrusion and in the vicinity of xenoliths, the increased volatiles may be a function of dehydration of wall rock or xenolith. The late stage reactions are, however, not restricted to these rocks, as rocks from the centre of the intrusion also show these effects. A feature of all the rocks is the strong zonation of plagioclase and, occasionally, the pale-mauve Ca-rich pyroxenes. Strong zonation reflects either fairly rapid crystallisation, or growth from liquid trapped between rapidly accumulating crystals, and, hence, isolated from the

over lying magma. (Orthocumulus growth of Wager et al, 1960). The latter mode is considered more likely in Unit A, as no obvious evidence exists for rapid crystallisation.

The observed reaction effects in rocks away from the margins or xenoliths, are interpreted as resulting from 'closed system' volatile fractionation, within the trapped liquid. Initially, pale-mauve pyroxene crystallised from the trapped liquid between the plagioclase crystals, but continued to react with the liquid, which became progressively enriched in volatiles, with fractionation in the trapped liquid.

Plagioclase shows no signs of reaction. This, and the observed reactions in the mafic and oxide phases, is consistent with the continuous and discontinuous reaction series respectively, of Bowen (1928) and Osborne (1978).

The rocks from Unit A, it was noted earlier, show evidence of hydrothermal alteration, which was presumed to be sub-solidus. It is unlikely, however, that any real distinction exists between very late magmatic (deuteric) alteration, and early sub-solidus, hydrothermal alteration. The latter is, thus, a continuation of processes occurring in the earlier, magmatic stages. The upper stability limit of prehnite is approximately 400°C (Liou 1971), which indicates that hydrothermal reactions had been operative down to, at least, this temperature.

3.5. THE GEOCHEMISTRY OF THE UNIT A GABBROS

The X-Ray fluorescence analysis and data reduction procedures are described in Appendix Three, together with the tabulated major and trace element analyses and calculated CIPW norms.

The variation of major and trace elements in the gabbros is shown in figure 3.6 a and b, plotted against MgO. The MgO content reflects the composition and modal abundance of pyroxene in the gabbros and is, therefore, a good indicator of fractionation within the intrusion, as pyroxene becomes more Fe enriched and less modally abundant towards the centre of the intrusion. Also shown in figure 3.6, is the compositional range of the aphyric lavas, and the complete range of porphyritic and non-porphyritic basic lavas from the Eycott Volcanic Group, from Fitton (1971). Figure 3.7 shows the analysed gabbros plotted on an AFM diagram, together with the compositional range of the aphyric lavas and porphyritic lava groundmass compositions. From both figures 3.6 and 3.7, it will be seen that there is good general agreement between the compositions of the gabbros and lavas, supporting a possible cogenetic origin, with the gabbros representing crystal accumulations of plagioclase, pyroxene and ilmenite from the fractional crystallisation of the Eycott Volcanic Group lavas.

Fitton (op cit) noted that opaque oxides became a phenocryst phase at approximately 55 Wt% SiO_2. In the gabbro intrusion ilmenite is an early crystallising phase, suggesting that the gabbros crystallised from a basaltic andesite composition. The phenocryst compositions in the porphyritic lavas are similar to the compositions of the gabbroic phases, providing further supporting evidence for their cogenetic origin.

The fact that subunits A2 and A3 contain Ca-poor pyroxene, suggests that the composition of the lava parental to these subunits, was slightly different (more Mg+Fe rich) than the parental lava of subunit A 1.

The negative correlation of incompatible trace elements (Ba, Rb, Y, Nb and Zr) with MgO content, supports a model of in situ differentiation after emplacement of a single batch of magma, to produce subunit A1, with slightly later intrusion of batches of magma of slightly differing composition, to form subunits A2 and A3.

No conclusions have been drawn for the physical mechanisms of differentiation in Unit A.

FIGURE 3.1.

Analysed plagioclase core compositions from Unit A gabbros, plotted in part of the ternary felspar diagram (Orthoclase-Albite-Anorthite).

■ Subunit A1

▼ Subunit A2

▲ Subunit A3

Dashed line shows the extent of zonation within the plagioclase margins.

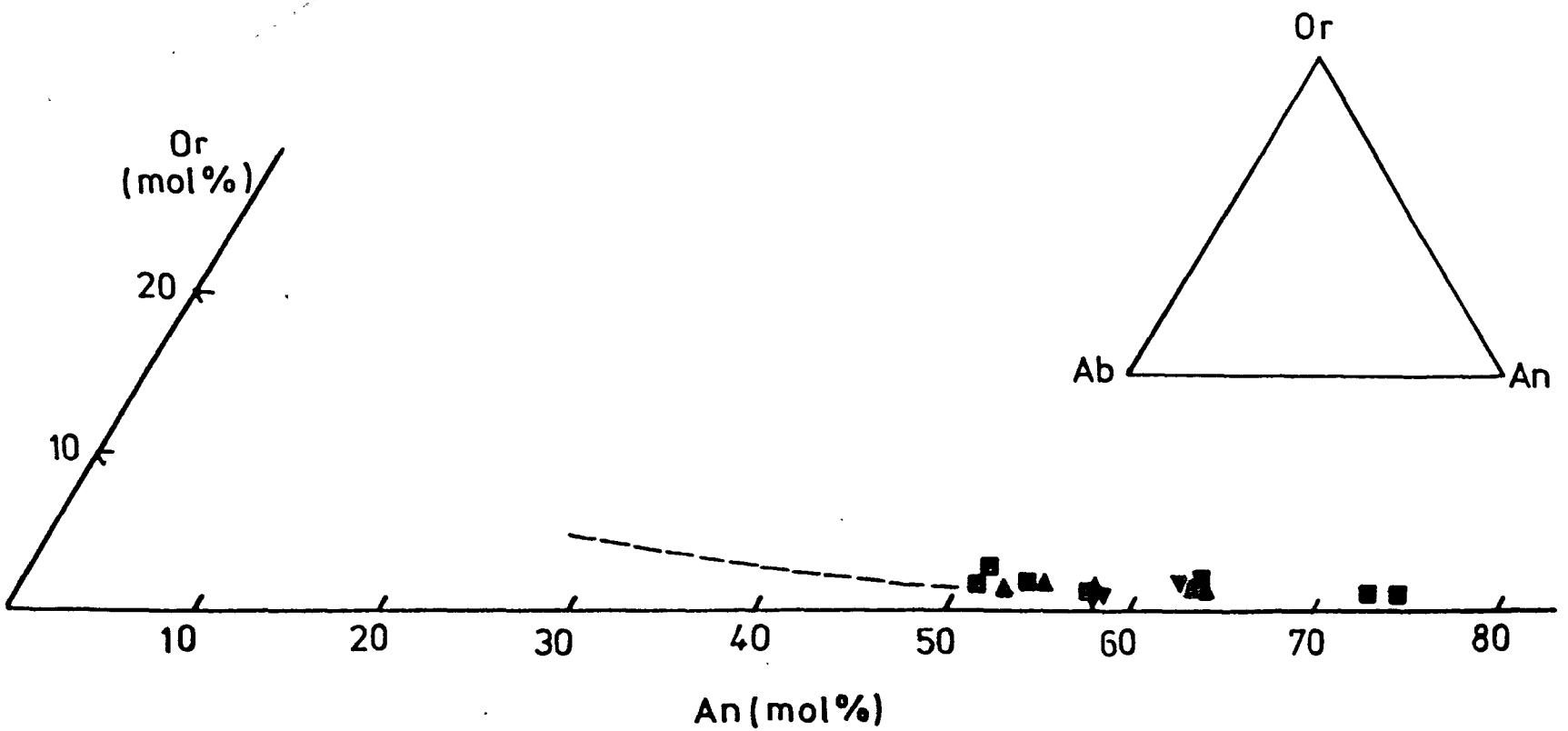
Or
(mol%)
20
10
Or
Ab
An
10
20
30
40
50
60
70
80
An (mol%)

FIGURE 3.2.

Analysed pyroxene analyses from Unit A gabbros, plotted in the pyroxene quadrilateral (Diopside-Hedenbergite-Ferrosilite-Enstatite).

A) ■ Pale-mauve Ca-rich pyroxenes, subunit A1.

□ Pale-green Ca-rich pyroxenes, subunit A1.

B) ▼ Subunit A2.

▲ Subunit A3.

Tie lines join coexisting Ca-rich and Ca-poor pyroxenes. Dashed line(S) is Skaergaard trend from Brown (1957), and Brown and Vincent (1963).
Compositional range of augite phenocrysts from Eycott Volcanic Group lavas is shown by dash-dot line on figure A. (From Fitton, 1971).

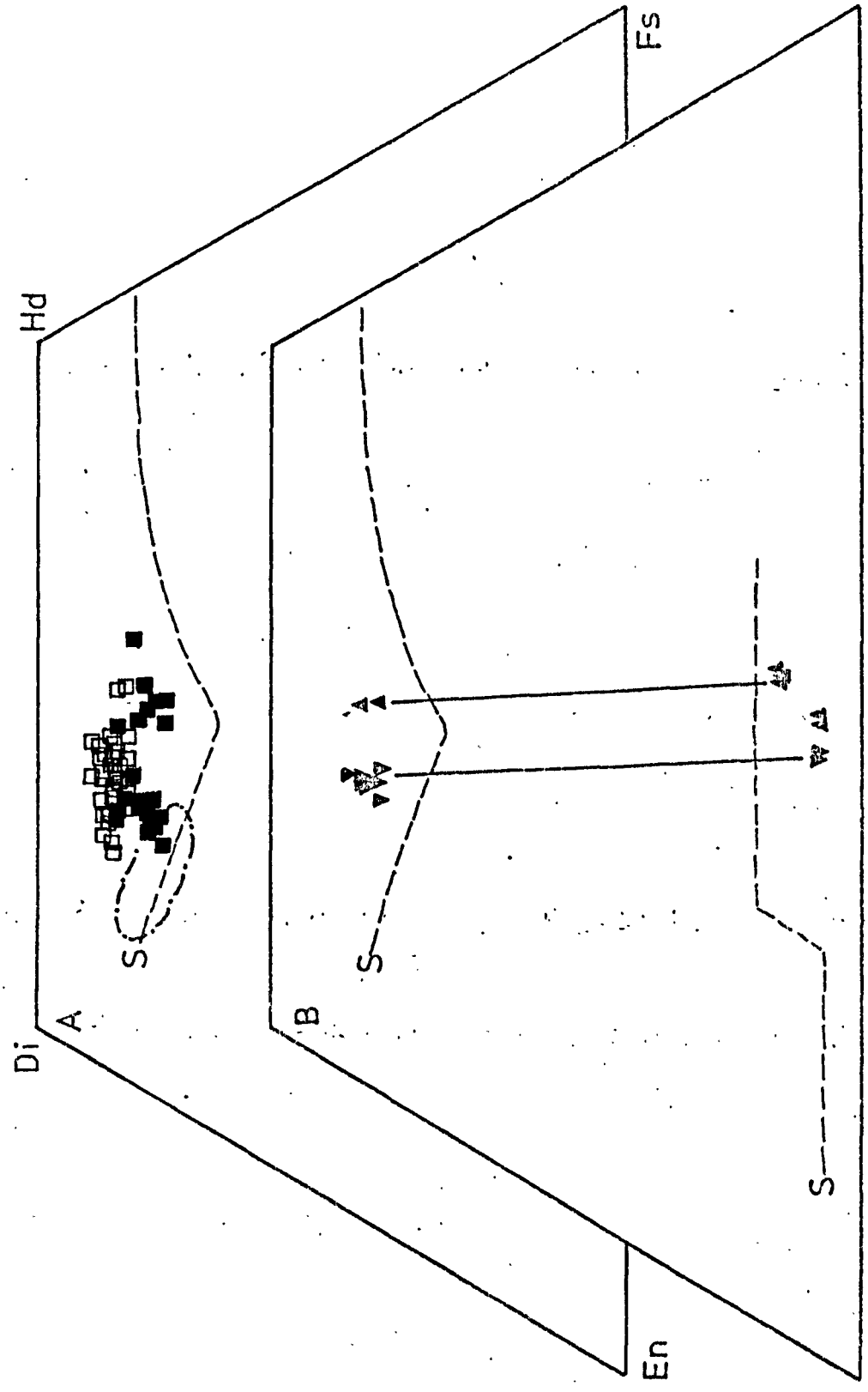
Hd
Fs
Di
En
A
B
S
S

FIGURE 3.3

Biotite analyses plotted in terms of At% Fe and Al, on basis of 22 oxygens.

Ann = Annite. $K_2Fe_6[Si_6Al_2O_{20}](OH)_4$

Si = Siderophyllite. $K_2Fe_5Al[Si_5Al_3O_{20}](OH)_4$

Ea = Eastonite. $K_2Mg_5Al[Si_5Al_3O_{20}](OH)_4$

Ph = Phlogopite. $K_2Mg_6[Si_6Al_2O_{20}](OH)_4$

■ Unit A

o Ardnamurchan cone sheets (Walsh, 1975)

● Palisades Sill (Walker et al, 1973)

FIGURE 3.4

Analysed amphiboles from Unit A gabbros plotted in part of ternary system Ca-Fe-Mg, together with coexisting Ca-rich pyroxenes (upper symbols) and tie lines. Symbols as in figure 3.1.

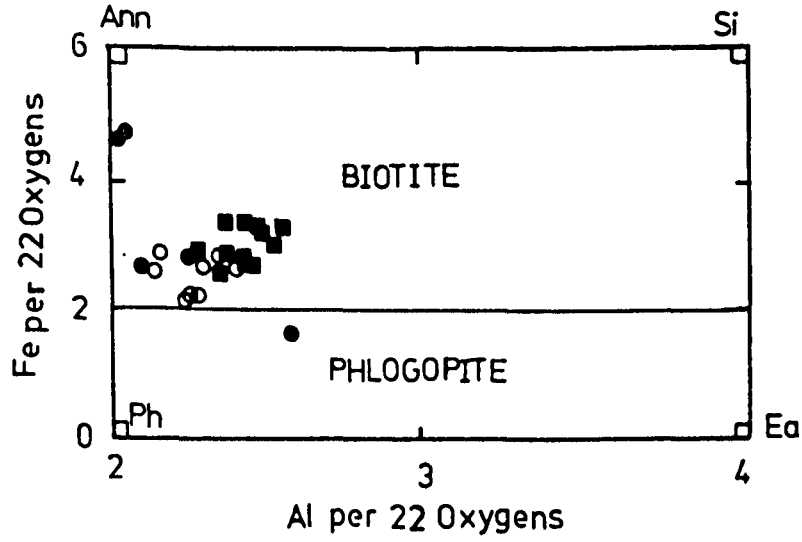
Ann
Si
6
4
2
0
BIOTITE
PHLOGOPITE
Ph
Ea
2
3
4
Fe per 22 Oxygens
Al per 22 Oxygens

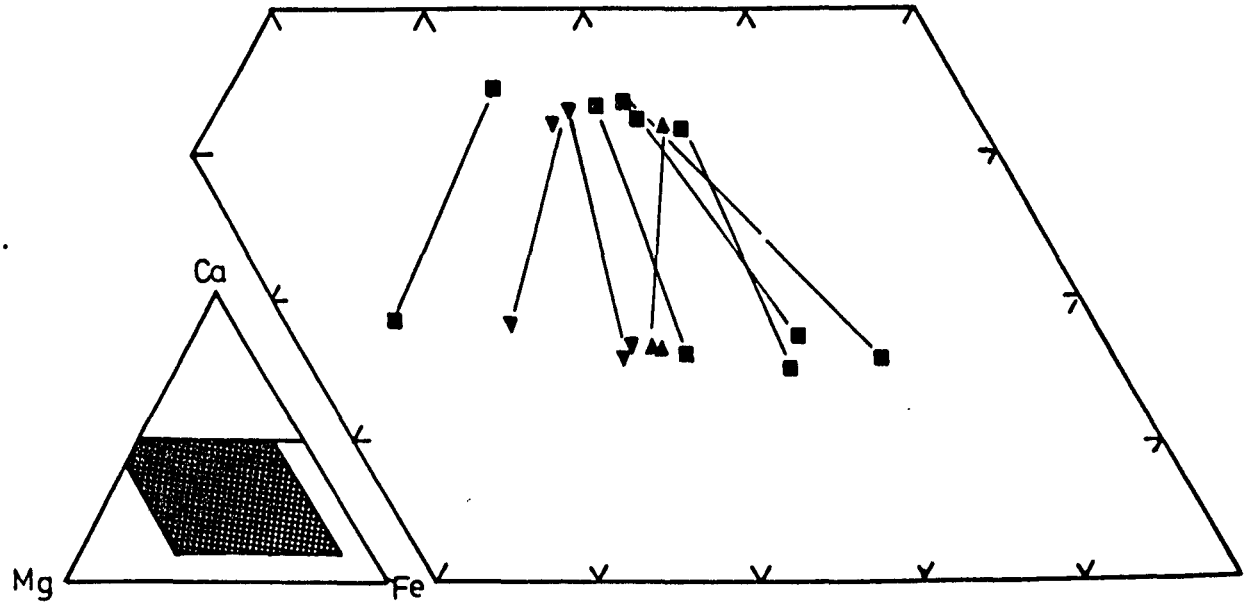
Ca
Mg
Fe

FIGURE 3.5.

Plagioclase-Ca rich pyroxene relationships in the Unit A gabbros. Symbols as in figure 3.1.
Pal.Palisades sill trend (Walker et al., 1973)
Sk. Skaergaard trend (Wager and Brown, 1968)

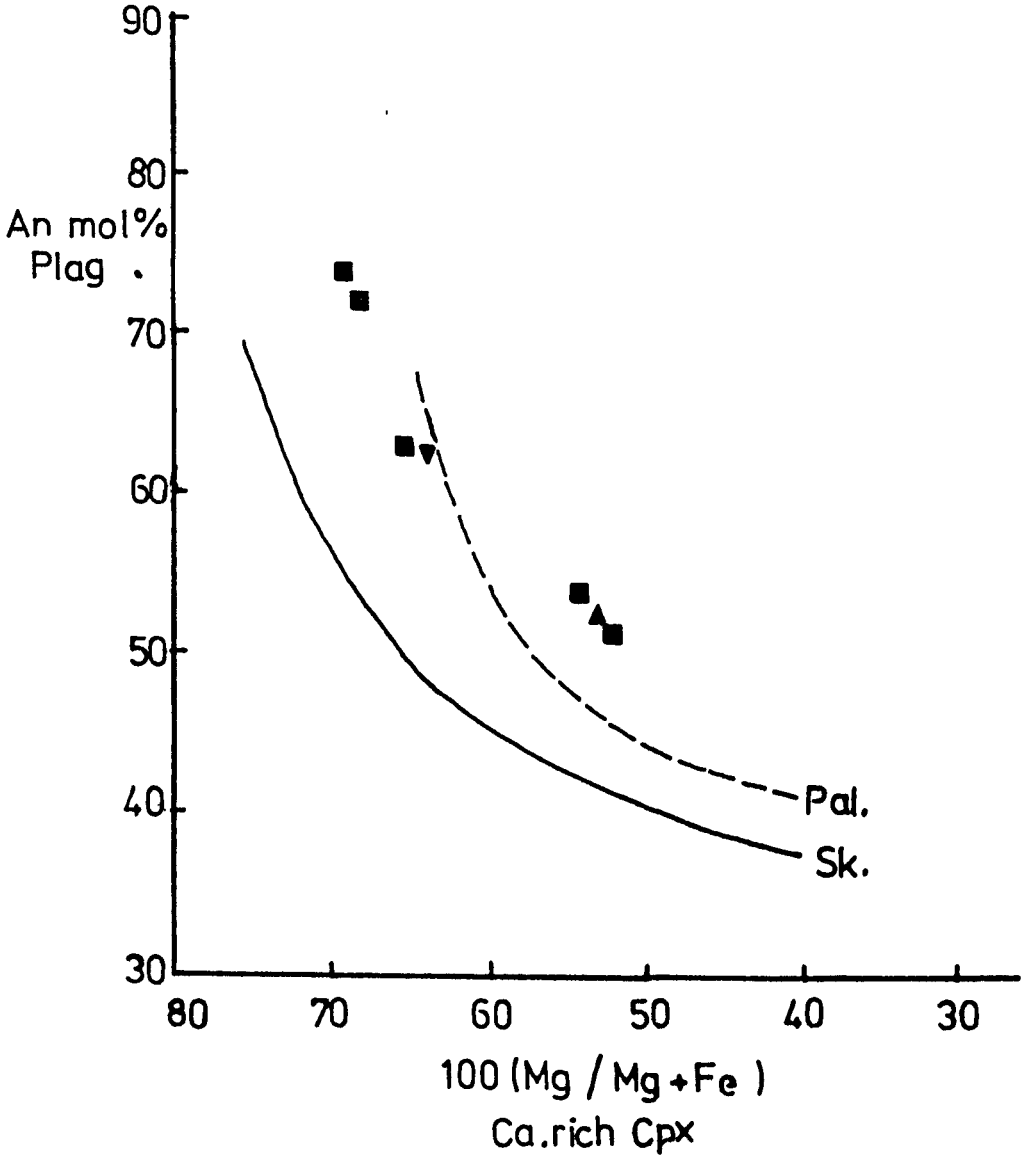
90
80
An mol%
Plag
70
60
50
40
30
80
70
60
50
40
30
Pal.
Sk.
100 (Mg / Mg + Fe)
Ca.rich Cpx

FIGURE 3.6.

a. Major element (Wt%) variation of Unit A gabbros, plotted against MgO (Wt%) content.

b. Trace element (ppm) variation of Unit A gabbros plotted against MgO (Wt%) content.

Symbols as in figure 6.1.

Compositional limits of basic aphyric lavas from the Eycott Volcanic Group are shown by a dashed line, that of the complete range of basic, porphyritic and non-porphyritic lavas is shown by a dash-dot line. Data from Fitton (1971).

3.6a

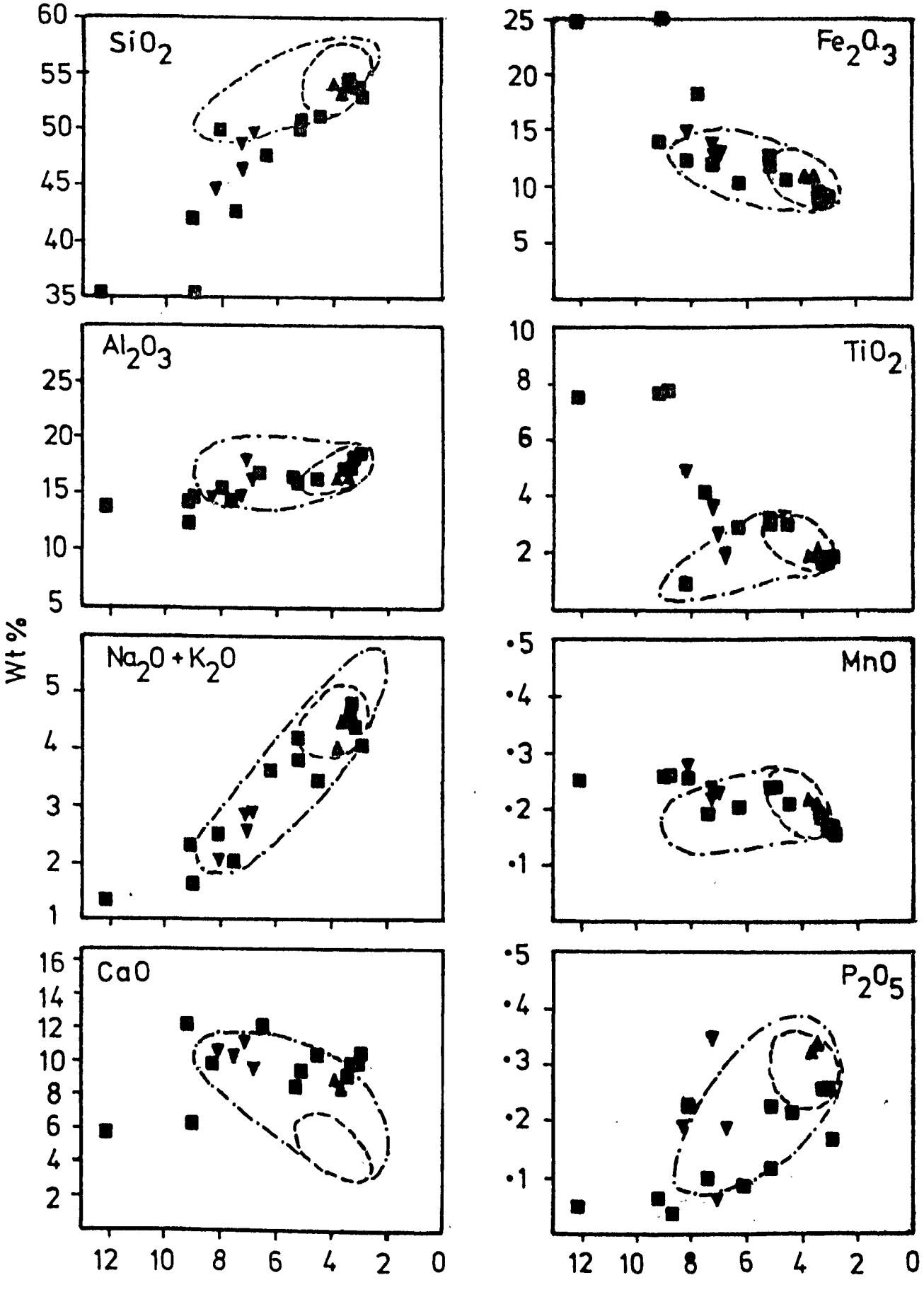

3.6b

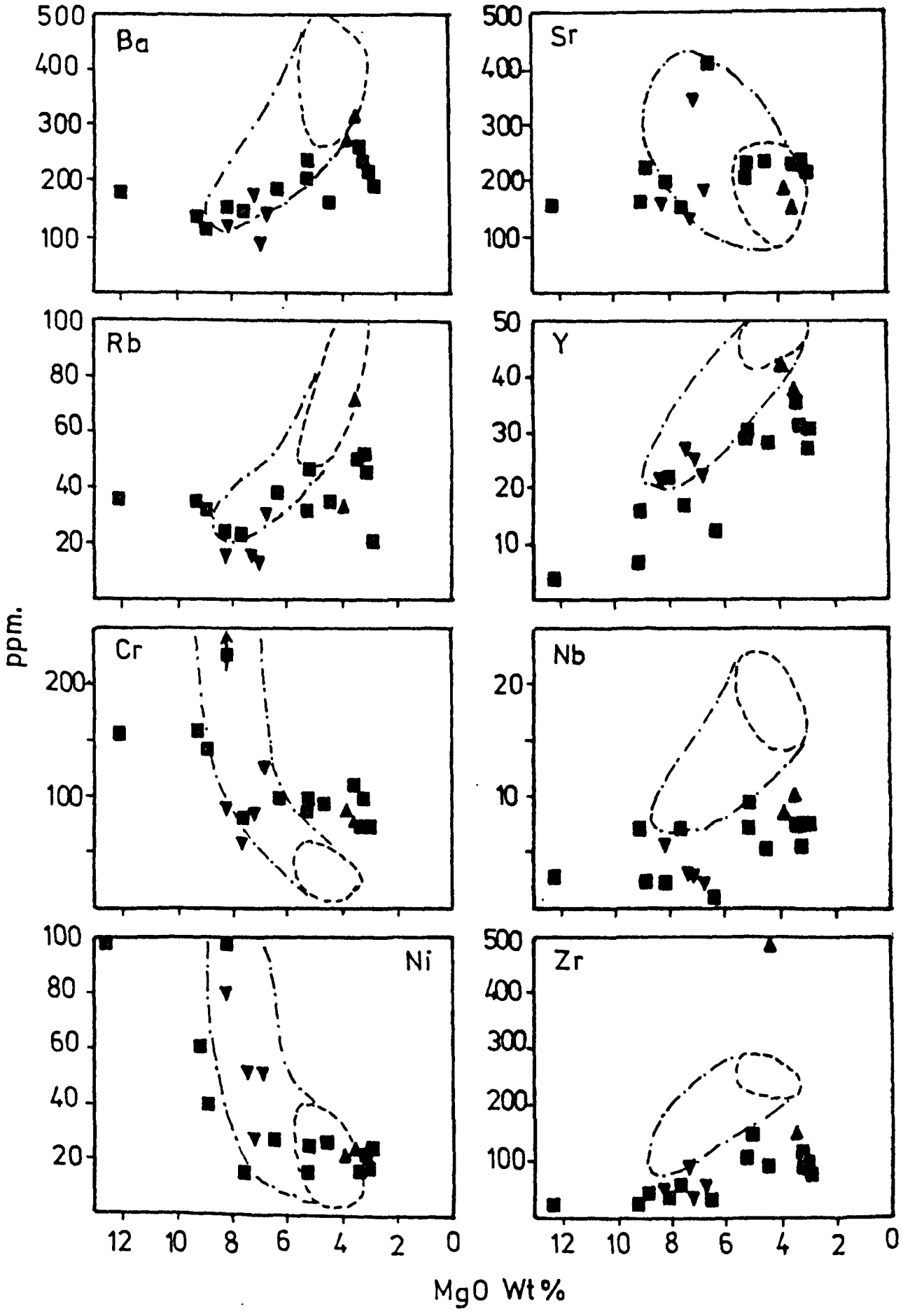
Ba
Sr
Rb
Y
Cr
Nb
Ni
Zr
ppm.
MgO Wt%
500
400
300
200
100
100
80
60
40
20
50
40
30
20
10
200
100
20
10
12
10
8
6
4
2
0

FIGURE 3.7.

A.F.M. plot of analysed gabbros from Unit A, together with the compositional range of basic aphyric lavas, and porphyritic lava groundmass compositions from the Eycott Volcanic Group (Fitton, 1971)
Symbols as in figure 6.1.

A = $Na_2O + K_2O$; F = Total iron as Fe_2O_3; M = MgO.

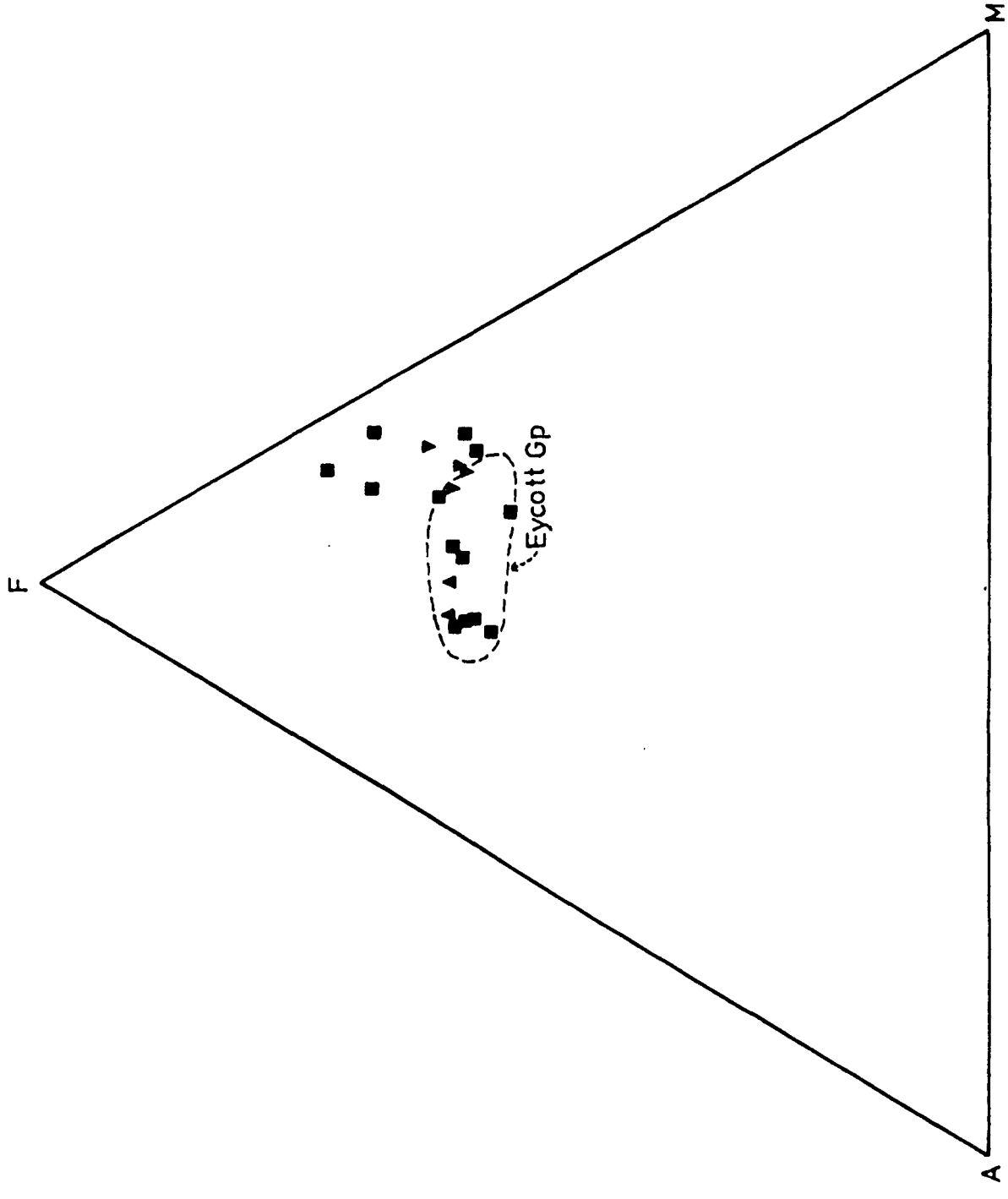
F
M
A
Eycott Gp

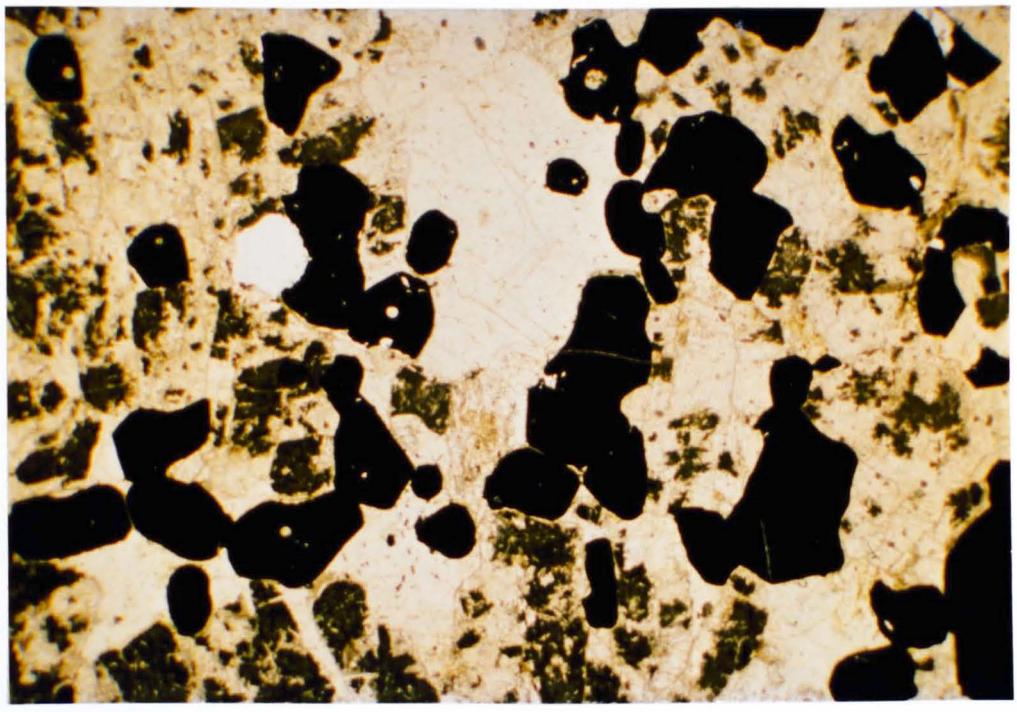

PLATE 3.1 Photomicrograph : Plagioclase-ilmenite gabbro from the northern margin of subunit A1. Note the chain-like growths of the opaque phase.
(20798. PP. Width of field - 8 mm).

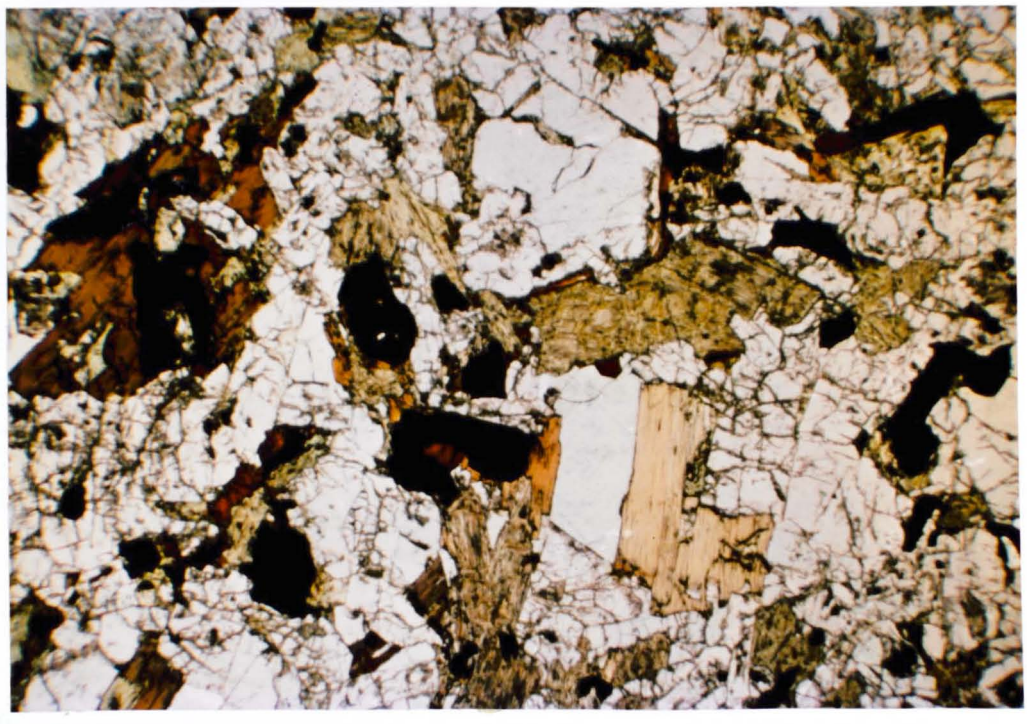

PLATE 3.2 Photomicrograph : Plagioclase-ilmenite-biotite-pyroxene gabbro from the southern margin of subunit A1. The pyroxene is pseudomorphed, in part, by secondary amphibole.
(17389. PP. Width of field - 8 mm).

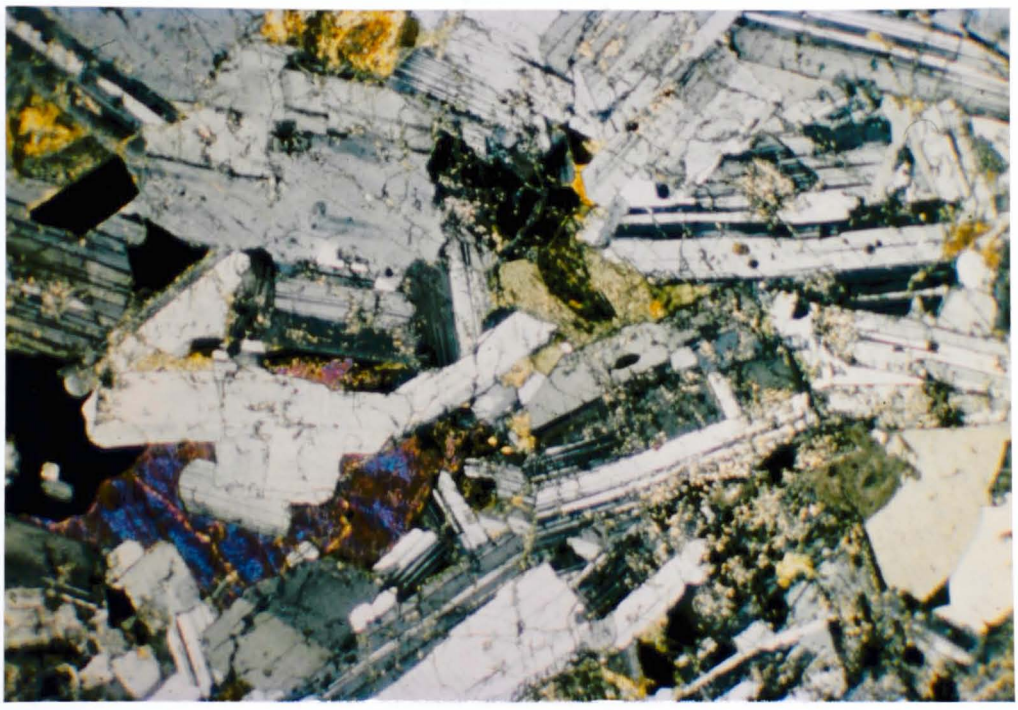

PLATE 3.3 Photomicrograph : Plagioclase gabbro from subunit A1, with interstitial pyroxene, ilmenite and quartz. The gabbro shows a faint lamination. (46. XP. Width of field - 8 mm).

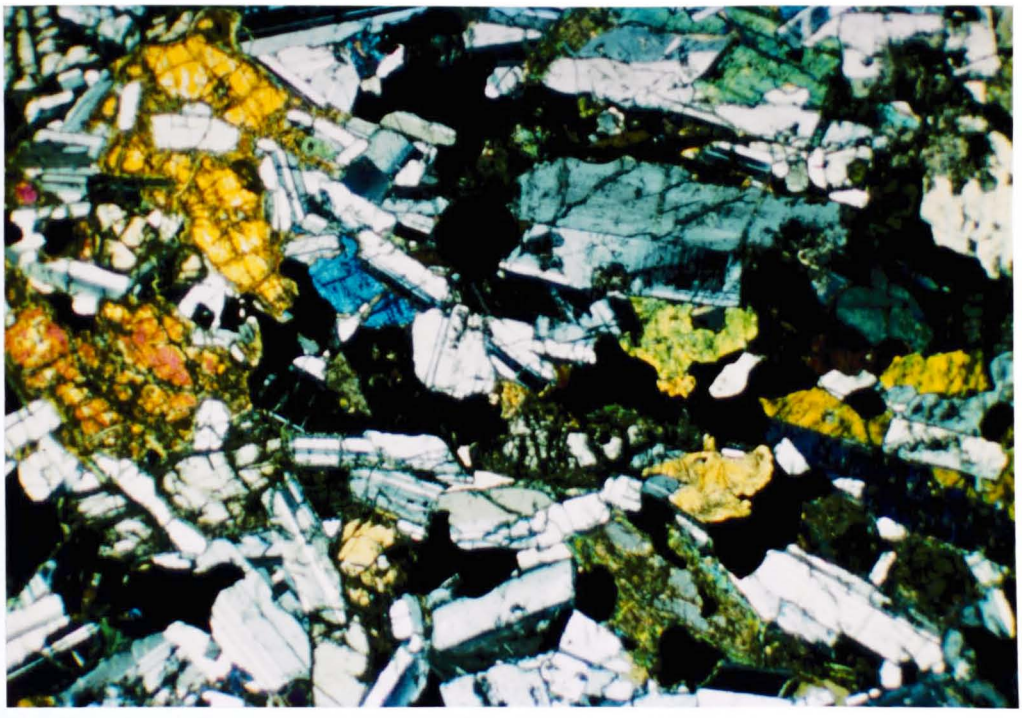

PLATE 3.4 Photomicrograph : Laminated plagioclase-ilmenite - hypersthene - augite gabbro. The hypersthene and augite are forming the interstitial grains in the upper left and the centre right respectively. (117. XP. Width of field - 8 mm).

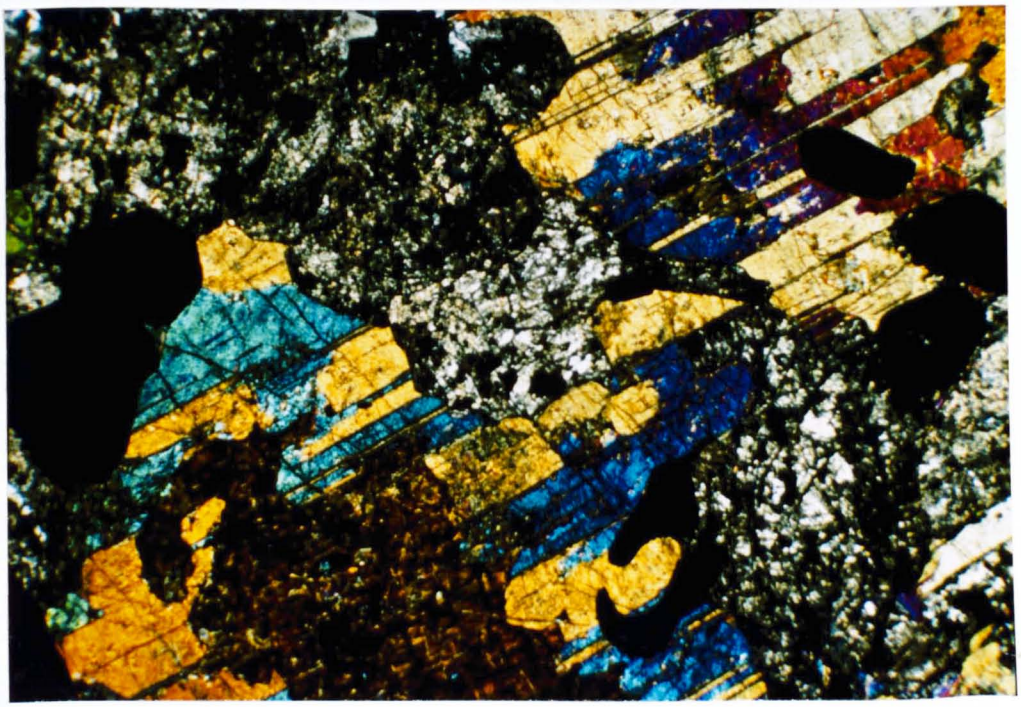

PLATE 3.5 Photomicrograph : Partially pseudomorphed ophitic augite, in subunit A1 plagioclase - ilmenite - pyroxene gabbro. The pyroxene shows repeated twinning on (100). (88. XP. Width of field - 8 mm).

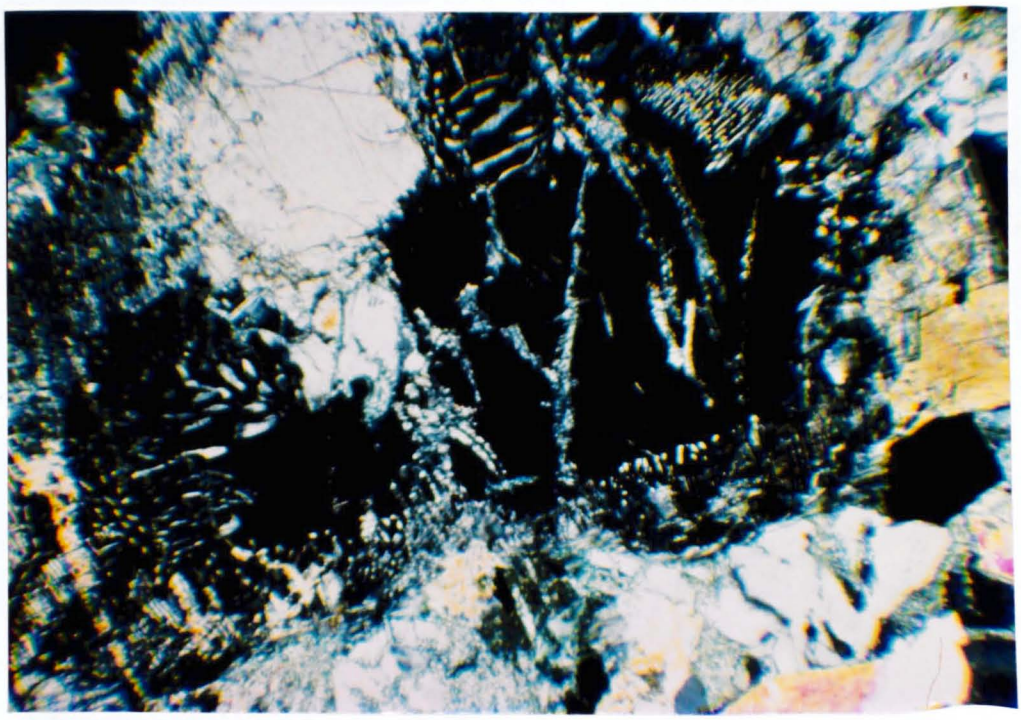

PLATE 3.6 Photomicrograph : Inverted pigeonite, showing hypersthene core, mantled by zones showing blebby and oriented pre-inversion exsolution of augite (152, XP. width of field - 3 mm).

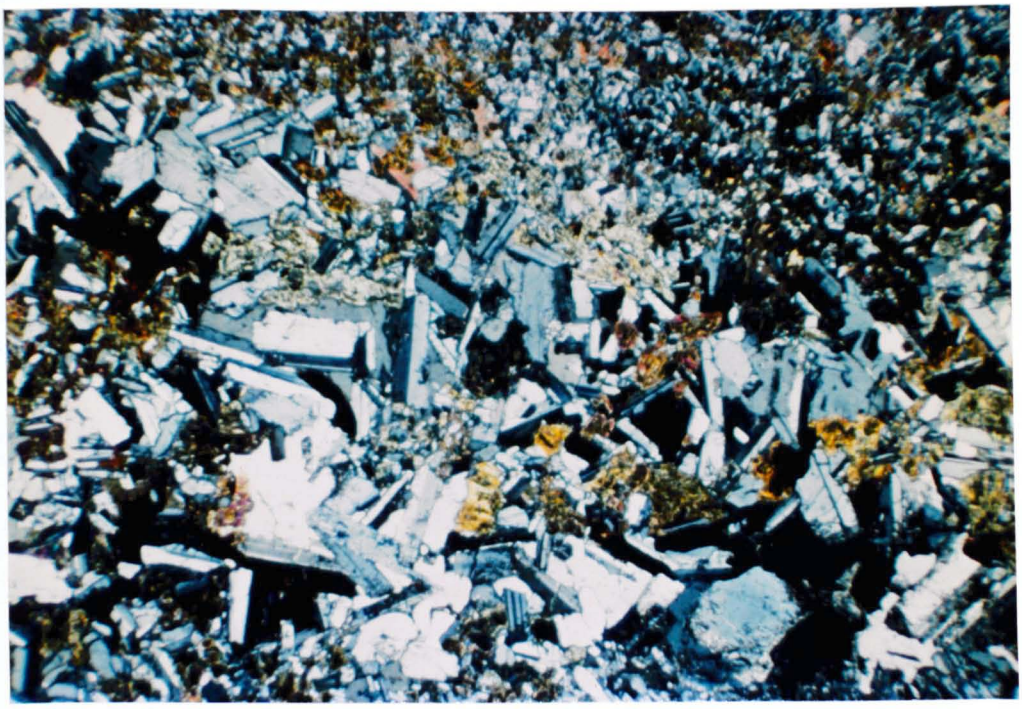

PLATE 3.7 Photomicrograph : Thin plagioclase-rich vein cross cutting hornfelsed xenolith of lava. Interstitial ilmenite, augite, biotite and quartz are present. (5. XP. Width of field - 5 mm).

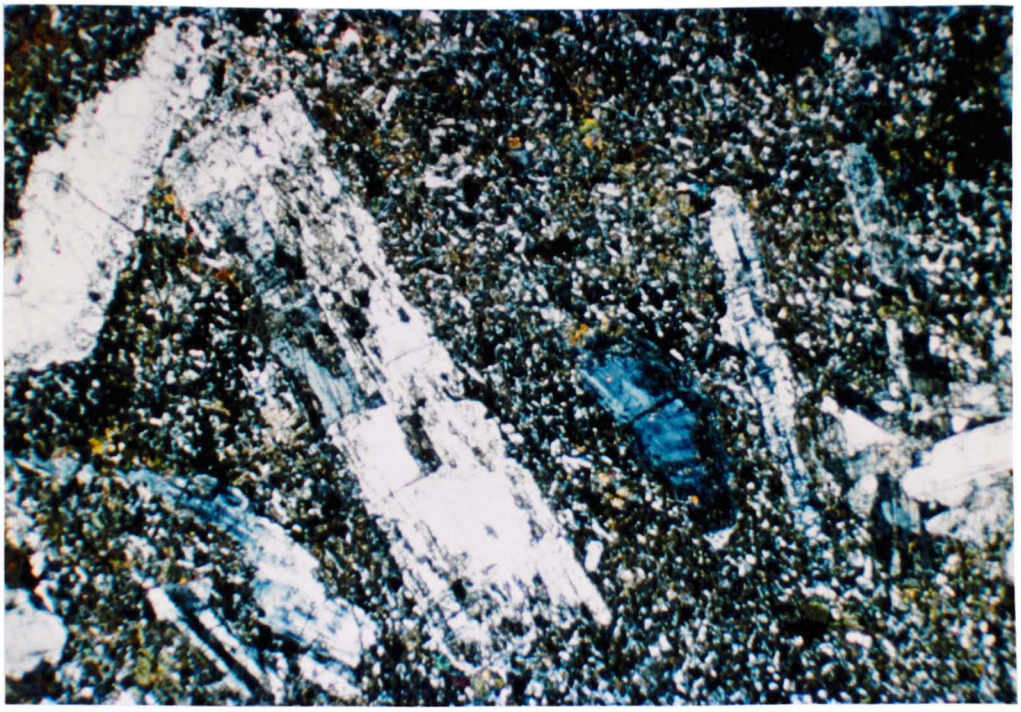

PLATE 3.8 Photomicrograph : Hornfelsed xenolith of plagioclase-Porphyritic Eycott lava. The ground mass is recrystallised and contains biotite. The relict phenocrysts show marginal sieve texture.
(165. XP. Width of field - 8 mm).

CHAPTER FOUR

THE PETROGRAPHY AND MINERALOGY OF UNIT B

4.1 PETROGRAPHY

The primary mineralogy of Unit B is fairly simple. Calcium-rich clinopyroxene, plagioclase and Fe-Ti oxides, both ilmenite and titanomagnetite, are the major phases throughout the fractionation sequence. Other phases occur only in certain subunits, or throughout in small amounts but become relatively abundant in a particular subunit. They are apatite in B2, amphibole in B3, and zircon in B4. Some phases occur only rarely or in trace amounts, they include epidote, allanite, pyrrhotite and pyrite. Quartz and alkali felspar occur throughout as micrographic intergrowths, but their coarseness and abundance vary greatly, the significance of which is discussed in later sections.

No olivine exists. The occurrence of calcium-poor pyroxene is restricted to exsolution lamellae in calcium-rich pyroxene.

Textural relationships vary considerably throughout the unit, and it is not easy to define the typical occurrence and form of any particular phase. Nor is it instructive to present typical modes, as the proportions of major phases vary considerably within each subunit.

The 'typical' occurrence and form of the major phases throughout the fractionation sequence is described for each phase, and the effects of alteration summarised in the following section. The most important textural variations

are then described and discussed in separate sections. Modal variations, and the significance of petrographic observations to the petrogenesis of Unit B, are deferred until Chapter Six, after the section describing the mineral chemistry. Modes when quoted in the following text are weight per-cent modes. Plates 4.1 to 4.6 show photomicrographs of rocks from subunits B2 to B5.

4.1.1. Plagioclase.

Plagioclase is present in all the subunits of Unit B. It occurs in roughly equal proportions with pyroxene in subunits B1 and B2, however, it becomes the dominant phase in subunit B3, and reaches up to 65 modal % in the ferrogranophyres of B4. In B5 it forms phenocrysts or glomeroporphyritic aggregates with other plagioclase crystals or mafic crystals. Typically it occurs in well formed tabular prisms, or laths, and although it shows considerable size variation, most crystals are between 2 to 5 mm. in length. In laminated samples individual crystals reach up to 1 cm. in length. Twinning is very common on Carlsbad and Albite Laws, and occasionally on Pericline Laws. The albite and pericline twins are usually fairly fine. Elongated crystals tend to show only a single Carlsbad twin and in the more fractionated subunits, untwinned crystals are common. Virtually all crystals show normal zonation but the degree of zonation varies, often being quite strong marginally. Oscillatory zoning occurs in subunit B5 but usually shows only a single reversal.

4.1.2. Pyroxenes.

Calcium rich pyroxene occurs throughout the fractionation

sequence. It is roughly equal in abundance to plagioclase in subunits B1 and B2, but becomes subordinate in B3 to B5, where it rarely exceeds 20 modal %. It normally occurs as euhedral eight sided prisms, typically 1-2 mm in length, although elongation up to 8 mm does occur. Elongate forms have a tendency to subophitic and occasionally subskeletal morphology (Pl.4.7.). Both euhedral and subskeletal forms can occur in the same section. In more mafic rocks, which are more susceptible to hydrothermal alteration, the pyroxenes are often a pale green colour, but otherwise they are pale brown. In the pegmatitic facies of some subunits, the pale green type predominates. Normal zonation is a common feature, but is usually only slight except in subunit B1, where marked marginal zonation occurs. Thin exsolution lamellae of a calcium-poor pyroxene, exsolved parallel to the (100) cleavage plane, occur throughout the fractionation sequence but are not a common feature. The pyroxenes of subunit B2 often have a core region that is crowded with very fine opaque material (Pl.4.8.), possibly an iron oxide phase. Whether it is an exsolution phenomena or a lower temperature equilibration phenomena is not certain, but the boundary of the core-region is often very sharp, and has euhedral form.

4.1.3. Amphiboles.

Amphibole is a minor phase throughout the fractionation sequence, but is most abundant in subunit B3, when it can equal pyroxene modally. It rarely, however, exceeds 5 modal %. While blue-green or pale-olive fibrous amphibole is of secondary hydrothermal origin, the amphibole referred to here is undoubtedly magmatic in nature. It is generally strongly

ple ochroic in shades of pale-brown, green and straw-yellow. It occurs both as a discrete phase, rarely exceeding 5 mm. in length, or as a mantling to pyroxene crystals (Pl.4.9.). The mantle is usually partial but can be complete, and the pyroxene-amphibole boundary is sharp. Amphibole is a common feature of the pegmatitic facies.

4.1.4. Iron-Titanium Oxides.

Ilmenite and titanomagnetite occur in subunits B1 to B4 but only the latter has been detected in B5. In B1 the oxides appear to be late forming, being excluded from the plagioclase and pyroxene, but are euhedral in form, and up to 0.5 mm. in size. Both ilmenite and magnetite are most abundant in the ferrogabbros of B2, where they are early crystallising phases, forming up to 20% of the mode. They reach up to 2 mm. in size and are subhedral in form, occasionally they are sub-skeletal.

From B3 to B5 the amount of Fe-Ti oxide rapidly decreases in abundance, rarely exceeding 5 modal %, and usually forms small (0.5 mm) subhedral crystals. In these rocks they also commonly occur in association with the pyroxene, often as inclusions within the latter, notably when the pyroxene has elongate and subskeletal form. The ilmenite is homogeneous, but the titanomagnetite has very thin lamellae of ilmenite, exsolved in a Widmanstatten trellis pattern, on (111). Oxide phases are very susceptible to hydrothermal alteration, and commonly have been altered to a dark red-brown or grey semi-opaque material. Magnetite has been particularly affected, and often only the exsolved ilmenite lamellae remain. In

some sections a second, apparently later, homogeneous magnetite has formed, probably during hydrothermal alteration.

4.1.5. Apatite.

Apatite forms small (0.5 mm) slightly elongated hexagonal prisms in the more fractionated parts of subunit B1. It is most abundant in subunit B2, however, (Pl.4.2.), where euhdral prisms up to 1 mm. in size form up to 5 modal %. They are enclosed by pyroxene, plagioclase and opaque oxides, indicating their early nucleation and growth. Small crystals occur in the more basic members of subunit B3, but become very scarce in more fractionated rocks.

4.1.6. Zircon.

Zircon occurs in the more fractionated members of all the subunits. It is most abundant, however, in subunit B4, where the high level of zirconium (600ppm.) suggests that zircon forms approximately 0.05 modal %. Except in pegmatitic facies, crystals rarely exceed 0.3 mm. in size, and form cubic or sub-prismatic sections. They appear to be magmatic, and no evidence for relict, inherited, zircons exists. Commonly the zircons occur in association with the mafic phases, particularly in subunit B5, where they almost exclusively occur in the glomeroporphyritic clusters (Pl.4.6.). When they occur in association with amphibole, they produce dark pleiochroic haloes.

4.1.7. Quartz and Alkali felspar.

Quartz occurs as discrete grains throughout the sequence, but probably results from hydrothermal re-equilibration. Most

of the quartz,however, is micrographically intergrown with alkali felspar. The intergrowths increase in abundance laterally within the vertical sheets of the various subunits, and also in the pegmatitic facies of the subunits, the significance of which is discussed in later sections. The coarseness of the intergrowths varies considerably from one subunit to another, also within subunits, particularly in the pegmatitic facies, when it is almost graphic. Many of the granophyres of subunit B5 contain spherulitic intergrowths in addition to micrographic, and are occasionally microfelsitic. In coarser intergrowths the alkali felspar is seen to be perthitic. No discrete alkali-felspar crystals have been detected, except in the pegmatitic facies.

4.1.8. Accessory phases.

Primary epidote, mantling allanite (Pl.4.16.) occurs very rarely in the pegmatitic facies of subunit B3. The allanite has euhedral form and is very dark brown in colour. The epidote is pale green. Pyrrhotite and pyrite exist in very small amounts. Other phases occur very occasionally and probably result from hydrothermal alteration, principally of Fe-Ti oxides. They include biotite, sphene and rutile.

4.1.9. Hydrothermal alteration.

Hydrothermal fluid (presumably,principally water) - rock interaction varies considerably in degree, but not in effect. Primarily because of their more basic and mafic mineralogy, subunits B1 and B2 have been more susceptible to alteration. The alteration is often selective on a microscopic scale, affecting some phases but not others, and inhomogeneous

on a centimetre scale, affecting, say, pyroxene in one area but not in another, sometimes producing a spotting effect in hand specimen, most notable in the pegmatitic facies of subunits B2 and B3, (plate 2.1)

Plagioclase becomes sericitised or occasionally albitised, notably in subunit B1, where almost complete alteration has prevented any optical or microprobe determination of the core compositions. In strongly zoned crystals sericitisation is seen to be restricted to the more calcic core regions. Pyroxene is replaced by pale ochre coloured anthophyllite or blue-green actinolitic hornblende. The latter also replaces plagioclase and the alkali-felspar of micrographic intergrowths. Fe-Ti oxides are oxidised and replaced by haematite, leucoxene, sphene, rutile and occasionally biotite. Amphibole is replaced by biotite and blue-green actinolitic hornblende.

Alteration is rarely complete and in more fractionated rocks (B3 to B5) is often only incipient, and restricted to sericitisation of plagioclase cores. This suggests that the hydrothermal fluids, whatever their composition, are more or less in equilibrium with the more fractionated rocks.

4.1.10. Variations in Texture.

4.1.10.1. Crystal growth rate dependent textures:

Disequilibrium growth textures, particularly in pyroxenes, are a common feature of rocks in Unit B, but are best developed in subunit B2, along the southern margin where the ferrogabbro is closely adjacent to the northern contact of unit A, in

the lower FurtherGill Sike region (MR 3512,3339, ; Sample 135).

Plagioclases are elongate and curved, reaching up to 1 cm. in length. They have a core which is mantled by a more basic zone, followed by normal zonation to the margins. The zonation is continuous, without sharp breaks. P yroxenes show curved, branching, and 'corkscrew' growth forms, up to 3 cm. in length (Pl.4.10.). The corkscrew effect is suggested by two lines of evidence. The birefringence changes along the length of single pyroxene crystals, and the (100) twin plane, when present, migrates from a central position to the margin, when the twin plane disappears as the section becomes parallel to (010). Small euhedral grains of opaque-oxides occur in the cores of the pyroxene. Apatites are skeletal or needle like, (Pl.4.11.), and their length to breadth ratio (l:b) has increased up to 20:1. Occasionally a subhedral central prism is elongated at either end, along the c-axis, with thin needle like growths producing an overall length of up to 1 cm. Fe-Ti oxides are also skeletal, but this form is very often obscured by later resorbtion effects.

The plagioclase form and zonation are similar to those produced from melts in the system albite-anorthite with undercooling (ΔT), below the liquidus, of 100-200^{o}C (Lofgren, 1974). Hollow, elongate, skeletal crystals grow initially and become infilled and moulded by lower temperature components, as ΔT converges on liquidus temperatures. A similar interpretation was proposed by Wager and Brown (1968, p.112) for textures shown by plagioclases from the Marginal Border Group of the Skaergaard intrusion.

Elongate, curved, and branching phenomena in olivines have been produced experimentally in charges of ultrabasic and basic composition for various ΔT's (Donaldson, 1976), while similar morphologies in olivines and pyroxenes have been noted in natural examples by Donaldson (1974), Lofgren and Donaldson (1975) and Fleet (1975). No examples of the corkscrewing phenomena have been described in natural pyroxenes, to the author's knowledge.

Crystal growth may occur by at least three mechanisms; continuous growth, surface nucleation, and screw dislocation (Uhlmann, 1972, Kirkpatrick, 1975). Kirkpatrick et al (1976) performed growth rate experiments at various ΔT's, which indicated that the type of growth can be distinguished by the dependence of growth rate on the degree of undercooling. They found that in melts of anorthite and diopside, anorthite grew by surface nucleation, and diopside by screw dislocation. Diopside was only the second silicate material known to do so. It is clearly possible that pyroxenes will produce spiral crystals by a screw dislocation growth mechanisms, given certain conditions of growth rate and undercooling.

Elongate and skeletal apatites and skeletal Fe-Ti oxides are common phenomena in quickly cooled differentiated dolerites. Wyllie et al (1962) produced skeletal, hollow, and elongate apatites in dynamic crystallisation experiments of phosphorous bearing compositions. They related increased length to breadth ratios to Δ T, but did not calibrate the relationship.

The features described in the ferrogabbros of subunit B2 are, thus, interpreted as being produced by undercooling,

or supersaturation, of the Fe, Ti and P enriched melt. Rapid growth of phases has occurred normal to the cooling surface in the manner described by Lofgren and Donaldson (1975). Such textures are similar to 'Willow lake layering", as described originally by Taubeneck and Poldervaart (1960), but have since been termed comb layering by Lofgren and Donaldson (op. cit).

Disequilibrium phenomena produced by rapid growth occur in other subunits. The pyroxenes at the margin of subunit B1 (MR 3513, 3392, Plate 4.12.) show sector zoning. Simple forms predominate ((110) and (100)), and fractionation of elements has occurred between sectors. Subskeletal and hollow pyroxenes occur in subunits B3, B4 and B5 (Plate 4.7. a and b). Disequilibrium growth produces a characteristic chemistry within pyroxenes, and further discussion of this aspect of these pyroxenes is deferred until the section dealing with pyroxene chemistry (section 4.2.2).

A further point of interest relating to the hollow, subskeletal pyroxenes in subunits B3 to B5, is the occurrence of opaque oxides concentrated in chains along the length of these pyroxenes. It is suggested that the rapid growth of the pyroxene, particularly along the C-axis, has caused rapid depletion of pyroxene components in the immediate magma surrounding the crystal.

While these components are diffusing toward the crystal surface from the surrounding melt a condition of constitutional supercooling exists with respect to oxide components at the growing front of the pyroxene. Super-saturation of oxide components, causes inhomogeneous nucleation

of Fe-Ti oxides on the growing pyroxene crystal, and after a period of growth become trapped, and isolated from further growth, by the advancing crystallisation of the pyroxene.

The spherulitic growth of quartz and alkali felspar in the B5 granophyre, must be considered evidence of rapid growth produced by undercooling in the acidic melt.

4.1.10.2. Pegmatitic facies.

Pegmatitic facies occur in different sheets and subunits, but show very similar textural and mineralogical changes from their associated rocks. These changes can be described under three headings; textural changes, growth of new phases, and replacement and resorbtion textures.

Textural changes : Plagioclase changes from euhedral prismatic crystals to elongate tabular laths or prisms, up to 2 cm. in length (Pl.4.13.). It tends to lose its albite twinning although a single carlsbad twin is usually retained. The crystals also show strong normal zonation. Pyroxenes become less abundant, but much larger, occasionally up to 2 cm. in length. They become elongated and subophitic, and change from pale brown to pale green, although sometimes only near the margins. The pyroxenes are untwinned, unlike the supercooled pyroxenes of subunit B2, but do show corkscrew growth (Pl.4.14.), as indicated by variation in birefringence along their length. Apatite consistently changes morphology with increasing pegmatitic development, from euhedral hexagonal prisms, to more elongate prisms, and finally to elongate needles (Pl.4.13.) with l:b ratios of up to 60:1. Zircons change from small square sections, becoming much larger

(~ 1mm) and showing sub prismatic form (Pl.4.15.). A form of optical zonation is apparent, but may reflect individual growth zones. No relict cores were observed. Quartz-alkali felspar intergrowths change from micrographic to graphic, with spectacular feather and regular cuneiform growths. The alkali felspar shows fairly coarse perthite exsolution

Growth of new phases : Amphibole rims grow on pyroxenes (Pl.4.9.), and discrete amphiboles often grow to spectacular sizes, up to 8 cm. in length. Epidote and allanite (Pl.4.16.) occasionally grow as new phases. Interstitial carbonate becomes more abundant.

Replacement and resorbtion effects : Fe-Ti oxides show a peculiar resorbtion effect, different to that developed by hydrothermal alteration. A 'sausage' texture develops, with worm like relicts of ilmenite, set in plagioclase or pyroxene, and occasionally showing no apparent reaction products. The original outline of the crystal is often still apparent. (Pl.4.17.)

Another effect, observed in the loose blocks between the head of Further Gill Sike and Pike summit, is the very spectacular growth of a dendritic mafic phase (Pl.4.18. a and b), probably originally pyroxene, but now amphibole. These dendritic forms grow up to 20 cm. in length and consist of thin (~ 5mm) radiating or parallel growths, often with a single origin. The elongate growths have small teeth like projections normal to the growth direction.

4.1.10.3. Plagioclase rich segregations.

Many of the samples from subunits B2 and B3 show igneous lamination. In one particular laminated ferrogabbro (MR 3405, 3355 Sample 163) , thin schlieren and segregations up to 5 cm. in width occur. They are composed largely of well formed tabular laths of plagioclase, up to 5 mm. in length, and showing little zonation. Clusters of small apatite prisms occur interstitially to the laths. Small euhedral Fe-Ti oxides are scattered throughout the segregation and pale brown ophitic pyroxene is occasionally found. Quartz and alkali felspar intergrowths occur very occasionally. The margins of the segregation are fairly sharp in hand specimens, but are diffuse on the microscopic scale. The margins show features common to both the segregation and the matrix, over distances of 5 mm. The segregations also show lamination.

4.1.10.4. Xenoliths, hybrid, and contact features.

The dark patchy areas in the granophyre from lower Scurth (MR 3510,3388), and the darker granophyre from south of Round Knott (MR 3345, 3372), have thin acicular amphiboles in a plagioclase-alkali felspar-quartz felsitic matrix. In both areas they are cut by pink microfelsitic veins of quartz and alkali felspar. These darker coloured variants possibly represent hybrid granophyres or resorbed and reacted xenoliths, but also may be hybrids associated with the emplacement of subunit B1. A xenolith of acid material in the margin of subunit B1 on Round Knott, is a flowbanded rhyolite whose origin is unestablished. Fine grained xenoliths of

micro gabbroic material, consisting largely of plagioclase, amphibole, and Fe-Ti oxides, occur in the margin of subunit B1, north of Carrock Fell summit (MR 3414, 3394, Specimen 35). They possibly represent reacted autoliths of subunit B1 material. Veins of dark material cut the granophyric xenoliths in subunit B4 in the cliffs at the head of Further Gill Sike (MR 3503, 3342, Specimens 124-126). The veins are of B3 and B4 material, with fairly coarse, but not pegmatitic, granophyric intergrowths. The xenoliths themselves are either fine grained pyroxene-plagioclase granulites, presumably recrystallised B3 or B4 materials, or they show abundant acicular pleochroic amphiboles in a matrix of discrete grains of quartz, alkali felspar and plagioclase. They are probably of hybrid origin, as suggested by their textures, but whether from B4 and B5 or some other material, has not been determined. Small granular acidified xenoliths of Eycott type lava occur occasionally in some of the subunits.

Specimens of subunit B5 granophyre, close to the margins of subunit B1 or B4 and from the screens in the Further Gill Sike region, show the effects of hornfelsing. The micrographic intergrowths are recrystallised giving a 'micro blebby' appearance.

4.2. MINERAL CHEMISTRY

This section describes the mineral chemistry of the main groups of minerals. Emphasis is placed on chemical variation with fractionation, and the physio-chemical controls on crystallisation. Mineral analyses were obtained by

electron-microprobe. The analysis procedure and conditions, data reduction, and mineral analyses are described and tabulated in Appendix two. No data have been obtained for apatites or zircons.

4.2.1. Plagioclase.

The plagioclases of subunit B1 are extensively altered, especially the cores, so no systematic analysis was possible. Analyses of core compositions of plagioclases from subunits B2 and B5 are represented in figure 4.1, in terms of the end member molecules Orthoclase-Albite-Anorthite (Or-Ab-An).

Each of the subgroups forms a distinct cluster of analyses, which has partly formed the basis for division into subgroups B2, B3, B4 and B5. The plagioclases from the subunit B2 ferrogabbros are An57-52, those from B3 are An47-44, and from B4 + B5 ferrogranophyres and granophyres, An36-26. The B5 plagioclases show marked marginal increase in Or. Zonation is usually normal and fairly marked.

Most of the chemical variation in the plagioclases is described by the single coupled-substitution $SiNa \rightleftharpoons AlCa$. Ab content increases with decreasing temperature. K_2O also increases with Ab content, but generally remains below 3.5 Or%, except in subunit B5, where marginal zonation to Or_{10} occurs. There is an illdefined relationship between the Fe content of the plagioclases, and whole-rock Fe content. FeO varies from 0.6 Wt% in B2 to 0.18 Wt% in B5.

Plagioclase is the only felspar to crystallise as a liquidus phase, and,therefore,the plagioclase liquidus minimum is not confined to the two-felspar solvus in the system

An-Ab-Or (Carmichael, 1963). This probably accounts for their low K_2O content, which together with the absence of other K_2O bearing phases, may account for the increase in K_2O/Na_2O with fractionation. Figure 4.2 is a plot of normative whole-rock felsic components in the system Ab-Or-SiO_2-H_2O (Tuttle and Bowen, 1958), for subunits B3 to B5. The rocks all plot in the Ab field, with a trend away from Ab with increasing fractionation. They show a close correlation with the inferred Skaergaard liquid trend, (Wager and Brown, 1968; Carmichael, 1963). The trend does not intersect the two-felspar thermal valley, nor the quartz-felspar surface at PH_2O 1.5 $kg.cm^{-2}$. This accounts for the presence of only one felspar, and the absence of quartz phenocrysts in the rocks from unit B, alkali felspar and quartz being restricted to granophyric intergrowths.

4.2.2. Pyroxenes.

Figure 4.3 shows the variation in principal end-member components for the complete range of calcium-rich clino-pyroxenes from unit B. Figure 4.4 A to K, shows the detailed variation within the five subunits.

The suite, as a whole, shows a marked trend towards iron enrichment. The range of compositions is from Wo45En44Fs11 to Wo44En1.5Fs44.5, with a minimum at approx-imately Wo40En35Fs35. Normal zonation reflecting substitution of $Mg \rightleftharpoons Fe^{2+}$, within a particular specimen or single pyroxene, is usually fairly limited, less than 0.10 Fe/Fe + Mg, except in subunit B1 where individual pyroxene show marginal zonation of 0.30 Fe/Fe + Mg.

The overall trend is subparallel to the Skaergaard trend (Brown, 1957; Brown and Vincent, 1963), but is notably enriched in the Wo component, compared to the latter. The trends do, however, show some convergence at Fe-rich compositions. There is no evidence in the Unit B rocks of Ferro β Wollastonite inversion, as in the Skaergaard rocks (Brown & Vincent 1963).

Boyd and Schairer (1962) and Kushiro and Schairer (1963) have shown experimentally that augites crystallising at lower temperatures, are likely to contain less $(FeMg)SiO_3$ component, than those crystallising at higher temperatures. This effect is presumably a function of the shape of the two pyroxene solvus. Ross et al (1973) show the solvus to be convex toward the Di-Hd join, and wider at lower temperatures. It has been shown that H_2O has had a significant role in the evolution of the Unit B magma (Chapter 6). The high CaO content of the Ca-rich pyroxene may be a function of low liquidus temperature, produced by high water content, and the expansion of the two-pyroxene solvus at lower temperatures. Low temperature liquidus-solidus relations do not, however, explain the lack of a Ca-poor pyroxene phase. This can only be explained by the liquidus minimum being in the one-pyroxene field, and not intersecting the solvus to produce cotectic crystallisation of Ca-rich and Ca-poor pyroxene.

It is clear, however, that the Unit B trend is related in some way to the solvus, as it shows a minimum Wo composition, and the pyroxenes throughout the range occasionally show very thin exsolution lamellae of calcium-poor pyroxene,

unlike mildly alkaline trends (Gibb, 1973), or thoroughly alkaline trends, which are subparallel to the Di-Hd join, and tend to be more Wo-enriched than even the Unit B trend. Unless diffusion was inhibited, thus preventing more widespread exsolution of Ca-poor pyroxene, the abundance of calcium in the Unit B pyroxenes is probably very similar to that at the time of crystallisation. The Unit B trend, as a whole, is very similar to the sub-solidus Ca-rich pyroxene trend of the Skaergaard intrusion, as determined by electron-probe microanalysis (Nwe and Copley, 1975; Nwe, 1976). The trend of Brown (1957) and Brown and Vincent (1963) was constructed from bulk analyses of pyroxene separates, and thus includes any component of exsolved Ca-poor pyroxene, and represents the composition of the pyroxenes at the solidus-solvus intersection. It is probable that the subsolidus Skaergaard trend, and the Unit B trend, are constrained by the lower temperature limit of effective diffusion, as suggested by Elsdon (1971) for the Kap Edvard Holm pyroxene trend.

The two-pyroxene solvus must represent a significant departure from thermodynamic ideality, as do regions of immiscibility in silicate melts. Irvine (1975), has observed experimentally the tendency for cotectic boundaries to skirt around regions of non-ideality (immiscibility) in silicate melts. It seems possible therefore, that under certain circumstances, the liquidus minimum in the augite field, if sufficiently close to the two-pyroxene solvus, might show a tendency to skirt around it rather than intersect it. It would thus prevent the separation of a discrete calcium-poor pyroxene, but the resultant Ca-rich trend would show the

features typical of tholeiitic trends, namely a Ca-minimum, and subsolidus exsolution of Ca-poor pyroxene.

The position of the pyroxene minimum is undoubtedly controlled by factors which affect the stability field of Ca-poor pyroxene (Campbell and Nolan, 1974). The stability field is related either to the reappearance of cumulus olivine (Poldervaart and Hess, 1951; Lindsley and Muncz, 1969; Campbell and Nolan, 1974), or to a peritectic reaction between pigeonite and liquid (Brown, 1957; Nwe and Copley, 1975; Nwe, 1976), causing a shift of the intersection of the liquidus minimum towards the Ca-rich limb of the solvus, to eventually become decoupled to form a liquidus minimum in the one-pyroxene field (Muir, 1954). Whatever the cause of the pyroxene minimum, it is surely the phase relationships and the shape of the solvus at the limit of the two-pyroxene field that are the controlling factors, as in Unit B neither Ca-poor pyroxenes nor olivine are liquidus phases. Parameters such as αSiO_2, P, and T (Campbell and Nolan, 1974) or fO_2 (Carmichael et al, 1970) influence the position of the minimum and the size of the solvus.

There seems to be a very strong correlation of the pyroxene minimum, with the crystallisation of Fe-Ti oxides in most tholeiitic suites. The stability of Fe-Ti oxides is principally influenced by the fO_2 of the magma (Osborne, 1959). It may be, therefore, that fO_2 and Fe-Ti oxide stability is influencing the position of the minimum, rather than the stability field of Ca-poor pyroxene. The apparent Ca-enrichment of the Ca-rich pyroxene trend, after the

minimum composition, may be a result of Fe depletion in the liquid consequent upon Fe-Ti oxide crystallisation, thus, it should be interpreted as a lack of Fe-enrichment in the pyroxene rather than an enrichment of Ca. Notably, the rate of increase of Fe in the Ca-rich pyroxenes does show a slight decrease, over the initial range of crystallisation of Fe-Ti oxide. The crystallisation of Fe-Ti oxides causes a marked change in liquid composition and melt structure in tholeiitic liquids, notably, $aSiO_2$ and activity of alkalis increase. The $aSiO_2$ has a controlling effect on the stability of Ca-poor pyroxene (Campbell and Nolan, 1974). The suppression of Ca-poor pyroxene may, therefore, be a secondary effect of Fe-Ti oxide crystallisation. The effect of increased activity of alkalis, may be to increase the width of the pyroxene solvus, and therefore enhance the subsequent apparent Ca-enrichment in the Ca-rich pyroxenes.

Campbell and Nolan (1974) suggest that beyond the pyroxene minimum, the Ca-rich pyroxene composition is no longer confined to the solvus and migrates towards the Di-Hd join. The implications of this would be that fractional crystallisation of Ca-rich pyroxene alone does not control the evolution of the residual liquid, which becomes depleted in CaO, and that participation of a Ca-poor phase, such as olivine or magnetite, is necessary to cause augite to become more calcic (Huebner and Turnock, 1980). If the Ca-rich pyroxene composition was not confined to the solvus, it would become a function of melt composition. It is surprising, therefore, that most Ca-rich pyroxene trends from tholeiitic

rocks, tend to converge in the Fe-rich p ortion of the pyroxene quadrilateral, and intersect the Fs-Hd join at between Wo40 and Wo44. It is also of note, that Lindsley and Munoz (1969) found experimentally that Hd_{ss} in equilibrium with pure fayalite and silica, at low pressure and 930°C, had the composition Wo40Fs60.

The existence of sub-solidus exsolution lamellae of Ca-poor pyroxene in Fe-rich pyroxenes crystallised in the one pyroxene field in Unit B and in other tholeiitic intusions, suggests that the pyroxene crystallised above the pyroxene solvus. At the lower liquidus temperatures of Fe-rich pyroxenes, it is unlikely that the solidus was far above the minimum temperature for effective diffusion to allow redistribution of the Ca-poor pyroxene component. Thus, the existence of exsolution lamellae at all, supports the contention that the liquidus minimum was not far above the solvus surface.

It is suggested that althought the Ca-rich pyroxenes were crystalising in the one-pyroxene field, the two-pyroxene solvus still had a profound effect on the crystallisation path of the Fe-rich pyroxenes, beyond the pyroxene minimum. Ross et. al. (1973), show the solvus to be assymmetrical towards the Ca-rich compositions, with the rate of steepening of the solvus limb, increasing with decreasing temperature. Figure 4.5, modified from Ross et. al. (op. cit.), shows that because of the assymmetry, pyroxenes A1 and B1, crystallising at liquidus minima close to the crest of the solvus, at temperatures X1 and Y1, will have differing Wo contents.

With fractionation at lower temperatures, pyroxenes A2 and B2, crystallising at X2 and Y2 will have converging Wo contents, despite the same differences in liquidus temperatures, because of the steepening limb of the solvus.

Figure 4.6 shows the variation of minor components Al, Ti and Mn plotted against $100.Mg/(Mg+Fe)$ (FM), a good indication of the degree of fractionation. Al and Ti decrease in concentration with fractionation up to approximately FM = 70; then show a very slight increase to a maximum at approximately FM = 80, followed by a further decrease. Zoned core-margin analyses for Al and Ti are joined by tie lines. In subunits B1 and B4 to B5, the tie lines are subparallel with the overall trends, in subunits B2 to B3, however, the tie lines run oblique or even normal to the main trends, indicating that pyroxene is not controlling Al and Ti fractionation in the liquid. Mn increases with fractionation, but shows a slight flattening of slope between FM50 to 80, probably related to the cotectic crystallisation of Fe-Ti oxides (ilmenite contains 4-5 Wt % MnO). Na is low and shows no systematic variation. Cr is high, up to 0.55%Cr_2O_3, in pyroxenes of subunit B1, but falls off very rapidly.

Figure 4.7a shows the variation of Al with Si. The fields for the subunits have been outlined for clarity, and core-margin analyses are joined by tie lines. Some of the lateral spread is possibly as a result of error in Si determination (see Appendix Two), however, the overall trends are considered representative of actual variation. There is a lateral spread within each subunit, about Al+Si = 2.0 atoms,

with most of the analyses showing an excess of Al over that required to fill the z site. Points also fall below the line, however, and may indicate incorporation of Ti into the z site. The Al contents are fairly high and show a negative correlation with fractionation. Figure 4.7b shows the variation of Ti with Al. Both Al and Ti are high, and while Al shows a negative correlation with fractionation, Ti shows less tendency to do so. The Al:Ti ratio, therefore, shows a systematic decrease from subunit B1 to B5, although there is considerable overlap, as there is with Si v. Al. Within the subgroups Al:Ti decreases with decreasing Al content.

Excess of Al over that required to fill the z site suggests incorporation of Ca-Tschermaks' molecule ($CaAl_2SiO_6$), as does Al:Ti ratios of greater than 4:1. Al:Ti ratios between 4:1 and 2:1 suggest incorporation of $R^{2+}TiAl_2O_6$ (Yagi and Onuma, 1967; Bence et al., 1971).

The negative correlation of Ca-Tschermaks molecule ($CaAl_2SiO_6$) with fractionation, could be related to increasing a_{SiO_2} in the melt (Carmichael et al 1970), according to the reaction:

$$CaAl_2SiO_6 + SiO_2 \rightleftharpoons CaAl_2Si_2O_8$$

in Pyroxene in melt in Plagioclase

Campbell and Borley (1974) relate the uptake of $CaAl_2SiO_6$ to increased $a_{Al_2O_3}$ and decreased a_{SiO_2}, which is supported by the observations of Barberi et al. (1970), who show that the $CaAl_2SiO_6$ content of the pyroxene is low when plagioclase

crystallises early, thus decreasing αAl_2O_3 and increasing αSiO_2. This is also consistent with the Unit B data, as Ca-Tschermaks decreases in pyroxene with fractionation, as plagioclase becomes more dominant. Gibb (1973), however, relates the Al content in the pyroxene to the Ti uptake, as there is a positive correlation of Al with Ti. As Ti drops in the pyroxene during Fe-Ti oxide crystallisation, so does Al. The Al:Ti ratio remains constant, suggesting that $R^{2+}TiAl_2O_6$ is the dominant substitution, however, and not $CaAl_2SiO_6$. One of the features of the Unit B pyroxenes is that they have crystallised fairly rapidly as evidenced by skeletal growth, sector zoning, and corkskrew growth, attributed to growth under supercooled conditions. Grove and Bence (1977; 1979), Coish and Taylor (1979), and Gamble and Taylor (1980), have shown experimentally, in synthetic and natural compositions, both terrestrial and lunar, that Ti and Al uptake is dependent on rate of crystallisation. While activity relationships may have an effect on Al and Ti uptake in the Unit B pyroxenes, the metastable incorporation of $CaAl_2SiO_6$ and $R^{2+}TiAl_2O_6$ molecules, during rapid growth is considered to be a contributing factor to the higher Al and Ti contents, as compared to other tholeiitic trends.

Sector zoning is shown in the augites of subunit B1, but especially well in sample 32. There are slight differences of interference colour and extinction angle between adjacent sectors. The prismatic face (100), and the (100) sector are shown in stippled ornament in figure 4.12. The adjacent unstippled sector is the non-prismatic sector, and is designated as (110) or (010), but could also be a (111)

type sector. Analysed points are also shown. The analyses are tabulated in Appendix Two, and the average analyses for prismatic and non-prismatic sectors are shown in table 4.1. The averages exclude points 9 and 10, as these show the extent of normal marginal zonation. Table 4.1 also shows the distribution coefficients between the sectors for all the elements analysed (K_D = concentration in prismatic sector/concentration in non-prismatic sector). The distribution coefficients indicate that Al, Ti, Cr, Fe, Ca and Na are preferentially fractionated into the prismatic sector, while Si, Mg and Mn are enriched in the non prismatic sectors. Ca/Ca+Fe+Mg values are 0.45 in the (100) sector and 0.44 in the adjacent sectors. The Al/Si and Al/Ti sectorial interrelationships have been indicated in figures 4.7. a and b.

Many occurrences of sector or 'hourglass' zonation have been described, principally in titanaugites from alkalic hypabyssal and volcanic rocks. A review is given by Deer et al. (1978). Nakamura and Coombs (1973) and Nakamura (1973) describe sector zoned pyroxenes from a tholeiitic dolerite, which have a Ca/Ca+Mg+Fe distribution opposite to that shown in the Unit B augites, and which show no intersectorial variation between Al and Ti. In this respect the subunit B pyroxenes are more similar to alkaline types.

Mechanisms for sectorial fractionation have been proposed by Dowty (1976), Hollister and Gancarz (1971), Leung (1974), Nakamura (1973), and Thompson (1972). It is well established that sectorial fractionation is produced on surfaces of adjacent crystal faces, simultaneously

TABLE 4.1 :

Average analyses for prismatitic (100) and non-prismatic sectors (110) (010) (111) from sector zoned pyroxenes in sample 32 (Analysed points shown in figure 4.8 and are tabulated in full in Appendix 2).

K_D = concentration in prismatic sector / concentration in non-prismatic sector

	PRISMATIC SECTOR	NON-PRISMATIC SECTOR	K_D
SiO_2	49.95	51.13	0.98
Al_2O_3	3.41	2.04	1.67
TiO_2	1.18	0.79	1.49
Cr_2O_3	0.31	0.23	1.35
FeO	7.40	7.21	1.03
MnO	0.27	0.32	0.84
MgO	14.96	16.10	0.93
CaO	22.13	21.86	1.01
Na_2O	0.30	0.22	1.36
TOTAL	99.91	99.90	
ATOMIC PROPORTIONS ON THE BASIS OF 6 OXYGENS			
Si	1.866	1.903	
Al	0.150	0.089	
Ti	0.034	0.022	
Cr	0.009	0.007	
Fe	0.231	0.224	
Mn	0.009	0.011	
Mg	0.833	0.892	
Ca	0.886	0.872	
Na	0.009	0.009	
number of points	6	6	

growing under identical conditions of pressure, temperature and composition of the surrounding melt, but differences of opinion exist as to the exact mechanism. It is undoubtedly related to two factors, the internal structure of the pyroxene, and probably also the difference in growth rate of different faces. These conclusions are drawn, because disequilibrium growths of olivine or plagioclase do not show sectorial fractionation, and pyroxenes which grow slowly under equilibrium conditions show the prismatic form with no sector zoning.

Because of the chain structure of the pyroxene, different crystal faces will present different structural sites to the magma for further growth at any particular time, that is, the proportion of M1, M2 and tetrahedral sites will differ on any one face. Leung (1974) suggests, therefore, that growth on different faces will deplete the magma differently with respect to Ca, Mg and Si, in front of different growing faces, constitutionally supercooling it with respect to Ti and Al. Metastable incorporation of Ti and Al would, thus, occur on those growth surfaces against which supercooling occurred . Nakamura (1973) interprets the growth of sectors in terms of the geometry of protosites, or partially formed structural sites. The geometry of the M1 and M2 protosites are most flexible on the (100) growth surface, as these deviate most from the true structural sites, consequently the composition of the (100) sector can deviate most prominently from equilibrium composition, by incorporating metastable molecules of the type $CaAl_2SiO_6$ or $R^{2+}TiAl_2O_6$.

Most of the models are based on the metastable incorporation of Ti and Al (and Cr). Increased Al and Ti uptake have been shown experimentally (Gamble and Taylor, 1980) to be a function of rapid crystallisation rate, whereas Mg, Fe and, to a lesser extent, Ca are essentially rate independent. The experimental results, thus, confirm the hypothesis that sector zoning is dependent on rapid crystallisation and incorporation of metastable molecules.

4.2.3. Plagioclase-pyroxene relationships.

Figure 4.9, shows the relationships between core compositions of coexisting calcium-rich clinopyroxenes and plagioclases, in terms of Mg/Mg+Fe and An% respectively. Within the subunits, the plagioclase compositions change relatively little, but are associated with a pronounced decrease in the Mg-number of the pyroxene. The subgroups B2, B3, and B4 with B5, show differing An contents. The dashed line connecting the start of each trend is considered to represent the fractionation trend of the magma, whilst the horizontal trends are a reflection of in situ fractionation within each unit after emplacement. The proposed fractionation trend of the magma is similar to fractionation trends shown by other tholeiitic intrusions.

A number of possible explanations exist to explain the plagioclase-pyroxene relationships within the subunits. Plagioclase may have been a phenocryst phase on emplacement of the magma, whereas pyroxene crystallised after intrusion, the iron-enrichment, thus, reflecting fractionation in the magma after emplacement, which is shown in the plagioclase by continued zonation. The above effect may be enhanced by the

ability of pyroxenes to re-equilibrate with the fractionating melt more easily than plagioclase. (Wager and Brown, 1968). A second contributing factor may be the suppression of the plagioclase liquidus-solidus relationships by increased volatiles(Yoder etal,1957) due to lateral fractionation of volatiles within the sheets. The Mg/Fe ratio of the pyroxene is not affected by lower liquidus temperatures, plagioclase compositions therefore initially remain constant with decreasing temperature, while pyroxene compositions reflect normal cooling trends. A similar relationship in the Upper Layered Series of the Kap Edvard Holm intrusion has been interpreted in this manner (Elsdon, 1971).

No plagioclase analyses are available for subunit B1. Extrapolation of the proposed fractionation trend in figure 4.9 back to pyroxene core compositions from subunit B1, suggests that the plagioclase in equilibrium with the pyroxene core composition would be approximately An75.

4.2.4. Amphiboles.

Discussion of amphibole chemistry is hampered by the ubiquitous presence of Fe^{3+}, since the microprobe analysis returns all Fe as FeO. Various methods for calculating the Fe^{3+} content of amphiboles have been proposed (Robinson et al. 1971; Leake, 1978).

It is necessary to estimate the Fe^{3+}/Fe^{2+} ratio before any attempt can be made to correctly classify amphibole analyses. An increase in the proportion of Fe^{3+} reduces FeM4, and therefore NaA. Si also decreases with a resultant increase in Al^{IV} ,

balanced by lower Al^{VI}. These parameters are all commonly used in amphibole classification.

A commonly used diagram for classifying amphiboles is a plot of tetrahedrally coordinated Al (Al^{IV}) against A-site occupancy. As defined by Ross et al. (1969), A = (Ca+Na+K+FeM4-2.0), where FeM4 is the excess of Fe over 5.0 in the Y site. Figure 4.10a shows the analysed amphiboles from Unit B with all Fe calculated as FeO. Figure 4.10b. show the analyses with some Fe recalculated as Fe^{3+}, by the method of Leake (1978), in which Fe^{3+}/Fe^{2+} is increased until the Z+Y site occupancy shows no excess over 13.0 atoms. This reduces FeM4 to zero, and therefore reduces A-site occupancy by increasing NaM4 to fill the X-site. The effect is to move the amphibole plots from Edenite towards Tschermakite. The two above cases are considered to represent the minimum and probable maximum limits of Fe^{3+} respectively. Table 4.2 shows representative analyses calculated by both methods. It will be noted that the Fe^{3+}/Fe^{2+} atomic ratio is generally low, averaging .2 with a range from .05 to .32. For maximum Fe^{3+}, $Si+Al^{IV}$ falls short of 8.0 atoms by an average of .14 atoms, but reaching .24 atoms, and Al^{VI} is usually, therefore, near zero. Considering the low Fe^{3+}/Fe^{2+} ratio, it seems unlikely that considerable Fe^{3+} occurs in the Z-site, Cr is also generally very low. Consideration of these points, implies that the calculated Fe^{3+}/Fe^{2+} ratio is probably too high, and the actual value probably lies somewhere between the maximum and minimum cases.

Figures 4.11 a-d, show the classification of Unit B amphiboles, using the scheme proposed by Leake (1978).

TABLE 4.2 :

Minimum and maximum cases for Fe_2O_3 recalculation for representative amphibole analyses from Unit B.

Minimum. all Fe is FeO
Maximum. calculated by method of Leake (1978)
for discussion see text.

Oxide wt%	52/1 min		52/1 max		135/1 min		135/1 max	
SiO_2	43.21		43.21		45.50		45. 0	
TiO_2	1.36		1.36		1.33		1.33	
Al_2O_3	5.80		5.80		4.87		4.87	
Cr_2O_3	0.07		0.07		0.04		0.04	
FeO	30.36		25.50		25.61		19.14	
Fe_2O_3	-		5.40		-		7.22	
MnO	1.06		1.06		0.45		0.45	
MgO	3.01		3.01		7.07		7.07	
CaO	9.99		9.99		10.32		10.32	
Na_2O	2.27		2.27		1.76		1.76	
K_2O	0.64		0.64		0.37		0.37	
Total	97.76		98.31		97.31		98.07	
Atomic proportions on the basis of 23 oxygens								
Si	6.96	8.01	6.86	7.94	7.12	8.0	6.99	7.87
Al^{IV}	1.05		1.09		0.88		0.88	
Al^{VI}	0.06		-		0.02		-	
Ti	0.16		0.16		0.16		0.15	
Cr	0.01		0.01		0.01		0.01	
Fe^2	3.91	5.00	3.39	5.06	3.11	5.0	2.46	5.13
Fe^3	-		0.65		-		0.84	
Mn	0.14		0.14		0.06		0.06	
Mg	0.72		0.71		1.64		1.63	
Ca	1.72		1.70		1.73		1.70	
FeM_4	0.18	2.00	-	2.00	0.24	2.0	-	2.0
NaM_4	0.10		0.30		0.03		0.30	
NaA	0.61	0.74	0.40	0.53	0.50	0.57	0.22	0.29
K	0.13		0.13		0.07		0.07	
Fe^{3+}/Fe^{2+}	-		.18		-		.27	
$Mg/Mg+Fe^{2+}$	.15		.17		.33		.40	

Minimum and maximum cases for Fe^{3+} have been plotted on figures a+b and c+d respectively. Amphiboles from subunit B1 are actinolitic hornblendes, those from subunits B2 to B5 range from ferroactinolitic hornblende, through ferrohornblende to ferroedenite, depending on the Fe^{3+}/Fe^{2+} ratio.

In figure 4.12 the amphiboles are plotted in terms of Ca, Fe and Mg in the pyroxene quadrilateral, with tie lines connecting coexisting clinopyroxene-amphibole pairs. The tie lines show a consistent orientation, any variation probably reflects zonal variation in Fe/Mg ratio in the pyroxenes, the amphiboles showing little variation in this respect. Figure 4.12 is plotted with total Fe as FeO. An increase in the Fe^{3+}/Fe^{2+} ratio reduces the vertical scatter in Ca, and alters the $Mg/Mg+Fe^{2+}$ ratio in the amphibole, thus, slightly changing the slope of the tielines. Unit B amphiboles show a consistent change in chemistry with decreasing Mg/Mg+Fe ratio.

Figure 4.10 shows that Al^{IV} and A-site occupancy increase, and Si decreases, with apparent decrease in temperature and increasing fractionation as indicated by Mg/Mg+Fe ratio. Mn and Ti also increase, Mn from .05 to .15 atoms and Ti from .1 to .2 atoms. Apart from the simple charge - balanced exchange reactions of $Mg \rightleftharpoons Fe + Mn$ and $Na \rightleftharpoons k$, the main substitution in the amphiboles is that of edenite (or ferroedenite) $Si \rightleftharpoons NaA.Al^{IV}$. The extent of this substitution is dependent on the Fe^{3+}/Fe^{2+} determination as explained. However, the generally low values of Fe^{3+}, together with the very low or zero Al^{VI}, and low Ti, suggest that Al-Tschermakite and Ti-Tschermakite

substitutions are restricted, if present at all. Richterite substitution is possible, as Ca is generally less than 2.0 atoms, but this is also likely to be restricted considering the probable presence of FeM4.

The dependence of amphibole chemistry on temperature, whole rock bulk chemistry, and oxygen fugacity (fO_2), is not clearly defined, but has been investigated by Helz (1973). Helz found that for a given starting composition, Al^{IV}, Ti and A-site occupancy, show positive correlations and temperature dependence. Al^{IV} was found to be proportional to $Al^{VI}+2Ti$, while Al^{IV}, from the tschermakite component, increases by two as the edenite substitution increases by one. Helz suggested that crystal chemical constraints in the hornblende require that tschermakite substitution be balanced by edenite substitution. This would minimise, or balance, intra-crystalline strains produced in the amphibole structure by tschermakite substitution. This conclusion is supported by variation in A-site occupancy with liquid bulk composition, with respect to total alkalis, at a constant Al^{IV} content. Coupled tschermakite substitution thus appears to be the dependent variable which strains the structure and requires compensating substitution of edenite. Edenite substitution is thus independent of tschermakite substitution.

Unit B amphiboles have little tschemakite but substantial edenite substitution, supporting Helz's conclusion. However, the observed increase in edenite substitution with decreasing fractionation and temperature, is in contradiction with the findings of Helz, that edenite substitution decreases with

decreasing temperature.

Helz (op cit) found no experimental correlation between whole rock SiO_2 and Al_2O_3 contents and Si and Al in amphibole. Jakeš and White (1972) found a positive dependence of Si and Al in amphibole, on either temperature or bulk rock SiO_2 content, in continental margin and island arc volcanic rocks. These data, however, may not be applicable to iron-enriched tholeiitic amphiboles.

The distribution coefficient K_D, $((Fe/Mg)_{Am} x (Mg/Fe)_{px})$ should approach one as temperature increases, if the Mg-Fe exchange between the two minerals follows ideal solution laws. Fe, however, is strongly partitioned into the amphibole, a large departure from ideality, which is probably related to structural constraints. Kretz (1960) showed that as Fe increased in hornblende, both alkalis and Al increased, because of ionic size differences between Mg^{2+} and Fe^{2+}. Amphibole chemistry, and particularly Fe uptake, is very sensitive to fO_2 (Helz, 1973). Low fO_2 produces low Mg/Mg+Fe. High fO_2 exerts external controls, causing the expansion of the Fe-Ti oxide field. This is reflected in amphibole chemistry by lower Ti contents. Popp et al. (1977) found that on the tremolite-actinolite join, solution limits of the Fe-end member, increased with decreasing fO_2. The overall effect of decreasing fO_2, is to produce Fe-enriched amphiboles, in which the uptake of Ti, Al and alkalis is favoured. This could account for the observed increase in edenite or ferroedenite substitution with decreasing temperature, in Unit B amphiboles, and the associated limited increase in Ti. Ti is low anyway in the more fractionated subunits due to

separation of Fe-Ti oxides in subunit B2.

Leake (1971) notes that natural edenitic amphiboles are rare in igneous rocks, and suggests that low liquidus temperatures are essential to stabilise them. Although little experimental work has been undertaken on the phase relations of edenite-ferroedenite, Colville etal. (1966) have synthesised edenite and ferroedenite at 850°C and 2KbPH_2O, and 600°C and 3KbPH_2O respectively, thus supporting Leake's observation. Leake (op cit) used data from Dodge et al. (1968) and Haslam (1968) to define a 'limit' for igneous amphibole compositions. This is shown in figure 4.13, a plot of Si against Ca+Na+K, together with data from Unit B. The higher temperature ferroedenitic amphiboles from Unit B plot on this 'limit', but the more fractionated ones lie beyond this limit towards ferroedenite (SS). This suggests that liquidus temperatures were low, a point noted from the pyroxene data in section 4.2.2. Onuki (1966) and Kretz (1960) have shown that K_D , defined above, is temperature dependent, increasing with increasing temperature or grade of metamorphism. Helz (1973) confirmed this dependence and produced a rough calibration curve, although Kretz and Jen (1978) have shown that the temperature dependence may not be linear. Extrapolation of Heltz's K_D temperature curve gives temperatures in the range of 700-750°C for the Unit B amphiboles. While these may be rather low temperatures, they support the low liquidus temperature hypothesis.

4.2.5. Iron-Titanium Oxides.

Both ilmenite (ilmenite-haematite$_{SS}$) and titano-magnetite (magnetite-ulvospinel$_{SS}$) appear as major phases in the latter stages of subunit B1, but are most abundant in

B2. Both phases crystallise in B3 but in B4 and B5 the spinel phase is dominant, and may be the only oxide phase in some specimens. It was noted in section 4.1 that the Fe-Ti oxides were particularly susceptible to hydrothermal alteration. Ilmenites show resorbtion, but remain relatively homogeneous. Magnetites, however, except in subunits B3 to B5, are highly resorbed, leaving a trellis of ilmenite lamellae in a semi-opaque, red-brown or grey material. It has been very difficult, therefore, to obtain satisfactory microprobe data from the magnetites. Commonly, totals are low or contain unacceptably high proportions of SiO_2. When totals were reasonable, ilmenite lamellae created problems of inhomogeneity, the lamellae being too small to probe on the one hand, and defocussed beam analysis prevented, on the other, by resorption and alteration effects. For these reasons, only seven analyses of titanomagnetites are presented, together with ilmenite data, in Appendix Two.

Electron microprobe analysis only provides values for total Fe as FeO, the data, therefore, have been corrected for Fe_2O_3, using the method of Carmichael (1967). The recalculated data are presented in figure 4.14, a ternary plot of FeO-TiO_2-Fe_2O_3. FeO includes molecular equivalents of $R^{2+}O$ oxides, MnO, MgO and CaO when present; Fe_2O_3 includes $R_2^{3+}O_3$ oxides, Al_2O_3 and Cr_2O_3; and TiO_2 includes SiO_2. The rhombohedral phase shows very limited solid-solution, with a maximum of 5% haematite and are thus, virtually pure ilmenite. The spinel phase, however, shows a greater range of solid-solution, from 38-64% ulvospinel. In grains which show ilmenite lamellae, the ulvospinel % is a minimum, as the

lamellae are interpreted as resulting from subsolidus oxidation of ulvospinel. (Vincent and Phillips, 1954; Buddington and Lindsley, 1964).

In view of the apparently oxidised nature of the titanomagnetites, it is surprising that the ilmenites show such a low Fe_2O_3 content. The almost ubiquitous presence of divided red-brown oxide material, in association with the ilmenites suggests that Fe_2O_3, as haematite, has been selectively removed during hydrothermal alteration. In this respect, Martin and Piwinskii (1969), have shown experimentally that Fe fractionates into the vapour phase at subsolidus temperatures, and Sweeton and Baes (1970) suggest that removal of Fe from magnetites in aqueous solutions occurs as soluble hydroxides. Further evidence of removal of Fe, as Fe_2O_3, is suggested by figure 4.15, which shows the coexisting ilmenite-haematite$_{ss}$ ulvospinel-magnetite$_{ss}$ projected onto the fO_2 - temperature plane. (Buddington and Lindsley, 1964). The apparently oxidised assemblages give fO_2 values of 10^{-25} to 10^{-22}, at temperatures of approximately 580-650°C. The points lie near the experimentally determined QFM buffer curve (Eugster and Wones, 1962).

No pertinent conclusions concerning magmatic conditions of fO_2 and temperature can be drawn from these data. They do, however, in conjunction with petrographic evidence, indicate that substantial re-equilibration of the ilmenite-haematite SS and ulvospinel-magnetite SS, has occurred during the hydrothermal alteration. There is evidence for oxidation followed

by resorption and selective removal of Fe_2O_3 (or $FeO.Fe_2O_3$), but these effects may have been late magmatic or subsolidus. The occurrence of resorbed ilmenite crystals with no apparent bi-products may suggest that conditions were still magmatic when these effects started. The appearance of Fe-Ti oxides at a fairly late stage in the evolution of the magma, as indicated from the coexisting plagioclase and pyroxene compositions, suggests that fO_2 conditions during fractionation remained fairly low. fO_2 conditions are discussed in Chapter Six.

MnO occurs in appreciable amounts, up to 5.5 wt% in ilmenite and 1.8 wt% in magnetite. There is a very crude positive relationship between the degree of fractionation, and the MnO content in the magnetites, but the values are variable in the ilmenites. The partitioning of Mn between ilmenite and magnetite conforms to normal patterns. (Buddington and Lindsley, 1964; Neumann, 1974) K_D (MnO ilmenite/MnO in magnetite) values average approximately 3.0 which is slightly high for tholeiitic rocks, indicating that preferred oxidation of Fe^{2+}, with respect to Mn^{2+}, may have occurred under conditions of increase fO_2 (Anderson, 1968; Czamanske and Mihalik, 1972).

Of the minor elements, Si, Al, Cr, Mg and Ca have been recorded. Si and Ca may be due to silicate impurities. No systematic variation in the other elements occurs. Vanadium is undoubtedly present in the magnetite, but was not determined.

Durham University SCIENCE 30 OCT 1980 SECTION Library

FIGURE 4.1.

Analysed plagioclase core compositions from Unit B rocks, plotted in part of the ternary felspar diagram, (Orthoclase-Albite-Anorthite).

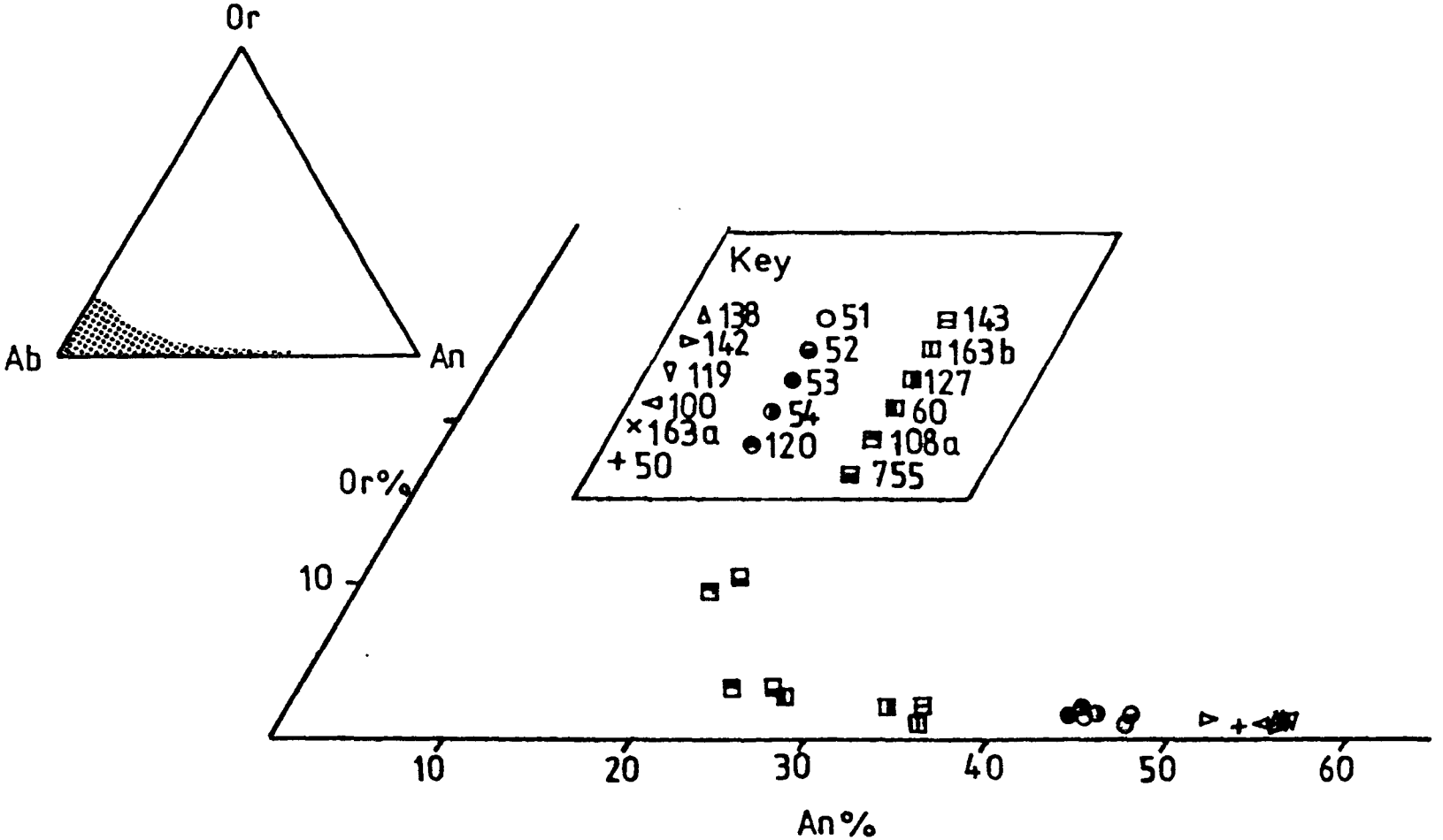
Or
Ab
An
Key
138
51
143
142
52
163b
119
53
127
100
54
60
163a
120
108a
50
755
Or%
10
10
20
30
40
50
60
An%

FIGURE 4.2.

Normative whole-rock felsic components (Qz + Or + Ab >50 %) for subunits B3, B4 and B5, projected onto the Ab-Or-SiO_2 plane. (after Tuttle and Bowen, 1958).

● B3; o B4; × B5:

The Quartz-Felspar field boundary at H_2O vapour pressures of 500,1000 and 2000 $Kg.cm^{-2}$ is shown. The dashed line is the Skaergaard trend in this system (Carmichael, 1963).

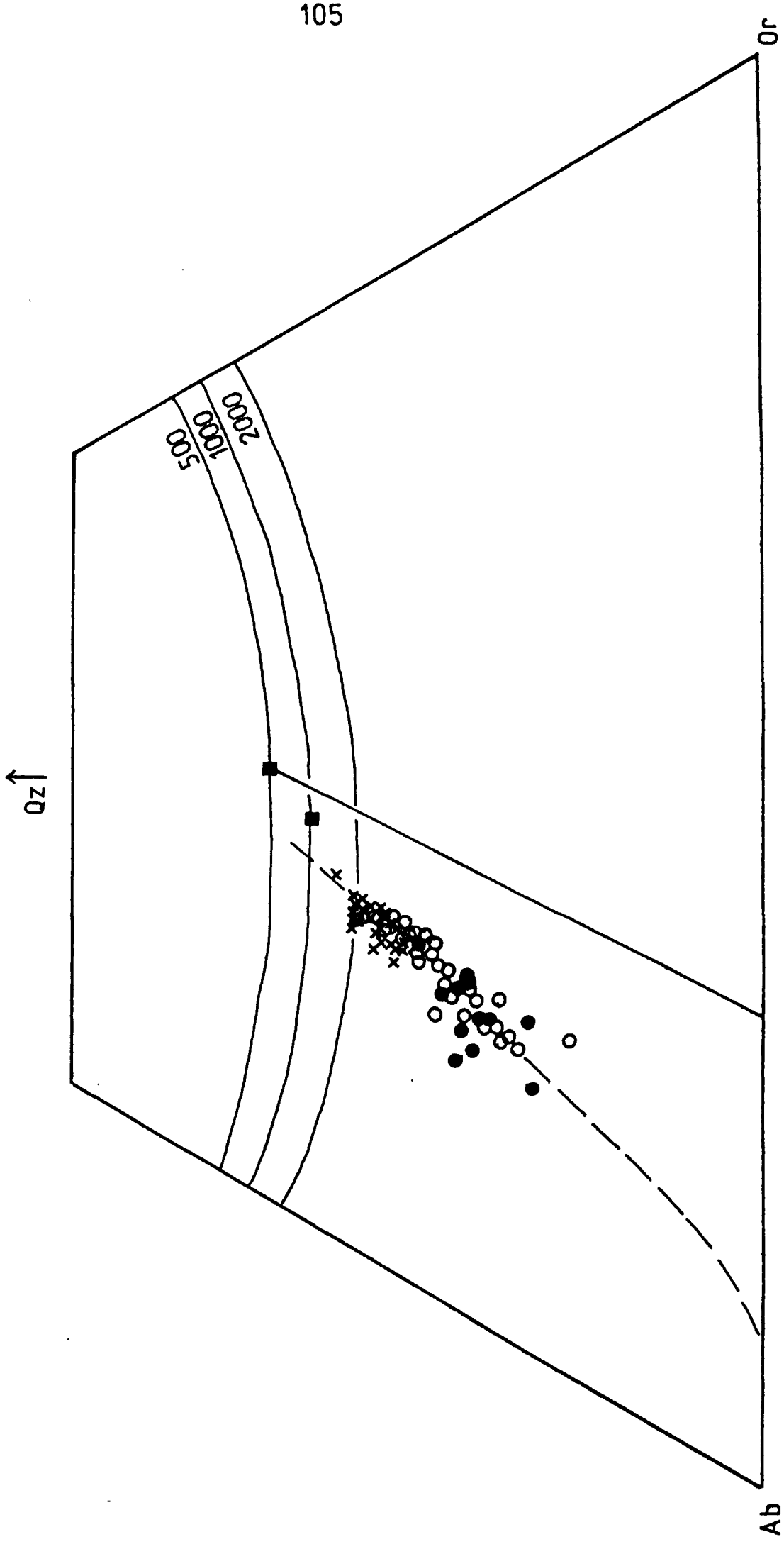
Or
Ab
Qz
500
1000
2000

FIGURE 4.3.

Calcium rich clinopyroxene analyses from Unit B, plotted in the pyroxene quadrilateral. (Diopside-Hedenbergite-Ferrosilite-Enstatite).

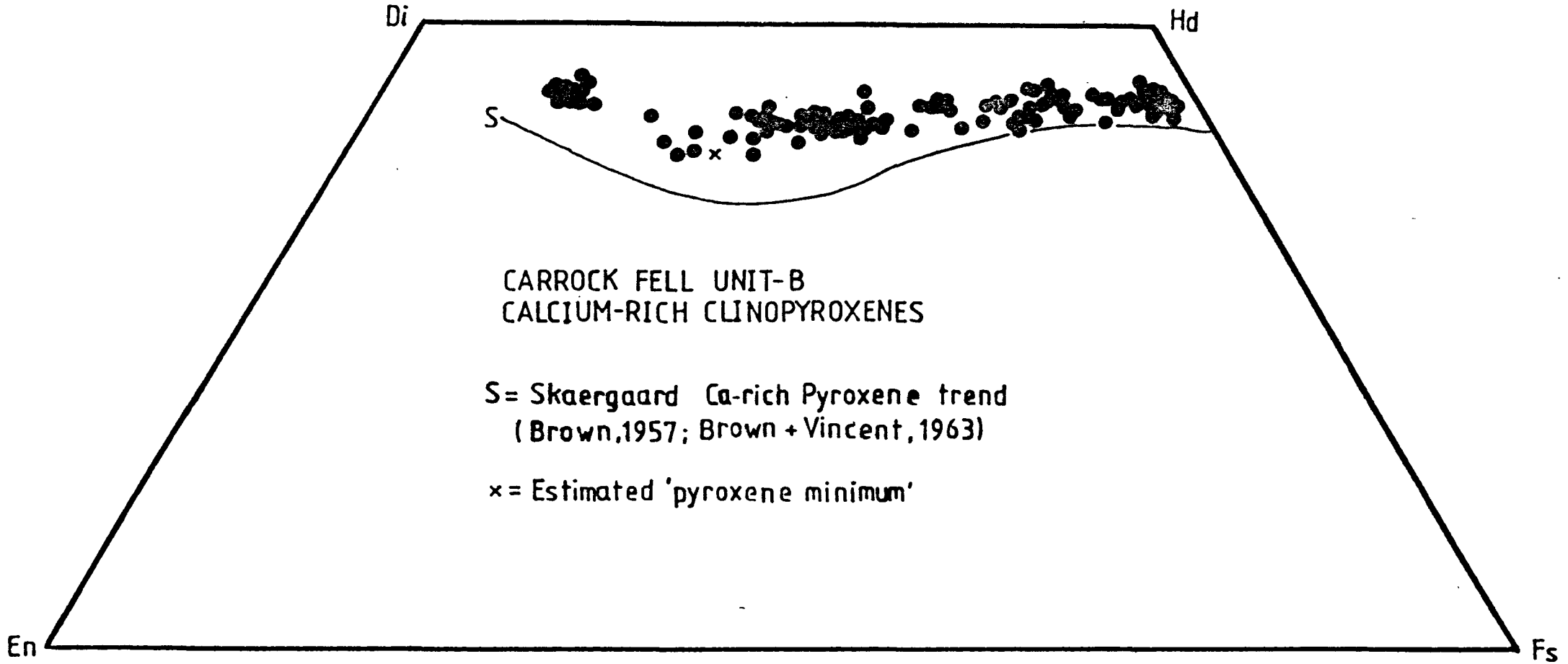

CARROCK FELL UNIT-B
CALCIUM-RICH CLINOPYROXENES

S = Skaergaard Ca-rich Pyroxene trend
(Brown, 1957; Brown + Vincent, 1963)

x = Estimated 'pyroxene minimum'

FIGURE 4.4.

Ca-rich pyroxene analyses, plotted in part of the pyroxene quadrilateral.

A. Subunit B1 (tielines connect analyses from zoned crystals)

B. Subunit B2, traverse 6.

C. Subunit B2, Further Gill Sike region.

D. Subunit B3, traverse 2.

E. Subunit B3, traverse 1.

F. Subunit B3, traverse 5.

G. Subunit B4, traverse 6.

H. Subunit B4, traverse 1.

I. Subunit B4, traverse 5.

J. Subunit B4, traverse 4.

K. Subunit B5.

Dashed line is the Skaergaard trend

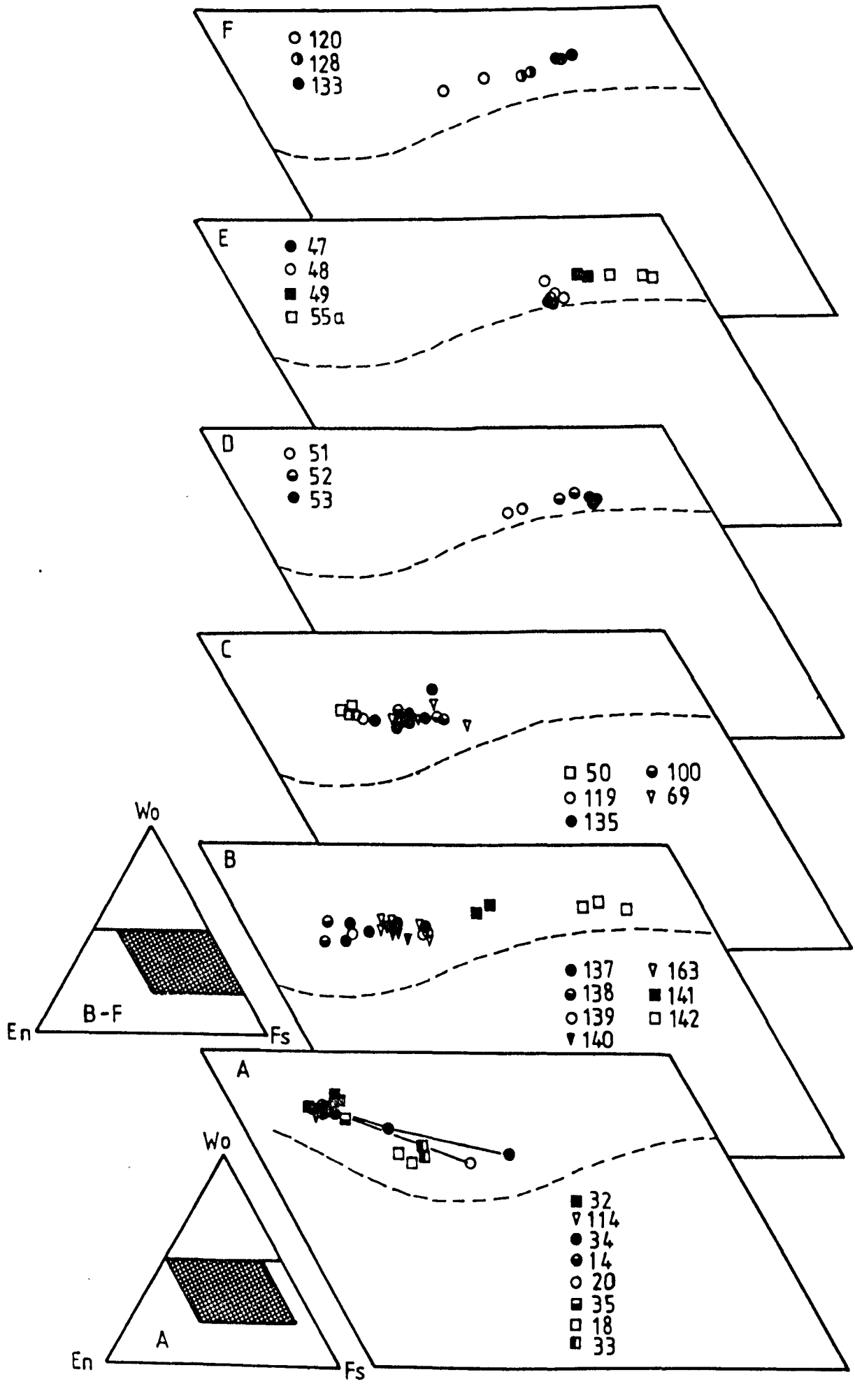
F
120
128
133
E
47
48
49
55a
D
51
52
53
C
50
100
119
69
135
B
137
163
138
141
139
142
140
A
32
114
34
14
20
35
18
33
Wo
En
Fs
B-F
Wo
En
Fs
A

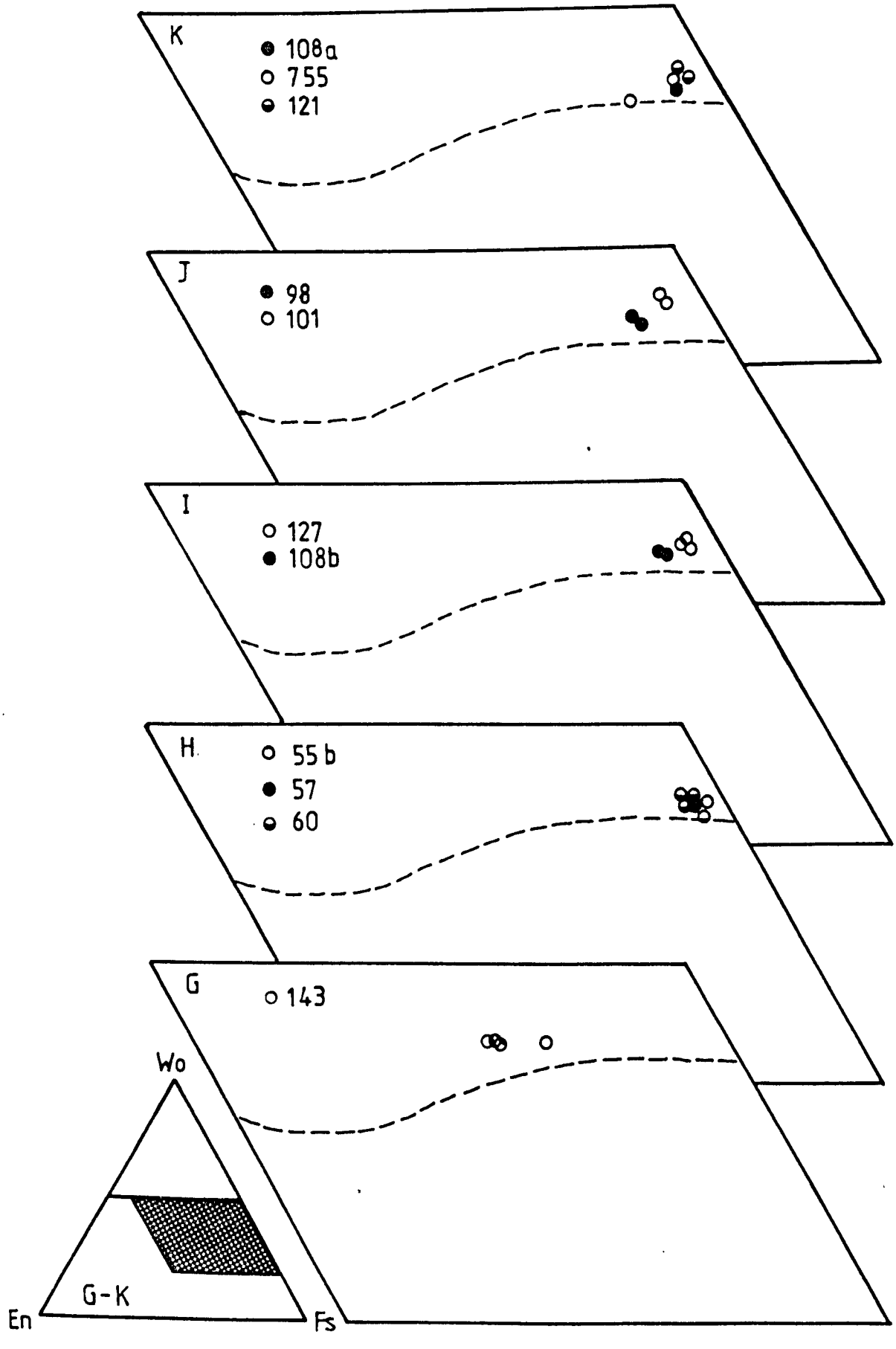
K
108a
755
121
J
98
101
I
127
108b
H
55 b
57
60
G
143
Wo
G-K
En
Fs

FIGURE 4.5.

Pseudobinary phase relations across parts of the pyroxene quadrilateral. Sections S1 and S2 correspond to sections S1 and S2 marked on the pyroxene quadrilateral below. Dashed lines on lower diagram represent hypothetical pyroxene trends.

For explanation see section 4.2.2.

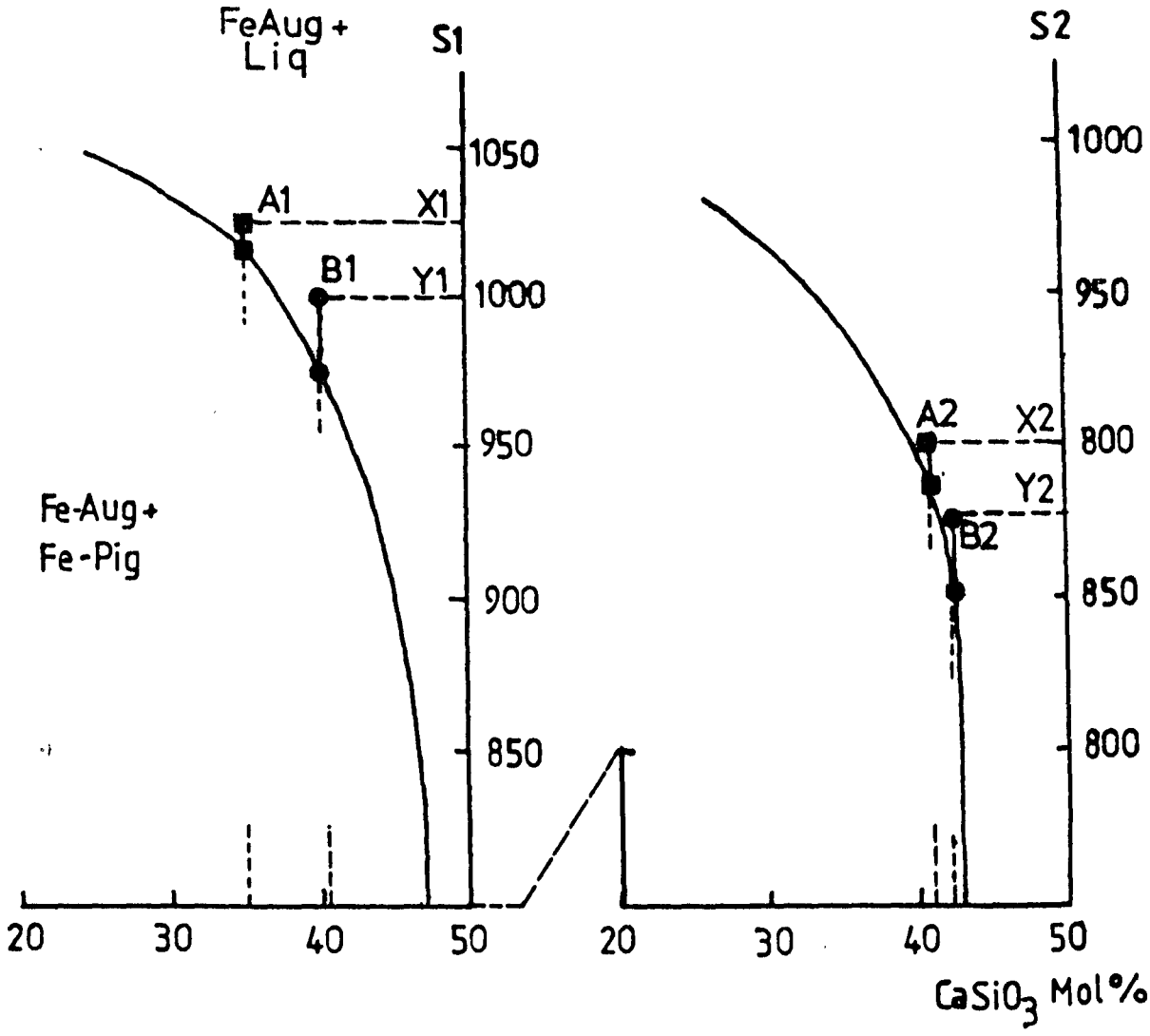
FeAug + Liq
S1
S2
1050
1000
950
900
850
800
A1
X1
B1
Y1
A2
X2
Y2
B2
Fe-Aug +
Fe-Pig
20
30
40
50
CaSiO3 Mol%

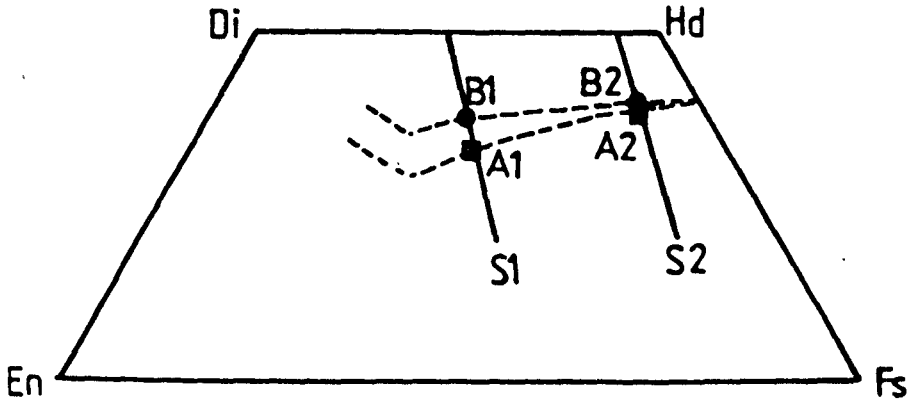
Di
Hd
B1
B2
A1
A2
S1
S2
En
Fs

FIGURE 4.6.

Variation in minor pyroxene components (at%) plotted against 100.Mg/Mg+Fe.

◆ B1; ▽ B2; ● B3; o B4; × B5;

◈ Analyses from prismatic sector of sector zoned pyroxene in B1.

◈ " "non-prismatic " " "

Tie lines join core-margin analyses in single crystals

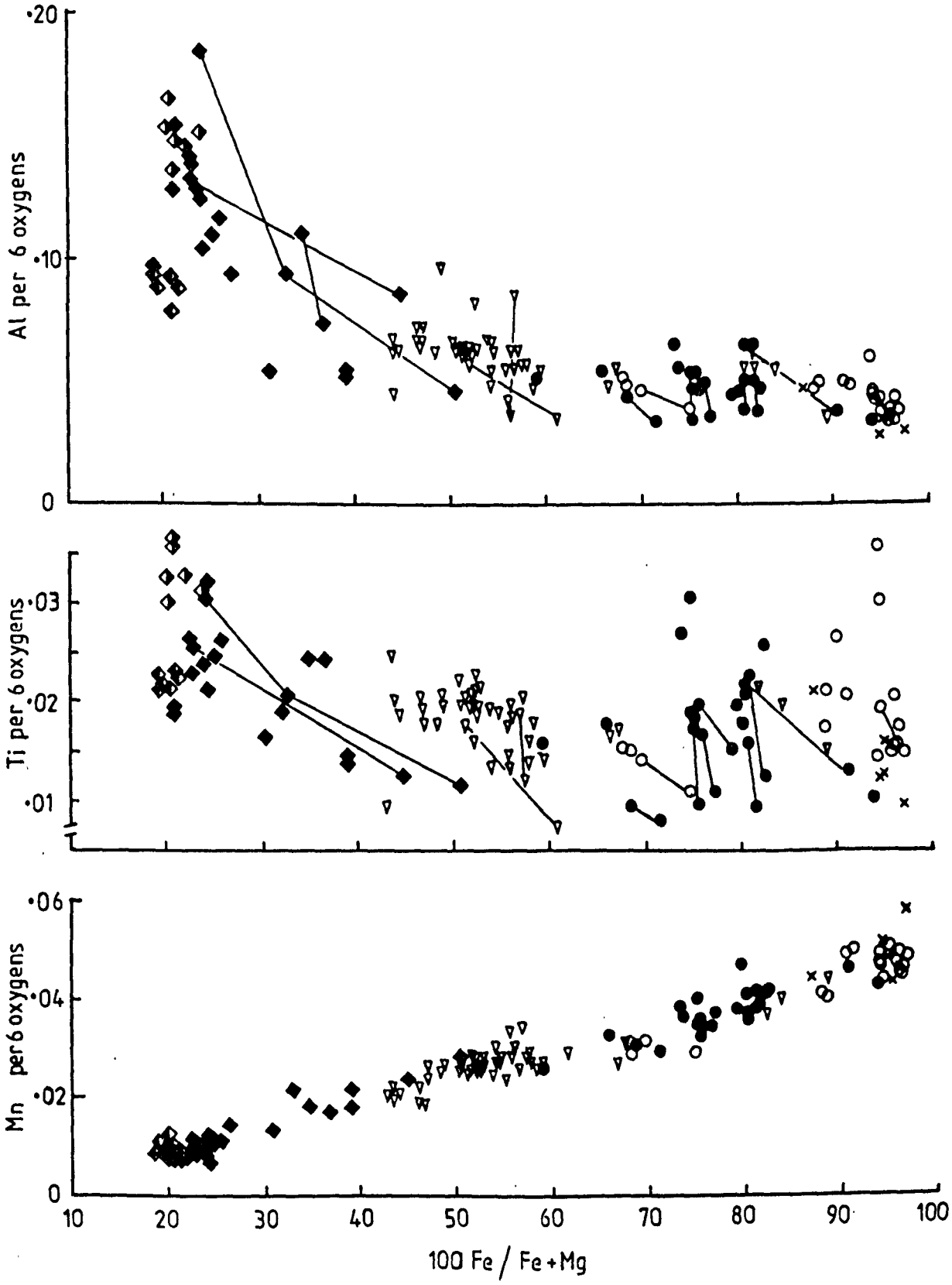
·20
·10
0
Al per 6 oxygens
·03
·02
·01
Ti per 6 oxygens
·06
·04
·02
0
Mn per 6 oxygens
10
20
30
40
50
60
70
80
90
100
100 Fe / Fe+Mg

FIGURE 4.7.

a) Si v. Al (At%) for pyroxenes from Unit B.

b) Al v. Ti (At%) for pyroxenes from Unit B.

Solid lines surround fields for each subunit and are for clarity only.

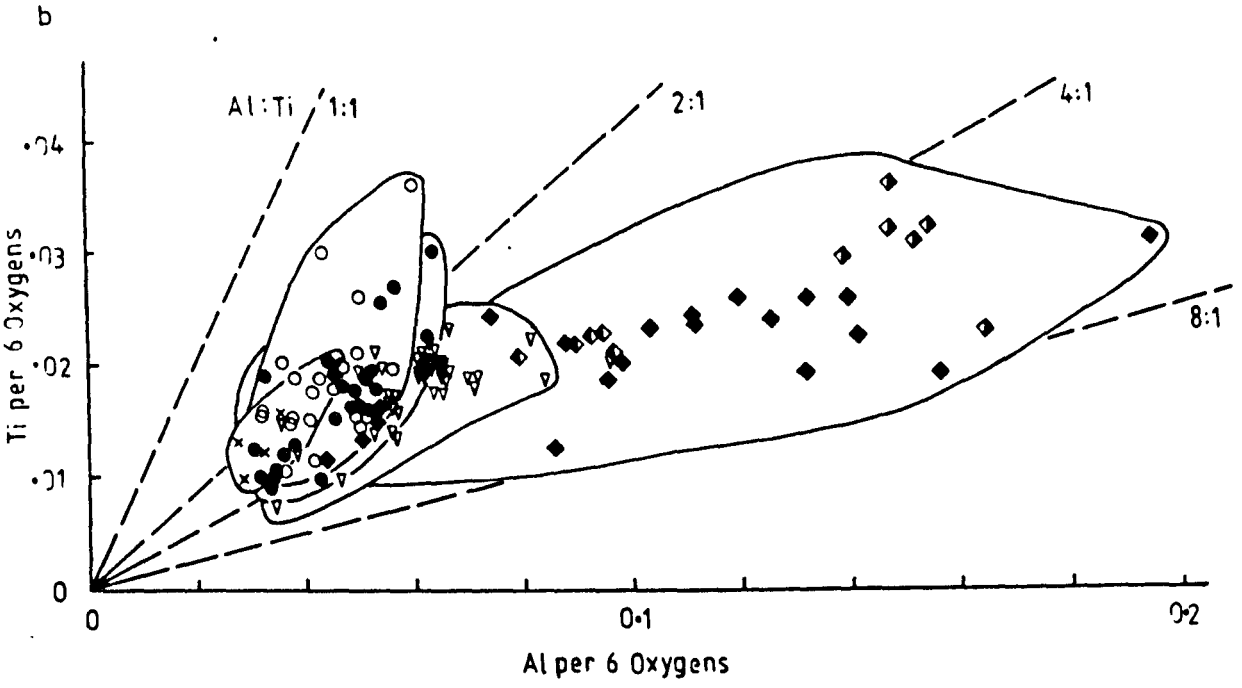
b
Al:Ti 1:1
2:1
4:1
8:1
·04
·03
·02
·01
0
Ti per 6 Oxygens
0
0·1
0·2
Al per 6 Oxygens

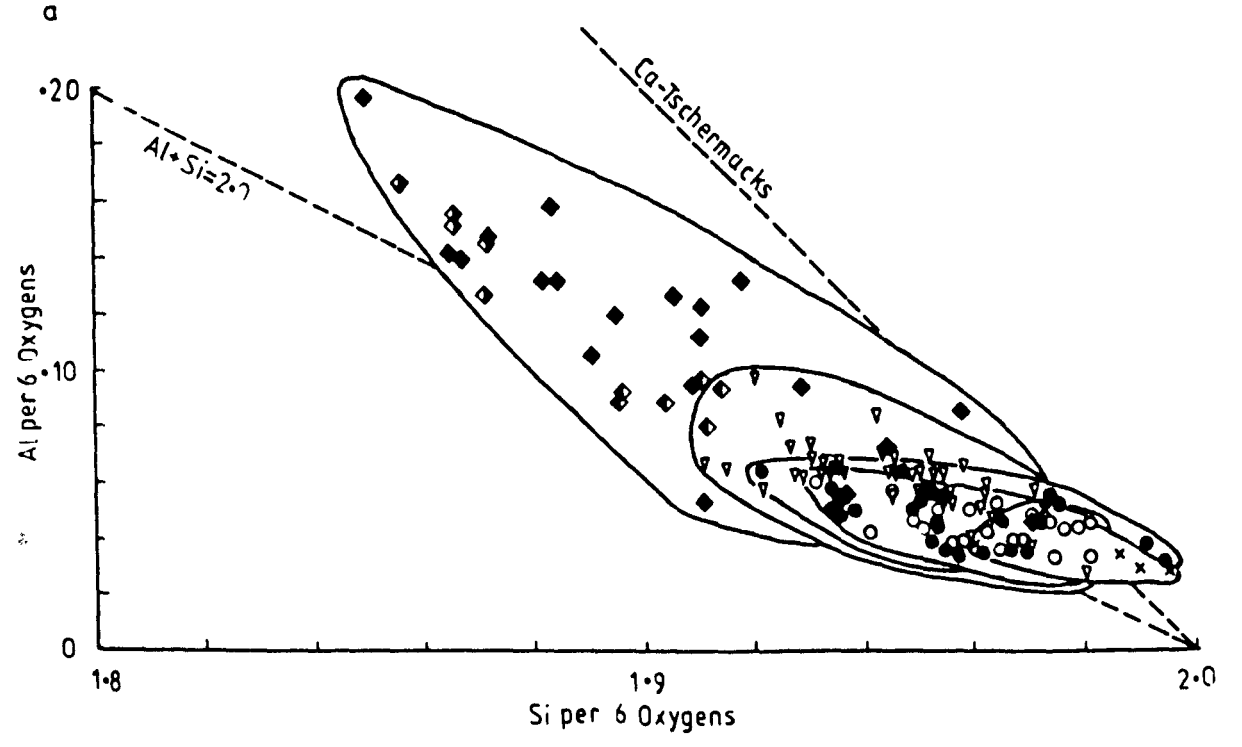
a
·20
·10
0
Al per 6 Oxygens
Ca-Tschermacks
1·8
1·9
2·0
Si per 6 Oxygens

FIGURE 4.8.

Sketches of sector zoned pyroxenes from Sample 32, Subunit B1. Stippled sector is prismatic sector. Numbered points are analysed points. Analyses appear in Appendix two .
(inclusions are of ilmenite and plagioclase).

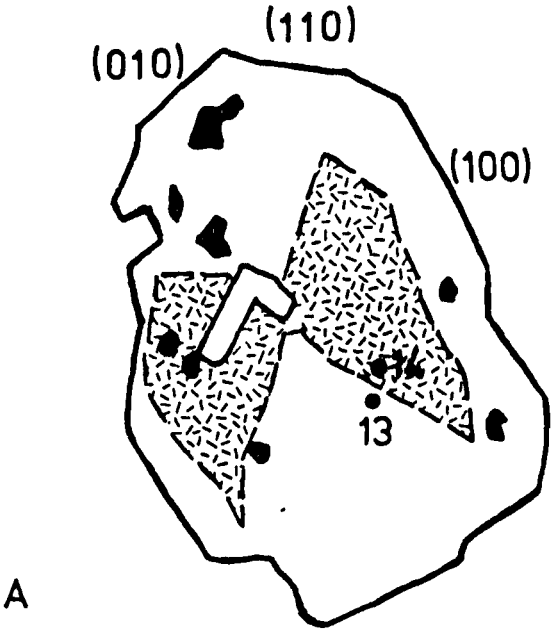

A

1mm.

B

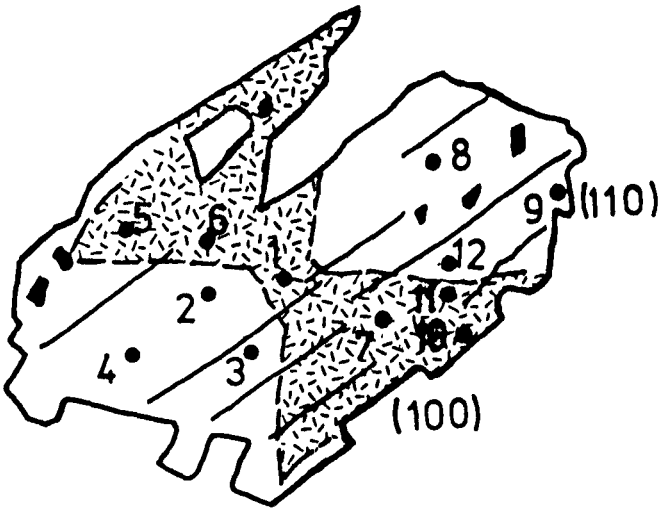

FIGURE 4.9.

Plagioclase-Ca-rich pyroxene relationships in Unit B. Symbols as in figure 4.1, with additional optically determined plagioclases numbered.

Dashed line indicates postulated 'magmatic' trend

Trends Sk. and Pal. are Skaergaard trend (Wager and Brown, 1968) and Palisades trend (Walker et al., 1973) respectively.

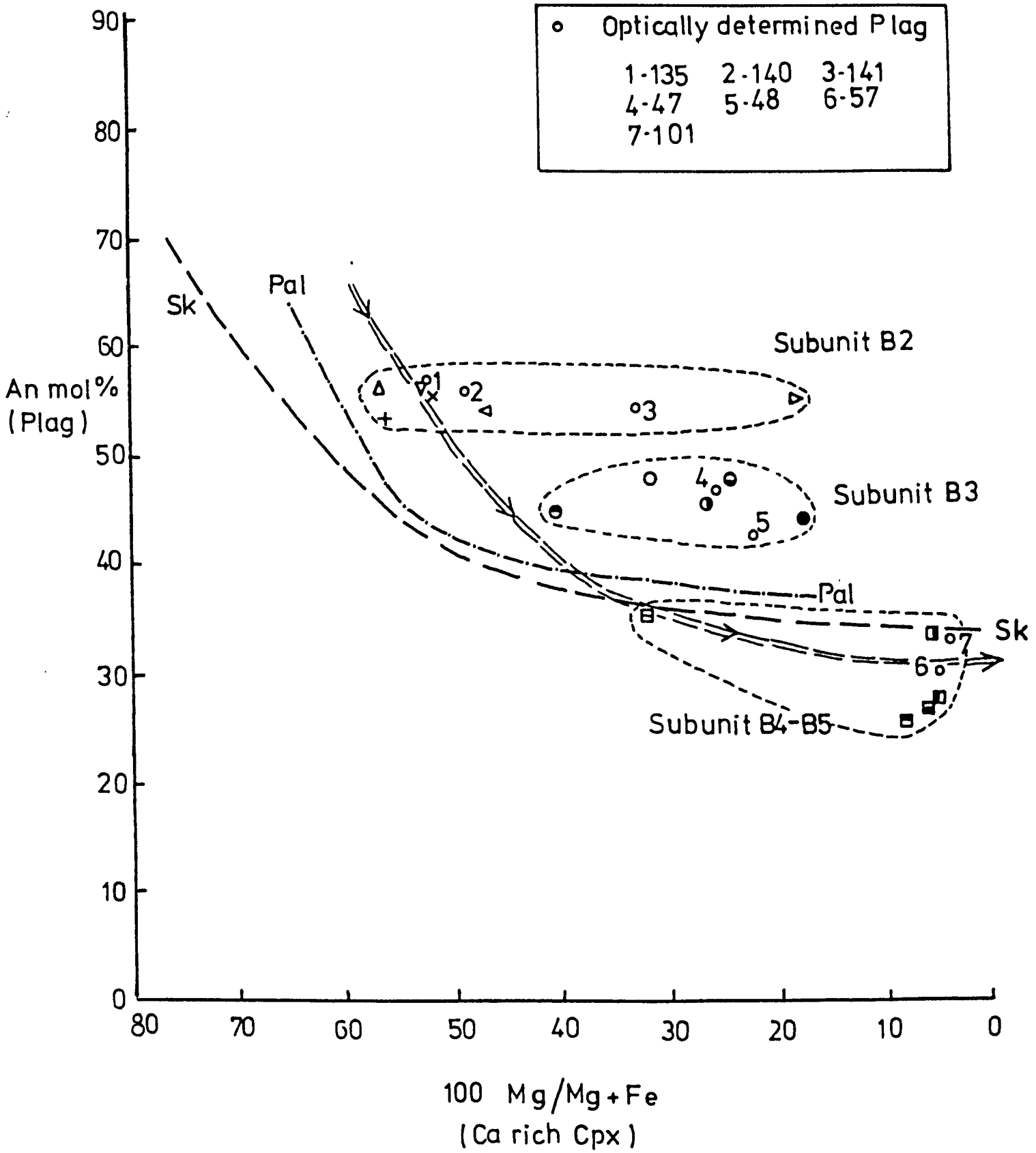
Optically determined Plag
1-135 2-140 3-141
4-47 5-48 6-57
7-101
Sk
Pal
Subunit B2
Subunit B3
Pal
Sk
Subunit B4-B5
An mol%
(Plag)
100 Mg/Mg+Fe
(Ca rich Cpx)
90
80
70
60
50
40
30
20
10
0
80
70
60
50
40
30
20
10
0

FIGURE 4.10.

Plot of tetrahedrally coordinated Al (Al^{IV}) v. A-site occupancy for analysed amphiboles of Unit B with all Fe as FeO (A), and some Fe recalculated to Fe_2O_3 (B), by method of Leake (1978).

Symbols as in figure 4.12.

Ts = Tschermakite

Pa = Pargasite

Ed = Edenite

Tr = Tremolite

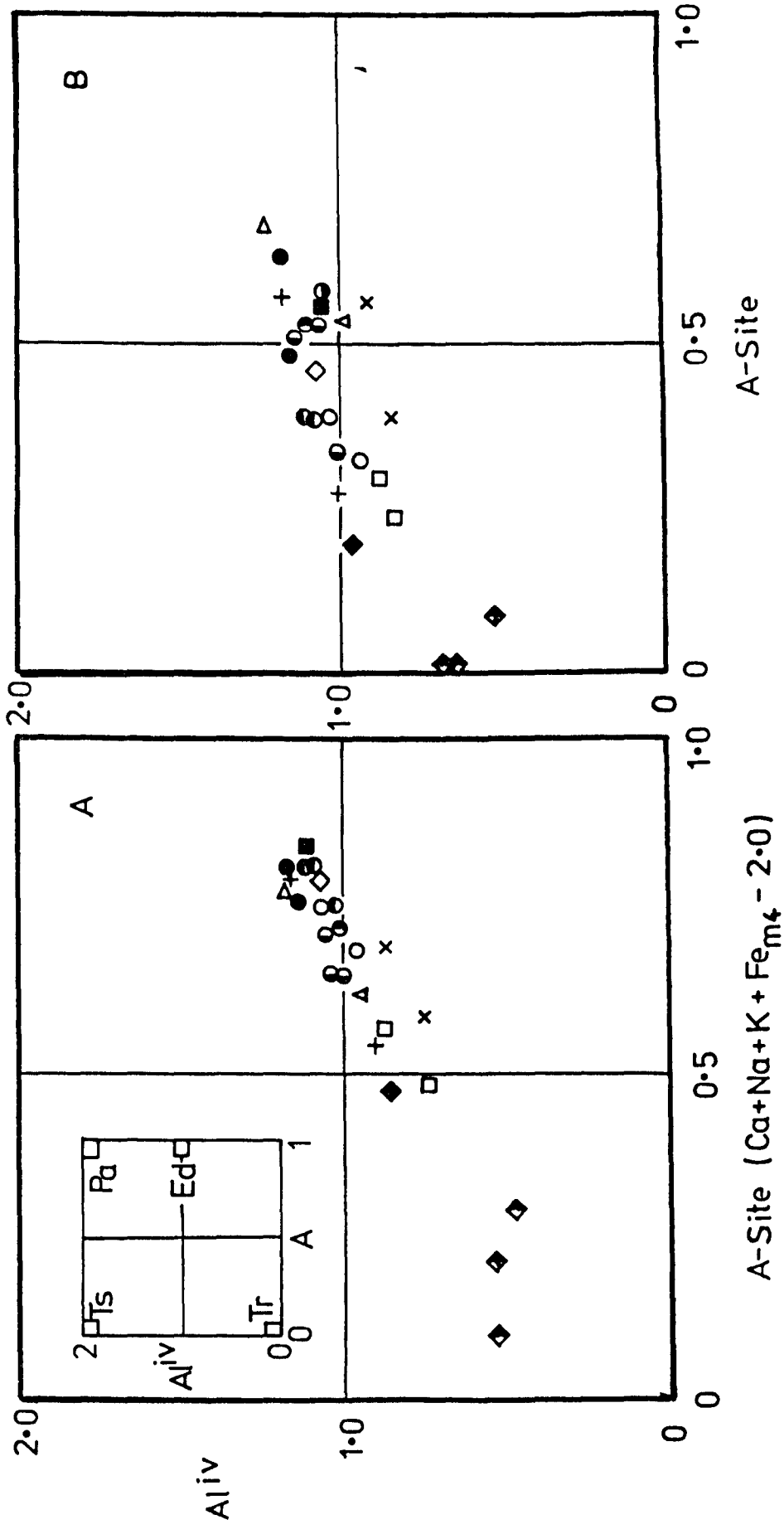
A
B
2·0
1·0
0
0·5
1·0
Al^{iv}
A-Site (Ca+Na+K+Fe_{m4} - 2·0)
A-Site
Ts
Pa
Ed
Tr
A
Al^{iv}
2
0
1

FIGURE 4.11.

Amphibole analyses plotted in classification diagrams of Leake (1978).

A and B show all Fe as FeO

C and D have some Fe recalculated as Fe_2O_3.

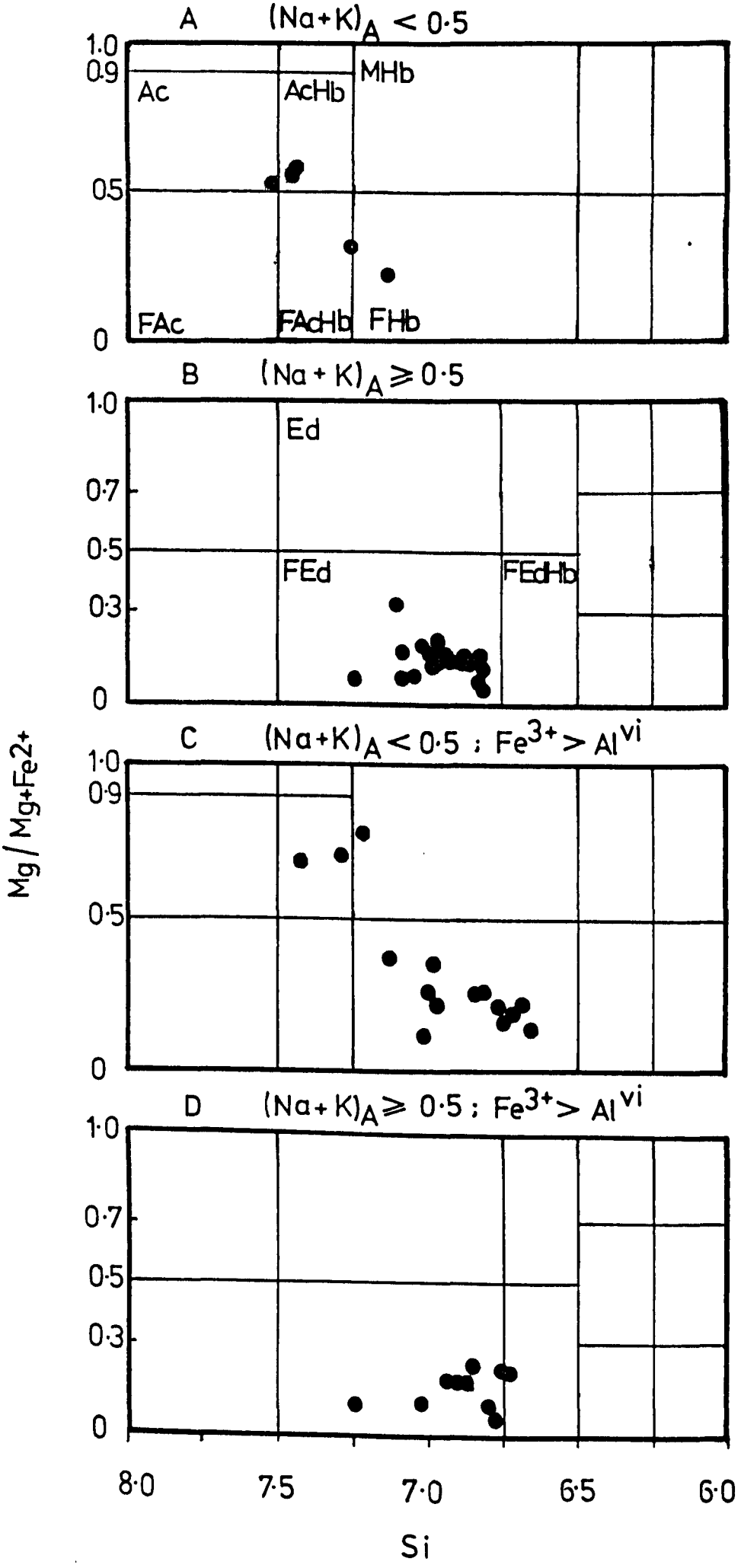
A (Na+K)A < 0·5
1.0
0.9
0.5
0
Ac
AcHb
MHb
FAc
FAcHb
FHb
B (Na + K)A ≥ 0·5
1·0
0·7
0·5
0·3
0
Ed
FEd
FEdHb
C (Na+K)A < 0·5 ; Fe3+ > AlVI
1·0
0·9
0·5
0
D (Na+K)A ≥ 0·5 ; Fe3+ > AlVI
1·0
0·7
0·5
0·3
0
8·0
7·5
7·0
6·5
6·0
Si
Mg / Mg+Fe2+

FIGURE 4.12.

Analysed amphibole analyses from Unit B, plotted in part of the ternary system Ca-Mg-(Fe+Mn). Also plotted are coexisting pyroxene analyses (upper symbols) with adjoining tie lines
All Fe is FeO.

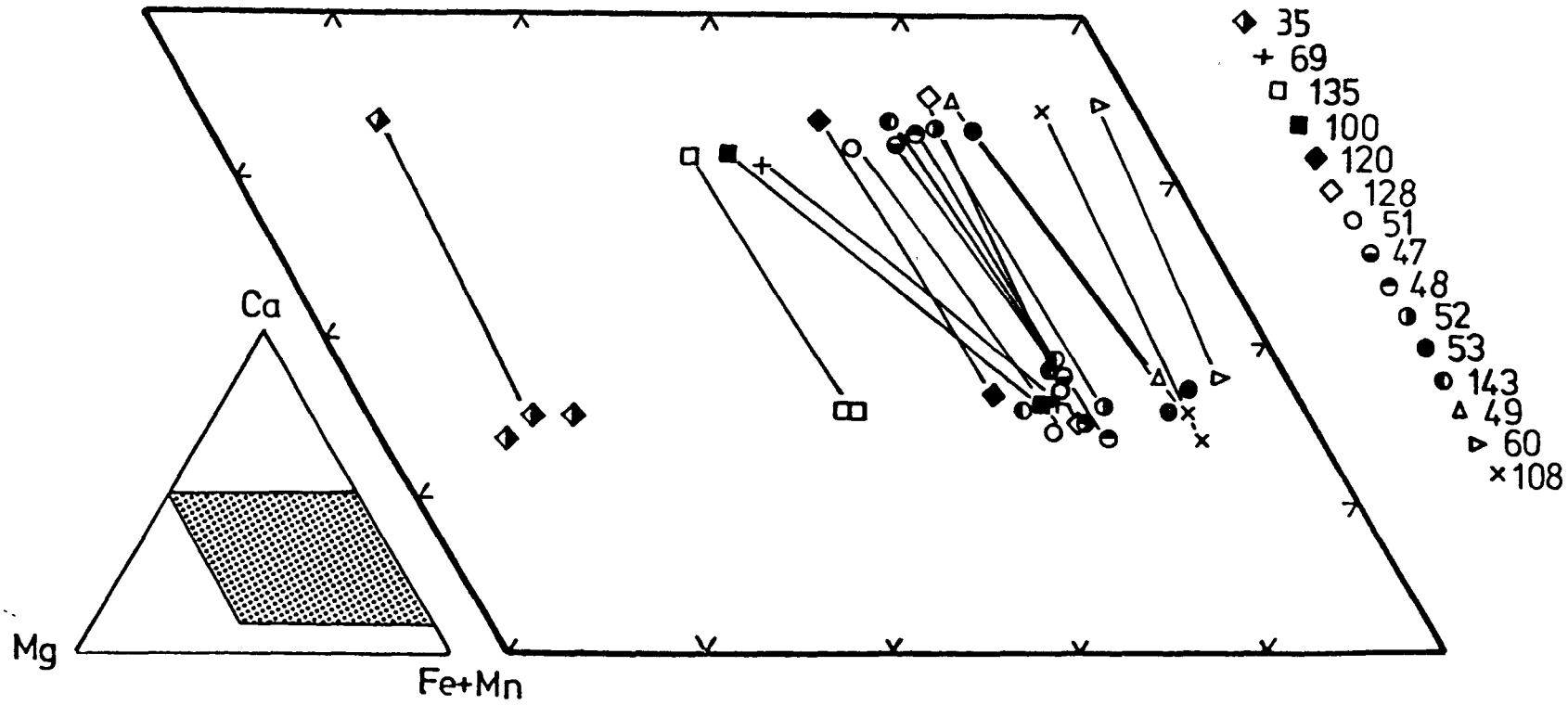
Ca
Mg
Fe+Mn
35
69
135
100
120
128
51
47
48
52
53
143
49
60
108

FIGURE 4.13.

Si v (Ca + Na + K) for analysed amphiboles from Unit B.

Dashed line indicates limit of igneous amphibole compositions (Leake, 1971). Enclosed areas are compositions of amphiboles from Dodge et al (1968), and Haslam (1968).

Ts = Tschermakite

Pa = Pargasite

Ed = Edenite

Tr = Tremolite

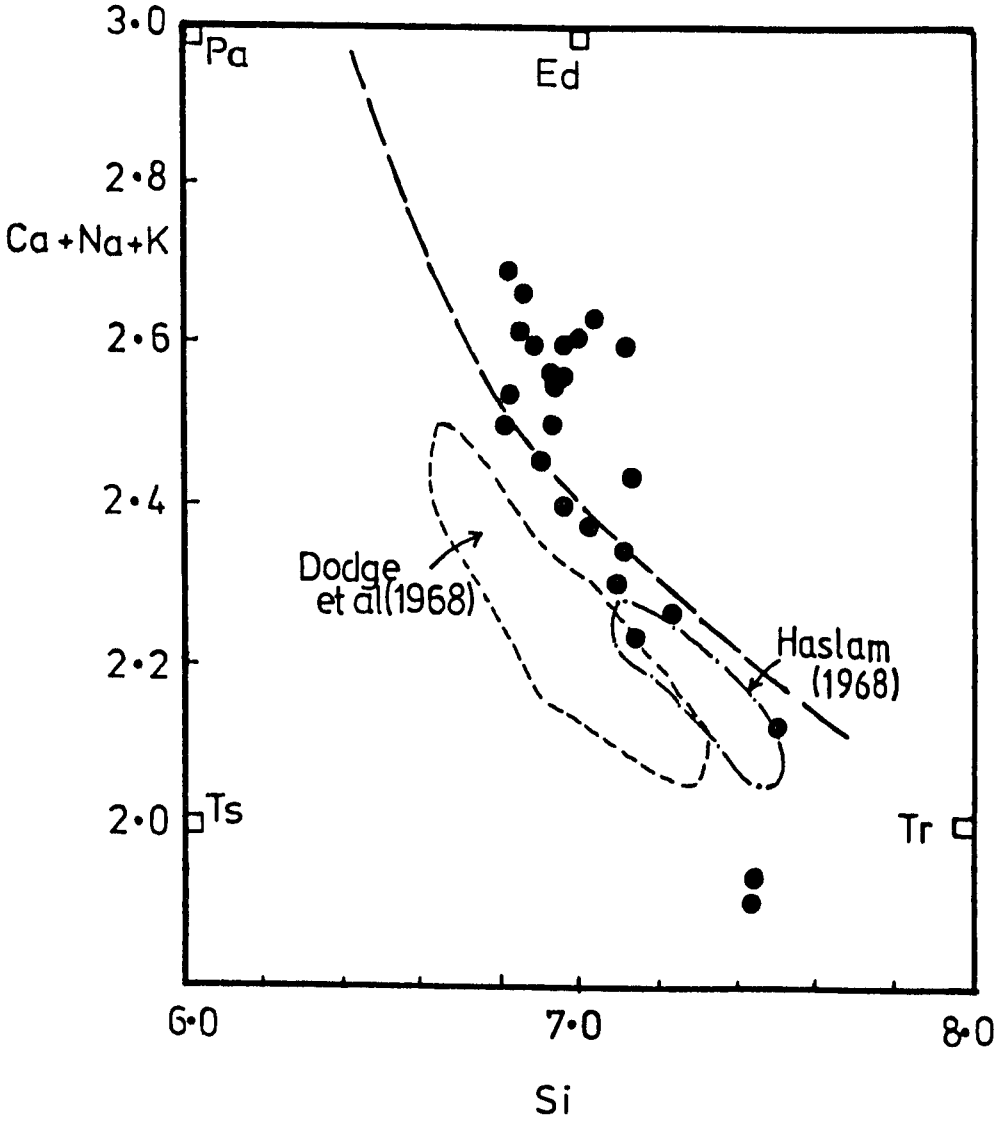
3·0
2·8
2·6
2·4
2·2
2·0
Ca+Na+K
Pa
Ed
Ts
Tr
Dodge et al(1968)
Haslam (1968)
6·0
7·0
8·0
Si

FIGURE 4.14.

Analysed ilmenite and titanomagnetite analyses, recalculated by method of Carmichael (1967), plotted in ternary diagram Fe_2O_3-FeO-TiO_2
Tie lines join coexisting rhombohedral and spinel phases.

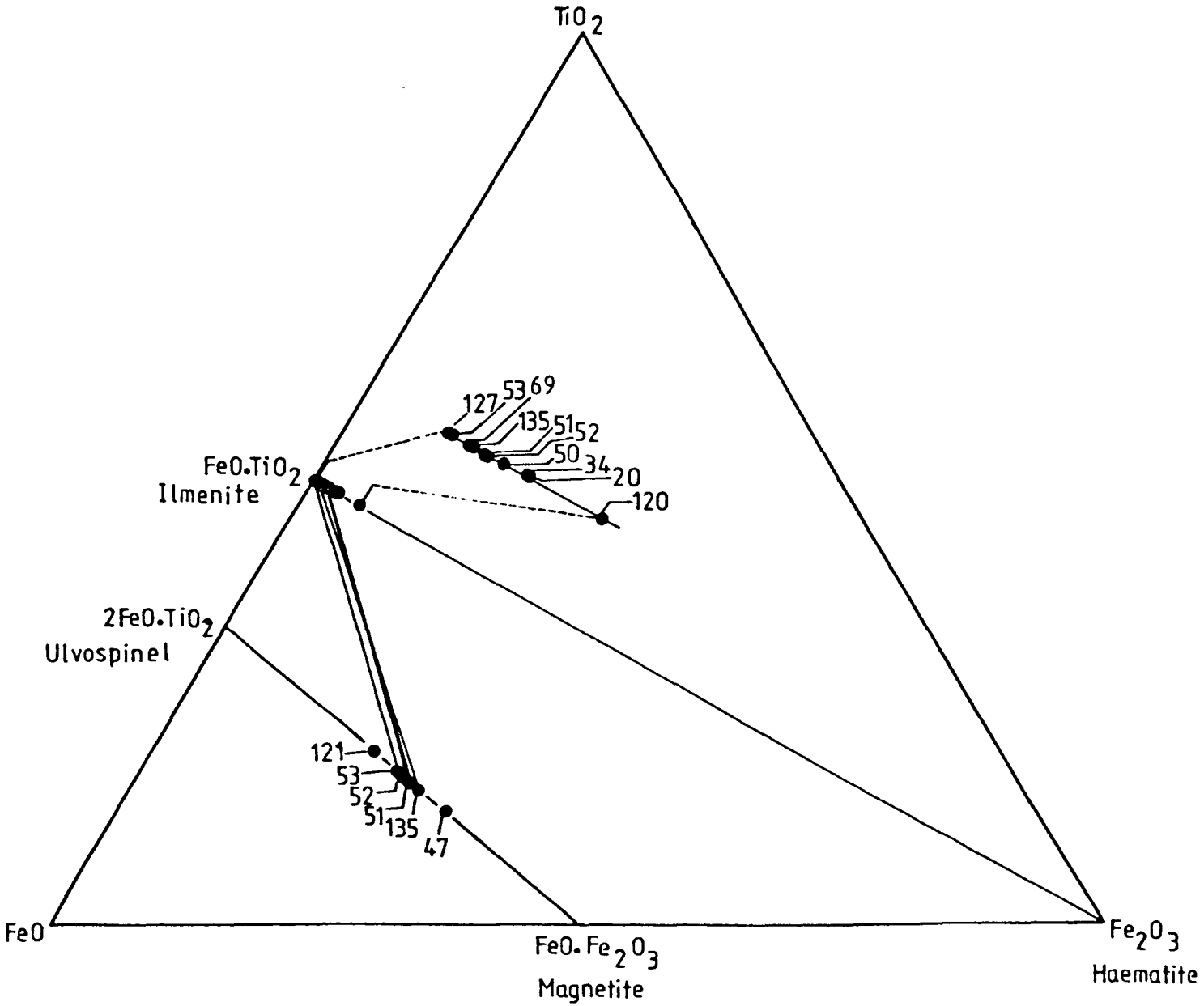
TiO2
FeO.TiO2
Ilmenite
2FeO.TiO2
Ulvospinel
FeO
FeO.Fe2O3
Magnetite
Fe2O3
Haematite
127
53
69
135
51
52
50
34
20
120
121
53
52
51
135
47

FIGURE 4.15.

Compositions of coexisting ilmenite-haematite$_{SS}$ and magnetite-ulvospinel$_{SS}$, projected onto the fO_2-temperature plane. (Buddington and Lindsley, 1964). Dashed lines are experimentally determined buffer curves from Eugster and Wones (1962).
HM = Haematite-magnetite; QFM = Quartz-magnetite-fayalite; MW = Magnetite-wustite.

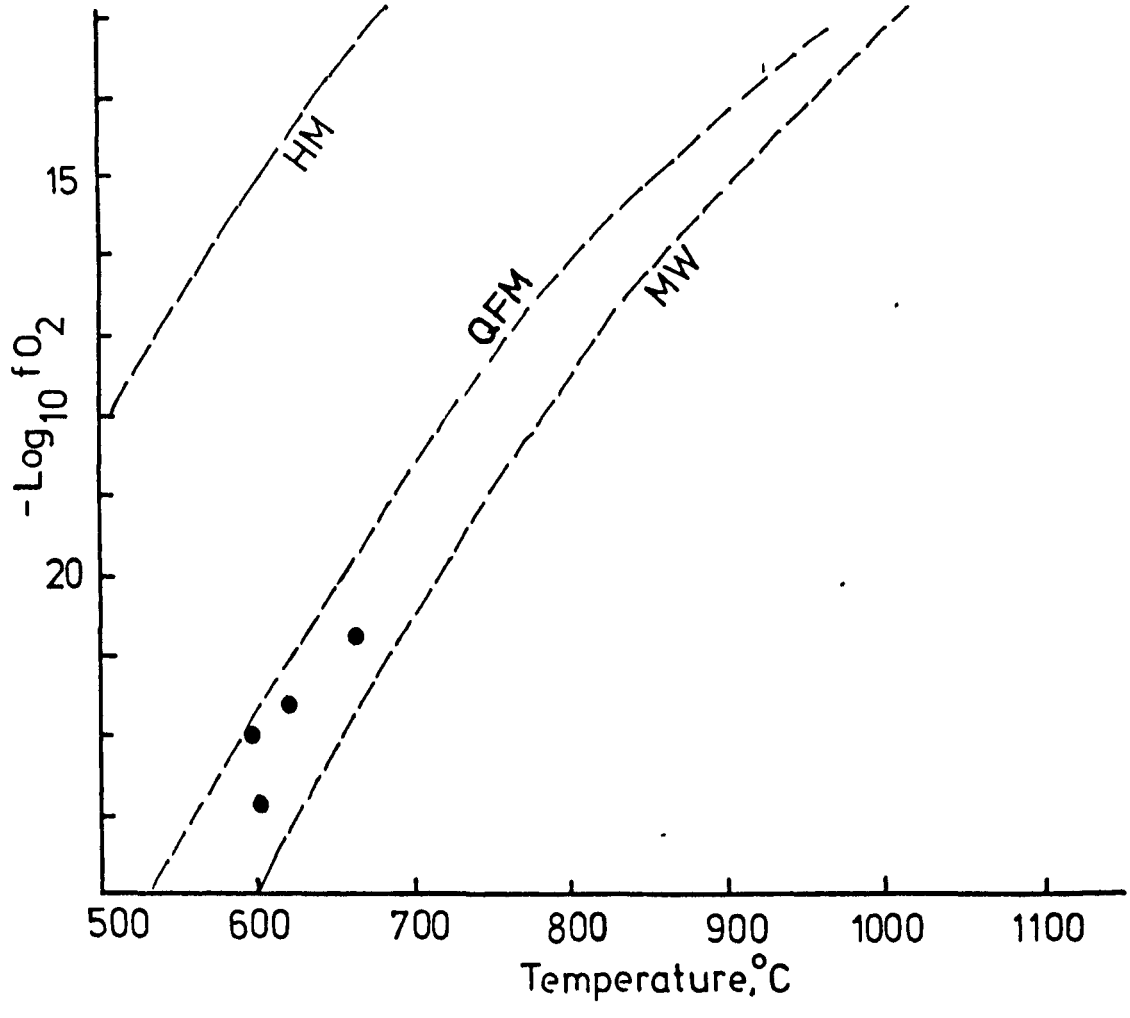
HM
QFM
MW
15
20
$-\mathrm{Log}_{10}\,fO_2$
500
600
700
800
900
1000
1100
Temperature, °C

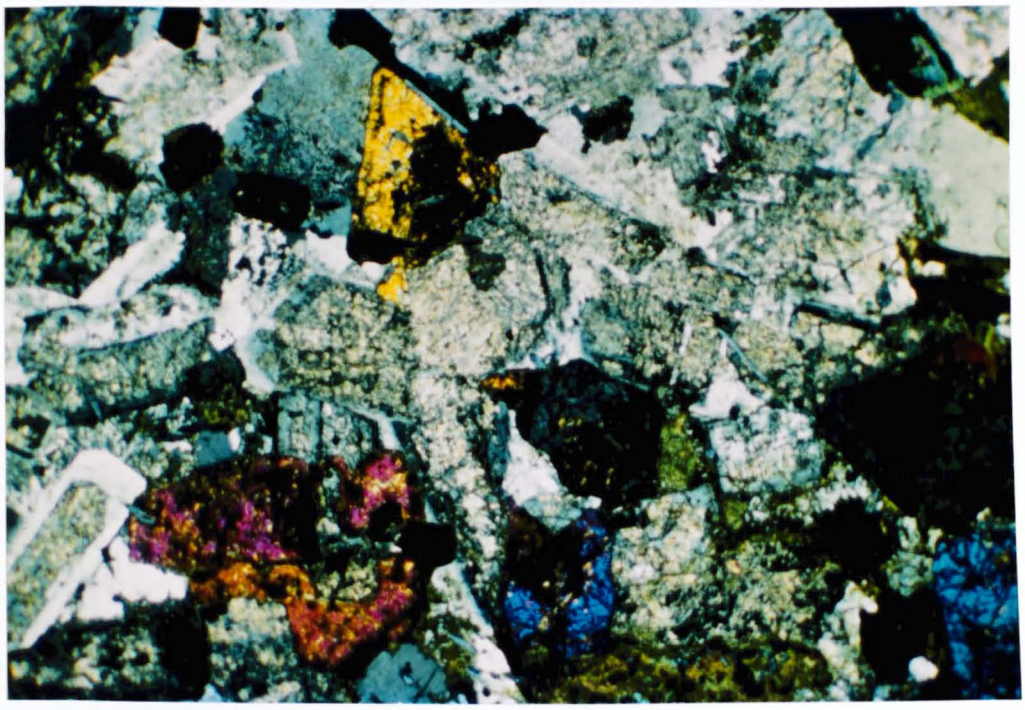

PLATE 4.1 Photomicrograph : Subunit B2 Plagioclase augite - oxide - apatite ferrograbbro.
(50. XP. Width of field - 8 mm).

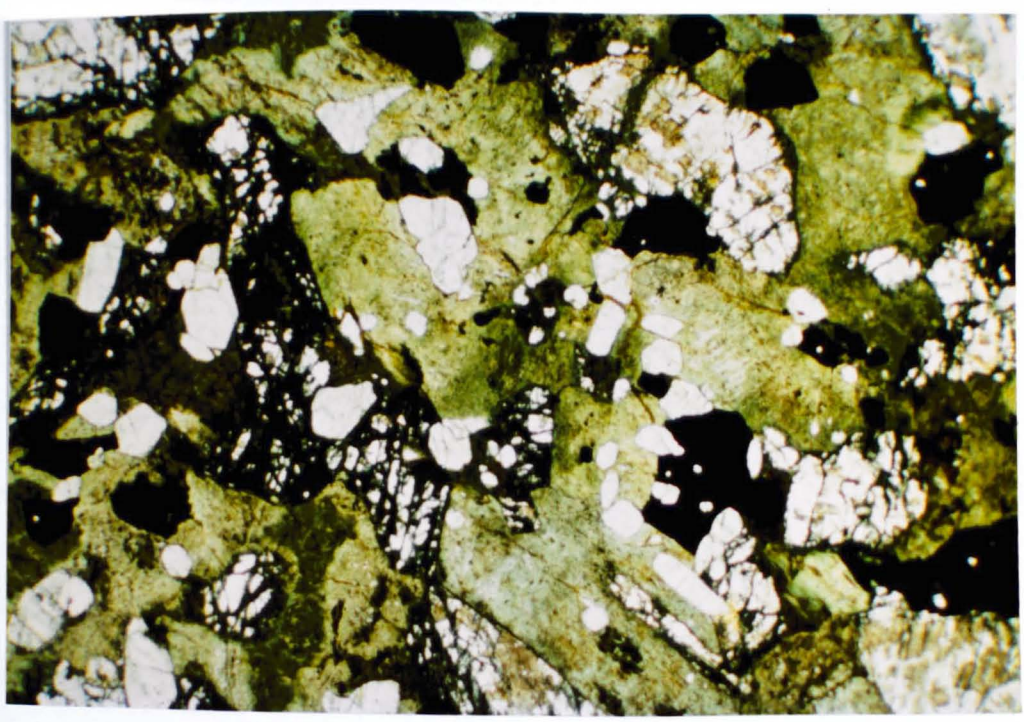

PLATE 4.2 Photomicrograph : Subunit B2 Apatite - oxide rich ferrograbbro. Both plagioclase and pyroxene are pseudomorphed by amphibole.
(44. PP. Width of field - 8 mm).

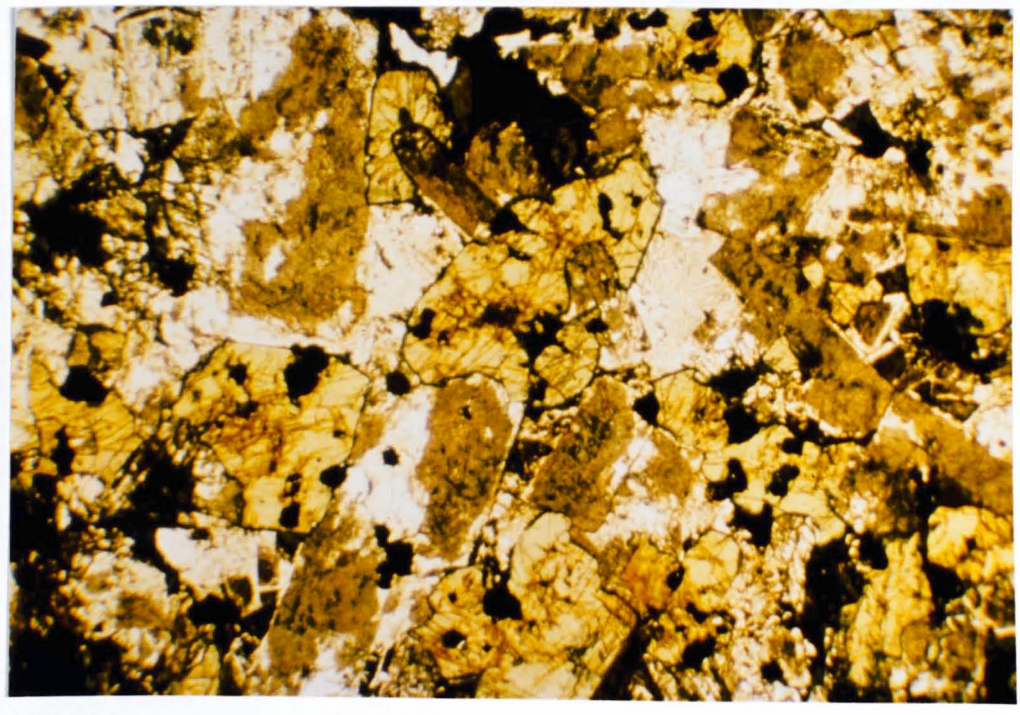

PLATE 4.3 Photomicrograph : Subunit B3 Plagioclase - ferroaugite - oxide ferrodiorite
(120. PP. Width of field - 7 mm).

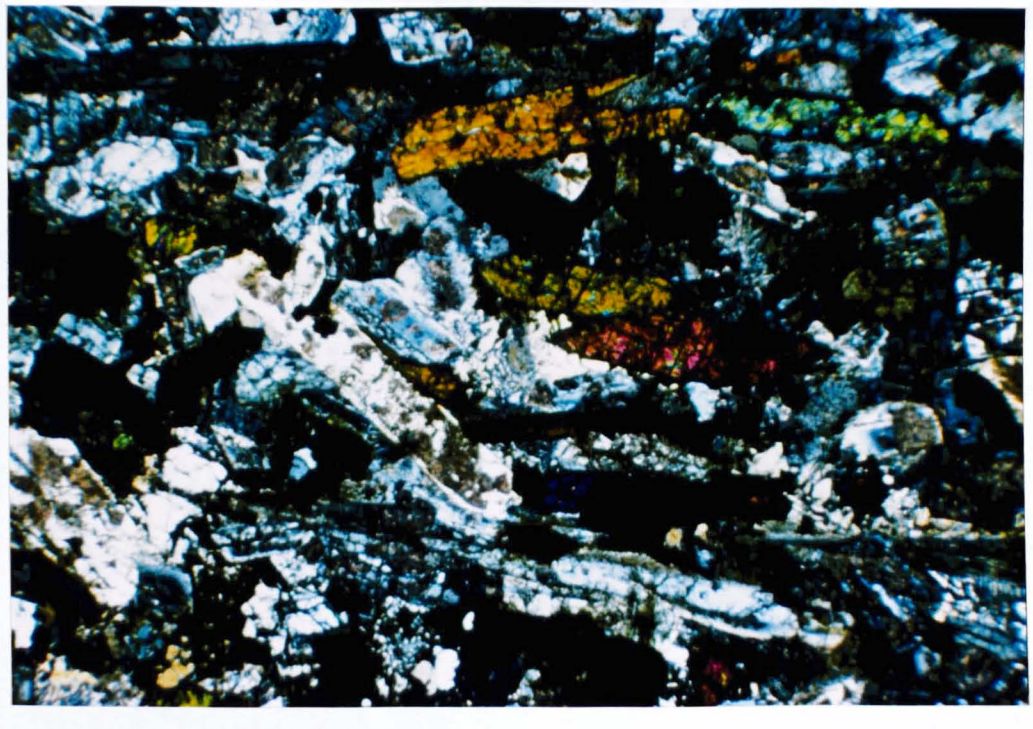

PLATE 4.4 Photomicrograph : Subunit B3. Laminated plagioclase - ferroaugite - oxide ferrodiorite
(47. XP. Width of field - 8 mm).

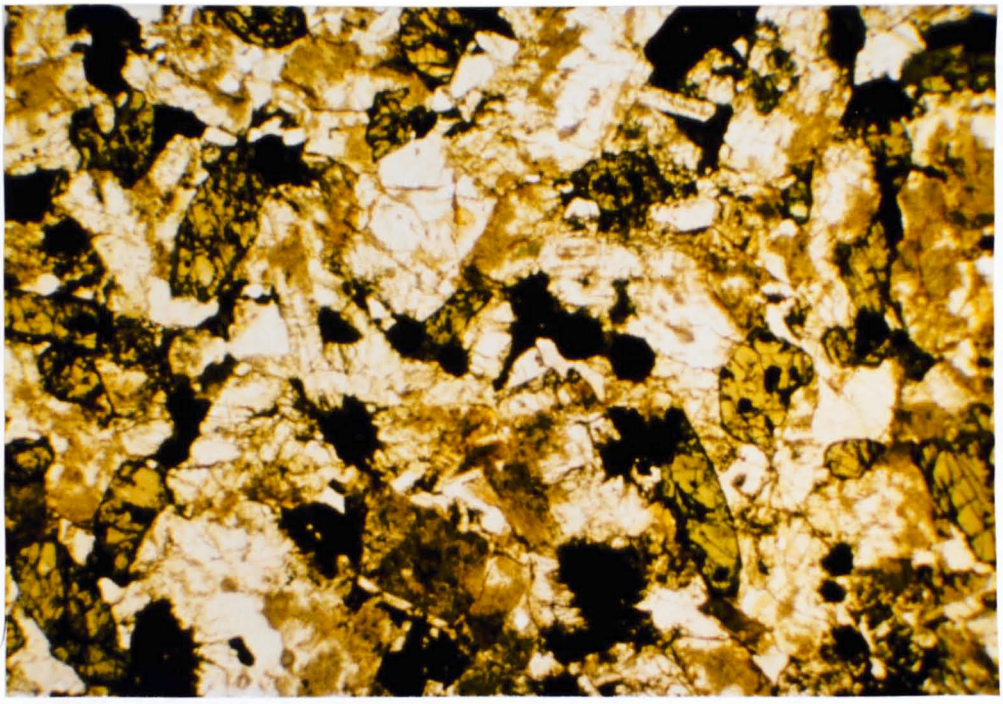

PLATE 4.5 Photomicrograph : Subunit B4. Plagioclase - ferrohedenbergite - oxide ferrogranophyre.
(127. PP. Width of field - 8 mm)

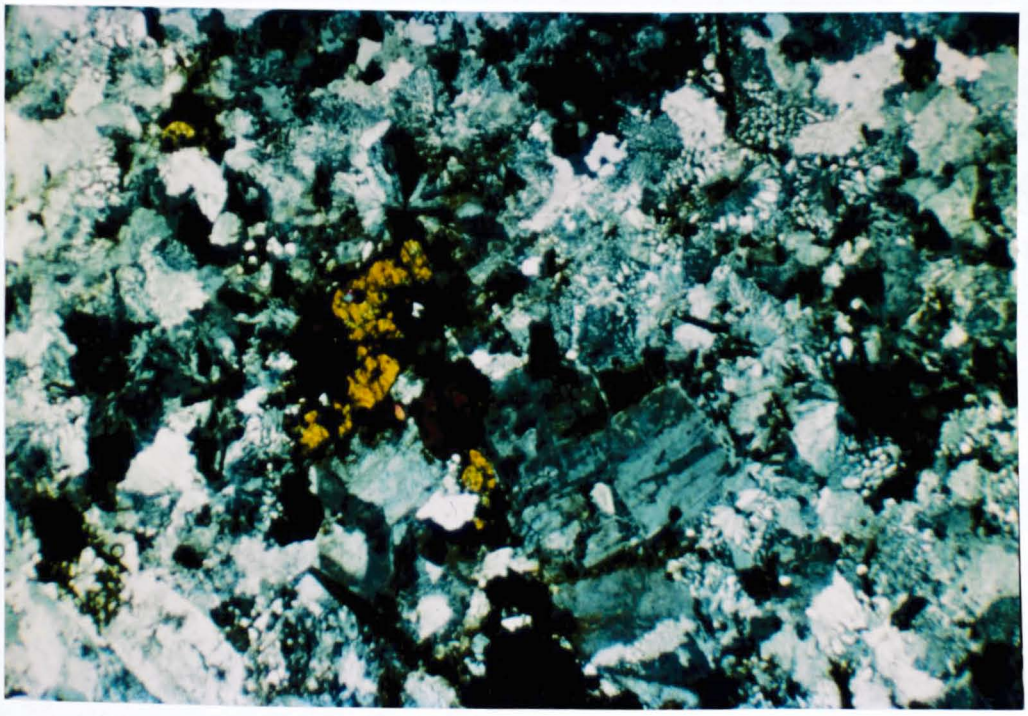

PLATE 4.6 Photomicrograph : Subunit B5. Porphyritic cluster of ferrohedenbergite - plagioclase - magnetite crystals in sub-sperulitic granophyre. Note also highly birefringent zircon crystals to the left of centre.
(16184. XP. Width of field - 8 mm)

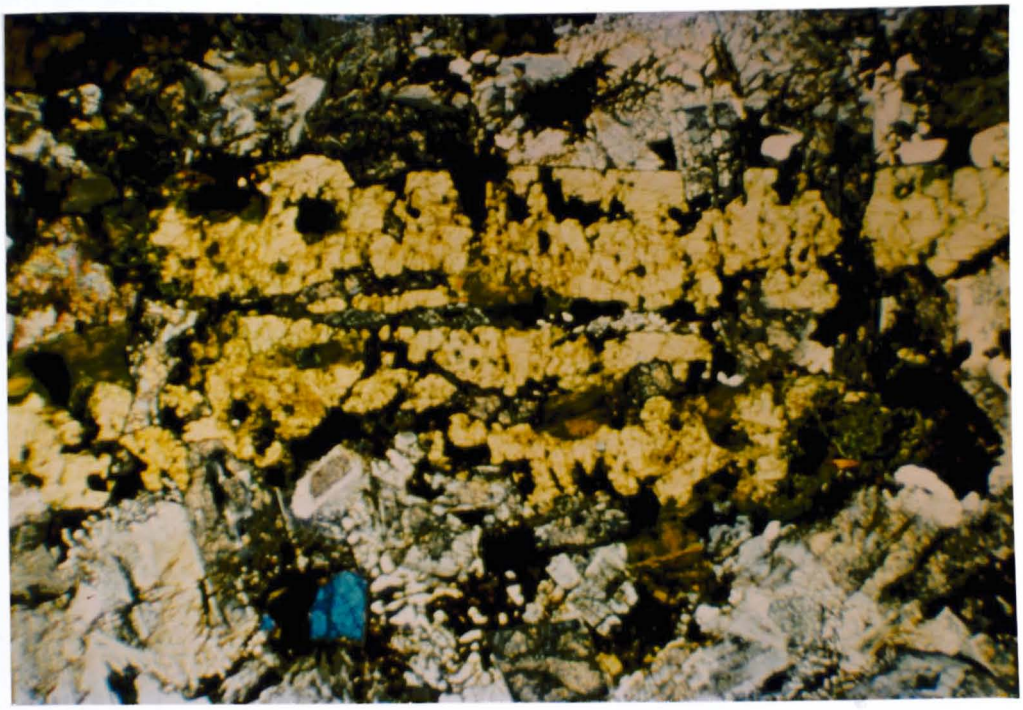

PLATE 4.7a Photomicrograph : Elongate skeletal, subophitic ferroaugite in subunit B3. (48. XP. Width of field - 8 mm).

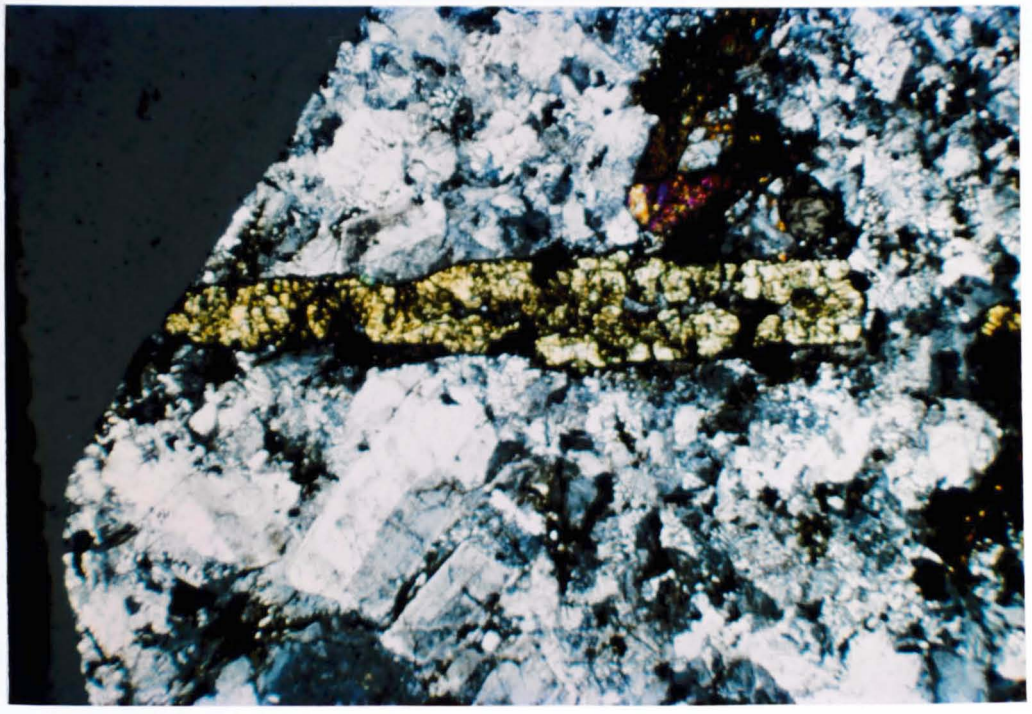

PLATE 4.7b Photomicrograph : Elongate, skeletal, subophitic ferrohedenbergite in subunit B5 granophyre. (16184. XP. Width of field -8 mm).

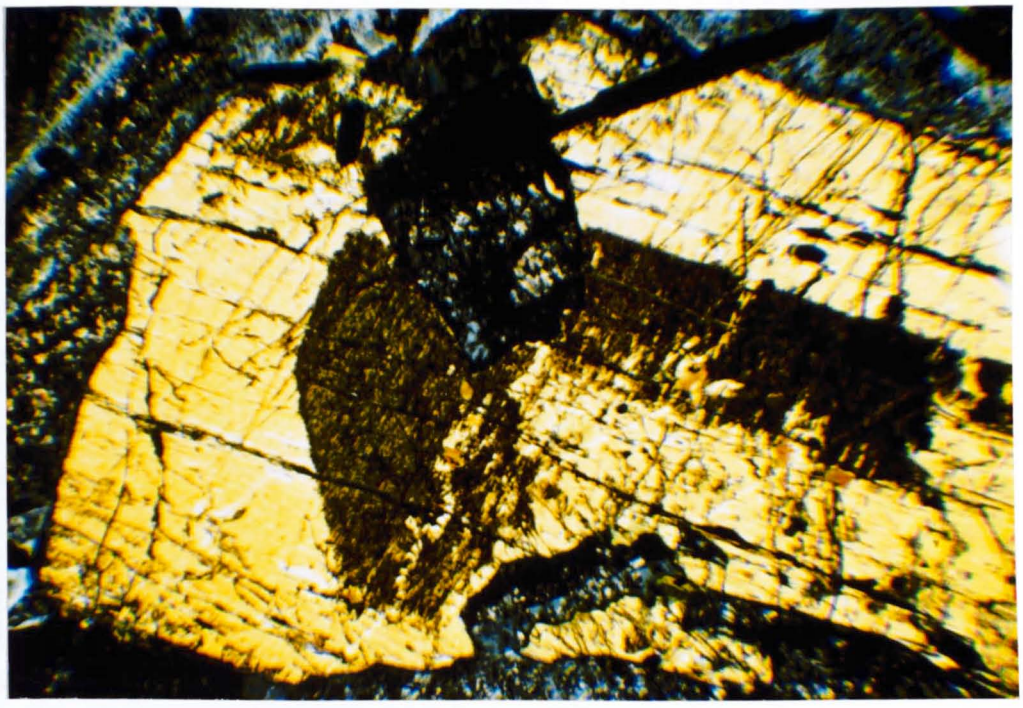

PLATE 4.8 Photomicrograph : Augite from subunit B2, showing euhedral core-region crowded with inclusions. (50. XP. Width of field - 2 mm).

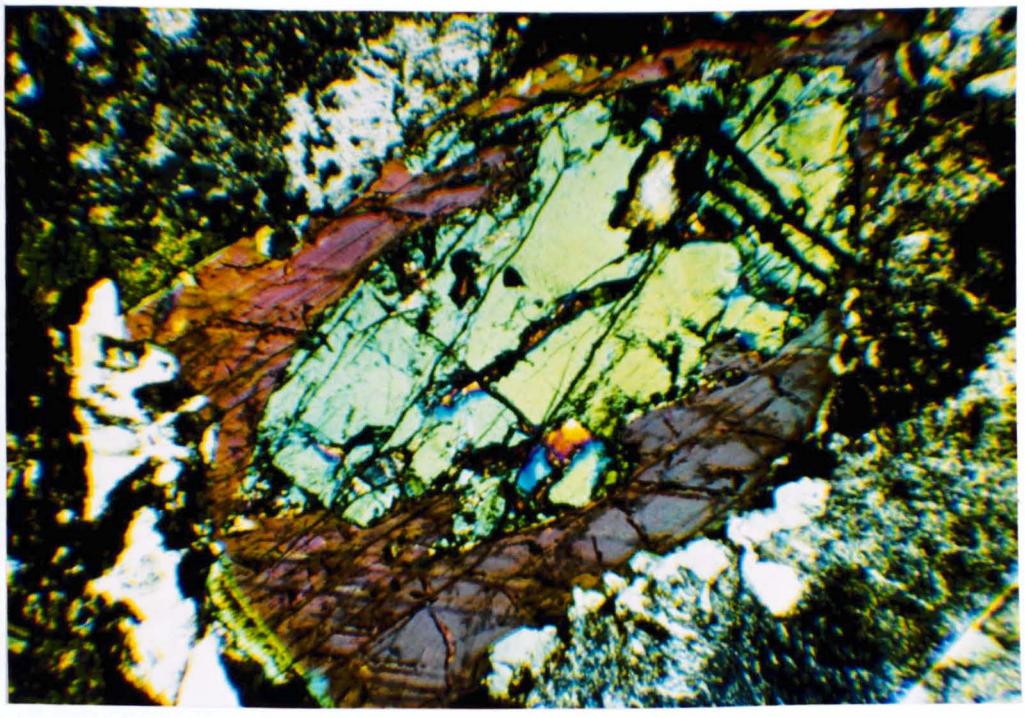

PLATE 4.9 Photomicrograph : Ferroedenitic amphibole mantling ferroaugite in subunit B3. (48. XP. Width of field - 1.5 mm).

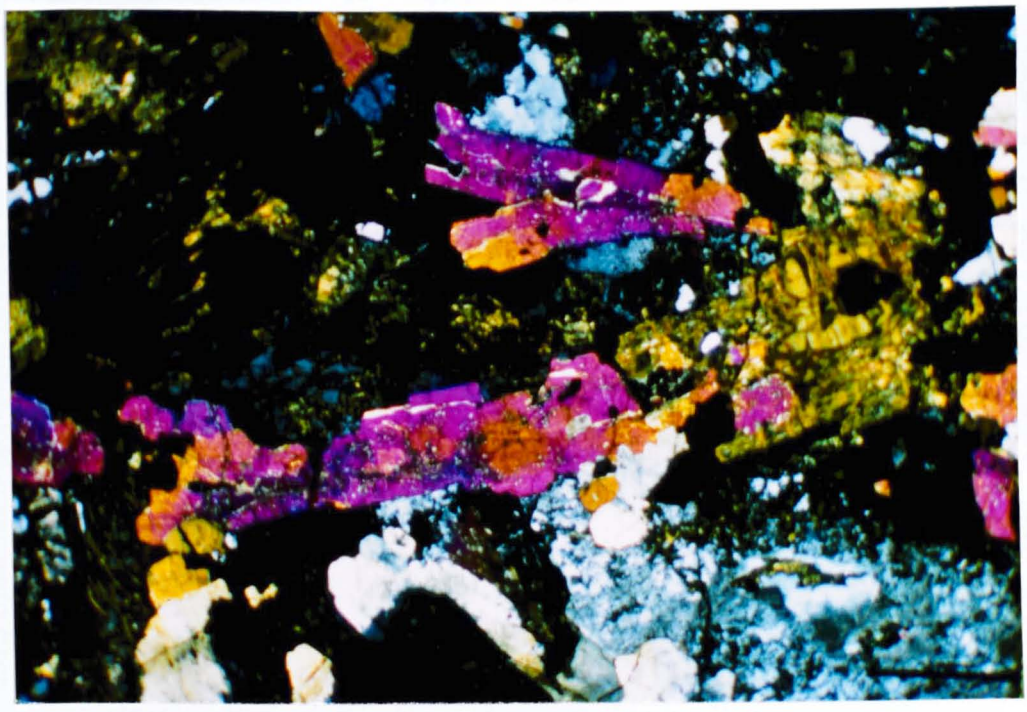

PLATE 4.10a Photomicrograph : Elongated augite showing branching phenomena in Subunit B2. (135. XP. Width of field - 8mm).

PLATE 4.10b Photomicrograph : Elongated augite showing 'corkscrew growth' phenomena, in subunit B2. (135, XP. Width of field - 8 mm).

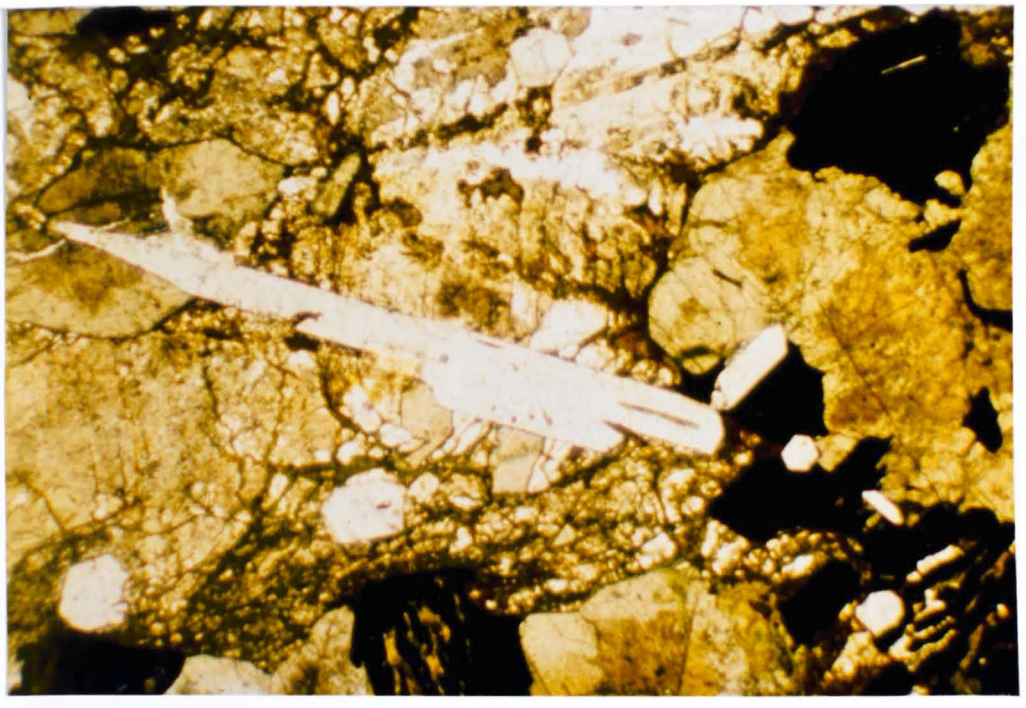

PLATE 4.11 Photomicrograph : Elongate, subskeletal apatite in subunit B2.
(135. PP. Width of field - 5 mm).

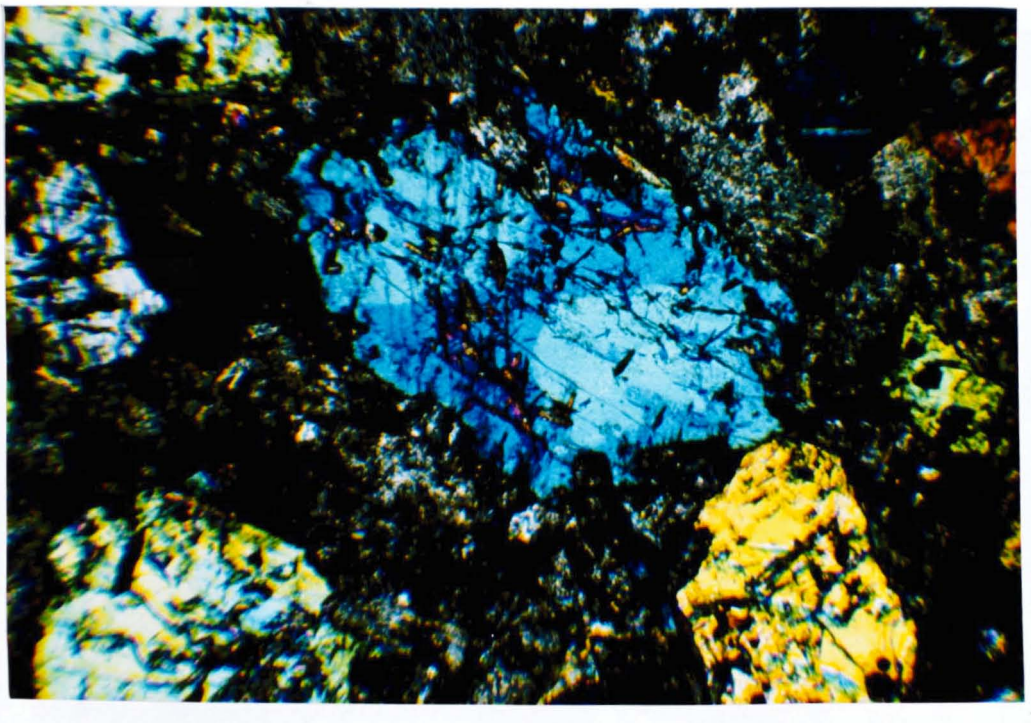

PLATE 4.12 Photomicrograph : Sector zoned augite in subunit B1. The prismatic sectors (100) are the darker sectors.
(32. XP. Width of field - 2.5 mm).

PLATE 4.13 Photomicrograph : Large tabular plagioclase laths, thin elongate needles of apatite and large zircon crystal (lower centre) set in ground mass of quartz - alkali felspar. Subunit B3 pegmatite-granophyric-ferrodiorite. (134. PP. Width of field - 5 mm).

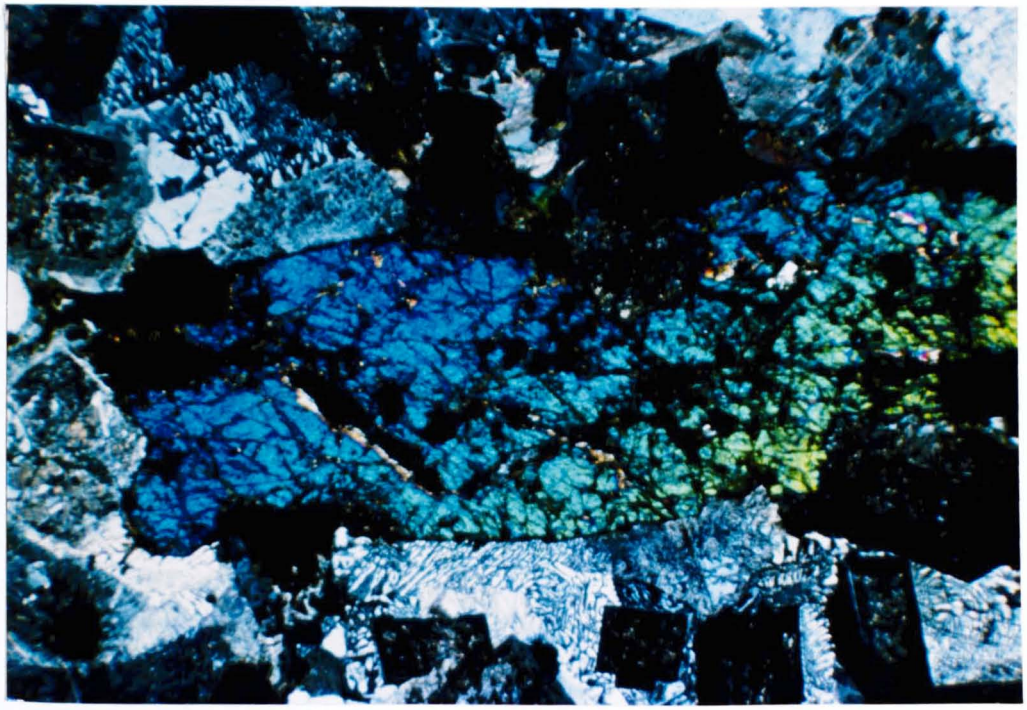

PLATE 4.14 Photomicrograph : Elongate ferroaugite crystal showing corkscrew growth (change in birefringence along the section) in pegmatitic ferrodiorite of subunit B3. (48. XP. Width of field - 8 mm).

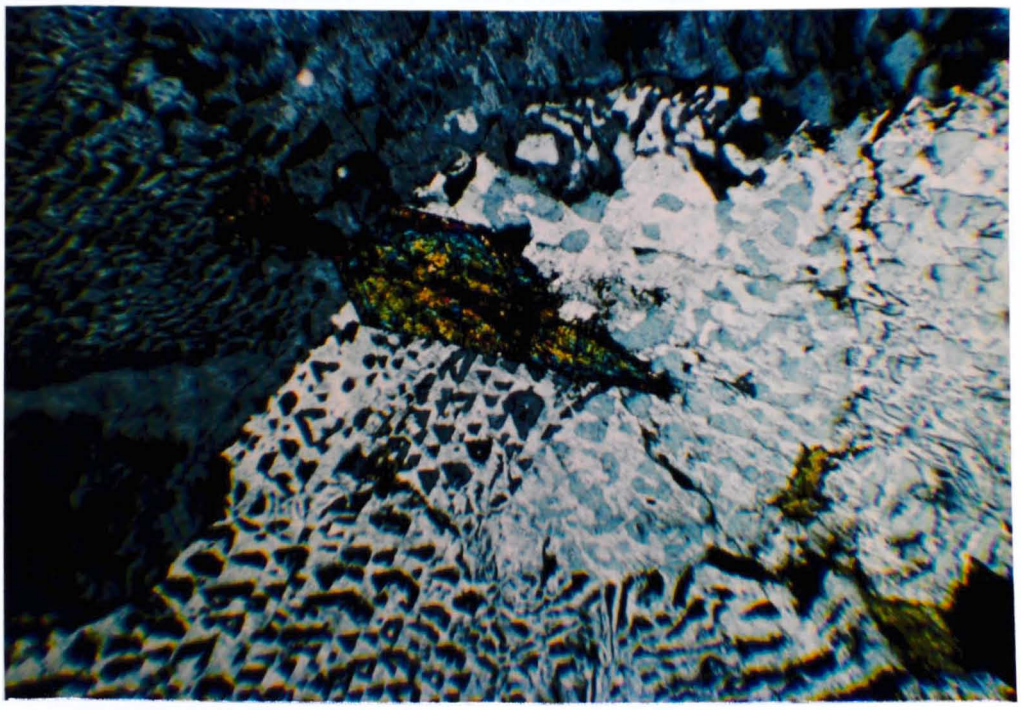

PLATE 4.15 Photomicrograph : Prismatic zircon crystal set in coarse groundmass of cunieform intergrowths of perthite and quartz. Subunit B3 pegmatitic ferrodiorite. (134. XP. Width of field - 3 mm).

PLATE 4.16 Photomicrograph : Allanite crystal, mantled by epidote in pegmatitic ferrodiorite of subunit B3 (49. XP. Width of field - 1.5 mm).

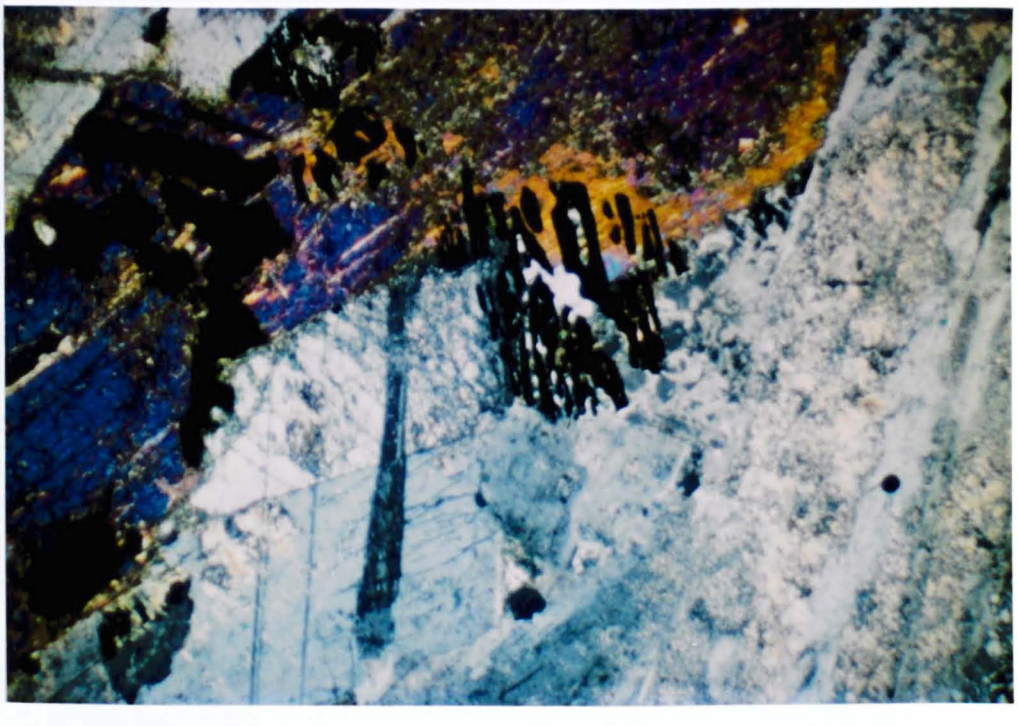

PLATE 4.17 Photomicrograph : Resorbed ilmenite in pegmatitic ferrogabbro of subunit B2. The pyroxene is mantled by amphibole.
(100. XP. Width of field - 6 mm).

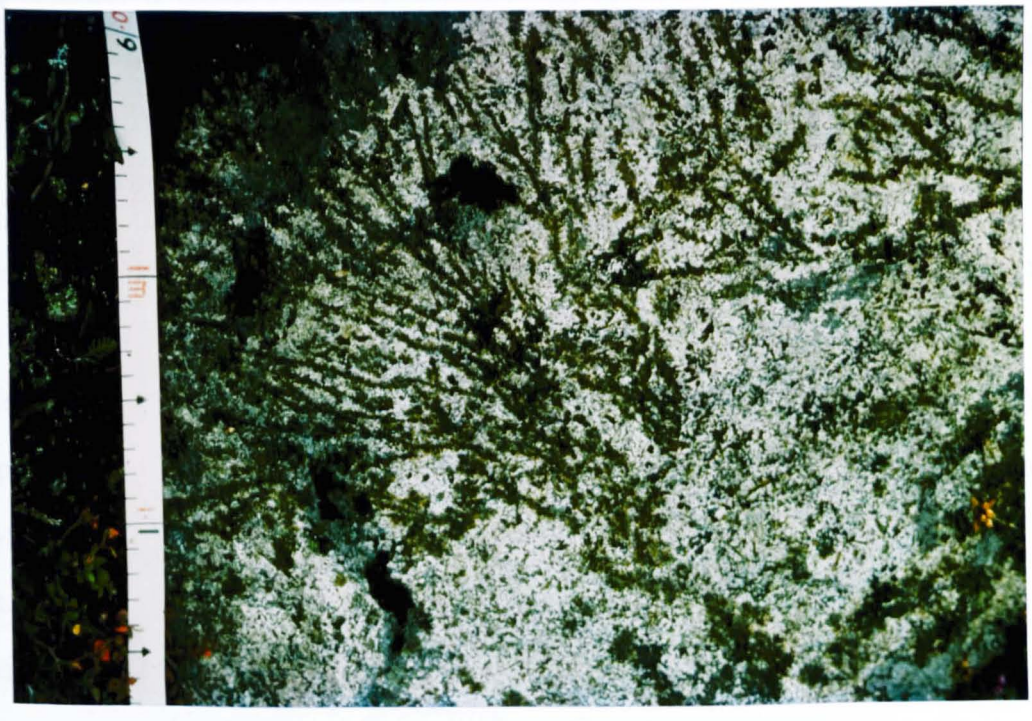

PLATE 4.18 a.b. Dendritic mafic phase in pegmatitic ferrodiorite, in loose blocks above the cliffs at the head of Further Gill Sike (MR 3490. 3340).

CHAPTER FIVE

THE GEOCHEMISTRY OF THE UNIT B ROCKS

5.1. INTRODUCTION.

Most of the data used in this chapter were produced by X-ray fluorescence (XRF) spectrometry. A small number of analyses are from Eastwood et al. (1968) and Fitton (1971). Eight analyses were provided by R.N. Thompson (written comm. 1978) and are gratefully acknowledged. The XRF methods and data are presented in Appendix Three. Rare earth element (REE) and selected trace element data were produced by instrumental neutron activation analysis (INAA), on my behalf by O.W. Thorpe (written comm. 1979) on an exchange basis with the Open University, and their help is also gratefully acknowledged. The INAA data and methods are presented in Appendix Three . The CIPW norms have been calculated and are tabulated in table A3.4.

The classification and nomenclature of the Unit B subgroups, is based on their occurrence as discrete mappable units, and on the core compositions of the clinopyroxene and plagioclase. A purely chemical classification is hindered by two main problems. Firstly, most of the rocks contain variable proportions of trapped liquid, and secondly, some of the subunits contain pegmatitic facies in which there is an increased proportion of graphic or micrographic intergrowths, relative to non-pegmatitic rocks. Most classifications, in general, are based on the allocation of arbitrary boundaries, whether they be based on field, mineralogical, or chemical parameters, and within most genetically related suites, variation is usually

continuous anyway. This is certainly true in the case of the Unit B rocks, and is reflected in the bulk-chemistry. Within each subunit there is a range of chemical variation, and chemical overlap within the subgroups.

Petrographic evidence indicates that hydrothermal alteration has occurred, particularly in the more mafic rocks. Detailed oxygen isotope and trace element studies have shown that for granitic suites from Mull (Walsh et al. 1979), Skye (Moorbath and Thompson, 1980), and the Bushveld complex (McCarthy and Fripp, 1980), hydrothermal groundwater-rock interaction has not substantially modified the whole-rock compositions. The fairly low $Sr^{87/86}$ ratio of 0.707 for the Unit B granophyres (Rundle, 1979), together with the low scatter of points about variation trends, especially with respect to the more mobile, large ion lithophile (LIL) elements, suggests that water-rock interaction has not had any simple modifying effect on the whole-rock chemistry. No detailed oxygen or strontium isotope data are available for Carrock Fell rocks, but in the light of recent studies, the assumption has been made that the observed bulk chemistry represents the original elemental distributions.

Most of the rocks of Unit B, are composed of accumulated crystals, residual micrographic intergrowth, and overgrowths on the crystals from the trapped liquid. The high degree of zoning and rapid crystallisation,suggest that equilibrium was never maintained between crystals and liquid, and, therefore, that perfect, or Rayleigh, crystal fractionation occurred. Rapid crystal growth would also tend to reduce large scale movement of crystals relative to liquid,

and, therefore, it is probably reasonable to assume that most of the rocks contain a fairly high proportion of 'trapped liquid'. In order to assess the proportion of trapped liquid represented by a particular bulk-rock analysis, incompatible elements are used. A true incompatible element has a bulk distribution coefficient, D, of zero.

$$D = X^a.K^{a/l} + X^b.K^{b/l} \text{ ---- } + X^n.K^{n/l}$$

where, X^a = Wt fraction of phase a in fractionating assemblage

$K^{a/l}$ = partition coefficient between phase a and the liquid

n = number of phases in fractionating assemblage.

No element is truly incompatible, because of the effect of minor fractionating phases, especially in evolved rocks (Wood, 1978; Pearce and Norry, 1979), and only K, Rb and Ba have D close to zero (Cox et al., 1979), for the phase assemblage in the Unit B fractionation sequence. The fraction of trapped liquid, relative to the whole-rock analysis, has been termed the residual porosity, R, (Morse, 1979).

$$R = C_S/C_L$$

where, R = residual porosity

C_S = concentration of excluded component in rock

C_L = concentration of excluded component in magma in equilibrium with fractionating assemblage.

In Unit B, the residual porosity can only be calculated for the plagio-ferrogranophyres of subunit B4, because B5 is the only liquid composition known.

TABLE 5.1 :

Residual porosity calculations for subunit B4 samples using B5 granophyre (less 20% crystals) as residual liquid composition.

Residual porosity (R) = C_S/C_L

C_S = Concentration of excluded component in rock
C_L = Concentration of excluded component in magma in equilibrium with fractionating assemblage.

	Sample 39	Sample 39 less 20% xls assuming D=0	Sample 60	R	Sample 129	R
Wt%K_2O	3.40	4.30	2.42	.56	2.00	.47
ppm Rb	133	164	90	.55	74	.45
Ba	610	753	543	.72	466	.62
Nb	34	42	26	.62	18	.43
Zr	536	662	280	.43	168	.25
Y	117	144	73	.51	78	.54
AvR =				.565±.10		.460±.12

The compositions of fractionating phases in subunits B4 and B5 are the same. The assumption can, therefore, be made that the B5 granophyre represents the compositon of the residual liquid in the subunit B4 rocks. The B5 granophyres, however, contain up to 20% crystals, (see table 6.1), therefore, the bulk composition of those must be removed from the B5 composition, before any calculation of R can be performed on subunit B4 rocks. Table 5.1 shows the calculation of R, for two of the more crystal-rich rocks of B4. Zr and Ba are considered the most compatible of the elements shown, and these show the greatest scatter in the values of R. Table 6.1 shows sample 60 to have 23% modal quartz and alkali felspar. Therefore as the calculated residual porosity is 56%, then 56 - 23 = 33 Wt% of the crystals must represent overgrowths from the trapped liquid.

5.2. MAJOR ELEMENT VARIATION.

The major element variation is best illustrated graphically by interelement plots. The choice of a suitable fractionation index as an abscissa, however, is always a difficult one. The various possibilities, discussed with their relative merits, are reviewed in Cox et al. (1979) and Wilcox (1979). The use of an incompatible element, or enrichment factor, was not considered satisfactory, in view of the lack of an initial liquid composition, and the variable compatibility of most, so-called, incompatible elements (Wood, 1978). Indexes based on Fe/Mg ratio, are ideal for tholeiitic lava sequences, however, the evolved nature of the Unit B rocks does not aid graphical representation with this type of index. Also, the analytical error on Mg determinations is higher at the low

concentrations in the more evolved subunits. Despite the disadvantages of using SiO_2 as a fractionation index, it was considered the best indicator of variance within the suite, and, therefore, has been used as the abscissa in the variation diagrams.

Figure 5.1, shows the Harker variation diagrams for the major and minor elements, together with the variation in composition of the phases forming the bulk of the rocks. The early trends, in subunits B1 and B2, do not show a liquid line of descent, but reflect the cryptic variation within the phases, the changing proportions of phases, the incoming of new phases, and the varying proportion of trapped liquid. The trends of subunits B3 to B5, however, are, more or less, straight lines. These straight lines are mixing-lines between the bulk composition of the crystallising phases and the trapped liquid compositions, but must also correspond to the liquid line of descent of the magma. To illustrate this point, Table 5.2 shows the compositions of two of the evolved Unit B rocks, with for comparison, compositions of selected lavas from the Eastern Iceland tholeiitic suite (Wood, 1978).

The overall chemical variation is entirely consistent with the observed petrographic and cryptic variation described in chapter four.

Figure 5.2a, shows the compositions of Unit B rocks, plotted on an AFM diagram. Figure 5.2b, shows plotted compositions from tholeiitic lava trends, (solid circles) tholeiitic sills (open squares) and the assumed Skaergaard liquid trend. (Data sources are given in the figure caption). It would appear that the degree of relative Fe-enrichment is dependent on the rate of cooling. The doleritic and gabbroic

TABLE 5.2 :

Comparisons of bulk-rock compositions from Unit B, with liquid compositions from the Eastern Iceland Tholeiitic province.

	49	P443	39	I6
SiO_2	63.87	63.70	72.84	71.60
Al_2O_3	13.65	13.50	13.35	12.97
Fe_2O_3*	9.73	8.33	3.71	3.76
MgO	0.70	0.80	0.21	0.30
CaO	3.89	3.70	1.26	1.12
Na_2O	4.30	4.35	4.77	4.58
K_2O	2.63	2.43	3.40	3.39
TiO_2	0.67	0.79	0.26	0.28
MnO	0.32	0.21	0.12	0.10
P_2O_5	0.22	0.10	0.08	0.02

49 - B3 pegmatitic ferrodiorite

P443 - Icelandite (Wood, 1978)

39 - B5 granophyre

I6 - Rhyolite (Wood, 1978)

trends show greater degrees of relative Fe-enrichment, with maximum occurring at higher FM ratios.

The bulk pyroxene-liquid FeO-MgO distribution coefficient, $K_D = \left[X^{PX}_{FeO} / X^{PX}_{MgO}\right] \div \left[X^{L}_{FeO} / X^{L}_{MgO}\right]$, is essentially independent of rate of crystallisation, (Bence et al,1971; Gamble and Taylor, 1980), and while it is, to a certain extent, dependent on the presence or absence of other mafic phases, it does remain fairly constant with fractionation within a particular suite. Pyroxene-liquid data from Carmichael, (1960), Wood (1978), and Stern (1979), suggest that a K_D value of 0.28 is a good estimate for tholeiitic liquids. Ranges of FM ratios have been calculated for liquids that, according to the estimated pyroxene-liquid K_D, should be in equilibrium with the pyroxenes from subunits B1 to B5, and are shown in table 5.3. Also shown in table 5.3 are the lava compositions corresponding to the calculated FM ranges from the Eastern Iceland tholeiitic suite. Subunit B1 corresponds to a low-Mg basalt, extending towards ferrobasalt in the more fractionated pyroxenes. Subunit B2, rather surprisingly, would appear to correspond to Icelandite compositions. Subunits B3 to B5, should be in equilibrium with rhyolites with successively higher FM ratios.

It must be recognised that the doleritic and gabbroic trends do not represent liquid trends, but the changing compositions of the crystallising phases, and the residual porosity. The Fe-maximum in a gabbroic, or doleritic, rock usually corresponds to the point at which Fe-Ti oxides crystallise from the liquid, which, to a certain extent, is related to fO_2. The differences in the FM ratio of the Fe-Maximum, therefore, relate to the different temperatures at which the Fe-Ti oxide

TABLE 5.3 :

MgO-FeO data for pyroxene from Unit B, together with FM ratios for coexisting lavas using Pyroxene-Liquid bulk MgO-FeO distribution coefficient.

$$K_D = \frac{X^{Px}_{FeO} \,/\, X^{Px}_{MgO}}{X^{L}_{FeO} \,/\, X^{L}_{MgO}} = 0.28$$

SUBUNIT	MgO (Wt%)	FeO (Wt%)	Mg/Mg+Fe (At%)	LAVA FM (Wt%)	LAVA TYPE (Wood, 1978)
B1	14.5	8.5	.76	70	Low Mg Basalt
B1(18)	13.0	13.5	.63	77	Ferrobasalt
B2	9.5	17.0	.50	86	Icelandite
B3	6.0	23.0	.32	92	Rhyolite
B4 B5	1.0	28.5	.05	97	Rhyolite

stability field is intersected, for a given fO_2. It is possible that the Fe-Ti oxide stability field is expanded, as fO_2 increases as the lavas come into contact with atmospheric oxygen upon extrusion. It is perhaps worthy of note, in this respect, that Fe-Ti oxides usually occur in the groundmass, rather than as phenocryst phases in most lavas.

An additional possibility, expanded upon in Chapter Six, is that the lower liquidus temperatures, the degree of Fe-enrichment, and the crystallisation of Fe-Ti oxides, may be influenced by a stable, or metastable, two-liquid solvus in the latter stages of fractionation.

5.3. TRACE ELEMENT VARIATION.

The trace element variation is shown, plotted against SiO_2 in figure 5.3. Cr and Ni are not shown as their abundances in subunits B2 to B5 were at, or near, detection limits, nor are the trace elements determined by INAA. The variation is described in groups of elements with similar geochemical characteristics. Partition coefficients, where quoted, are between crystal and liquid.

Nickel, chromium and cobalt :

All these elements decrease with fractionation and partition preferentially into pyroxene. The decreasing Cr/Ni ratio indicates that the K_D for Cr is greater than for Ni between pyroxenes and liquid.

Scandium :

Because of its ionic radius and charge, Sc should replace Mn Fe^{3+} or Ti and, thus, would be expected to concentrate in Fe-Ti oxides or Fe-rich pyroxenes. No data are available

for B1 but a decrease from B2 to B5 is in general agreement with this.

Zirconium and Hafnium :

Both Zr and Hf increase with fractionation and show a maximum in subunit B4 of 620 and 13.53 ppm. respectively . Zircon is the only Zr+Hf bearing phase in the fractionation sequence and is modally most abundant in subunit B4.

Niobium and Tantalum :

Both increase with fractionation. Their ionic size and valency suggest that Nb and Ta should behave similarly to Ti and thus partition into Fe-Ti oxides. This effect is not observed but may be masked by low abundance levels anyway.

Zinc :

Zn substitutes for Fe^{2+} in Fe-rich pyroxene and magnetite. There is an increase from B1 to a maximum in subunit B4, then a significant decrease into B5. Either the K_D for pyroxene - melt is very compositionally dependent, or a separate Zn bearing phase is crystallising in B4 to B5 in very small amounts.

Yttrium :

Y increases with fractionation. In acidic rocks, hornblende, pyroxene, zircon and apatite all have $K_D > 1.0$, but their effect on the observed Y distribution in Unit B is not apparent.

Strontium, Rubidium and Barium :

The Sr/Rb and Sr/Ba covariance are shown in figure 5.4a and b respectively. Both trends show a 'dog leg' shape, with a well defined trend through subunits B3 to B5, but more

scatter in B1 and B2. Both the Rb/Sr and Ba/Sr ratios increase with fractionation. Strong zonation in minerals indicates that equilibrium has not been maintained between melt and crystal, and that fractionation has tended towards being perfect. The Rayleigh equation, describes the behaviour of an element during perfect fractionation.

$$C_l/C_o = F^{(D_a - 1)}$$

C_o = concentration of element in original melt

C_l = concentration of element in residual melt

F = weight fraction of melt remaining

D = Bulk distribution coefficent for element a

$$D_a = \Sigma_i K_a^i \cdot X_i$$

K_a^i = distribution coefficient for element a in phase i

X_i = weight fraction of phase i

Also shown in figure 5.4 are vectors indicating the change in composition of melts as a result of monomineralic fractionation, with the numbers indicating per cent of crystals removed. Partition coefficients are those from Arth (1976). The vectors in the insets in figure 5.4 show the direction of evolution of fractionated liquids, calculated from the modal observations, for each subunit. (see table 6.1).

Alkali element ratios do not vary significantly throughout the fractionation suite, confirming their incompatibility in the crystallising phases, and the limited effect that hydrothermal alteration has had on their distribution. The ratios are: $K_2O/Ba = 0.0054 \pm .0008$, $K_2O/Rb = .029 \pm .005$, $Rb/Ba = .020 \pm .05$ (errors are $\pm$ 1SD).

Uranium and Thorium :

Th increases from B1 to B5 and U would also be expected to do the same. Both are highly incompatible.

Rare Earth Elements (REE) :

The chondrite normalised REE patterns are shown in figure 5.5a for samples from subunits B2, B4 and B5. The normalising data are from Nakamura (1974) and Thorpe et al. (1977). All the rocks are Light REE enriched. $(Ce/Yb)_N$ however varies slightly, decreasing from 3.93 in subunit B2, to 2.92 in B4, and increases again to 3.19 in B5. Total REE increase from B2 to B5, but enrichment factors for light, intermediate and heavy REE differ, (La = 3.17, Sm=1.44, Yb=3.16). Figure 5.6 shows the variation of the total REE (as measured by Sm_N), and the slope of the REE pattern (as measured by Ce/Yb_N). Also shown are vectors for the change in composition of residual liquids produced by fractional crystallisation of the phases in Unit B, assuming Rayleigh fractionation. More points would be desirable but the variation is considered significant, considering the precision of the INAA data. Because of the high K_D for total REE, and the characteristic shape of the normalised REE pattern for apatite (Irving 1978), the apatite control dominates the ferrogabbro pattern. It also accounts for the different REE enrichment factors, as the normalised pattern for apatite shows heavy and light REE depletion with respect to intermediate REE. The pattern of 142, 148 and 39 is more representative of the liquid composition, as plagioclase, pyroxene and Fe-Ti oxides all have $K_D < 1.0$. Plagioclase fractionation would produce a decrease in Ce/Yb_N, this is, however, masked by the plagioclase accumulation on the one hand,

counteracting its effect in the liquid, and secondly, and perhaps more importantly, the effect of zircon fractionation in subunit B4, is to increase Ce/Yb_N. The high K_D for total REE for zircon means that a small amount of zircon fractionation has an apparently disproportionate effect on the REE patterns. The increase in Ce/Yb_N from B4 to B5 is most likely to be the effect of zircon. Plagioclase has, however, had a dominating effect on the REE pattern, indicated by the negative europium anomaly (Eu/Eu^*_N = .60), in B5. Both B2 and B4 show a slight negative europium anomaly. The effect of plagioclase fractionating early in the sequence on the europium anomaly is counteracted by the plagioclase accumulation in these rocks, although K_D for Eu is compositionally dependent, increasing in more acidic rocks.

For comparative purposes, the normalised REE patterns of the Skaergaard U2B ferrogabbro (Haskin and Haskin, 1968) and selected patterns from the Eastern Iceland ferrobasalt - rhyolite suite (Wood,1978) are shown in figure 5.5b. While variations in detail occur, the broad similarities are obvious, and related by the same processes of fractional crystallisation, (Wager and Brown, 1968; Wood, 1978). Negative europium anomalies are very common, almost ubiquitous, features of high level granitic rocks in tholeiitic provinces, attesting to the role of plagioclase fractionation in their evolution. (Walsh et al. 1979; Thorpe et al. 1977; Wood, 1978; Stern, 1979).

5.4 SUMMARY.

Comparisons of the chemistry of tholeiitic lava suites and tholeiitic intrusions with Unit B, confirms the tholeiitic nature of the latter. With fractionation, the chemical changes

can be summarised as follows ; Ca, Mg, Cr, Ni and Co, all decrease; Fe*, Ti,Mn, Sc, P all show an initial increase to a maximum in B2, and then decrease in abundance; of the other high field strength (HFS) transition metals and Lanthanides, Zn, Zr, Hf and Eu show a maximum in B4, then decrease, all the others increase systematically but show varying degrees of incompatibility; LIL elements are all highly incompatible; AL and Sr vary in basic rocks, show a maximum in B4, then decrease. Si shows a decrease into B2, then increases to B5.

FIGURE 5.1.

Harker variation plots for major elements (Wt%) in Unit B rocks.

◆ B1; ▽ B2; ● B3; O B4; × B5.

Also shown are compositional ranges for pyroxenes, plagioclases, Fe-Ti oxides and apatite (on P_2O_5 v. SiO_2 only) from subunits B1 to B5.

Pyroxene (Px) ◪ B1; ◘ B2; ◪ B3; ◘ B4; □ B5.

Plagioclase (Pl) ◇ B1; ◇B2; ◇B3; ◇B4; ◇B5.

Fe-Ti oxide (Mt,Il) ■

Apatite ▮

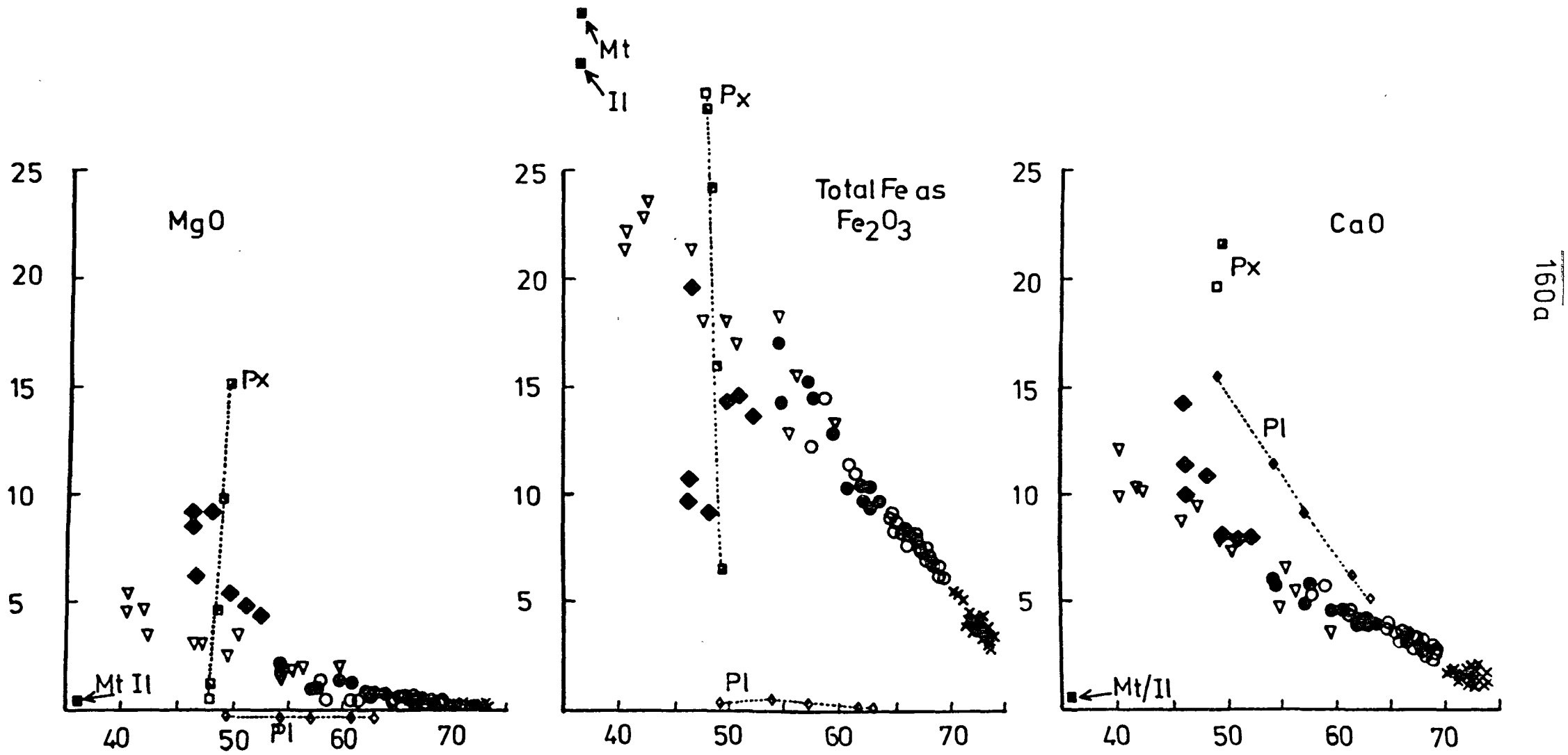
Mt
Il
Px
MgO
Total Fe as
Fe_2O_3
CaO
Px
Pl
Mt Il
Pl
Pl
Mt/Il
25
20
15
10
5
40
50
60
70

160a

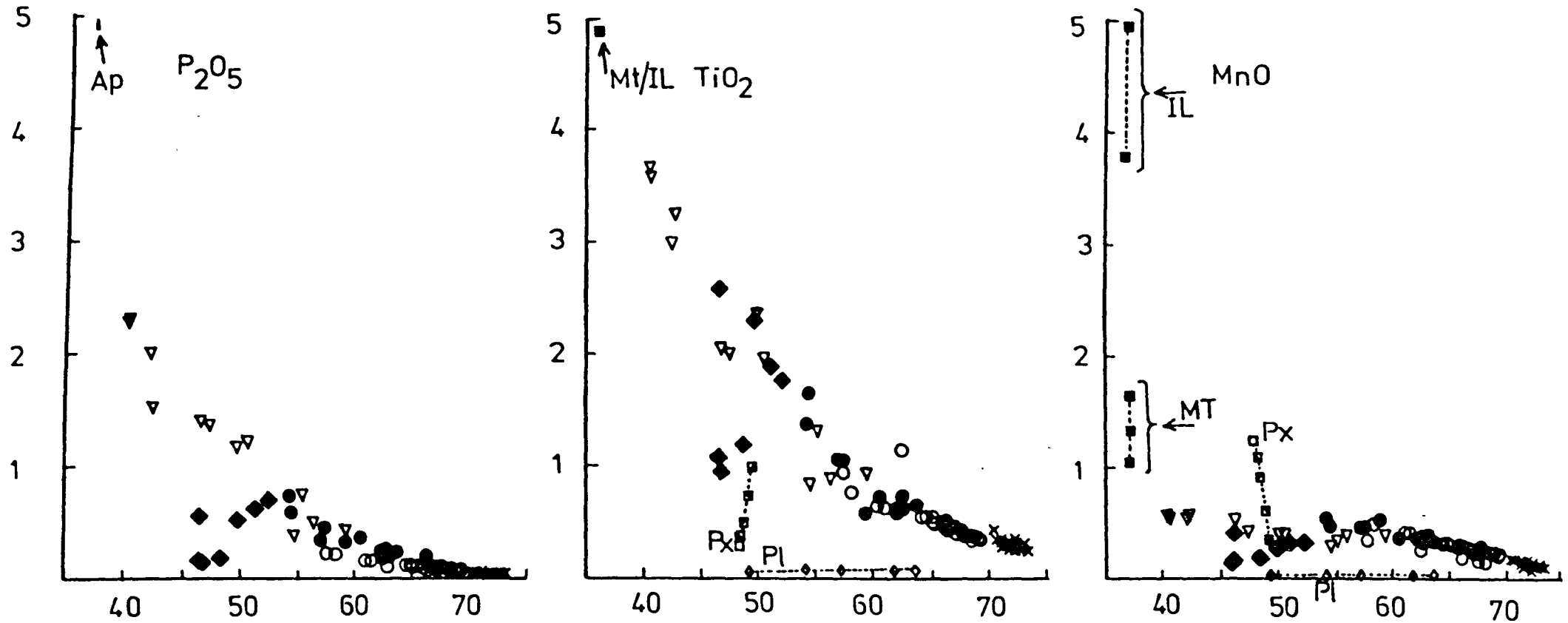
5
4
3
2
1
Ap
P_2O_5
40
50
60
70
Mt/IL TiO_2
Px
Pl
MnO
IL
MT
Px
Pl

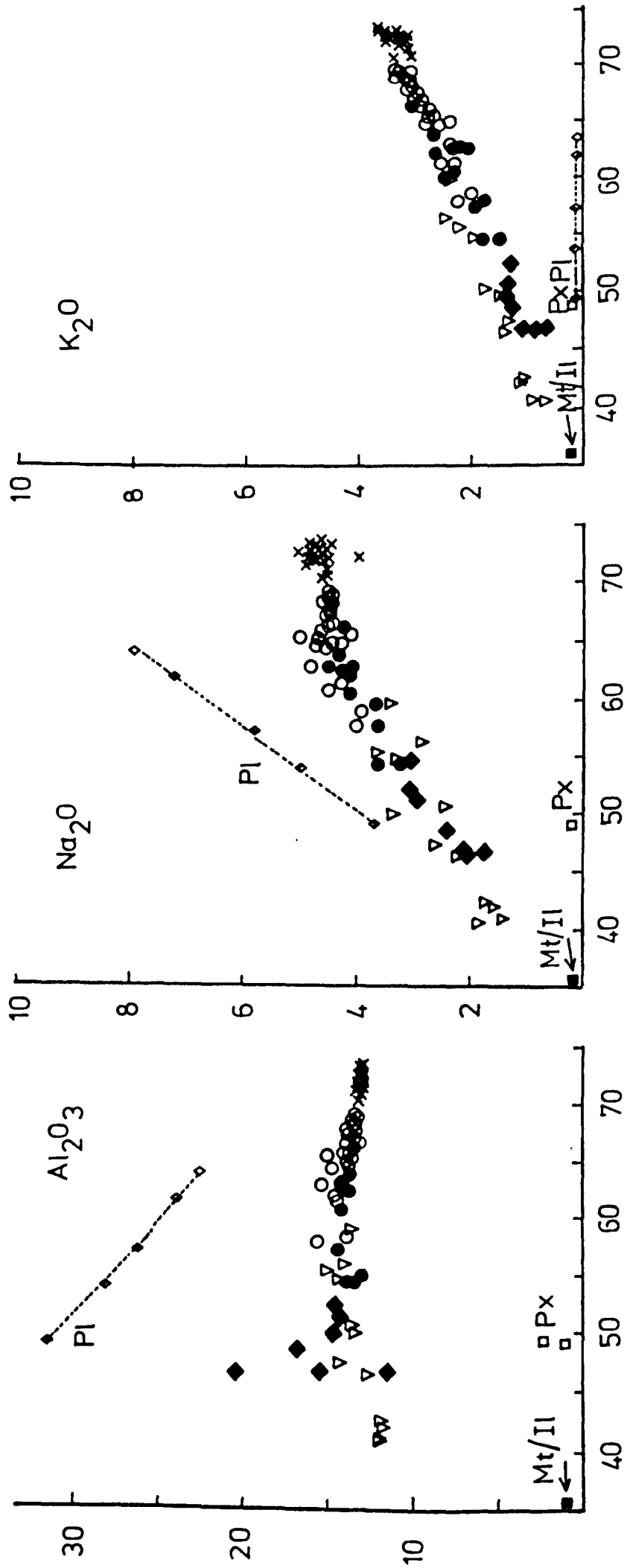
Al_2O_3
Pl
Mt/Il
Px
Na_2O
Pl
Mt/Il
Px
K_2O
Mt/Il
Px
Pl
10
20
30
40
50
60
70
2
4
6
8
10

FIGURE 5.2.

a) A.F.M (Wt%) plot of analysed rocks from Unit B. Symbols as in figure 5.1.
A = Na_2O + K_2O; F = Total iron as Fe_2O_3; M = MgO

b) A.F.M. plot of analysed rocks from tholeiitic lava suites (Cornwall, 1951; Carmichael, 1964; and Wood, 1978), tholeiitic dolerite sills (Walker et al, 1952; Hotz, 1953; McDougall, 1962; Hawkes, 1966; and Walker, 1969) The Skaergaard projected liquid trend (Wager and Brown, 1968) is also shown.

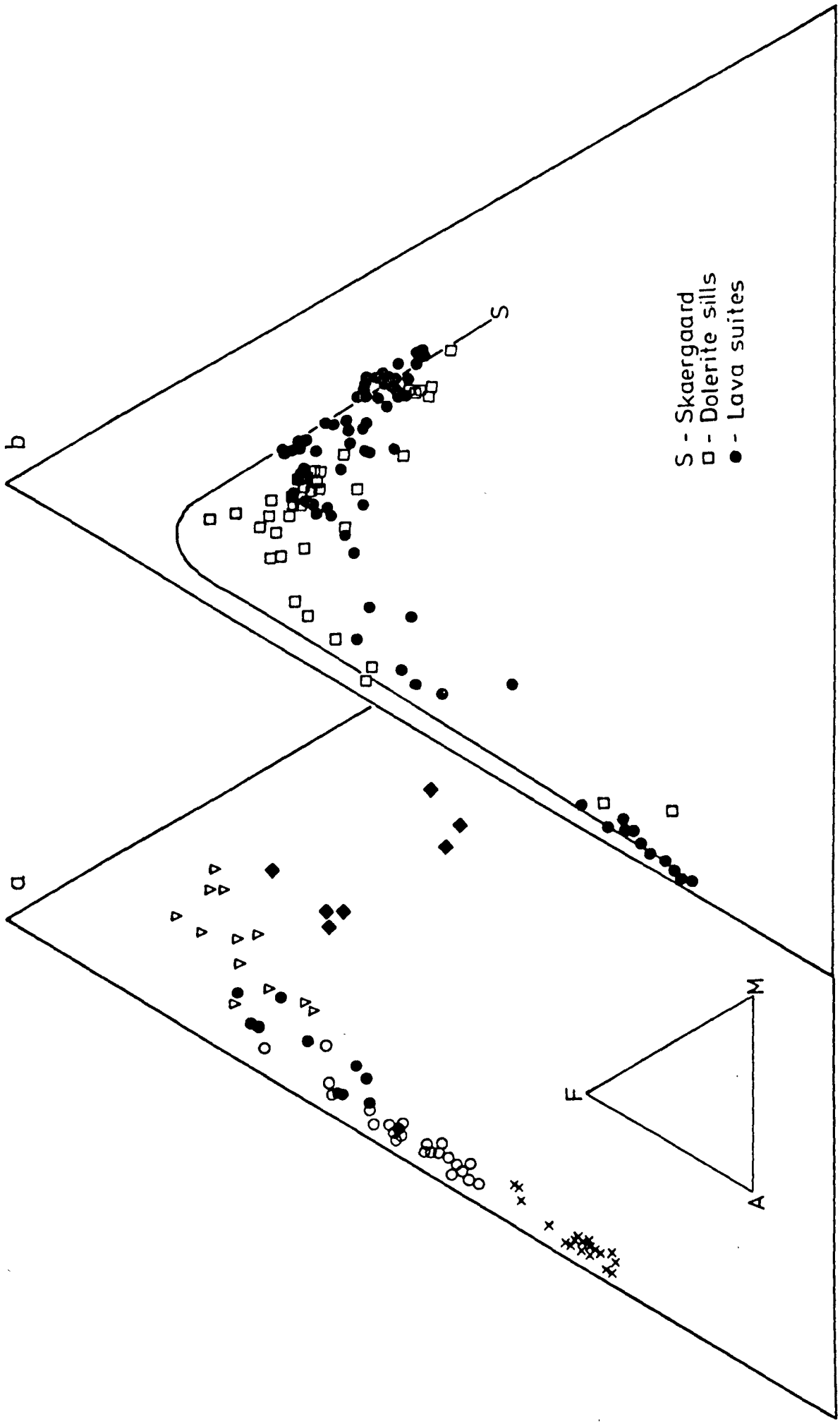
a
b
S
S - Skaergaard
□ - Dolerite sills
● - Lava suites
F
M
A

FIGURE 5.3.

Harker variation plots for trace elements (p.p.m) in Unit B rocks.

Symbols as in figure 5.1.

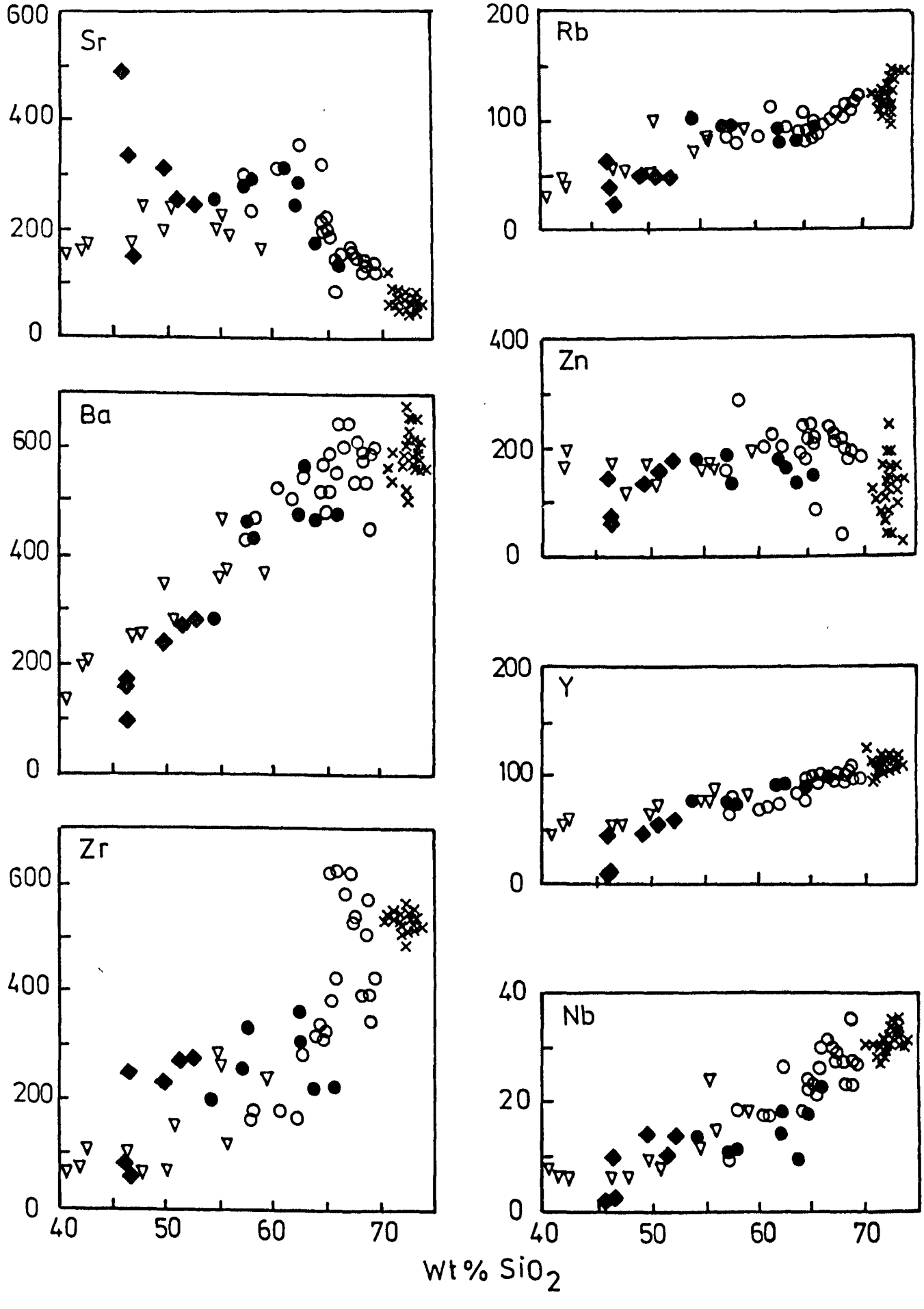
Sr
Rb
Ba
Zn
Y
Zr
Nb
600
400
200
0
100
20
40
50
60
70
Wt % SiO2

FIGURE 5.4.

Sr-Rb (a) and Sr-Ba (b) covariance in analysed rocks from Unit B. Symbols as in figure 5.1. The vectors in the upper right indicate the change in composition of melts as a result of perfect (Rayleigh) monomineralic fractionation (see Text). The numbers indicate the percentage of ilmenite (Il); magnetite (Mt); quartz (Qz); clinopyroxene (Cpx); basic plagioclase (Pl_b); acid plagioclase (Pl_a); and alkali-felspar (Ksp) removed. The vectors in the insets show the direction of evolution of fractionating liquids, calculated from the modal observations for each subunit.

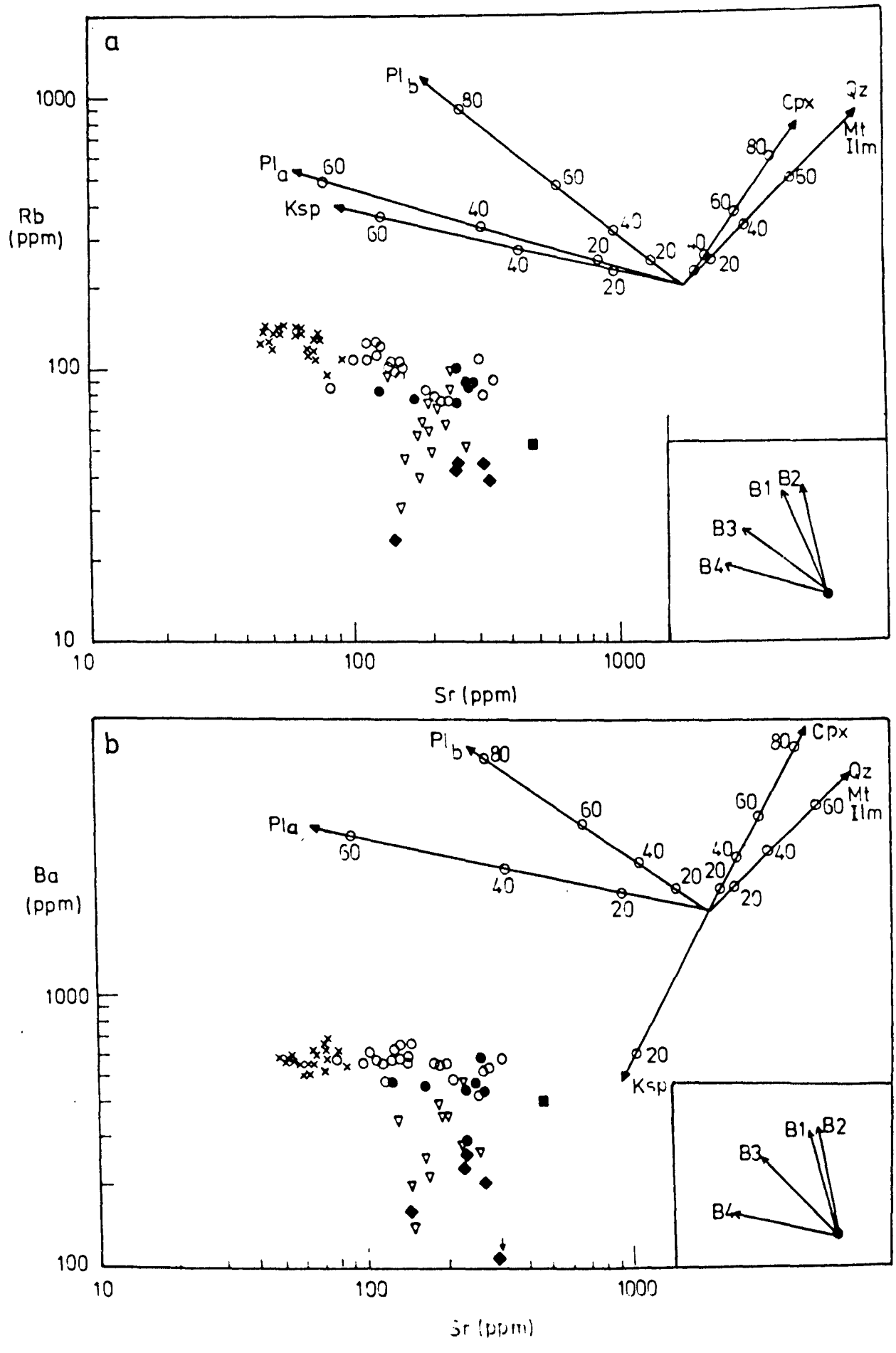
a
Rb (ppm)
Sr (ppm)
1000
100
10
10
100
1000
Pl b
Pl a
Ksp
Cpx
Qz
Mt
Ilm
80
60
40
20
0
B1
B2
B3
B4
b
Ba (ppm)
Sr (ppm)
1000
100
10
10
100
1000
Pl b
Pl a
Ksp
Cpx
Qz
Mt
Ilm
80
60
40
20
B1
B2
B3
B4

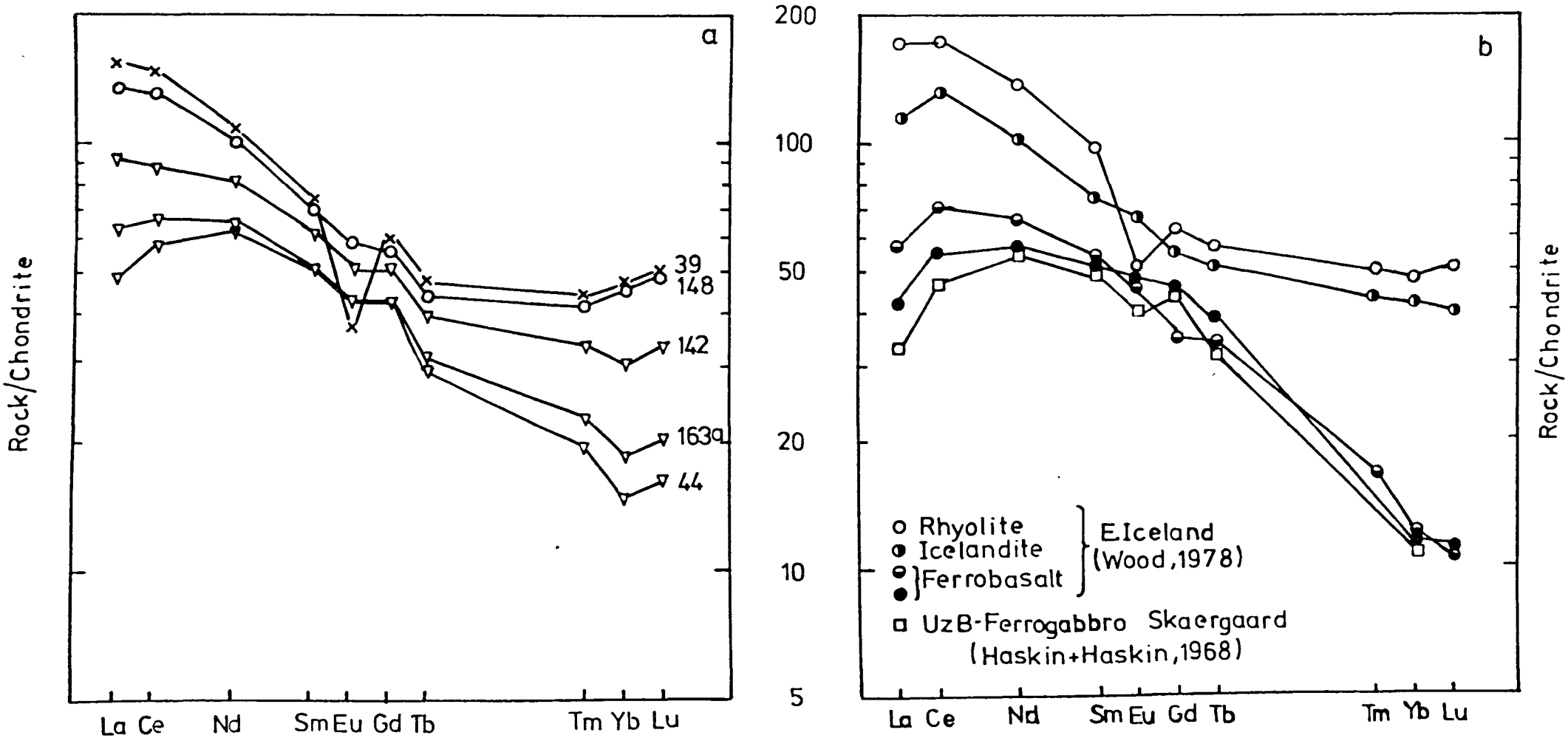
a
b
Rock/Chondrite
200
100
50
20
10
5
39
148
142
163a
44
La Ce Nd Sm Eu Gd Tb Tm Yb Lu
Rhyolite
Icelandite
Ferrobasalt
E.Iceland
(Wood, 1978)
UzB-Ferrogabbro Skaergaard
(Haskin+Haskin, 1968)

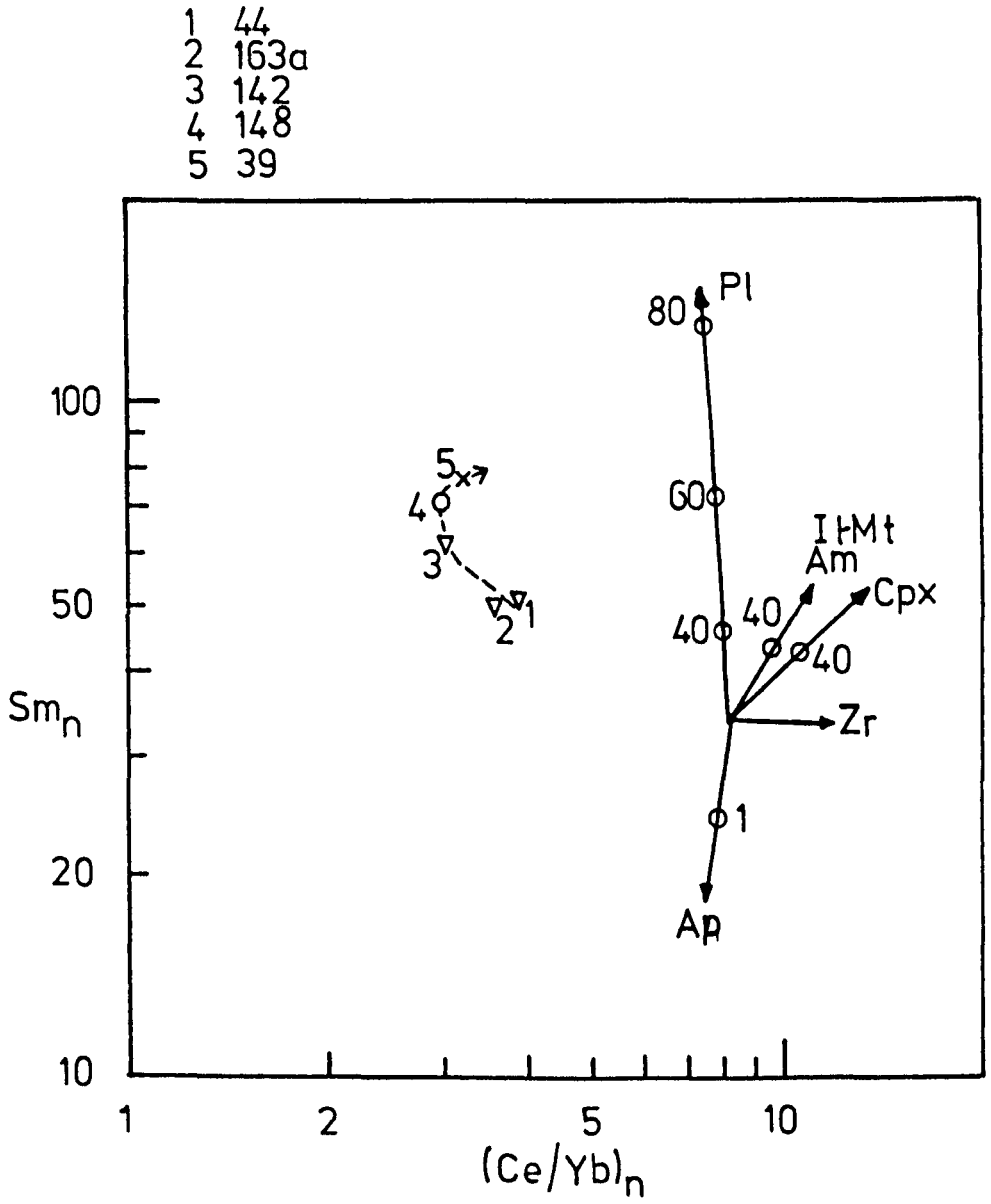
1 44
2 163a
3 142
4 148
5 39
Pl
80
60
40
40
40
40
Ilmt
Am
Cpx
Zr
1
Ap
5
4
3
2
1
100
50
20
10
Sm$_n$
1
2
5
10
(Ce/Yb)$_n$

CHAPTER SIX

THE EMPLACEMENT AND FRACTIONATION OF UNIT B

6.1 EVIDENCE FOR IN SITU FRACTIONATION

It was noted in Chapter Two that Unit B was composed of a series of sheets, sub-vertical in form, varying in width from 3 m. to 50 m. Their individual lengths could not be established because of lack of continued exposure, but some undoubtedly extend for over 2 km. Whatever the phase relationships and controls on the fractionation of the liquid parental to the exposed rocks of Unit B, evidence exists for in-situ fractionation of the separate sheets after emplacement at their 'present' levels. The evidence falls under the following general headings; modal variation, pegmatitic facies, cryptic variation, and incompatible element variation.

Modal variation: Modal concentrations were measured using a Swift point-counter. Methods described in Chayes (1956) were employed. 500-1000 points were counted per slide. Optical modal determinations have inherent limitations (Chayes, op. cit; Wright and Okamura, 1977), but were also hampered, especially in subunits B1 and B2, because of alteration effects. Modes are presented in table 6.1, showing the variation in each subunit, and are approximate only for subunits B1 and B2.

Modal variation histograms are shown in figure 6.1 a-d, for samples collected at intervals across various sheets of subunits B3 and B4, in traverses 1,2,5 and 6. The mode of

TABLE 6.1 :

MODAL ANALYSES FOR ROCKS FROM UNIT B.
MODES = Wt%. Aproximate only for subunits B1 and B2.

Subunit	Sample	Pl	Px+Am	Fe-Ti Oxide	Qz/Af	Ap
B1	32	40	42	8		
	20	50	28	10	10	1
B2	137	35	40	17	3	5
	142	50	10	5	35	1
B3	51	52.0	17.3	5.0	24.6	0.2
	52	51.1	16.2	5.6	27.0	0.1
	53	43.6	12.0	3.0	41.3	tr
B4	60	63.5	8.0	5.5	23.0	
	64	35.0	7.0	2.0	56.0	
	127	53.5	16.5	6.0	24.0	
	126	61.5	10.0	3.0	26.5	
	109	54.5	8.0	2.0	35.5	
	143	65.5	11.0	3.5	21.0	
	148	38.0	8.5	1.0	52.5	
B5	E16184	9.5	7.5	2.0	81.0	

Key : Pl. Plagioclase
Px. Pyroxene
Am. Amphibole
Fe-Ti oxide. magnetite and ilmenite
Qz/Af. Quartz-alkali felspar intergrowths
Ap. Apatite

subunit B5 is shown for comparison (figure 6.1 e). Figure 6.1 a, b and c show the variation across three sheets from subunit B4. In specimens from the southern margins (143, 60 and 127), plagioclase is the dominant phase, forming 55 to 60%, with mafic phases forming 10 to 20%, and quartz-alkali felspar intergrowths the remainder. The northernmost specimens (148, 64 and 109) show a substantial increase in quartz and alkali felspar, up 50 to 60% of the mode, while plagioclase, forming 30-40%, still exceeds mafic phases which now form less than 10% of the mode. The horizontal distance over which these changes take place varies from 38 m. (143 to 148), to 35 m. (127 to 109), to 5 m. (60 to 64). Similar variation occurs over a distance of 2 m. in subunit B3 (51 to 53 in figure 6.1 d). These modal variations indicate a decreasing proportion of plagioclase and mafic phases, and an increase in the amounts of 'trapped liquid', represented by the micrographic intergrowths, laterally across the sheets from south to north. The actual percentage of trapped liquid would be greater, in any particular sample, than the percentage of micrographic intergrowth, as a result of continued over-growth on the earlier formed higher temperature crystals.

Pegmatitic facies: The occurrence and nature of the pegmatitic facies has been described in section 4.1.10. It has been attributed to saturation in the melt of an aqueous phase, by crystallisation of anhydrous phases. These pegmatitic facies invariably form on the northern margin of the sheets in which they occur, thus, indicating the probability of lateral volatile fractionation across the sheets. Although

upward fluxing cannot be entirely ignored, it would be most likely to occur in regions where the proportion of melt to crystals was the greatest, which from the evidence of modal variations would be on the northern margins anyway.

Cryptic variation: The plagioclase core compositions show little variation across the sheets, but this has been attributed, in part, to their phenocrystic nature, and to the thermal effectsof volatiles in lowering the liquidus-solidus relationships in the plagioclases. Pyroxenes, however, can show substantial cryptic variation from south to north across individual sheets, and was illustrated, in terms of principal end-members components, in figure 4.4. Figure 4.4B, for example, shows the variation in subunit B2 across traverse six. The majority of the variation occurs over the northern 20% of the sheet, in the more fractionated and pegmatitic facies of the ferrogabbro. Figure 4.4E, shows the variation in subunit B3 across traverse one. It will be noted that there is a significant increase in the Wo component, which coincides with the abrupt change into pegmatitic facies (sample 48, traverses the boundary). This may be an effect of increased vapour pressure, causing the local expansion of the two-pyroxene solvus. The cryptic variation in the pyroxenes, indicates that major elements have fractionated laterally across the sheets from south to north.

Incompatible element variation: The variation in zirconium across three sheets of subunit B3 and B4, is plotted against MgO and CaO in Figure 6.2 .

A general relationship exists between the Zr content and the position of the sample in the sheet. Zr increases by up to a factor of four across the sheets from south to north, indicating in-situ fractionation of the liquid. The major element concentration also varies, in a manner reflecting the cryptic variation and abundance of the pyroxenes.

The treatment of Zr (or Y, or Nb) as truly incompatible elements, is not strictly valid, as indicated by the variation in enrichment factors across the sheets between Zr, Y and Nb. It was also noted in Chapter Five that the zircon becomes a liquidus phase in subunit B4, however, the very small nature of the initial nucleii would probably allow them to be transported in the migrating liquid, and therefore, in effect, still reflect Zr fractionation across the sheets.

6.2 THE EMPLACEMENT OF UNIT B

Before discussion of the mechanisms of in-situ fractionation, it would be pertinent to consider the order of emplacement of the various subunits, and the thermal regime that existed at the time of their emplacement.

Figure 6.3 , shows the proposed sequence of intrusion of the five subunits of Unit B, in the Further Gill Sike region. The Carrock Fell granophyre, subunit B5, was intruded along the contact of Unit A, and the Skiddaw Group or Eycott Volcanic Group, either as a single stock, or as a series of subvertical sheets (A). The cooling granophyre, comparatively voluminous compared to later subunits, acted as a source of heat throughout the emplacement of subunits B2 to B4. Subunit

B4 was emplaced, as a subvertical sheet, along the southern margin of the, still hot, granophyre (B), slightly hornfelsing it and stoped off sheets of it. Crystallisation proceeded, initially, against the cooler southern wall, but progressed inwards towards the northern margin. The ferrodiorite, subunit B3, was then intruded in a similar manner along the southern margin of B4 (C), the cooling ferrogranophyre of B4, contributing to the heat flow from north to south. Cooling most rapidly on the southern margin, the ferrodiorite became saturated with respect to volatiles, by progressive crystallisation inwards of anhydrous phases, leading to development of a pegmatitic facies along its northern margin, and under the roof. The ferrogabbro of subunit B2 was intruded and crystallised in a similar manner, with conductive heat loss from the cooling of subunit B3 contributing to the overall thermal gradient from north to south (D). The thermal gradient must have still been high enough to cause supercooling of the iron-rich magma against Unit A, resulting in localised comb layering. Emplacement of the successive sheets also must have been fairly rapid, as at no time did the thermal gradient cease to exist from north to south, indicating that the Unit A rocks had not reached thermal equilibrium, even on emplacement of subunit B2. On the other hand, there was sufficient time between the emplacement of successive sheets, to allow some crystallisation inward from the southern margin. Successive sheets were therefore intruded against a semi-solid medium. It is perfectly possible that successive sheets became contaminated along their northern margin, by interstitial

liquids from the previously intruded sheet. This effect could have enhanced the fractionation effect and possibly contributed to the saturation of volatiles along the northern margin of the later sheet, and also account for the lack of chilled margins between sheets. Sample 55(MR 3518,3339), traverses the contact between the ferrodiorite pegmatitic facies of subunit B3, and the pyroxene-plagioclase granophyre of B4. Microscopically features exist from both subunits over 0.5 to 1.0 cm., and electron micro-probing has indicated that the phases are in equilibrium over the contact region. (Compare the marginal analysis of pyroxene 55a, a large pyroxene from the pegmatitic facies, with the analysis of pyroxene 55b, a small euhedral pyroxene from subunit B4, in figure 4.4H and E respectively).

The thermal gradient from north to south would have been generated by the cooling of the subunit B5 granophyre, by conductive heat loss through the wall, but would be enhanced by the emplacement of successive magmas each with a higher liquidus temperature.

It is surprising that pegmatitic facies have developed in the more basic members of the suite, in subunits B3 and B4, but not in the granophyres, as these, under closed system volatile fractionation, should be saturated before more basic melts with higher liquidus temperatures. It is possible that the cooling of the subunit B5 and B4 rocks, had initiated a hydrothermal convection cell, and that influx of ground-water occurred during emplacement of subunits B3 and B2, thus increasing the water content of the magma, which then became

saturated on further crystallisation. Figure 6.3E, shows the last event in the evolution of Unit B, the emplacement of subunit B1, into the northern and central parts of the subunit B5 granophyre, splitting it into two, the southern part being the Carrock Fell granophyre, and the northern the Rae Crags granophyre. Cooling of the B1 magma would have occurred initially in a uniform thermal regime, and thus crystallisation was from both margins inwards as the magma cooled by conduction from both walls, causing residual liquids to become concentrated in the central region. The hydrothermal convective cell was operating at the time of emplacement of subunit B1 as the alteration effects are most pronounced in this subunit. Local melting of the granophyre occurred on the emplacement of subunit B1, producing the back-veining and hybridisation effects, observed at Round Knott (MR 3345, 3372) and Scurth (MR 3510, 3388).

It is very interesting to note, that the proposed sequence of intrusion of the subunits, which seems to fit the field and petrographic observations most closely, is the reverse order of the fractionation sequence. It would therefore be attractive to speculate that the order of intrusion reflects the emptying of a vertically differentiated magma chamber.

6.3 MECHANISM OF FRACTIONATION IN UNIT B

Layering and related phenomena have provided the central theme for the interpretation of differentiation processes in igneous rocks (Wager and Brown, 1968). Much

recent work and debate, however, has centred on the mechanisms of crystallisation and accumulation in magma chambers, and on the mechanisms of fractionation in silicate melts (i.e. McBirney and Noyes, 1979). In particular, the role of gravity in accumulation of crystals (Wager et al., 1960; Wager and Brown, 1968) has come under close scrutiny in the light of measurements on physical properties of magmas, particularly viscosity, density and yield strength (Murase and McBirney, 1973; McBirney and Noyes, 1979). The application of fluid dynamic, thermochemical and physical principles to processes in magma chambers has opened up a new area of research, and in the light of present changing ideas, and still, as yet, limited knowledge of the dependence of physical properties on other variables, it would be unwise to do more than speculate about the mechanism of in situ fractionation within Unit B. Several pertinent conclusions may be drawn however.

It would appear that gravity played only a minor role, if any, in producing the observed distribution of crystalline phases within the sheets, as the sheets are essentially sub-vertical. Except on a local scale in subunit B1, and then only of a diffuse nature, no rhythmic layering phenomena exist in Unit B. Lamination when present is parallel to the margins of the sheets. The lack of scatter about the chemical variation trends of the Unit B rocks in figure 5.1 suggests that little, if any, differential accumulation of one phase relative to another occurred. These observations, together with the abundance of disequilibrium crystallisation

phenomena, comb layering and skeletal morphology, and the strong zonation of plagioclase and, to a lesser extent, pyroxenes produced by rapid crystallisation, suggest that crystallisation occurred in situ against the walls of the sub-vertical sheets, and in particular the southern margins in subunits B2 to B4. The rocks, in this respect, might be termed congelation cumulates (Wager and Brown, 1968).

The viscosity of silicate melts has been measured experimentally by Shaw (1969), Murase and McBirney (1973), and McBirney and Noyes (1979), and has been shown to increase substantially with crystallisation. Shaw (1965) suggests, however, that the effect of volatiles would be to reduce the viscosity, and that it would not increase in excess of one order of magnitude until more than half crystallised. Whatever the viscosity, the suspension of crystals in a vertical magma column, requires the crystal-liquid suspension to have a finite yield strength, in order to overcome the gravitational stress acting upon individual crystals, and hence, prevent settling or slump. It is significant in this respect that no evidence for slumping exist in the Unit B rocks. Rapid crystallisation undoubtedly contributed to the above requirement.

As noted in the previous section, a thermal gradient existed across the magma column within individual sheets, in some cases high enough to cause significant undercooling in the melt, thus, resulting in comb layered phenomena. Certainly, the gradient was always high enough to cause fairly rapid crystallisation and, hence, prevent equilibrium being maintained

between crystals and liquid. This is evident from strong zonation in the plagioclase, and incorporation of Al and Ti, metastably, in pyroxene. A direct consequence of the thermal gradient, will be a chemical potential gradient within the magma. It is unlikely that convection occurs to any great extent in intrusions less than 100 m. wide (Shaw, 1965), and therefore, that conductive heat loss, through the southern wall of each sheet, was the dominant cause of the thermal gradient.

In summary then, nucleation, probably inhomogeneously or by self nucleation (Campbell, 1978), occurred in conditions of supercooling along the southern walls of individual sheets, (both walls in the case of subunit B1). Continued rapid crystallisation within a high thermal gradient, prevented equilibrium of crystals with melt, and enhanced fractionation within the melt. It is unlikely that diffusion was the sole cause of fractionation, and some relative movement of crystals and liquid, by a method analogous to filter pressing, must have been operative. Rapid crystal growth would reduce the porosity of the crystal-liquid framework, until the point where liquid became trapped in the interstitial pore spaces. At this point, growth of crystals would continue from the trapped liquid, (orthocumuls growth of Wager et al., 1960). The residual liquid would crystallise as granophyric intergrowths, but would, as noted earlier, represent a smaller volume than the actual volume of trapped liquid. The more fractionated liquid in each subunit crystallised on the northern margin, and may have become contaminated by pore liquids from the southern margin of the adjacent sheet. Subunit B5 represents the most fractionated liquids, but these are considered to be near

eutectic melts, containing at most 20% crystals. The normative felsic components lie close to the ternary minimum at 1.5Kb PH_2O, in the system SiO_2-Ab-Or-H_2O. (figure 4.2).

6.4. THE WATER CONTENT OF THE UNIT B MAGMA.

At this point, it is interesting to speculate about the H_2O content of the magma, and its effects on crystallisation. Pegmatitic features, such as the corrosion of earlier formed phases, growth of H_2O - saturated phases, and especially the growth of large crystals (see section 4.1.10.2) which requires rapid transfer of nourishing materials to centres of nucleation, suggest that the magma may have become locally saturated with a low-viscosity aqueous phase. This aqueous phase would be largely H_2O, although CO_2, F and H_2S, were probably also present in small quantities, as endorsed by the occurrence of carbonate, amphibole, apatite, pyrrhotite and pyrite. The critical pressure of H_2O is 221 bars, (Carmichael et al., 1974), which is equivalent to a depth of 1 km. Regardless of temperature, therefore, the aqueous phase would be in a supercritical state, with no distinction between vapour and liquid, as suggested by Jahns and Burnham, (1969).

The effect of a low viscosity aqueous phase, probably 10^{-3} or 10^{-4} poise (Frank, 1961), would be to lower the isothermal viscosity of the melt. Burnham (1967), showed that the addition of 6.4 Wt%H_2O to a granitic melt, decreased the viscosity from 10^9 to 10^5 poise. Calculations following Shaw (1972), show that addition of 1.5 Wt%H_2O to a ferrodiorite liquid composition, decreases the viscosity by 1.5 orders of magnitude. The decreased viscosity is primarily a function of the depolymerisation effect of the H_2O on the silicate

framework structure in the melt. (Burnham, 1979a; 1979b). Lower viscosity is however counteracted, to a limited extent, by the thermal effects of lowering liquidus temperatures.

Initially individual magma pulses would be undersaturated with respect to H_2O on intrusion. With fractionation of anhydrous phases, such as plagioclase, pyroxene, and Fe-Ti oxides, the water content would increase until the magma becomes saturated by the aqueous phase, and a pegmatitic facies would develop. This seems to occur between 50-80% crystallisation of individual sheets, although there is considerable variation between sheets, and some show no pegmatitic facies. Because of later alteration effects, however, it is not possible to measure the water content of the magma quantitatively, although a semi-quantitative estimate can be made.

Figure 6.4, shows how crystallisation of anhydrous phases would affect the concentration of H_2O in a magma containing initially 0.5, 1.0, 2.0 and 3.0 Wt%H_2O. Crystallisation of the limited volume of anhydrous phases can be ignored, as formation of 5% amphibole or apatite, would lower the whole-rock H_2O content by only 0.1 Wt%H_2O. Also shown on figure 6.4, as dashed lines, are the water saturation levels under varying confining pressures, of andesitic and granite (pegmatitic) melts. (the data are from Hamilton et al., 1964, and Burnham and Jahns, 1962). An overburden of 2.5 km. at Carrock Fell, would produce a load pressure of approximately 1 kb. The exposed section would be equivalent to only 0.15 kb, and can therefore be ignored. At 1 kb and 60-70% crystallisation, the H_2O content at saturation would be approximately 4 Wt%,

equivalent to approximately 1.0 Wt%, before any crystallisation. The lower pressure stability of Fe-rich amphibole in acid rocks has not been determined experimentally, but Holloway and Burnham (1972), found experimentally that amphibole is stable down to 2 kb in tholeiitic basalt. This is likely to be lower in acidic rocks, but may indicate that the estimate of overburden was low.

The magmatic system is assumed to be closed with respect to H_2O in the above estimation. However, upward fluxing of the aqueous phase may have occurred, as the pegmatitic facies are more widely developed in higher exposures of the intrusion. Also, as noted in section 6.2, influx of water during hydrothermal circulation may have contributed to the overall H_2O content.

SiO_2, Al_2O_3, Na_2O and K_2O, are all soluble to varying degrees in an aqueous phase in equilibrium with a melt (Tuttle and Bowen, 1958; Carmichael et al, 1974; Burnham, 1979a;b) This may account for the increased proportion of quartz and alkali felspar intergrowths within the pegmatitic facies. The increased H_2O should tend to stabilise amphibole, but also, due to the dissociation of H_2O, should lead to an increase in fO_2, as the diffusivity of H_2 is considerably higher than O_2, and this certainly would account for the observed oxidation and resorbtion effects in the Fe-Ti oxides.

6.5 THE FRACTIONATION OF THE UNIT B MAGMA

From the petrographic and mineralogical observations made in the previous sections, it is possible to draw certain conclusions about the fractionation of the Carrock Fell Unit B magma.

The use of simplified phase diagrams, such as MgO-FeO-SiO_2 (Bowen and Schairer, 1935) or MgO-FeO-Fe_2O_3-SiO_2 (Muan and Osborne, 1956), is uninstructive to interpret the fractionation trend, as CaO is undoubtedly an important parameter.

Early liquids lay outside the stability fields of Ca-poor pyroxene or Mg-olivine and were confined to an augite-plagioclase univariant surface or cotectic. Rapid crystallisation would enhance the normal fractionation trend towards Fe-enrichment in the melt, by preventing continued re-equilibration of crystals with magma. This is the stage represented by the rocks of subunit B1. It is likely that fO_2 in the magma was fairly low at this stage and remained fairly constant, (Osborne, 1959; 1979; Roeder and Osborne, 1966), being buffered, primarily, by the magma composition and the precipitating phases, and therefore it did not drop with fractionation as in a system closed to oxygen. At fO_2 10^{-9}, in the system $CaAl_2Si_2O_8$ - Mg_2SiO_4 - Fe_2O_3 - SiO_2 (Roeder and Osborne, 1966) magnetite is a stable phase throughout the Fe-rich part of the system. A liquid fractionating along a univariant plagioclase pyroxene surface or cotectic, intersects the magnetite stability field, so that magnetite-pyroxene (augite) and plagioclase are in equilibrium with the liquid, the stage represented by subunit B2. (ilmenite and apatite are additional phases not represented by the above system).

Under lower fO_2 conditions, the liquid intersects the Fayalite stability field before the magnetite field, and leads to extreme Fe-enrichment with little SiO_2 enrichment.

At higher, or increasing fO_2 conditions the magnetite stability field becomes enlarged and the pyroxene-plagioclase univariant surface is reduced in size. Fe-encirchment can only be very limited in this case. Precipitation of low SiO_2 phases, magnetite, ilmenite, and apatite, causes the residual liquids to become enriched in SiO_2, and eventually intersect the silica minerals field. The $aSiO_2$ may, however, be buffered in the case of Unit B by plagioclase fractionation, thus preventing the actual intersection of the silica minerals field. This SiO_2 enrichment stage is defined by subunits B3 to B5. The fractionating liquid becomes depleted in Fe by continued magnetite and pyroxene crystallisation, the Fe/Fe+Mg ratio continues to increase, Na/Ca+Na increases, and K_2O increases as no potassium bearing phases crystallise. During this stage, the fO_2 probably remained fairly constant, but was buffered high enough to prevent fayalite crystallising, according to the reaction :

$$3Fe_2SiO_4 + O_2 \rightleftharpoons 2Fe_3O_4 + 3SiO_2$$

continued removal of magnetite, and buffering of $aSiO_2$ by plagioclase, probably buffered the fO_2 between the experimentally determined QFM and HM buffer curves (Eugster and Wones, 1962), but in the absence of meaningful data on coexisting Fe-Ti oxides, no quantitative relationship can be calculated. Textural evidence exists for a reaction relationship of Fe-pyroxene with liquid, to produce Fe-amphibole in subunits B3 to B5. Data from Fe-Ti oxides coexisting with Fe-amphibole in silica rich liquids (Carmichael, 1967) supports the higher oxygen fugacity in this range. The stability of Fe-amphibole with Si-rich liquid suggests that the H_2O may have had an

external buffering effect on the fO_2 of the liquid. Irvine (1976) showed that the existence of a metastable two-liquid solvus over large regions of the system Mg_2SiO_4 - Fe_2SiO_4 - $CaAlSi_3O_8$ - SiO_2, at 1 atm., and showed that the degree of relative iron or silica enrichment in fractionating liquids is dependent on the presence of $KAlSi_3O_8$, and its ability to suppress the solvus at higher liquidus temperatures. This system, and the role of silicate liquid immiscibility in the Unit B magma, but more specifically in tholeiitic magmas in general, is discussed fully in the following section.

6.6. THE ROLE OF SILICATE LIQUID IMMISCIBILITY (SLI) IN THE EVOLUTION OF THOLEIITIC ROCKS.

The discovery of a field of low temperature immiscibility in the system FeO-K_2O-Al_2O_3-SiO_2 (Roedder, 1951), at geologically reasonable compositions, and particularly, the discovery of widespread evidence for SLI in Lunar rocks (Roedder and Wieblen, 1970; 1971), has provoked much interest in the possible role of SLI in the evolution of magmas. Many authors have been prompted to propose SLI as a mechanism to account for the lack of intermediate compositions in naturally occurring iron rich and silica rich associations. Recent reviews of the 'state of the art' have been given by Roedder, (1978; 1979), but a summary of pertinent findings in experimental and natural systems, in the last decade, is given here.

It is not intended to enter into lengthy discussion on the theoretical basis of SLI, which is not at present, fully understood, principally because of our limited knowledge of the thermodynamic mixing properties of silicate species in melts. Silicate melts, however, have been discussed in terms

of the types of oxygen bonding between silicate and metal cations. (Toop and Samis, 1962). Hess (1977) interprets the structure of silicate melts, on the basis of bridging oxygen (Si-O-Si), non-bridging oxygen (Si-O-M) and free oxygen (M-O-M) bonding, in terms of the reactions that must occur when melts of metal oxide (MO) and SiO_2 are mixed.

Polymerised silicate melts contain a preponderance of bridging oxygens. In order to minimise the electrostatic repulsions between cations and neighbouring cations, however, non-bridging oxygens are required to coordinate high charge density cations, as these cations cannot enter into tetrahedral coordination in the framework structure of the melt. If the concentration of HFS, framework modifying, cations is high, the charge-screening demands are high. In polymerised melts this causes a positive excess free energy, which is minimised in the system by liquid-liquid separation. Cations of high charge-density partition into a basic, low-viscosity melt, where they can be effectively screened by non-bridging and free oxygens. The conjugate liquid is a more viscous, silica-rich tectosilicate liquid, in which aluminium is tetrahedrally coordinated, charge-balanced by coupled-substitution of low charge-density (LIL) cations. The sum of the free energy of the two separated melts is lower than the free energy of the homogeneous melt. The system is, thus, electrostatically and thermodynamically more stable (Seward, 1970).

The contribution of melt-melt interface energy, configurational entropy, and enthalpy terms, to the free-energy of the system, is discussed by Charles (1969), Hess (1977), Ryerson and Hess (1978; 1980), and Wood and Hess (1980).

Silicate liquid immiscibility is a function of non-ideal mixing of polymeric species, and this is reflected in phase equilibrium studies by the occurrence of a two-liquid solvus, or liquid miscibility gap, (LMG).

Roedder (1951) reported a stable, low temperature, LMG on the join Fayalite-Leucite-Silica (Fa-Le-SiO_2) at latm. This LMG has since been verified, and studied in more detail by Watson (1976), Biggar (1978), Roedder (1978), Freestone (1978), and Visser and Koster van Groos (1979a). The conjugate melts are a high-silica melt, L_S, enriched in Al_2O_3 and K_2O, relative to a high-iron melt, L_f. The system is quaternary over a limited range of temperatures, and shows a marked change in liquid compositions with temperature due to a plateau in the fayalite liquidus. The exposed solvus lies on the tridymite-fayalite cotectic, between an upper temperature of 1210°C and 1270°C, but disappears at a lower temperature, between 1110°C and 1160°C. The lower temperature of the exposed solvus represents a reaction of the type $Tr+L_f \longrightarrow Fa+L_S$, or a eutectic type reaction $Tr+L_f+L_S \longrightarrow Tr+Fa+L_S$. All authors note that there is a metastable extension of the solvus, linking the stable low temperature LMG, with the high temperature LMG, discovered by Greig (1927), in the silica-rich part of the system.

A stable LMG is not present in the related systems Nepheline-Fa-SiO_2, (Bowen and Schairer, 1938) or Le-forsterite-SiO_2 (Schairer, 1954). Naslund (1976), studied the effect of increased fO_2, and addition of sodium, as $NaAlSi_3O_8$ (Ab) in the system $KAlSi_3O_8$ (Or)-FeO-SiO_2. In the Na-free system,

the LMG expanded with increasing fO_2, because expansion of the magnetite stability field decreased the local relative temperature minimum in the system. The system Ab-FeO-SiO_2 showed no stable LMG, at low fO_2 (10^{-12} atm). At fO_2 = 10^{-9} atm., however, the LMG was stabilised, and continued to expand with increased fO_2.

The effects of addition of Al_2O_3 to related systems showing an LMG, (ie. SiO_2-TiO_2-MgO-CaO-FeO, Wood and Hess, 1980) is to reduce the SLI effect. The ability of Al_2O_3 to coordinate tetrahedrally with divalent ions in the silica-poor melt, reduces the structural contrast between the conjugate melts.

The high charge screening demands of TiO_2 and P_2O_5, however, have the effect of expanding the LMG, when added to systems showing SLI. (Watson, 1976; Ryerson and Hess,1978; 1980; Wood and Hess, 1980; Freestone,1978; Visser and Koster van Groos,1979b). The ability of phosphorous to complex with metal cations, increases the liquid-liquid distribution coefficient of those cations (Ryerson and Hess 1978; 1980; Visser and Koster van Groos 1979b). P_2O_5 and TiO_2 also have the effect of polymerising the melt by coupled-substitutions of the sort, $P^5+Al^3 \rightleftharpoons Si^4.Si^4$, and $Si^4 \rightleftharpoons Ti^4$. Addition of P_2O_5 and TiO_2 to the system FeO-K_2O-Al_2O_3-SiO_2, raises the maximum temperature of the LMG by 35°C/Wt% P_2O_5 added,and 25°C/Wt% TiO_2 added. The minimum temperature is lowered 25°C/Wt% P_2O_5 added, but no effect was produced on addition of TiO_2 (Visser and Koster van Groos 1979b). The effect of pressure on this system has been studied by Nakamura (1974), and in the P_2O_5 bearing system, by Visser and Koster van Groos (1979c). The expansion of the silica field relative to the Fa field, causes the stable LMG to disappear at pressures

above $6.5^{\pm}$1Kb. Addition of P_2O_5 increases the stability of the LMG by $4^{\pm}$1Kb/Wt%P_2O_5 added.

Thus, it is found that the size of the field of stable SLI, represents a balance between the tendency of the various components of the systems to promote, or suppress, the immiscibility, and their tendency to depress liquidus temperatures. In magmas, it may be expected to depend especially upon the depression of the liquidii of the mafic and oxide minerals, relative to the liquidus of plagioclase. Systems with high CaO, FeO, Fe_2O_3, FeO/MgO, P_2O_5 and TiO_2 have low liquidus temperatures, and additionally these elements, particularly P and Ti, have the effect of expanding the two-liquid solvus.

Tholeiitic magmas, therefore, should show a tendency to approach a stable LMG in the latter, iron-enriched, stages of fractionation, providing apatite and ilmenite do not crystallise in significant amounts prior to this. Lunar basalts commonly show SLI in their latter stages of crystallisation, (Roedder and Wieblen, 1970; 1971; Wieblen and Roedder, 1973; Hollister and Crawford, 1977). This is undoubtedly a function of their high Ti, P and Fe. Many rapidly cooled terrestrial basalts, however, also show late stage SLI, with, usually, globules of brown high-iron glass in a silica -rich interstitial glass (Roedder and Wieblen, 1971; De, 1974; Clochiatti, 1978; Roedder, 1978; Philpotts, 1978; 1979; see also Plates 6.1a and b). Some of the SLI observed in these examples may result from quenching into the metastable solvus (Biggar, 1979), but still confirms the existence of a solvus.

Fractional crystallisation experiments (as opposed to equilibrium experiments) have been conducted on synthetic lunar basalt compositions (Hess et al 1975), and on natural terrestrial examples, in order to establish whether low temperature liquids intersect a stable LMG (Dixon and Rutherford, 1979; Philpotts, 1979). All the experiments showed that the fractionating liquids intersect a stable LMG, but the degree of fractionation required to intersect the solvus, varies from 45 to 95%. Philpotts (1979) found that the stable LMG was intersected at higher temperatures with increasing fO_2. USGS standard diabase, W-1, shows no obvious evidence for SLI in thin-section, however, similar fractionation experiments conducted on this sample (Philpotts, op cit), show SLI between 1035 and 1040°C. McBirney and Nakamura (1974) and McBirney (1975) report SLI in experiments conducted on mixtures of Skaergaard Upper Zone and Upper Border Group compositions.

The origin of the Daly Gap (Daly, 1933) particularly in the Tertiary Thulean province, has received considerable attention and provoked much debate in the last 50 years. Both crystal fractionation of basalt, and partial melting of acidic crustal rocks by higher temperature mafic melts, have been proposed, amongst other hypotheses, to account for the observed bi-modal distribution of rocks in tholeiitic provinces. The pendulum has swung back and forth as new methods have enabled new approaches to the problem to be pursued. The problem has by no means been resolved yet, but present published consensus, in the Hebridean province at least, favours crystal fractionation of a basaltic parent (Thorpe et al, 1977; Thorpe, 1978) but with varying degrees of crustal contamination, (Walsh et al. 1979).

The similarity of the high-iron and high-silica conjugate melts produced in experiments, and observed naturally, to natural iron rich-silica rich associations, (ferrobasalt-rhyolite or ferrogabbro-granophyre), has prompted many authors to propose SLI as a mechanism to account for the observed lack of intermediate compositions - the Daly Gap - (De, 1974; McBirney, 1975; Philpotts, 1976; 1979; Rutherford et al. 1976; Wiebe, 1979).

Figure 6.7 shows the $K_D.L_F-L_S$(K_D = concentration of element in iron rich melt/concentration in silica-rich melt) calculated for the major elements for conjugate immiscible melts, from crystallisation experiments (Rutherford et al, 1976;Ryerson and Hess,1978), and from melt inclusions (Roedder and Wieblen, 1970). Also plotted are K_D's calculated for the Upper Zone B ferrogabbro and Upper Border Group transitional granophyre, from Skaergaard (Wager and Brown, 1968), and a subunit B2 ferrograbbro and B4 granophyre from Carrock Fell. It will be noted that there is very good agreement between the partitioning behaviour between immiscible melts, and the observed distribution of major elements between ferrogabbro and granophyres.

Theory predicts, and experiment shows, that HFS trace elements (ie Zr, Nb, Y, REE) behave identically to Fe, Ti, and P, in their partitioning behaviour. (Watson, 1976; Ryerson and Hess, 1978). They, therefore, concentrate in the high iron melt. A study of the distribution of HFS trace elements between natural ferrobasalt-rhyolite or ferrograbbo granophyre associations, however, shows the reverse of the observed effect for conjugate immiscible melts.

It has been shown that a stable LMG exists in fractionated tholeiitic compositions, resulting in a high iron and a high-silica conjugate pair, at geologically reasonable temperatures, and at reasonable levels of fractionation that would allow physical separation to occur. The observed trace element distribution, however, is not in accordance with fractionated granitic rocks being produced by a straightforward application of the silicate liquid immiscibility model.

Irvine (1976) found that in the system, Mg_2SiO_4 - Fe_2SiO_4 - $CaAl_2Si_2O_8$ - SiO_2 - $KAlSi_3O_8$, that the solvus extended metastably over large areas of the system, and that it had a profound effect on the shape of the liquidus surface and size of the primary phase volumes. It is termed the silica immiscibility effect (Irvine 1975). Non-ideality in silicate melts contributes to a positive excess free energy in the system. The experiments of Irvine show that the non-ideality extends beyond the compositional limits of the solvus. Consequently, liquids in the vicinity of miscibility gaps, either stable or metastable, have higher molar Gibbs free energies and, therefore, higher liquidus temperatures than they would if they were ideal. Non-ideality, thus, tends to shift liquid-solid equilibria in favour of the solid by raising melting temperatures. Liquidus temperature contours and liquidus boundaries in the vicinity of solvii will tend to be shifted or deflected away from them. In the potassium free system, Fo-Fa-An-SiO_2, the presence of a metastable solvus, caused the silica minerals field liquidus boundary to be deflected over the solvus, thus preventing substantial silica enrichment in liquids fractionating in the olivine and Ca-poor stability fields. The addition of potassium, as $KAlSi_3O_8$, depressed

the solvus, thus reducing the silica immiscibility effect. This causes the silica minerals field to contract relative to the olivine and Ca-poor primary phase volumes, thus, allowing residual liquids to become enriched in silica.

At lower temperatures in the system, however, the tridymite-fayalite-cotectic is depressed, so that it does not clear the solvus. This effect should be enhanced by the addition of even small amounts of P_2O_5 or TiO_2, especially if the metastable solvus had prevented substanial silica enrichment at higher temperatures. The evidence from tholeiitic basalts, presented earlier, suggests that at lower temperatures in the iron-enriched residual liquids, an LMG is stable or very nearly so.

It is instructive, therefore, to consider at this point, exactly what happens in terms of enrichment of elements and crystallisation of phases in late stage tholeiitic liquids, say, for example, the Carrock Fell Unit B magma. The presence of Fe, Ti and P, contributes both to low liquidus temperatures, and to expansion of the two-liquid solvus. In the Unit B magma, the liquid was precipitating plagioclase and augite. Plagioclase crystallisation contributes to further localised enrichment of the Fe, Ti and P in the interstitial liquid. Consider, therefore, the possibility that the residual liquid intersects a stable solvus. The simplified phase relationships become quaternary at this point, with Aug+Pl.+L_F+L_S. By analogy with the system K_2O-Al_2O_3-SiO_2-FeO, globules of L_S will appear in L_F and will continue to increase in volume, as the L_F reacts with augite. The augite, therefore, is growing at the expense of L_F, with continued increase in L_S. When L_F disappears

completely, the system becomes ternary, with Plag+Aug+L_S. The effect of P_2O_5 and TiO_2 would be to expand the solvus. The partitioning behaviour of P and Ti, means they concentrate in L_F. If for kinetic reasons, apatite or ilmenite had been unable to nucleate and crystallise before intersection of the solvus, the low viscosity of L_F, and high concentration of P and Ti in L_F, would probably cause them to nucleate and grow rapidly at the expense of L_F. The activity of P and Ti would, of course, be identical in both melts, but nucleation and crystallisation is less likely to occur in the high viscosity, high-silica melt. The HFS trace elements, Zr, Nb, Y, REE, etc., partition into the high-iron melt, but it is the crystal-liquid K_D for each element that will control the incorporation of those elements in to the crystallising phases. It is considered likely that crystallisation of augite, ilmenite and apatite from L_F, will affect the equilibrium between the conjugate melts, and the stability of the solvus, and may promote reaction between the crystals and liquids, and between the residual conjugate liquids. Certainly the structural contrast between the liquids will be reduced, and the tendency should be, therefore, for them to re-homogenise, leaving a silica rich liquid with low concentrations of Fe, Fi and P, but containing those HFS elements that did not partition significantly into the mafic phases. The bulk composition of the crystallised phases is essentially that of a ferrogabbro, but the bulk composition of the liquid is that of a granophyre or rhyolite.

The crystallisation of apatite is considered to lend support to the above model. In many intrusions, P_2O_5 concentration rises slowly to a point at which apatite crystallises

When it does, apatite crystallises out of proportion to the P_2O_5 concentration at saturation. Most tholeiitic lava sequences show P_2O_5 maxima rarely in excess of 1Wt%, yet crystallisation of 5-6% apatite in slowly cooled plutons, implies P_2O_5 contents of 2.5 to 3.0 Wt%. In some intrusions apatite may have concentrated by crystal settling but in others it can be shown that it grew in situ. Thus, it would seem that apatite suddenly became supersaturated in the melt. The above model accounts for the sudden, and apparently voluminous, appearance of apatite. The association of apatite with maxima in TiO_2 and FeO content in lavas, may suggest that the above process was operative for ilmenite and magnetite also.

The model assumes that the liquid actually intersects the stable solvus. If the solvus is, however, metastable, the tendency will be for the cotectic boundary to be deflected over the solvus, and form a temperature plateau, where the liquid composition changes considerably with only a small change in temperature. It has already been noted, that non-ideality in the regions close to the solvus shift equilibria in favour of the solid phase. Irvine (1976) notes, in this respect, that a melt held just above the solvus temperature was stable for some time, but that in the same melt at a slightly lower temperature, exsolution in fact initiated rapid crystallisation. Zdaniewski (1975) notes also, that nucleation and growth of phases promoted by the metastable solvus, is a common feature in ceramic systems. The possibility arises, therefore, that the structural changes in the melt solution that result from the effects of non-ideality surrounding the solvus, whether it be stable or metastable, may promote the nucleation and

growth of phases as described in the model above.

While Irvine (1975;1976)discusses the role of metastable SLI in relative iron, or silica, enrichment in the earlier parts of the fractionation sequence, the above discussion of silicate liquid immiscibility controlled crystallisation, may help to explain some of the phenomena observed in late stage tholeiitic rocks. It must be emphasised, however, that the dominant process in the earlier stages of differentiation, is still crystal fractionation, but that crystallisation in more evolved liquids may be influenced by SLI in a way that will enhance residual silica enrichment, and produce the apparent compositional gap between ferrogabbro and granophyre.

Little mention of magnetite crystallisation has been made in the above discussion. The magnetite stability field is expanded by increasing fO_2. The general effect of increased fO_2 on the solvus, however, is to expand it both in synthetic systems (Naslund, 1976), and in natural tholeiites (Philpotts, 1979). Extensive early crystallisation of magnetite under high fO_2 conditions, however, will have the effect of reducing the enrichment of iron in late stage magmas. (The effects of fO_2 and the stability of the magnetite field were considered in section 6.5).

SLI is not restricted to late stage tholeiitic rocks, indeed, the underlying principles of the above discussion apply to other rock types as well. SLI has been proposed to explain certain alkaline rock associations, (Philpotts, 1976) Carbonate-ijolite and carbonate-phonolite associations (Hamilton et al., 1979; LeBas and Handley, 1979) amongst many others.

It is suggested that further experimental work in two areas is required. Extension of the work in the systems, Fo-Fa-An-Or-SiO_2 (Irvine, 1976), and Fo-Fa-Di-Hd-Or-SiO_2 (Hoover and Irvine, 1978), to study the effect of the addition of geologically reasonable amounts of P_2O_5 and TiO_2. Secondly, detailed work is required in natural systems, to study the effect of the stable or metastable LMG, on liquidus relations of coexisting crystallising phases, and study the phase relations of the conjugate liquids themselves. Investigations should also be undertaken in the simpler synthetic systems, to study the effects of fCO_2 and fH_2O at pressure.

FIGURE 6.1.

Modal variation histograms for samples collected at intervals across various sheets in Unit B.

A. Subunit B4, traverse 6.

B. Subunit B4, traverse 1.

C. Subunit B4, traverse 5.

D. Subunit B3, traverse 2.

E. Subunit B5, sample E16184.

Specimens at right of diagrams are from the southern margins of each sheet, those on the left are from the northern margin.

Modes are in Wt%

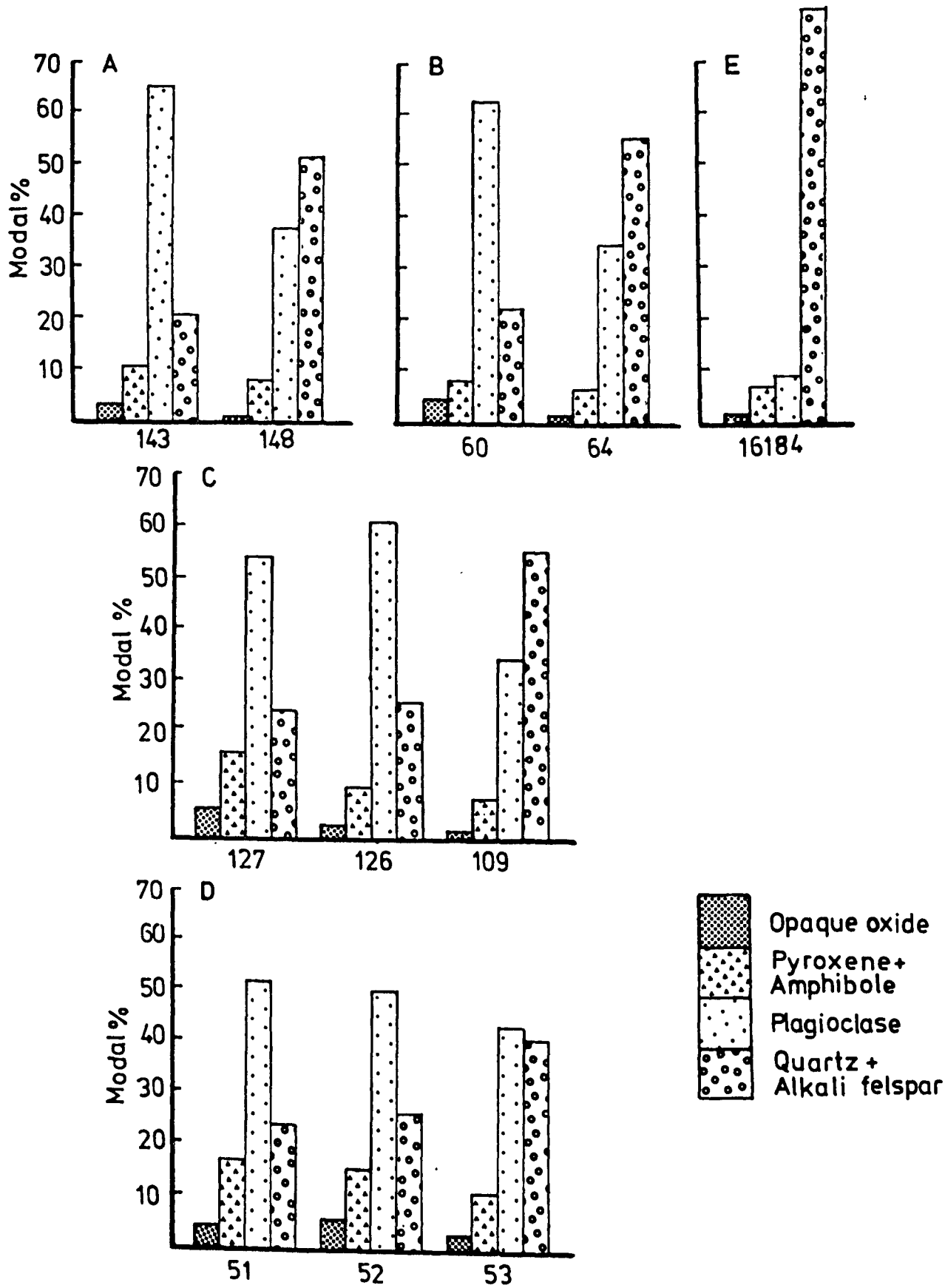
A
B
E
C
D
Modal %
70
60
50
40
30
20
10
143
148
60
64
161
84
127
126
109
51
52
53
Opaque oxide
Pyroxene+ Amphibole
Plagioclase
Quartz + Alkali felspar

FIGURE 6.2.

Zr v. MgO(A), and Zr v. CaO(B), for samples collected at intervals across various sheets

■ Traverse 2, Subunit B3

o Traverse 6, Subunit B4

● Traverse 5, Subunit B4

Points to the right of the trends are analysed samples from the southern margins of the sheets, those on the left are from the northern margins.

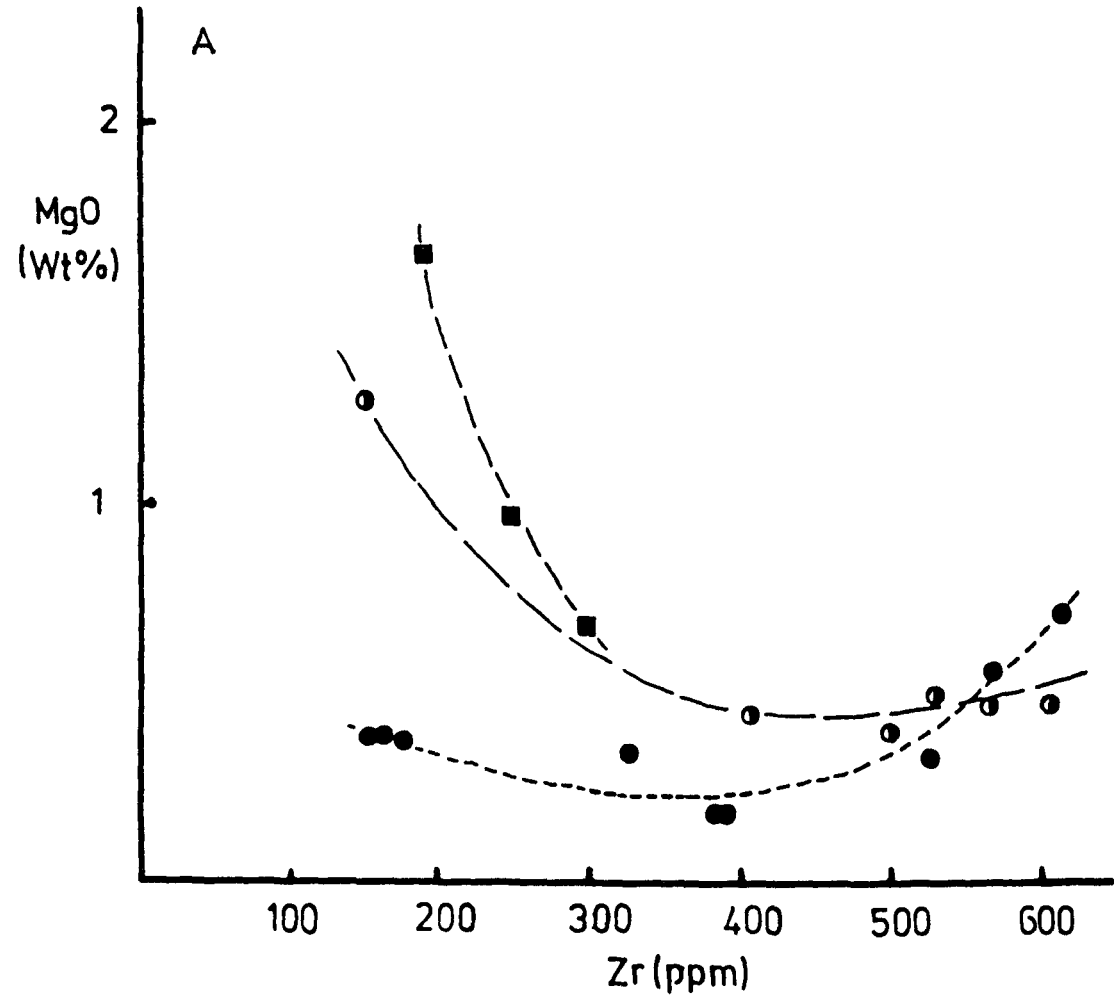
A
2
MgO
(Wt%)
1
100
200
300
400
500
600
Zr (ppm)

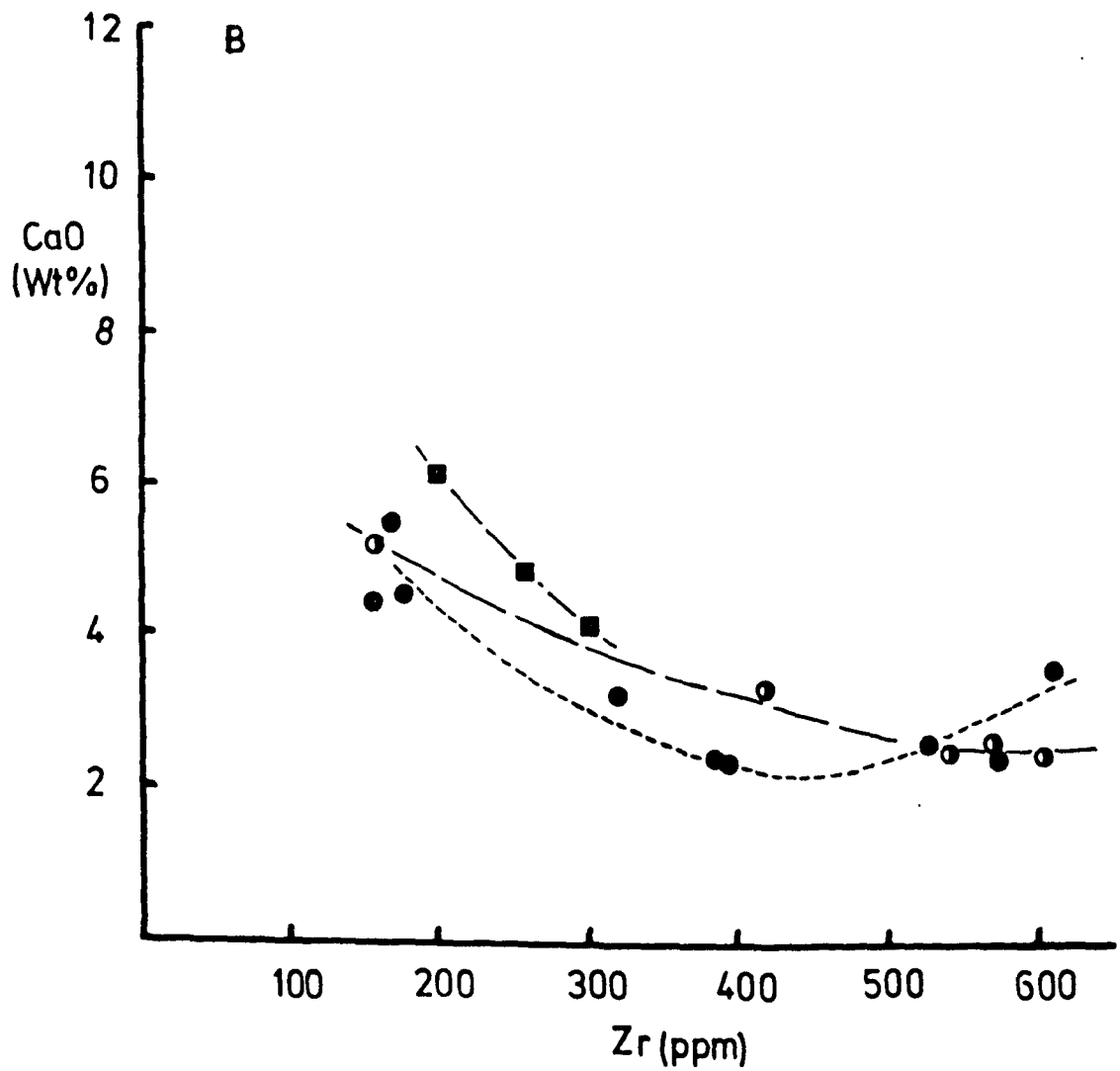
B
12
10
CaO
(Wt%)
8
6
4
2
100
200
300
400
500
600
Zr (ppm)

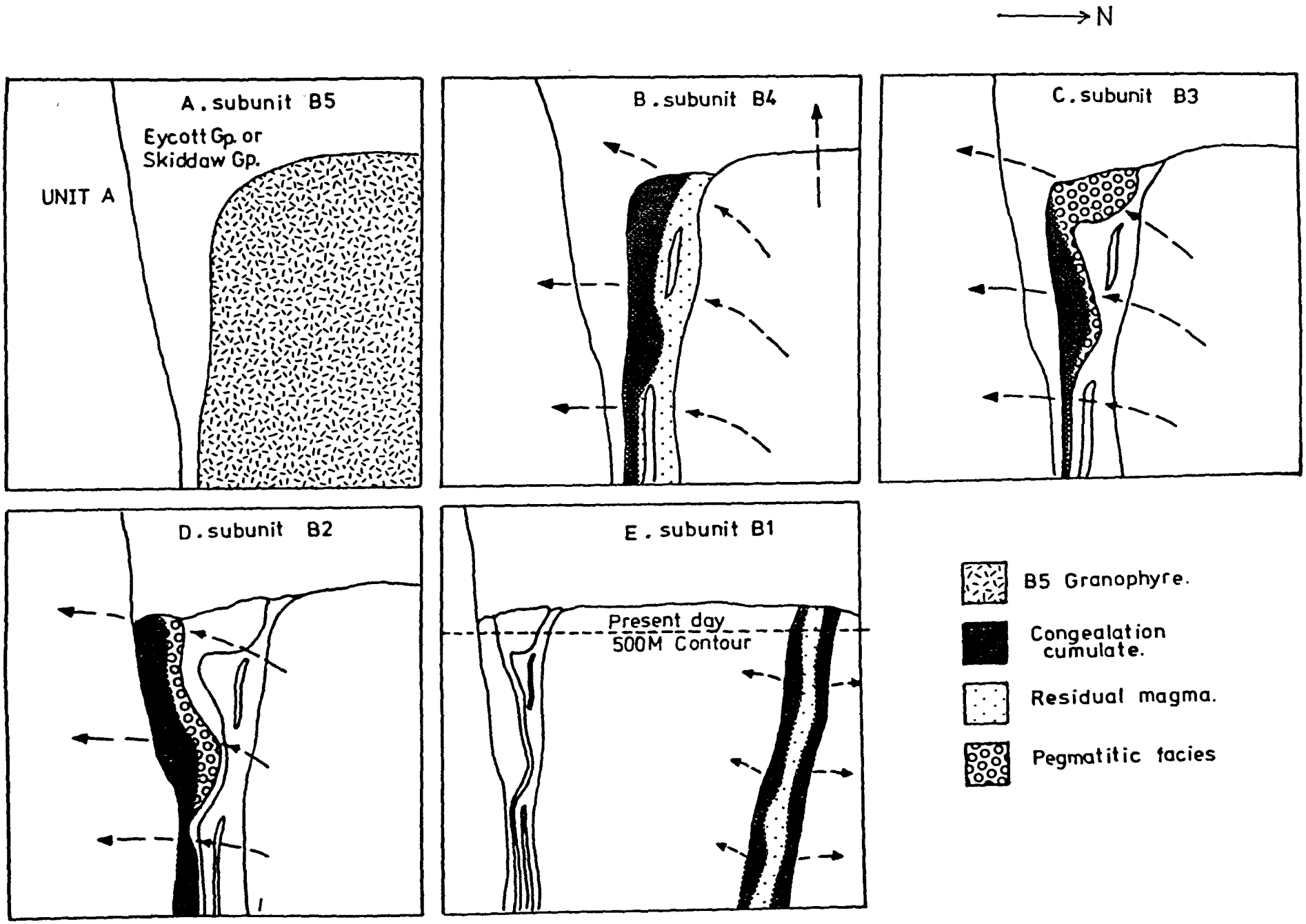
N
A. subunit B5
Eycott Gp. or
Skiddaw Gp.
UNIT A
B. subunit B4
C. subunit B3
D. subunit B2
E. subunit B1
Present day
500M Contour
B5 Granophyre.
Congealation
cumulate.
Residual magma.
Pegmatitic facies

FIGURE 6.4.

The change in Wt%H_2O of a melt, with degree of crystallisation of anhydrous phases.
Solid lines show the increase in Wt%H_2O with crystallisation of anhydrous phases, for initial concentrations of 0.5, 1.0, 2.0 and 3.0 Wt%H_2O. (calculated)
Dashed lines and values on right are water saturation levels at various total pressures in Andesite and Granite (pegmatite) compositions. (Data from Hamilton et al, 1965; Burnham and Jahns, 1962).
For further explanation see section 6.4.

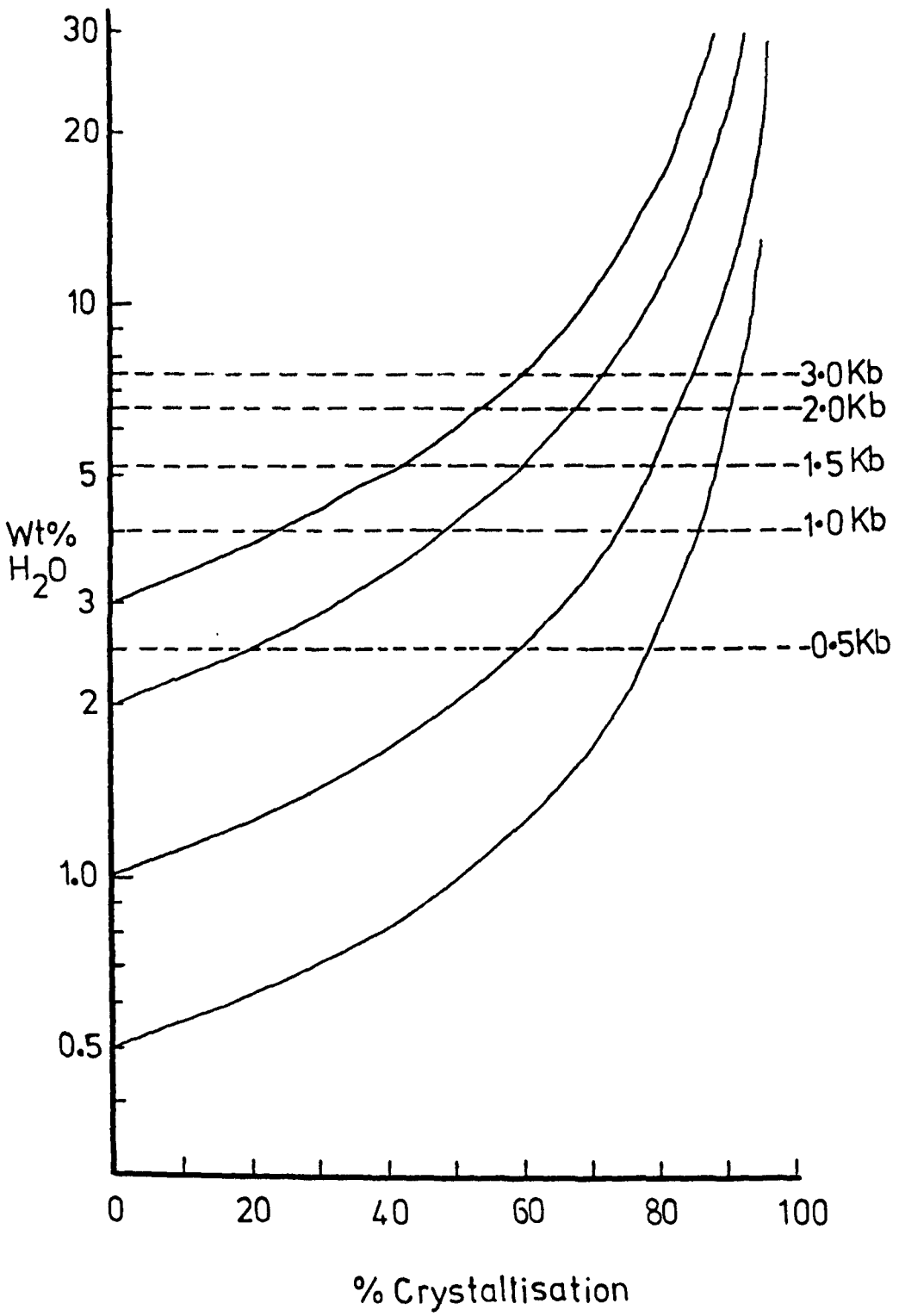
30
20
10
5
3
2
1.0
0.5
Wt%
H_2O
3·0Kb
2·0Kb
1·5Kb
1·0Kb
0·5Kb
0
20
40
60
80
100
% Crystallisation

FIGURE 6.5.

The distribution coefficients for major elements between iron-rich and silica-rich conjugate immiscible melts, from fractional crystallisation experiments on lunar compositions (Hess et al, 1975) and from lunar melt inclusions (Roedder and Wieblen, 1970; and Wieblen and Roedder, 1973).

Also shown are the calculated distribution coefficients of major elements between the Upper Zone B ferrogabbro and Upper Border Group transitional granophyre (data from Wager and Brown, 1968) and between subunit B2 ferrogabbro and subunit B4 ferrogranophyre from Carrock Fell

▽ Hess et al (1975) 12038

▼ " 75055

△ " 14310

▲ " felspar phyric basalt

□ Roedder and Wieblen (1970) silicate melt inclusions

■ Wieblen and Roedder (1973) "

○ Skaergaard

× Carrock Fell

$$K_D^{F-G} = \frac{\text{Concentration in iron rich melt}}{\text{concentration in silica rich melt}}$$

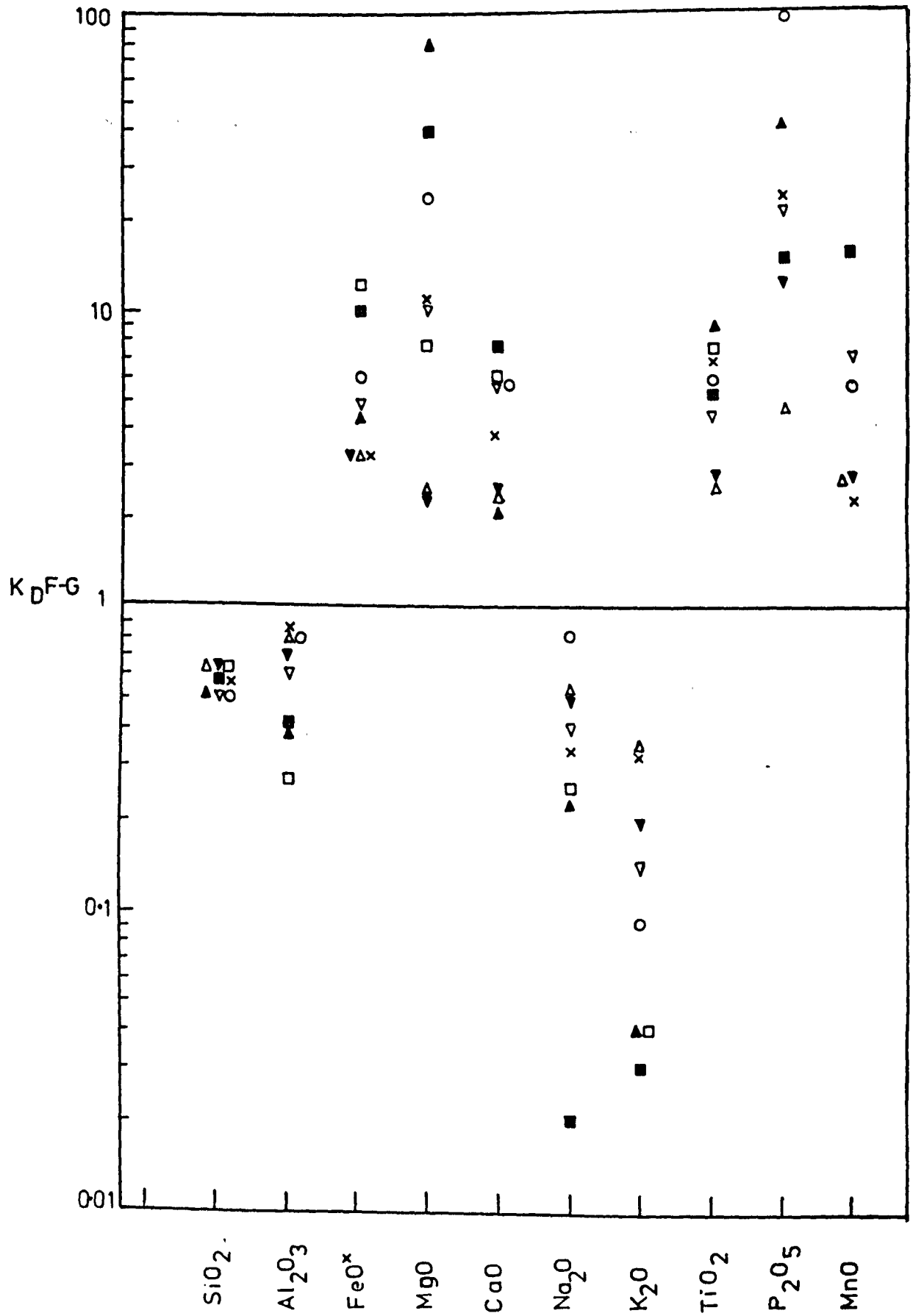
100
10
1
0·1
0·01
K_D^{F-G}
SiO_2
Al_2O_3
FeO^x
MgO
CaO
Na_2O
K_2O
TiO_2
P_2O_5
MnO

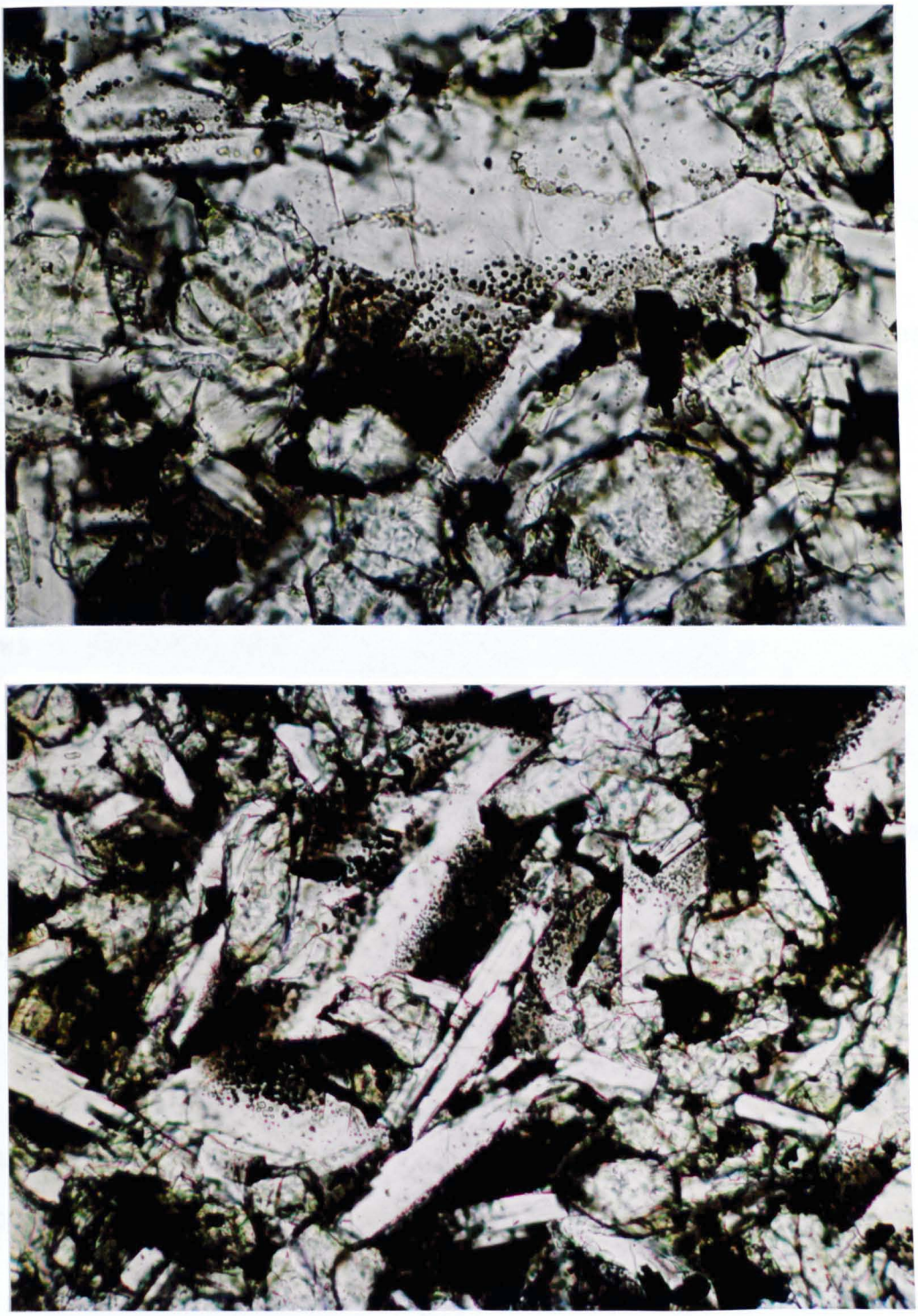

PLATE 6.1 a.b. Photomicrographs : Iron-rich immiscible globules (.005 mm dia.) in interstitial glass of tholeiitic basalt from middle series of Giants Causeway, Co.Antrim.
(PP. Width of field 0.5 mm).

CHAPTER SEVEN

SUMMARY AND CONCLUSIONS

7.1. UNIT A SUMMARY OF CONCLUSIONS

The Unit A gabbros form a dyke like multiple intrusion. They have been divided into three subunits A1, A2 and A3, on the basis of field mapping and primary mineralogy.

No evidence was forthcoming to support the contention that the Leucogabbros and Melagabbros of Eastwood et al (1968), were formed from separate injections of magma. These have been treated as one intrusion, Subunit A1. Variation is continuous from the melanocratic to the leucocratic gabbro. Plagioclase is the dominant phase, modally, in both types. The melagabbro is dark, principally because it shows a greater degree of secondary alteration, although ilmenite and Ca-rich pyroxene (augite) do decrease modally, from the margins to the centre of the intrusion.

Subunits A2 and A3 contain a Ca-poor pyroxene phase, hypersthene in A2, and inverted pigeonite in A3, and, therefore, probably represent a slightly different magma composition.

The mineralogy supports a high $aSiO_2$, but low fO_2. Substantial Fe-enrichment was prevented by early crystallisation of ilmenite however.

Late stage magmatic reactions are a feature of the Unit A gabbros. Pale-mauve Ca-rich pyroxene and ilmenite reacted with the late stage hydrous liquids, to produce a biotite + pale green Ca-rich pyroxene assemblage. The

stabilisation of a primary pale-green pyroxene and biotite, together with the low and high Wo contents of Ca-poor and Ca-rich pyroxenes respectively, and the extended compositional range of the hypersthene stability field compared to other slowly cooled tholeiitic intrusions, suggests a lower liquidus temperature than for those intrusions.

The stabilisation of primary late stage phases in the vicinity of large xenoliths of Eycott lava, and near the margins of the intrusion, may indicate that dehydration and selective leaching of K_2O from the xenoliths and country rock may have contributed to the lower liquidus temperature.

7.2 THE UNIT A GABBROS AND THE EYCOTT VOLCANICS

The petrography, mineralogy and chemistry of the Unit A gabbros shows striking similarities with the Eycott Volcanic Group lavas, and lends support to the contention (Fitton, 1971; Soper, 1974) that they may have been cogenetic.

Field evidence indicates that the Eycott Group are interbedded at their base, with the underlying Skiddaw slates (Eastwood et al, 1968; Downie and Soper, 1972). On micropalaeontological grounds, the Eycott Group have been dated as early Llanvirn in age, and it is possible that they span the Arenig-Llanvirn boundary (Downie and Soper, Op.cit; Millward et al, 1978).

The Unit A gabbros are intruded into folded Skiddaw slates at the base of the Eycott Volcanic Group, and therefore post-date the earliest volcanics. The Eycott lavas, and the massive psammite horizons in the Skiddaw Group are,

however, undeformed, which is probably a function of ductility and layer thickness contrasts (Soper and Moseley, 1978).

If the Unit A gabbros are indeed cogenetic with the lavas, and the petrological, geochemical and dating evidence would seem to support this, then there must have been intra-volcanic tectonism during the early Llanvirn, with the gabbros emplaced at a later stage in the evolution of the Eycott Volcanic Group. This deformation was associated with the early stages of uplift of the Skiddaw anticline, which Downie and Soper (1972), suggest was late or post Llanvirn but pre-Borrowdale volcanic. The evidence presented here may indicate that it extended, at least in its early stages, as far back as the early Llanvirn. Although it is not known what time span the Eycott Volcanic Group covered, their exposed thickness reaches a maximum on Binsey Hill of 2.5 km., but the actual thickness may be greater further to the north and east under the Carboniferous cover.

Palaeomagnetic evidence (Briden and Morris, 1973; Faller and Briden, 1978) suggests that the gabbros were intruded as a dyke-like body at their present position, with a slight allowance for post-Carboniferous tilting. The best estimate of the age of the complex, on palaeomagnetic grounds alone (Briden and Morris, op.cit), is Caradoc-Ashgill. Unfortunately, however, these results have low precision, and no allowance has been made for the fact that the gabbros of Unit A are significantly older than the Unit B gabbros. The magnetic remanence in the Unit A gabbros may, therefore, reflect resetting of the

palaeomagnetic data in the Unit A gabbros, by heat associated with the intrusion of the later, Caradoc-Ashgillian, Unit B suite.

7.3 THE EYCOTT VOLCANIC GROUP

It is generally accepted that the present-day Lake District region, in Ordovician times, lay close to a destructive plate boundary to the north, and formed from tectonism and volcanism associated with subduction southwards under the region (Moseley, 1978a). The finer details of the progressive closure of the Lower Palaeozoic Iapetus ocean, however, are still a matter of debate (see for example, Moseley, 1978b; McKerrow et al, 1978).

Fitton and Hughes (1970), noted the progressive north-south variation in Ordovician volcanic rocks, from the tholeiitic tendencies of the Eycott Volcanic Group, to the calc-alkaline Borrowdale Volcanics, and the predominantly alkaline volcanic rocks further south in Wales. They suggested that this north-south variation paralleled the variation across present day volcanic arc-continental margin provinces, as described by Kuno (1966).

Recent work has suggested that incompatible element modelling and inter-element ratios, when used in conjunction with REE, Cr and isotopic variation, can be used to distinguish between basalts erupted in different tectonic settings (Pearce and Cann, 1973; Pearce and Norry, 1979; Pearce, 1979). The variation in elemental abundances, elemental and isotopic ratios in different tectonic settings,

reflect source heterogeneities or different degrees of partial melting within the mantle (Pearce and Norry op cit; Hawkesworth et al, 1977; 1979). As no REE or isotope data are available for the lavas it would be unwise to speculate about the relative roles of various mantle processes. However, as an initial step to testing the applicability of the proposed model (Fitton and Hughes, op cit) a plot of (Zr/Y) v. Zr is shown in figure 7.1, for the Eycott Volcanic Group basalt and basaltic andesite compositions from Fitton (1971). This diagram (Pearce and Norry, op cit) serves to distinguish between island arc tholeiites (IAT), mid ocean ridge basalts (MORB), and within plate basalts (WPB). Many of the Eycott lavas are porphyritic, and, therefore, have undergone some degree of crystal fractionation. As long as no minor Zr or Y bearing phases are crystallising out, however, the Zr/Y ratio should not change significantly with small degrees of fractionation of plagioclase or pyroxene.

Figure 7.1 shows that, on the basis of Zr and Y variation, the Eycott Volcanic group are not island arc tholeiites but show affinities to WPB.

No REE data are available for the lavas, but the chondrite normalised REE patterns for two Unit A gabbros are shown in figure 7.2, and show LREE enrichment, with $(Ce/Yb)_N$ of 2·64 to 3·36. A combination of plagioclase, pyroxene or ilmenite fractionation should not alter the shape or slope of the normalised curve significantly, so the parental magma was likely to have been LREE enriched also. The

similarity of the trace-element chemistry of the gabbros and volcanics, and the $(La/Y)_N$ ratio of the Eycott volcanics, suggests that the latter were LREE enriched. Island arc tholeiites, however, have a characteristically flat, or LREE depleted pattern (Hawkesworth et al, 1977; Gill, 1970).

The available data suggests that the Eycott Volcanic Group lavas do not show affinities to Island arc tholeiites, although this does not contradict the interpretation of the Central Lake District and Wales Volcanics, (Fitton and Hughes, 1970). The chemistry of the Eycott Volcanics and the Unit A gabbros, however, do show similarities with lavas and gabbros from marginal basins (Weaver et al, 1979; Saunders et al, 1979). Although without isotope and detailed REE data, this correlation is very tentative, it is suggested that a more detailed study of these aspects of the lavas, might prove a fruitful area for further research into the plate tectonic evolution of the Southern Caledonides.

7.4 UNIT B SUMMARY OF CONCLUSIONS

Unit B has been divided into five subunits, on the basis of field mapping and mineralogy. The principal rock types of subunits B1 to B5 are ; gabbro, ferrogabbro, ferrodiorite, ferrogranophyre and granophyre respectively. The sequence shows continuous mineralogical and chemical variation, however, with considerable overlap between the subunits.

Ca-rich pyroxene and plagioclase occur throughout the suite. Apatite, ilmenite and titanomagnetite crystallise abundantly in subunit B2, but only the latter continues to crystallise into B5. Calcic-amphibole is most abundant in subunit B3, and zircon in B4. Plagioclase, pyroxene, and amphibole, all show strong cryptic variation, with increase in Na/Na+K in plagioclase, and increase in Fe/Fe + Mg in pyroxene and amphibole, leading to the formation of ferrohedenbergite and ferroedenite respectively. The physio-chemical controls on mineral chemistry, particularly in pyroxene and amphibole, have been studied in detail.

The chemical variation within the suite, is consistent with the cryptic variation within the phases, and the appearance of new liquidus phases, and is typically tholeiitic. Mg, Ca, Cr, Ni and Co show a continuous decrease with fractionation, and Fe, Ti, P, Mn and Sc show a maximum in B2 then decrease. Sr, Zn and Zr show a maximum in B4, and other incompatible elements increase continually into B5. The suite is LREE enriched and the B5 granophyre shows a negative Eu anomaly.

A hybrid interpretation for parts of the sequence has been discounted, but the sequence of exposed rocks are related by crystal fractionation of an evolved tholeiitic parent probably of a low Mg basalt or ferrobasaltic composition. Fractionation was enhanced by rapid crystallisation and subsequent filter pressing of interstitial liquid.

The crystallisation of magnetite and ilmenite in subunit B2, prevented extreme late stage Fe-enrichment,

but instead, caused residual Si-enrichment. This suggests that fO_2 remained constant during fractionation. $aSiO_2$ was high, thus preventing the liquid from intersecting the fayalite stability field, but was internally buffered by plagioclase, and quartz, therefore, was not a liquidus phase. The granophyre lay close to the ternary granite minimum at 1.5 Kb. H_2O. The evolved liquids were in equilibrium with late hydrothermal fluids, but more mafic rocks show the effects of hydrothermal alteration.

The suite shows considerable textural variation. Of particular note, are textures attributed to rapid cooling or supersaturation. Plagioclases show very strong zonation and pyroxenes, locally, show sector zoning, sub-skeletal morphology, and elongated corkscrew and branching growth phenomena. Regular changes in rock texture and crystal morphology, growth of hydrous phases, and resorbtion of Fe-Ti oxides, associated with saturation of an aqueous phase, occur with the development of pegmatitic facies.

Each subunit forms a subvertical sheet, which shows systematic and regular internal variations. Modal proportions of principal phases change, pegmatitic facies develop, phases show cryptic variation, and incompatible elements increase, laterally within each sheet. The regular variations are best explained by a model of in situ fractionation in response to an assymetric thermal gradient. The order of emplacement of the five subunits is the reverse of their order in the fractionation sequence.

7.5 UNIT B, AND THE c.420 Ma EVENT

It has been demonstrated that the B5 granophyres of Carrock Fell and Rae Crags, were produced by fractional crystallisation of a tholeiitic parent. They have been dated at 416±20 Ma (Rundle, 1979) and have an initial $Sr^{87/86}$ ratio of 0.70708±0.0016.

There are three other igneous events in the Caradoc-Ashgillian period (Rundle, 1979; Gale et al, 1979). The emplacement or extrusion of the Harestones Felsite (419±4 Ma; initial $Sr^{87/86}$ ratio = 0.70799±0.00029), the intrusion of the Ennerdale Granophyre (420±4 Ma; initial $Sr^{87/86}$ ratio = 0.70568±0.00024), and the extrusion of the Stockdale Rhyolite (421±3 Ma; initial $Sr^{87/86}$ ratio = 0.70766±0.00022). These rocks form the c 420Ma 'event' in the Lake District (Rundle, 1979). The initial $Sr^{87/86}$ ratios for the Stockdale Rhyolite, Carrock Fell Granophyres and Harestones felsite are all identical within experimental errors, but that of the Ennerdale Granophyre is slightly lower.

Apart from the Unit B gabbros, a dolerite (and supposed hybrids) associated with the Ennerdale Granophyre (Rastall, 1906), and a few intermediate minor intrusions cutting the Unit B suite, which may be significantly later, no other basic rocks of proven Caradoc-Ashgill age occur in the Lake District. It is proposed, however, that the other evolved rocks of the c.420 Ma event, were formed from a tholeiitic parent, in a similar manner to the Carrock Fell and Rae Crags granophyres.

The slightly high initial $Sr^{87/86}$ ratios, do not preclude an origin by fractional crystallisation. High initial

ratios can originate by selective crustal contamination (Pankhurst, 1977; Walsh et al, 1979) or source heterogeneity (Sun and Hanson, 1976; Sun and Nesbitt, 1977; Kyle, 1980). Certainly by Caradocian times, when the Iapetus ocean was closing, the mantle under the Lake District may have been significantly contaminated by radiogenic strontium from dewatering of the down-going oceanic slab.

The event that led to the production of the tholeiitic rocks is, however, open to debate. The Iapetus ocean was closing during Caradoc-Ashgillian times (Moseley, 1978a), but continent-continent collision did not occur until late Silurian, resulting in the major deformation and associated granite emplacement. There had been uplift and erosion, however, in pre-Caradocian times (Soper and Moseley, 1978) and the area was transgressed from north to south by a marginal sea in Caradoc-Ashgill times (Ingham and McNamara, 1978).

It is possible that the c.420 Ma event, represents the continental extension of a tectonic regime analogous to back arc spreading. (Elliott, 1976; Kyle, 1980), which would account for the tholeiitic nature of the event, the LREE enrichment, and the observed $Sr^{87/86}$ ratios.

FIGURE 7.1

(Zr/Y) v. Zr for lavas from the Eycott volcanic group (data from Fitton, 1971)

Porphyritic lavas

Porphyritic lava groundmass compositions and aphyric lavas

A Field of Island Arc Tholeiites

B Field of Mid Ocean Ridge Basalts

C Field of Within Plate Basalts

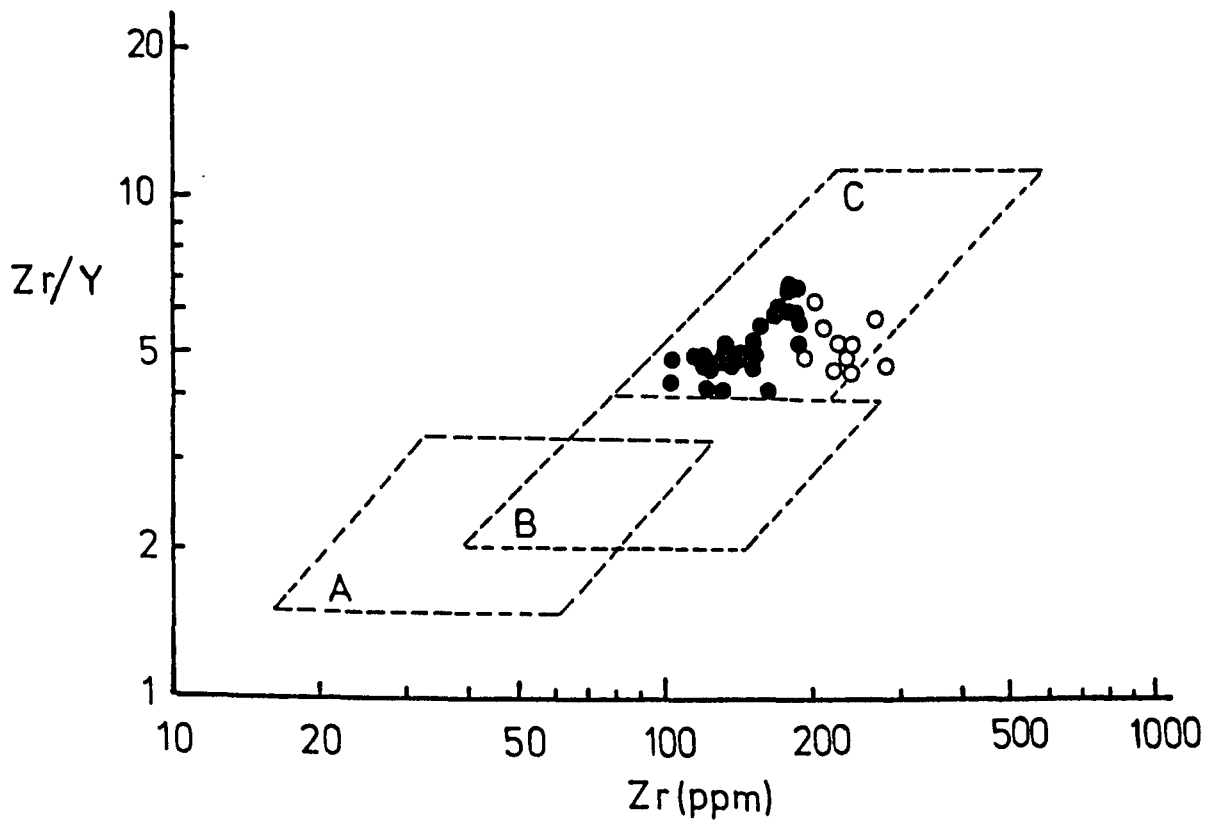
20
10
5
2
1
Zr/Y
A
B
C
10
20
50
100
200
500
1000
Zr (ppm)

FIGURE 7.2

Rare earth element chondrite normalised patterns for gabbros from subunit A1 and A3

(Normalising data from Nakamura, 1974
REE data in Appendix two)

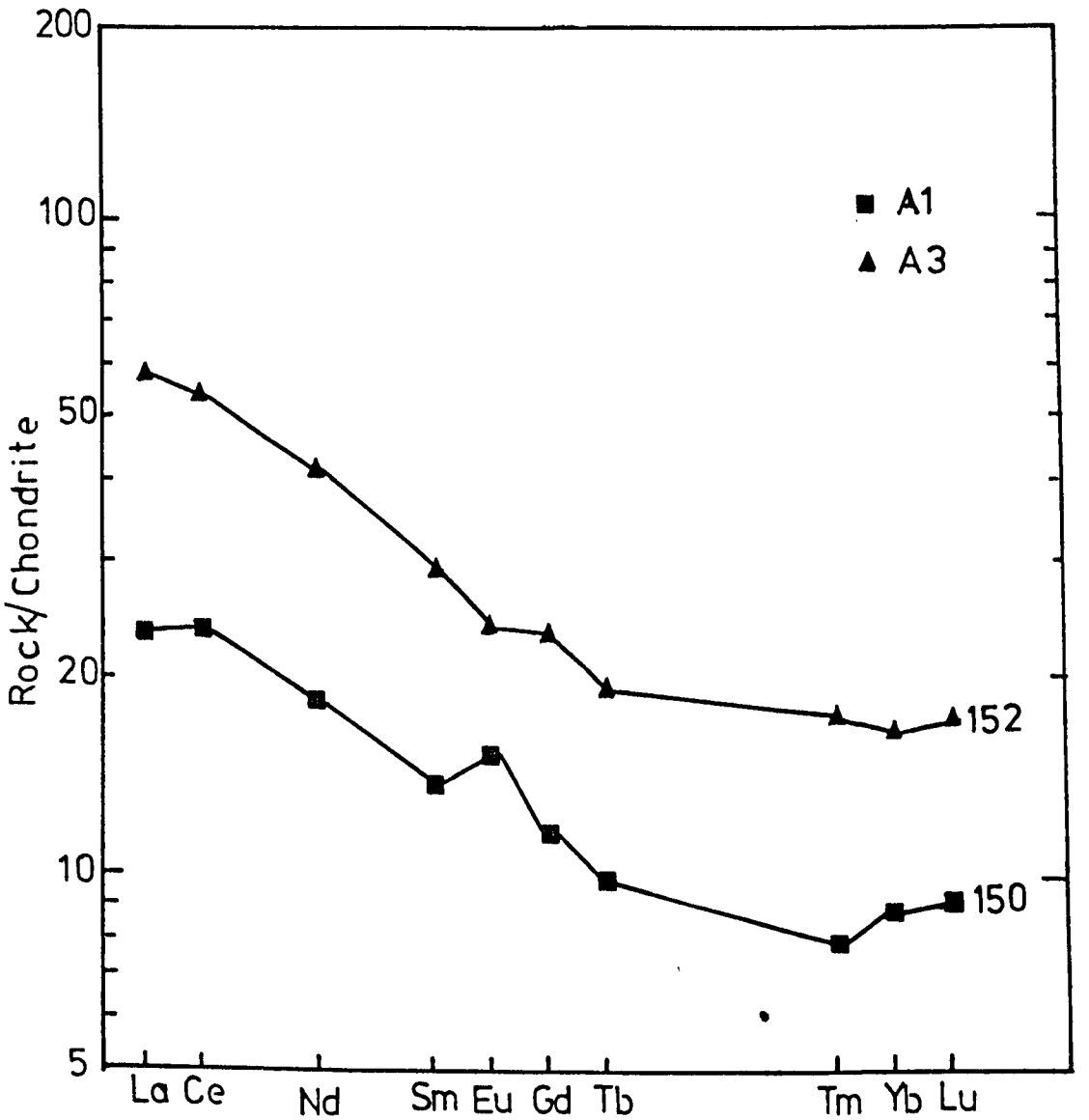
200
100
50
20
10
5
Rock/Chondrite
A1
A3
152
150
La Ce Nd Sm Eu Gd Tb Tm Yb Lu

REFERENCES

Anderson, A.T. Jr. (1968). Oxidation of the La Blache Lake Titaniferous magnetite deposit. Quebec. J. Geol. 76, 528.

Arth, J.G. (1976). The behaviour of trace elements during magmatic processes - A summary of theoretical models and their applications. J. Res. U.S. Geol. Surv. 4, 41-47.

Barberi, F., Bizouard, H. and Varet, J. (1971). The Nature of Clinopyroxene Fe-enrichment in alkalic and transitional magmas. Conrib. Mineral. Petrol. 33, 93-107.

Bence, A.E., Papike, J.J. and Lindsley, D.H. (1971). Crystallisation histories of clinopyroxenes in two porphyritic rocks from Oceanus Procellarum. Proc. Lunar Sci. Conf. 2nd. 559-574.

Biggar, G.M. (1978). Revision of the two-liquid field in the system SiO_2-FeO-Al_2O_3-K_2O. Prog. Exp. Petrol. 4th REP. NERC. 204-207.

Biggar, G.M. (1979). Immiscibility in tholeiites. Min. Mag. 43, 544-546.

Bowen, N.L. (1928). The Evolution of the Igneous Rocks. Princeton Univ. Press. Princeton, N.J. 320 pp.

Bowen, N.L. and Schairer, J.F. (1935). The system MgO-FeO-SiO_2. Am. J. Sci. 29, 151-217.

Bowen, N.L. and Schairer, J.F. (1938). Crystallisation equilibrium in nepheline-albite-silica mixtures with fayalite. J. Geol. 46, 397-411.

Boyd, F.R. and Schairer, J.F. (1962). The system $MgSiO_3$-$CaMgSi_2O_6$. Carnegie Inst. Yr. Bk. 61, 68-75.

Briden, J.C. and Morris, W.A. (1973). Palaeomagnetic studies in the British Caledonides III. Igneous rocks of the Northern Lake District, England. Geophys. J.R. Astr. Soc. 34, 27-46.

Brown, G.M. and Vincent, E.A. (1963). Pyroxenes from the late stages of fractionation of the Skaergaard Intrusion, E. Greenland. J. Petrol. 4, 175-197.

Brown, G.M. (1957). Pyroxenes from the early and middle stages of fractionation of the Skaergaard Intrusion, E. Greenland. Min. Mag. 31, 511-543.

Brown, G.M., Emeleus, C.H., Holland, J.G. and Phillips, R. (1970). Petrographic, mineralogic and X-ray fluorescence analysis of Lunar igneous type rocks and spherules. Science. 167, 599-601.

Brown, P.E., Miller, J.A. and Soper, N.J. (1964). Age of the Lake District Intrusions. Proc. Yorks. Geol. Soc. 34, 331-342.

Buddington, A.F. and Lindsley, D.H. (1964). Iron-titanium oxide minerals and synthetic equivalents. J. Petrol. 5, 310-357.

Burnham, C.W. (1967). Hydrothermal fluids at the magmatic stage In: H.L. Barnes (Ed) Geochemistry of Hydrothermal Ore Deposits. p. 34-76. Holt Reinhart and Wilson. New York.

Burnham, C.W. (1979a). Magmas and hydrothermal fluids In: Barnes, H.L. (Ed.) Geochemistry of hydrothermal ore deposits. 2nd Edn. Wiley and Sons Inc. New York.

Burnham, C.W. (1979b). The importance of volatile constituents In: H.S. Yoder Jr. (Ed) The Evolution of the Igneous Rocks. 50th Anniversary Perspectives - p. 439-478. Princeton Univ. Press. Princeton, N.J.

Burnham, C.W. and Jahns, R.H. (1962). A method for determining the solubility of water in silicate melts. Am. J. Sci. 260, 721-745.

Campbell, I.H. (1978). Some problems with cumulus theory. Lithos 11, 311-324.

Campbell, I.H. and Borley, G.D. (1974). The geochemistry of pyroxenes from the Lower Layered Series of the Jimberlana intrusion. Western Australia. Contrib. Mineral. Petrol. 47, 282-297.

Campbell, I.H. and Nolan, J. (1974). Factors affecting the stability field of Ca-poor pyroxenes, and the origin of the Ca-minimum in pyroxenes from tholeiitic intrusions. Contrib. Mineral. Petrol. 48, 205-219.

Carmichael, I.S.E. (1960). Pyroxenes and Olivines from some Tertiary acid glasses. J. Petrol. 1, 309-336.

Carmichael, I.S.E. (1963). The crystallisation of felspar in volcanic acid liquids. Q.J. Geol. Soc. (Lond.) 119, 95-131.

Carmichael, I.S.E. (1964). The petrology of Thingmuli, a Tertiary Volcano in Eastern Iceland. J. Petrol. 5, 435-460.

Carmichael, I.S.E. (1967). The iron-titanium oxides of salic volcanic rocks and their associated Mg-Fe silicates. Contrib. Mineral. Petrol. 14, 36-64.

Carmichael, I.S.E., Nicholls, J. and Smith, A.L. (1970). Silica activity in igneous rocks. Am. Min. 55, 246-263.

Carmichael, I.S.E., Turner, F.J. and Verhoogen, J. (1974). Igneous Petrology. McGraw Hill, New York. 739 pp.

Charles, R.J. (1969). The origin of immiscibility in silicate melts. Phys. Chem. Glasses. 10, 169-178.

Chayes, F. (1956). Petrographic modal analysis. Wiley and Sons Inc. New York.

Clocchiati, R. (1979). Découverte dans la mésostase des laves a affinité andésitique du Monte Arci, de verres riches en titane et phosphore et élargissement du domaine d'immiscibilité entre liquides silicates. C.R. Acad. Sc. Paris t. 289 D. 607-610.

Coish, R.A. and Taylor, L.A. (1979). The effects of cooling rate on texture and pyroxene chemistry in DSDP Leg 34 Basalt: A microprobe study. Earth Planet. Sci. Lett. 42, 389-398.

Coleman, R.G. and Peterman, Z.E. (1975). Oceanic Plagiogranite J. Geophys. Res. 80, 1099-1108.

Collingwood, R.G. (1938). The Hill Fort on Carrock Fell. Trans. Cumb. Westm. Aut. Arch. Soc. 38 (NS), 32-41.

Colville, P.A., Ernst, W.G. and Gilbert, M.C. (1966). Relationships between cell parameters and chemical compositions of monoclinic amphiboles. Am. Min. 51, 1727-1753.

Cornwall, H.C. (1951). Differentiation in the Keewanawan series and the origin of the copper deposits of Michigan. Geochim. Cosmochim.Acta 62, 159-202.

Cox, K.G., Bell, J.D. and Pankhurst, R.J. (1979). The interpretation of igneous rocks. George Allen and Unwin. London. 450 pp.

Czamanske, G.K. and Mihalik, P. (1972). Oxidation during magmatic differentiation. Finnmarka complex, Oslo area, Norway. Part I. 'The opaque oxides'. J. Petrol. 13, 493-509.

Daly, R.A. (1933). Igneous rocks and the Depths of the earth. McGraw Hill. New York. 598 pp.

De, A. (1974). Silicate liquid immiscibility in the Deccan Traps and its petrogenetic significance. Geol. Soc. Am. Bull. 85, 471-474.

Deer, W.A., Howie, R.A. and Zussman, J. (1978). Single Chain Silicates. Rock Forming Minerals V. 2A. 2nd Edn.

Dixon, S. and Rutherford, M.J. (1979). Plagiogranites as late-stage immiscible liquids in ophiolite and mid-ocean ridge suites: An experimental study. Earth Planet Sci. Lett. 45, 45-60.

Dodge, F.C.W., Papike, J.J. and Mays, R.E. (1968). Hornblendes from granitic rocks of the central Sierra Nevada Batholith, California. J. Petrol. 9, 378-410.

Donaldson, C.H. (1974). Olivine crystal types in Harrisitic rocks of the Rhum Pluton and Archaean spinifex rocks. Geol. Soc. Am. Bull. 85, 1721-1726.

Donaldson, C.H. (1976). An experimental investigation of olivine morphology. Contrib. Mineral. Petrol. 57, 187-213.

Downie, C. and Soper, N.J. (1972). The age of the Eycott Volcanic Group and its conformable relationship to the Skiddaw Slates in the English Lake District. Geol. Mag. 109, 259-368.

Dowty, E. (1976). Crystal structure and Crystal growth II: sector zoning in minerals. Am. Min. 61, 460-467.

Eastwood, T., Hollingworth, S.E. Rose, W.C.C. and Trotter, F.M. (1968). Geology of the country around Cockermouth and Caldbeck. Mem. Geol. Surv. U.K.

Elliot, D.H. (1976). The tectonic setting of the Jurassic Ferrar Group. Antarctica. Proceedings of the symposium on Andean and Antarctic volcanology problems. I.A.V.C.E.I. 357-372

Elsdon, R. (1971). Crystallisation history of the Upper Layered Series, Kap Edvard Holm E. Greenland. J. Petrol. 12, 499-521.

Eugster, H.P. and Wones, D.R. (1962). Stability relations of the ferruginous biotite, annite. J. Petrol. 3, 82-125.

Faller, A.M. and Briden, J.C. (1978). Palaeomagnetism of Lake District Rocks. In: F. Moseley (Ed). The geology of the Lake District. Yorks. Geol. Soc. Occ. Publ. 3, 17-24.

Firman, R.J. (1978). Intrusions. In: F. Moseley (Ed). The geology of the Lake District. Yorks. Geol. Soc. Occ. Publ. 3, 146-163.

Fitton, J.G. (1971). The petrogenesis of the calc-alkaline Borrowdale Volcanic G roup. Northern England. Unpublished Ph.D. Thesis University of Durham.

Fitton, J.G. and Gill, R.C.D. (1970). The oxidation of ferrous iron in rocks during mechanical grinding. Geochim. Cosmochim.Acta. 34, 518-524.

Fitton, J.G. and Hughes, D.J. (1970). Volcanism and Plate Tectonics in the British Ordovician. Earth Planet.Sci. Lett. 8, 223-228.

Flanagan, F.J. (1973). 1972 Values for international geochemical reference samples. Geochim. Cosmochim.Acta. 37, 1189-1200.

Fleet, M.E. (1975). Growth habits of Clinopyroxene. Can. Min. 13, 336-341.

Franck, E.U. (1961). Überkritisches Wasser als elektrolytisches Losungini Hel: Angew.Chemie. 73, 309-322.

Freestone, I. (1978). Liquid immiscibility in alkali-rich magmas. Chem. Geol. 23, 115-125.

Gale, N.H., Beckinsale, R.D. and Wadge, A.J. (1979). A Rb-Sr Whole-rock isochron for the Stockdale Rhyolite of the English Lake District, and a revised Mid-Palaeozoic time scale. J. Geol. Soc. Lond. 136, 235-242.

Gamble, R.P. and Taylor, L.A. (1980). Crystal/Liquid partitioning in Augite. Effects of cooling rate. Earth Planet.Sci. Lett. 47, 21-33.

Gibb, F.G.F. (1973). The zoned clinopyroxenes of the Shiant Isles Sill. Scotland. J. Petrol. 14, 203- 230.

Gill, J.B. (1970). Geochemistry of Viti Levu, Fiji, and its evolution as an island arc. Contrib. Mineral. Petrol. 27, 179-203.

Gordon, G.E., Randle, K., Goles, G.G., Corliss, J.B., Beeson, M.H. and Oxley, S.S. (1968). Instrumental Activation analysis of standard rocks with high resolution gamma ray detectors. Geochim. Cosmochim.Acta. 32, 369-396.

Green, J.F.N. (1917). The age of the chief intrusions of the Lake District. Proc. Geol. Assoc. 28, 1-30.

Greig, J.W. (1927) Immiscibility in silicate melts. Am. J. Sci. 13, 1-44; 133-154.

Groom, T.T. (1889). On a tachylyte associated with the gabbro of Carrock Fell, in the Lake District. Q. J. Geol. Soc. (Lond.) 45, 298-304.

Grove, T.L. and Bence, A.E. (1977). Experimental study of pyroxene-liquid interaction in quartz-normative basalt, 15597. Proc. Lunar Sci. Conf. 8th 1549-1579.

Grove, T.L. and Bence, A.E. (1979). Crystallisation kinetics in a multiply saturated basalt magma: an experimental study of Luna 24 ferrobasalt. Proc. Lunar Sci. Conf. 10th.

Hamilton, D.L., Burnham, C.W. and Osborne, E.F. (1964). The solubility of water and effects of oxygen fugacity and water content on crystallisation in Mafic magmas. J. Petrol. 5, 21-39.

Hamilton, D.L., Freestone, I.C., Dawson, B.J. and Donaldson, C.H. (1979). The origin of Carbonatite, by liquid immiscibility. Nature 279, 52-54.

Harker, A. (1894). Carrock Fell: A study of the variation of igneous rock masses. Part I, the Gabbro. Q. J. Geol. Soc. (Lond.) 50, 311-337.

Harker, A. (1895). Carrock Fell: A study of the variation in igneous rock masses. Part II The Carrock Fell granophyre Part III The Grainsgill Greisen. Q. J. Geol. Soc. (Lond.) 51, 125-48.

Harker, A. (1902). Notes on the igneous rocks of the English Lake District. Proc. Yorks. Geol. Polytech. Soc. 14, 487-93.

Haskin, L.A. and Haskin, M.A. (1968). Rare-earth elements in the Skaergaard Intrusion. Geochim.Cosmochim. Acta. 32, 433-447.

Haslam, H.W. (1968). The crystallisation of intermediate and acid magmas at Ben Nevis, Scotland. J. Petrol. 9, 84-104.

Hawkes, D.D. (1966). Differentiation of the Tumatumari-Kopinang dolerite intrusion. British Guiana. Bull. Geol. Soc. Am. 77, 1131-1158.

Hawkesworth, C.J., Norry, M.J., Roddick, J.C., Baker, P.E. Francis, P.W. and Thorpe, R.S. (1979). $^{143}Nd/^{144}Nd$, $^{87}Sr/^{86}Sr$, and incompatible element variations in calc-alkaline andesites and plateau lavas from South America. Earth Planet. Sci. Lett. 42, 45-57.

Hawkesworth, C.J., O'Nions, R.K., Pankhurst, R.J., Hamilton, P.J. and Evensen, N.M. (1977). A geochemical study of island arc and back arc tholeiites from the East Scotia Sea. Earth Planet. Sci. Lett. 36, 253-262.

Helz, R.T. (1973). Phase relations of basalts in their melting range at PH_2O = 5Kb, as a function of oxygen fugacity. Part I Mafic phases. J. Petrol. 14, 249-302.

Hess, P.C. (1977). Structure of Silicate melts. Can. Min. 15, 162-178.

Hess, P.C., Rutherford, M.J., Guillemette, R.W., Ryerson, F.J. and Tuchfield, H.A. (1975). Residual products of fractional crystallisation of Lunar magmas: an experimental study. Proc. Lunar Sci. Conf. 6th. 895-909.

Himmelberg, G.R. and Ford, A.B. (1976). Pyroxenes of the Dufek intrusion Antarctica. J. Petrol. 17, 219-243.

Holland, J.G. and Brindle, D.W. (1966). A self-consistent mass absorption correction for silicate analysis by X-ray fluorescence. Spectrochim. Acta 22, 2083-2093.

Hollister, L.S. and Crawford, M.L. (1977). Melt immiscibility in APOLLO 15 KREEP; origin of Fe-rich mare basalts. Proc. Lunar Sci. Conf. 8th. 2419-2432.

Hollister , L.S. and Gancarz, A.J. (1971) Compositional sector zoning in Clinopyroxene from the Narce area, Italy. Am. Min. 56, 959-979.

Holloway, J.R. and Burnham, C.W. (1972) Melting relations of basalt with equilibrium water pressure less than total pressure. J. Petrol. 13, 1-29.

Hoover, J.D. and Irvine, T.N. (1978). Liquidus relations and Mg-Fe partitioning in part of the system.
Mg_2SiO_4 - Fe_2SiO_4 - $CaMgSi_2O_6$ - $CaFeSi_2O_6$ - $KAlSi_3O_8$ - SiO_2
Carnegie Inst. Yr. Book 77, 774-784.

Hotz, P.E. (1953). Petrology of granophyre in diabase near Pittsburg, Pennsylvania. Bull. Geol. Soc. Am. 64, 676-704.

Huebner, J.S. and Turnock, A.C. (1980). The melting relations at 1 bar, of pyroxenes composed largely of Ca - Mg-, and Fe- bearing components. Am.Min. 65, 225-271.

Ingham, J.K. and McNamara, K.J. (1978). The Upper Ordovician rocks In: F. Moseley (Ed). The geology of the Lake District. Yorks. Geol. Soc. Occ. Publ. 3, 121-129.

Irvine, T.N. (1975). The Silica Immiscibility Effect in Magmas. Carnegie Inst. Yr. Book 74, 484-492.

Irvine, T.N. (1976). Metastable liquid immiscibility and MgO - FeO-SiO_2 fractionation patterns in the system Mg_2SiO_4 - Fe_2SiO_4 - $CaAl_2Si_2O_8$ - $KAlSi_3O_8$ - SiO_2.
Carnegie Inst. Yr. Book 75, 597-611.

Irving, J.A. (1978). A review of experimental studies of crystal-liquid trace element partitioning.
Geochim. Cosmochim.Acta. 42, 743-771.

Jahns, R.J. and Burnham, C.W. (1969). Experimental Studies of pegmatite genesis : I : a model for the derivation and cystallisation of granite pegmatites.
Econ. Geol. 64, 843-864.

Jakeš, P. and White, A.J.R. (1972). Hornblendes from Cal-Alkaline Volcanic rocks of Island arcs and continental margins.
Am. Min. 57, 887-902.

Kirkpatrick, R.J. (1975). Crystal growth from the melt: a review.
Am. Min. 60, 798-814.

Kirkpatrick, R.J., Robinson, G.R. and Hays, F.J. (1976). Kinetics of crystal growth from silicate melts. Anorthite and Diopside J. Geophys. Res. 81 5715-5720.

Kretz, R. (1960). The distribution of certain elements amongst coexisting calcic pyroxenes, calcic-amphiboles and bioties in skarns.
Geochim. Cosmochim. Acta 20 161-191.

Kretz, R. and Jen, T.S. (1978). Effect of temperature on the distribution of Mg + Fe^{2+} between calcic pyroxene and hornblends.
Can. Min. 16 533-539.

Kuno, H. (1966). Lateral variation of basalt magma across continental margin and Island arcs.
Bull. Volcan. 29, 195-222.

Kushiro, I. and Schairer, J.F. (1963). New data on the system Diopside-Forsterite-Silica.
Carnegie Inst. Yr.Bk. 62, 95-103.

Kyle, P.R. (1980). Development of heterogeneities in the Subcontinental mantle : Evidence from the Ferrar Group, Antarctica.
Contrib.Mineral.Petrol. 73, 89-104.

Leake, B.E. (1971). On Aluminous and Edenite Hornblendes.
Min.Mag. 38, 389-407.

Leake, B.E. (1978). Nomenclature on Amphiboles compiled for subcommittee on amphiboles, I.M.A.
Min.Mag. 42, 533-563.

Le Bas, M.J. and Handley, C.D. (1979). Variation in apatite composition in ijolitic and carbonatitic rocks.
Nature 279, 54-56.

Leung, I.S. (1974). Sector-zoned titanaugites: Morphology, crystal chemistry and growth.
Am. Min. 59, 127-138.

Lindsley, D.H. and Munoz , J.T. (1969). Subsolidus relations along the join hedenbergite - ferrosilite.
Am.J.Sci. 267, 295-324.

Liou, J.G. (1971). Synthesis and stability relations of prehnite.
Am.Min. 56, 507-531.

Lofgren, G.E. (1974). An experimental study of plagioclase crystal morphology. Isothermal crystallisation.
Am. J. Sci. 274, 243-273.

Lofgren, G.E. and Donaldson, C.H. (1975). Curved Branching crystals and differentiation in comb-layered rocks.
Contrib.Mineral.Petrol. 49, 309-319.

Martin, R.F. and Piwinskii, A.J., (1969). Experimental data bearing on the movement of iron in an aqueous vapour.
Econ.Geol. 54, 798-803.

McBirney, A.R. (1975). Differentiation of the Skaergaard intrusion.
Nature 253, 691-694.

McBirney, A.R. and Nakamura, Y. (1974). Immiscibility in late stage magmas of the Skaergaard intrusion.
Carnegie Inst. Yr.Bk. 73, 348-352.

McBirney, A.R. and Noyes, R.M. (1979). Crystallisation and Layering in the Skaergaard intrusion.
J.Petrol. 20, 487-554.

McCarthy, T.S. and Fripp, R.E.P. (1980). The crystallisation history of a granitic magma, as revealed by trace element abundances. J.Geol. 88, 211-224.

McDougall, I. (1962). Differentiation of the Tasmanian dolerites : Red Hills dolerite - granophyre association. Geol.Soc. Am. Bull. 73, 279-316.

McKerrow, W.S., Leggett, J.K. and Eales, M.H. (1978). Caledonian plate tectonics and the place of the English Lake District. Discussion. Geol.Soc.Am.Bull. 89, 1694-1695.

Millward, D., Moseley, F. and Soper, N.J. (1978). The Eycott and Borrowdale Volcanic rocks. In. F.Moseley (Ed). The geology of the Lake District. Yorks.Geol.Soc.Occ.Publ.3, 99-120.

Moorbath, S. and Thompson, R.N. (1980). Strontium isotope geochemistry and petrogenesis of the early Tertiary lava pile of the Isle of Skye, Scotland and other Basic rocks of the British Tertiary Province. An example of Magma-crust interaction. J.Petrol. 21, 295-322.

Morse, S.A. (1979). Kiglapait Geochemistry II. Petrography. J.Petrol. 20, 591-624.

Moseley, F. (1978a). An introductory review. In : F.Moseley (Ed) The Geology of the Lake District. Yorks. Geol.Soc. Occ.Publ.3, 1-16.

Moseley, F. (1978b). Caledonian plate tectonics and the place of the English Lake District. Reply. Geol.Soc.Am.Bull. 89, 1695-1696.

Muan, A. and Osborne, E.F. (1956). Phase equilibria at liquidus temperatures in the system $MgO-FeO-Fe_2O_3-SiO_2$ J.Am. Ceram. Soc. 39, 121-140.

Muir, I.D. (1954). Cyrstallisation of pyroxenes in an iron-rich diabase from Minnesota. Min. Mag. 30, 376-388.

Murase, T. and McBirney, A.R. (1973). Properties of some common igneous rocks and their melts at high temperatures. Bull.Geol.Soc.Am. 84, 3563-3592.

Nakamura, K. (1974). Determination of REE, Ba, Fe, Mg, Na and K, in Carbonaceous and ordinary chrondrites. Geochim. Cosmochim. Acta 38, 757-775.

Nakamura, Y. (1973). Origin of sector-zoning in igneous clinopyroxene. Am. Min. 58, 986-990.

Nakamura, Y. (1974). The system Fe_2SiO_4 - $KAlSi_2O_6$-SiO_2 at 15 kb. Carnegie Inst. Yr.Bk. 73, 352-354.

Nakamura, Y. and Coombs, D.S. (1973). Clinopyroxenes in the Tawhiroko tholeiitic dolerite at Moerat, North Eastern Otago, New Zealand.
Contrib.Mineral.Petrol.42, 213-228.

Naslund, H.R. (1976). Liquid immiscibility in the system $KAlSi_3O_8$- $NaAlSi_3O_8$-FeO-Fe_2O_3-SiO_2 and its application to natural magmas
Carnegie Inst. Yr.Bk.75, 592-597.

Neumann, E. (1974). The distribution of Mn^{2+} and Fe^{2+} between ilmenite and magnetite in igneous rocks.
Am.J.Sci. 274, 1074-1088.

Nwe, Y.Y. (1976). Electron-probe studies of the earlier pyroxenes and olivines from the Skaergaard Intrusion.E.Greenland.
Contrib.Mineral.Petrol. 55, 105-126.

Nwe, Y.Y. and Copley, P.A. (1975). Chemistry, subsolidus relations and electron petrography of pyroxenes from the late ferrodiorites of the Skaergaard intrustion. E.Greenland.
Contrib.Mineral.Petrol. 53,37-54.

Onuki, H. (1966). Mg-Fe^{2+} distribution between coexisting hornblende and Ca-rich pyroxene.
J.Japan. Ass.Miner.Petrol.Econ. 56, 266-255.

Osborne, E.F. (1959). Role of oxygen pressure in the crystallisation and differentiation of basic magma.
Am.J.Sci. 257, 609-647.

Osborne, E.F. (1979). The reaction principle In: H.S. Yoder, Jr. (Ed) The Evolution of the Igneous Rocks. 50th Anniversary perspectives. p.133-164.
Princeton Univ.Press. Princeton, N.J.

Pankhurst, R.J. (1977). Strontium isotope evidence for mantle events in the continental lithosphere.
J.Geol.Soc.Lond. 134, 255-268.

Paul, D.K., Potts, P.J., Gibson, I.L. and Harris, P.G. (1975). Rare-Earth abundances in Indian Kimberlites.
Earth Planet. Sci. Lett. 25, 151-158.

Pearce, J.A. (1979). Geochemical evidence for the erruptive setting of lavas from Tethyan ophiolites.
Proc.Int.Ophiolite Symposium Cyprus. (manuscript).

Pearce, J.A. and Cann, J.R. (1973). Tectonic setting of basic volcanic rocks determined using trace element analyses.
Earth Planet. Sci. Lett. 19, 290-300.

Pearce, J.A. and Norry, M.J. (1979). Petrogenetic implications of Ti, Zr, Y and Nb variations in volcanic rocks.
Contrib.Mineral.Petrol. 69, 33-47.

Philpotts, A.R. (1976), Silicate liquid immiscibility: Its probable extent and petrogenetic significance.
Am. J.Sci. 276, 1147-1177.

Philpotts, A.R. (1978), Textural evidence for liquid immiscibility in Tholeiites.
Min.Mag 42, 417-427.

Philpotts, A.R. (1979) Silicate liquid immiscibility in tholeiitic basalts.
J.Petrol.20, 99-118.

Pinsent, R.H. (1974), The emplacement and metamorphism of the Blue-River Ultramafic body Cassiar District. British Columbia, Canada.
Unpubl.Ph.D.Thesis Univ. Durham.

Poldervaart, A. and Hess, H.H. (1951). Pyroxenes in the crystallisation of basaltic magma.
J.Geol. 59, 472-489.

Popp, R.K., Gilbert, M.C. and Craig, J.R. (1977). Stability field of Fe-Mg amphibole with respect to oxygen fugacity.
Am. Min. 62, 1-13.

Rastall, R.H. (1906). The Buttermere and Ennerdale granophyre.
Q.J.Geol.Soc.(Lond) 62, 253-74.

Reeves, M.J. (1971). Geochemistry and mineralogy of British Carboniferous seat earths from Northern Coalfields.
Unpubl. Ph.D. Thesis. Univ. Durham.

Robinson, P. Ross, M. and Jaffe, H.W., (1971). Composition of the anthophyllite-gedrite series, comparisons of gedrite-hornblende and anthophyllite-gedrite solvus.
Am.Min 56,1005-1041.

Roedder, E. (1951). Low temperature liquid immiscibility in the system K_2O-FeO-Al_2O_3-SiO_2
Am.Min. 36, 282-286.

Roedder, E. (1978) Silicate liquid immiscibility in magmas and in the system K_2O-FeO-Al_2O_3-SiO_2 : An example of serendipty.
Geochim.Cosmochim. Acta. 42, 1597-1619.

Roedder, E. (1979). Silicate Liquid immiscibility in magmas. In. H.S. Yoder Jr. (Ed). The Evolution of the Igneous Rocks. 50th Anniversay Perspectives. p.15-47.
Princeton Univ.Press. Princeton.

Roedder, E. and Wieblen, P.W. (1970). Lunar petrology of silicate melt inclusions Apollo 11 rocks
Proc.Lunar Sci. Conf. 1st. 801-837.

Roedder, E. and Wieblen, P.W. (1971). Petrology of silicate melt inclusions Apoll 11 and Apoll 12 and Terrestrial equivalents
Proc.Lunar Sci. Conf. 2nd 507-528.

Roeder, P.L. and Osborne, E.F. (1966). Experimental data for the system $MgO-FeO-Fe_2O_3-CaAlSi_2O_8-SiO_2$ and their petrologic implications.
Am.J.Sc. 264, 428-480

Ross, M., Huebner, J.A. and Dowty, F. (1973). Deliniation of the one-atmosphere augite-pigeonite miscibility gap for pyroxene from Lunar basalt. 12021.
Am.Min. 58, 619-635.

Ross, M., Papike, J.J. and Shaw, K.W. (1969). Exsolution textures in amphiboles as indicators of subsolidus thermal histories
Spec.Paper. Mineral.Soc.Amer. 2, 275-299.

Routti, J.T. (1969), Sampo : A fortran IV program for computer analysis of gamma spectra from Ge (Li) detectors and for other spectra with peaks.
Am. Govt. Rept. 1969 UCRL-19452. 31 pp.

Rundle, C.C. (1979). Ordovician intrusions in the English Lake District.
J.Geol.Soc.Lond.136, 29-38.

Rutherford, M.J., Hess, P.C., Ryerson, F.J., Campbell, H. and Dick,P.A.(1976). The chemistry origin and petrogenetic implications of Lunar granite and monzonite.
Proc.Lunar Sc.Conf. 7 th. 1723-1740.

Ryerson, F.J. and Hess, P.C. (1978). Implications of liquid-liquid distribution coefficients to mineral-liquid partitioning.
Geochim. Cosmochim.Acta 42, 921-932.

Ryerson, F.J. and Hess, P.C. (1980). The role of P_2O_5 in silicate melts
Geochim. Cosmochim.Acta. 44, 611-624.

Saunders, A.D., Tarney, J., Stern, C.R and Dalziel, I.W.D. (1979). Geochemistry of mesozoic from Southern Chile.
Geol.Soc.Am.Bull.90, 237-258.

Schairer, J.F. (1954). The system $K_2O-MgO-Al_2O_3-SiO_2$: I, results of quenching experiments on four joins in the tetrahedron cordierite-forsterite-leucite-silica and on the join cordierite-mullite-potash felspar.
J.Am. Ceram.Soc. 37, 501-533.

Seward, T.P. (1970). Phase separation and liquid immiscibility. In: A.M.Alper (Ed) Materials Science and Technology Vol.1
Academic Press.

Shaw, H.R. (1965). Comments on viscosity, crystal settling and convection in granitic magmas.
Am.J.Sci. 263, 120-153.

Shaw, H.R. (1969). Rheology of basalt in the melting range.
J.Petrol. 10, 510-535.

Shaw, H.R. (1972). Viscosities of magmatic silicate liquids : an empiricle method of prediction.
Am.J.Sci. 272, 870-893.

Shepherd, T.J., Beckinsale, R.D. Rundle, C.C. and Durham, J. (1976). Genesis of Carrock Fell Tungsten deposits : Fluid inclusion and isotopic study Trans.Instn. Min.Metall. 85,B63-73.

Skillen, I.E. (1973). The igneous complex of Carrock Fell Proc. Cumb. Geol.Soc. 3, 363-86.

Soper, N.J. (1974). The rubidium-strontium age and field relations of the Threlkeld Microgranite.Discussion. Proc. Yorks.Geol.Soc. 40, 211-222.

Soper, N.J. and Moseley, F. (1978). Structure. In : F. Moseley (Ed) The geology of the Lake District. Yorks. Geol. Soc.Occ.Publ. 3, 45-67.

Stern, C. (1979). Open and closed system fractionation within two Chilean ophiolites and the tectonic implications. Contrib. Mineral. Petrol. 68, 243-258.

Streckeisen, A. (1976). To each plutonic rock its proper name. Earth Sci. Rev. 12, 1-34.

Sun, S.S. and Hanson, G.N. (1976). Rare earth evidence for differentiation of McMurdo volcanics. Ross Island Antarctica. Contrib.Mineral. Petrol. 54, 139-155.

Sun , S.S. and Nesbitt, R.W. (1977). Chemical heterogeneity of the Archaean mantle. Composition of the earth and mantle evolution. Earth Planet.Sci. Lett. 36, 429-448.

Sweeton, F.H. and Baes, C.F. Jr., (1970).The solubility of magnetite and hydrolysis of ferrous ion in aqueous solutions at elevated temperature. J.Chem. Thermodyn. 2, 479-500.

Taubeneck, W.H. and Poldervaart, A. (1960). Geology of the Elkhorn Mountains Northeastern Orgeon. Part 2,Willow Lake Intrusion. Geol.Soc. Amer.Bull. 71, 1295-1322.

Teall, J.J.H. (1885). On some quartz-felsites and augite granites from the Cheviot district. Geol. Mag.D. III, V.2 109-121.

Teall, J.J.H. (1888). British Petrography. London.

Thompson, R.N. (1972). Occillatory and sector-zoning in Augite from a Vesuvian lava. Carnegie Inst. Yr.Bk. 71, 463-470.

Thornton, C. and Tuttle, O. (1960) .Chemistry of igneous rocks I. Differentiation index. Am.J.Sci. 258, 664-684.

Thorpe, R.S. (1978). The parental basaltic magma of granites from the Isle of Skye. N.W. Scotland. Min.Mag. 42, 157-8.

Thorpe, R.S. Potts, P.J. and Sarre, M.B. (1977). Rare earth evidence concerning the origin of granites of the Isle of Skye N.W.Scotland. Earth Planet. Sci. Lett. 36, 111-120.

Toop, G.W. and Samis, C.W. (1962). Activities of ions in silicate melts. Trans. Metall. Soc. A.I.M.E. A224, 878-887.

Trechmann, C.O. (1882). Note on the so called 'hypersthenite' of Carrock Fell, Cumberland.
Geol. Mag. 9, 210-212.

Tuttle, O.F. and Bowen, N.L. (1958). The origin of granite in the light of experimental studies in the system $NaAlSi_3O_8$-$KAlSi_3O_8$-SiO_2-H_2O
Geol.Soc.Am.Mem. 74.

Uhlmann, D.R. (1972). Crystal growth in glass forming systems - A review. In: L.L. Hench and S.W. Freiman (Eds) Advances in Nucleation and crystallisation in Glasses.
Am.Ceram. Soc. Spec.Publ. 5.

Vincent, E.A. and Philips, R. (1954). Iron-titanium oxide minerals in layered gabbro of the Skaergaard intrusion. E.Greenland
Geochim.Cosmochim.Acta. 6, 1-26.

Visser, W. and Koster van Groos, A.F. (1979a). Phase relations in the system K_2O-FeO-Al_2O_3-SiO_2 at latm. with special emphasis on low temperature immiscibility.
Am. J.Sci. 279, 70-91.

Visser, W., and Koster van Groos, A.F. (1979b). Effects of P_2O_5 and TiO_2 on liquid-liquid equilibrium in the system
K_2O-FeO-Al_2O_3-SiO_2
Am.J.Sci. 279, 970-988.

Visser, W. and Koster van Groos, A.F. (1979c). Effect of pressure on liquid immiscibility in the system K_2O-FeO-Al_2O_3-SiO_2-P_2O_5
Am.J.Sc. 279, 1160-1175.

Wager, L.R., Brown, G.M. and Wadsworth, W.J. (1960). Types of Igneous cumulate.
J.Petrol. 1, 73-85.

Wager, L.R. and Brown, G.M. (1968) Layered igneous rocks.
Oliver and Boyd, Edinburgh.

Walker, F., Vincent, H.G.C. and Mitchell, R.L. (1952). The chemistry and mineralogy of the Kinkell Tholeiite. Stirlingshire
Min.Mag. 29, 895-908.

Walker, K.R. (1969). The Palisades Sill. New Jersey : A reinvestigation.
Geol.Soc.Am. Spec.Paper 3, 1-178.

Walker, K.R., Ware, N.G. and Lovering, J.F. (1973). Compositional variations in the pyroxenes of the differentiated Palisades Sill, New Jersey.
Geol.Soc.Am. Bull. 84, 89-110.

Walsh, J.N. (1975). Clinopyroxenes and biotites from the Centre III igneous complex, Ardnamurchan, Argyllshire. Min.Mag. 40, 335-345.

Walsh, J.N. Beckinsale, R.D., Skelhorn, R.R. and Thorpe, R.S. (1979). Geochemistry and petrogenesis of Tertiary granitic rocks from the Island of Mull. Northwest Scotland. Contrib. Mineral. Petrol. 71, 99-116.

Ward, J.C. (1876). On the quartz-felsite, syenitic and associated metamorphic rocks of the Lake District. Q.J.Geol.Soc (Lond) 32, 11-27.

Watson, E.B. (1976). Two-liquid partition coefficients : experimental data and geochemical implications. Contrib.Mineral. Petrol. 56, 119-134.

Weaver, S.D., Saunders, A.D. Pankhurst, R.J. and Tarney, J. (1979). A geochemical study of magmatism associated with the initial stages of back arc spreading. The Quarternary volcanics of Bransfield Strait from the South Shetland Islands. Contrib.Mineral. Petrol.68, 151-171.

Wiebe, RA. (1979). Fractionation and liquid immiscibility in an anorthositic pluton of the Nain Complex, Labrador. J.Petrol. 20, 239-269.

Wieblen, P.W. and Roedder, E. (1973). Petrology of melt inclusions in Apollo samples 15598 and 62295 and of clasts in 67915 and several Lunar soils. Proc. Lunar Sci. Conf. 4 th. 681-703.

Wilcox, R.E. (1979). The liquid line of descent and variation diagrams. In. H.S. Yoder Jr. (Ed) The Evolution of the Igneous Rocks. 50th Anniversary perspectives p.205-224. Princeton Univ.Press. Princton, N.J.

Wright, T.L. and Okamura, R.T. (1977). Cooling and crystallisation of tholeiitic basalt, 1965 Makaopuhi Lava Lake Hawaii. U.S. Geol. Surv. Prof. paper 1004.

Wood, D.A. (1978). Major and trace element variation in the Tertiary lavas of Eastern Iceland, and their significance with respect to the Iceland Geochemical Anomaly. J. Petrol.19, 393-436.

Wood, M.I. and Hess, P.C. (1980). The structural role of Al_2O_3 and TiO_2 in immiscible silicate liquids in the system SiO_2-MgO-CaO-FeO-TiO_2-Al_2O_3. Contrib.Mineral.Petrol. 72, 319-328.

Wyllie, P.J., Cox, K.G. and Biggar, G.M. (1962). The habit of apatite in synthetic systems and igneous rocks. J.Petrol.3, 238-243.

Yagi, K. and Onuma, K. (1967). The join $CaMgSi_2O_6$-$CaTiAl_2O_6$ and its bearing on the titanaugites.
J.Fac.Sci. Hokkaido Univ. Ser. 4.13, 463-483.

Yoder, H.S. Jr. , Stewart, D.B and Smith, J.R. (1957), Felspars : Carnegie Inst. Yr.Bk. 56,206-214.

Zdaniewski, W. (1975), D.T.A. and X-Ray analysis study of nucleation and crystallisation of MgO-Al_2O_3-SiO_2 glasses containing ZrO+TiO_2+CeO_2
J.Amer.Ceram. Soc. 58, 161-169.

APPENDIX ONE

SAMPLES

Table A1.1, lists all the samples used in this study. All the samples collected for this study are prefixed by 'RH77'. All the samples with five-figure numbers, (except 20798), are samples from the collecti on of the Geological Survey. These numbers are prefixed by 'E', and correspond to the numbers in Eastwood et al (1968). Four samples have been used from the collection of the Department of Geological Sciences at Durham. They are 755, 1537, 1536 and 20798 : they are prefixed by 'D'. Analyses from Fitton (1971) are prefixed by 'CN' and those from R.N.Thompson (written comm. 1978) are prefixed by 'ME'. A brief description of the samples is given in Table A1.1 together with eight-figure grid references. The grid references refer to O.S.1:10000 sheets NY33 SE/SW. The abbreviations in the descriptions are; Pl. Plagioclase, Px. Pyroxene, Mt. Titano-magnetite, Il. Ilmenite, Am. Amphibole, Ap. Apatite and Bi. Biotite. Notes; T. Thin section, P. Probe analyses of one or more phases (see Appendix two), A. Whole-rock analysis (see Appendix Three).

In Table A1.1 map references given for the six traverses refer to either end of the traverse. The six sample traverses are shown in more detail in figure A1.1.

Table A1.1

SAMPLE NUMBER	DESCRIPTION	MAP REFERENCE	NOTES
SUBUNIT A1			
2	Bi-Il-Pl-Px gabbro	3552 3242	T, P.
5	Pl rich vein in xenolith	3555 3248	T.
46	Pl gabbro	3390 3328	T, P, A.
67	Altered melanocratic gabbro	3515 3335	T.
87	Altered ilmenite gabbro	3515 3336	T, P, A.
88	Pl-Il-Px gabbro	3515 3333	T, P, A.
89	Altered ilmenite gabbro	3515 3336	T.
115	Pl gabbro-altered	3515 3290	T, P, A.
116	Pl gabbro	3530 3300	T.
118	Altered ilmenite gabbro	3506 3335	T, A.
136	Pl-Il-Px gabbro	3434 3341	T, P, A.
150	Bi-Il-Pl-Px gabbro	3548 3245	T, P, A.
151	Pl-Px-Il gabbro	3550 3270	T, P, A.
153	Pl gabbro	3536 3294	T,A.
156	Pl gabbro	3480 3306	T, A.
158	Pl-Il-Px gabbro	3450 3285	T, P, A.
159	Pl-Il-Px gabbro	3420 3290	T, P, A.
160	Alt Pl-Il-Px gabbro	3320 3340	T, P.
161	Pl-Il gabbro	3385 3290	T, A.
170	Pl gabbro	3492 3309	T, P.
D20798	Il-Pl gabbro		T.
E17389	Bi-Il-Pl-Px gabbro		T, P.
E15249	Bi-Il-Pl-Px gabbro		T, P.
E16180	Pl-Il-Px gabbro		T, A.
E15242	Pl-Il-Px gabbro		T, P.
E16181	Pl-Il-Px gabbro		T, P, A.
CN7			A.
CN64			A.
SUBUNIT A2			
45	LAM Pl-Px-Il gabbro	3362 3340	T, A.
117	LAM Pl-2Px-Il gabbro	3525 3307	T, P, A.
154	LAM Pl-Px-Il gabbro	3510 3315	T, A.
155	LAM Pl-Px-Il-Bi gabbro	3486 3317	T, A.
D1536	LAM Pl-Px-Il gabbro		T, P.
D1537	LAM Pl-Px-Il gabbro		T, P.

SAMPLE NUMBER	DESCRIPTION	MAP REFERENCE	NOTES
E17390	LAM Pl-Px-Il gabbro		T.
E16192	LAM Pl-Px-Il gabbro		T.
E23545	LAM Pl-Px-Il gabbro		T.
SUBUNIT A3			
152	Pl-2Px-Ilm-Bi-Qz gabbro	3545 3281	T, P, A.
157	Pl-2Px-Ilm-Bi-Qz gabbro	3470 3285	T, A.
E17263	Pl-2Px-Ilm-Bi-Qz gabbro		T.
CN16			A.
CN17			A.
XENOLITHS IN UNIT A			
4	Fine grained xenolith	3555 3250	T.
5	Gabbroic vein in xenolith	3555 3248	T.
162	Eycott lava xenolith	3415 3280	T.
167	Pegmatitic gabbro (A1)+ xenolith	3380 3294	T.
SUBUNIT B1			
14	Pl-Px gabbro	3351 3378	T, P, A.
18	Pl-Px-Mt-Il-Ap ferrogabbro	3343 3374	T, P, A.
20	Pl-Px-Mt-Il gabbro	3415 3394	T, P, A.
21	Cognate xenolith in gabbro	3415 3394	T.
32	Pl-Px gabbro	3513 3392	T, P.
33	Pl-Px-Mt-Il-(AP) gabbro	3508 3395	T, P, A.
34	Pl-Px-Mt-Il-(AP) gabbro	3493 3398	T, P, A.
35	Pl-Px-Mt-Il gabbro + cognate xenolith	3414 3394	T, P.
114	Pl-Px gabbro	3374 3387	T, P.
E16182			A.
CN11			A.
SUBUNIT B2 FURTHER GILL SIKE REGION			
50	Pl-Px-Mt-Il-Ap ferrograbbo	3517 3338	T, P, A.
69	Pegmatitic Pl-Px-Mt-Il-Ap ferrogabbro	3513 3339	T, P.
100	Pegmatitic granophyric ferrogabbro	3506 3342	T, P, A.

SAMPLE NUMBER	DESCRIPTION	MAP REFERENCE	NOTES
103	Pegmatitic granophyric ferrogabbro	3506 3341	T, P, A.
119	Pl-Px-Mt-Il-Ap-ferrogabbro	3505 3338	T, P.
135	Comb-layered ferrogabbro	3512 3339	T, P.
SUBUNIT B2 TRAVERSE SIX			
44	Pl-Px-Mt-Il-Ap ferrogabbro	3345 3362	T, A.
137	"	3404 3354	T, P, A.
138	"		T, P, A.
139	"		T, P, A.
140	"		T, P, A.
141	Pegmatitic granophyric ferrogabbro		T, P, A.
142	"	3403 3356	T, P, A.
163 a/b	Laminated plagioclase segregation in ferrogabbro		T, P, A.
SUNIT B3 TRAVERSE ONE			
47	Laminated Pl-Px-Mt-Il-Am ferrodiorite	3518 3339	T, P, A.
48	"		T, P.
49	Pegmatitic-granophyric ferrodiorite		T, P, A.
54	"		T, P, A.
55a	"	3518 3339	T, P.
SUBUNIT B3 TRAVERSE TWO			
51	Pl-Px-Mt-Il-Am ferrodiorite	3517 3338	T, P, A.
52	"		T, P, A.
53	Granophyric Pl-Px-Mt-Il-Am ferrodiorite	3517 3338	T, P, A.
SUBUNIT B3 TRAVERSE FIVE			
120	Pl-Px-Mt-Il-Am ferrodiorite	3501 3340	T, P, A.
128	"		T, P.
133	Pegmatitic granphyric ferrodiorite		T, P.
134	"	3502 3341	T, P.

SAMPLE NUMBER	DESCRIPTION	MAP REFERENCE	NOTES
SUBUNIT B4 TRAVERSE ONE			
55b	Pl-Px-Mt plagioferrogranophyre	3518 3339	T, P.
56	"		T, A.
57	"		T, P, A.
59	"		T, A.
60	"		T, P, A.
64	"		T, A.
65	"	3518 3341	T, A.
SUBUNIT B4 TRAVERSE THREE			
70	Pl-Px-Mt plagioferrogranophyre	3513 3340	T, A.
74	"	3515 3340	T, A.
SUBUNIT B4 TRAVERSE FOUR			
96	Pl-Px-Mt plagioferrogranophyre	3507 3344	T, A.
98	"		T, P, A.
101	"	3507 3343	T, P, A.
SUBUNIT B5 TRAVERSE FIVE			
108b	Pl-Px-Mt plagioferrogranophyre	3503 3344	T, P.
109	"		T, A.
110	"		T, A.
111	"		T, A.
112	"		T, A.
113	"		T, A.
126	"		T, A.
127	"		T, P, A.
131	"		T, A.
129	"	3502 3340	T, A.
SUBUNIT B5 TRAVERSE SIX			
143	Pl-Px-Mt plagioferrogranophyre	3403 3356	T, P, A.
144	"		T, A.
145	"		T, A.
146	"		T, A.
147	"		T, A.
148	"	3403 3362	T, A.

SAMPLE NUMBER	DESCRIPTION	MAP REFERENCE	NOTES
SUBUNIT B5	Rae Crags Granophyre		
8		3430 3430	T.
9	dark with acicular mafics	3350 3416	T, A.
10	dark with acicular mafics	3345 3420	T.
11	dark fine grained	3342 3426	T.
12	dark fine grained	3325 3427	T, A.
13	acicular mafics	3310 3425	T, A.
SUB UNIT B5	Carrock Fell Granophyre		
15	dark hornfelsed	3351 3375	T, A.
19	dark hornfelsed	3414 3391	T, A.
22	dark fine grained inhomogeneous	3515 3386	T.
24	felsic vein in hybrid granophyre	3515 3386	T.
27	dark fine grained acicular mafics	3513 3388	T.
30	brick red	3505 3388	T, A.
31	brick red	3507 3392	T, A.
36	pink	3418 3389	T, A.
37	pink	3418 3382	T, A.
38	pink	3417 3374	T, A.
39	pink	3417 3366	T, A.
40	grey-pink	3490 3360	T, A.
42	pink	3494 3360	T, A.
43	pink	3498 3363	T, A.
62	hornfelsed screen in FGS	3519 3340	T, A.
63	hornfelsed screen in FGS	3519 3340	T, A.
66	hornfelsed screen in FGS	3516 3341	T, A.
82	hornfelsed screen in FGS	3514 3341	T, A.
90	grey	3507 3345	T, A.
104	pink	3502 3346	T, A.
105	grey	3503 3345	T, A.
106	grey	3503 3345	T, A.
107	grey	3503 3344	T, A.
108a	pink	3503 3344	T, P.
121	hornfelsed screen in FGS	3503 3343	T, P, A.
149	hornfelsed grey	3403 3363	T, A.
D755	pink		T, P.
E16184	pink		T, A.
CN10			A.
CN71			A.

SAMPLE NUMBER	DESCRIPTION	MAP REFERENCE	NOTES
MISCELLANEOUS SAMPLES			
58	lava xenolith in B4 ferrogranophyre	3518 3339	T.
123	hybrid granophyric xenolith + mafic vein	3503 3342	T.
124	hybrid ferrogranophyre	3503 3342	T.
125	hybrid ferrogranophyre	3503 3342	T.
130	hybrid ferrogranophyre	3505 3342	T.
164	felsite xenolith in subunit B1	3345 3372	T.
165	granophyric back vein in hybrid granophyre	3345 3372	T.
R.N. THOMPSON DATA			
B2 ME2	ferrogabbro	3517 3338	A.
B3 ME4	ferrodiorite		A.
B3 ME8	ferrodiorite		A.
B3 ME9	ferrodiorite		A.
B3 ME 10a	ferrodiorite		A.
B3 ME 10b	pegmatitic ferrodiorite		A.
B4 ME 12	plagioferrogranophyre		A.
B5 ME 14	hornfelsed granophyre	3519 3340	A.

FIGURE A1.1

The six sample traverses. The grid references given refer to the sample at the southern end of each traverse -

. Sample, with sample number

. boundary - certain

. boundary - less certain

Peg . Pegmatitic facies

. Tree

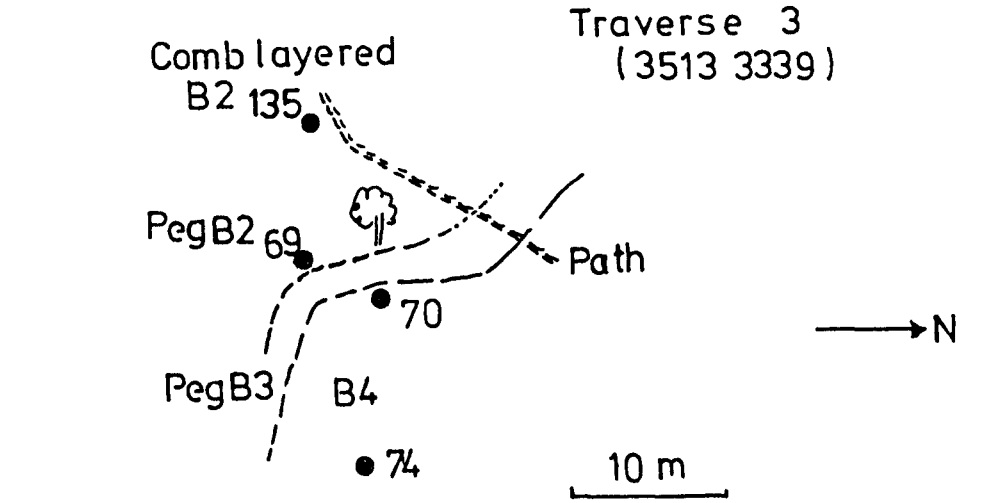

Traverse 2 (3517 3338)

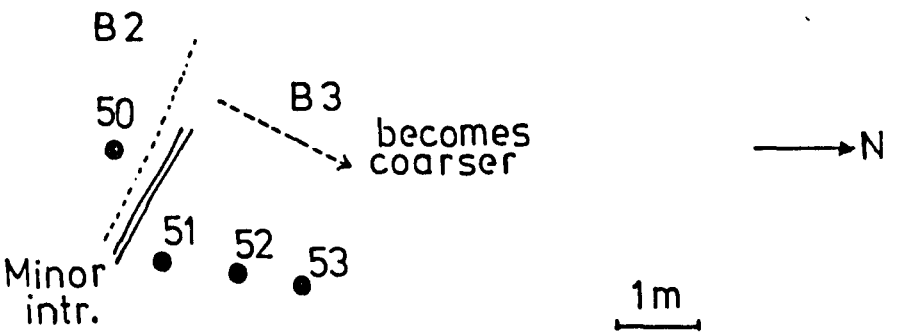

Traverse 1 (3518 3338)

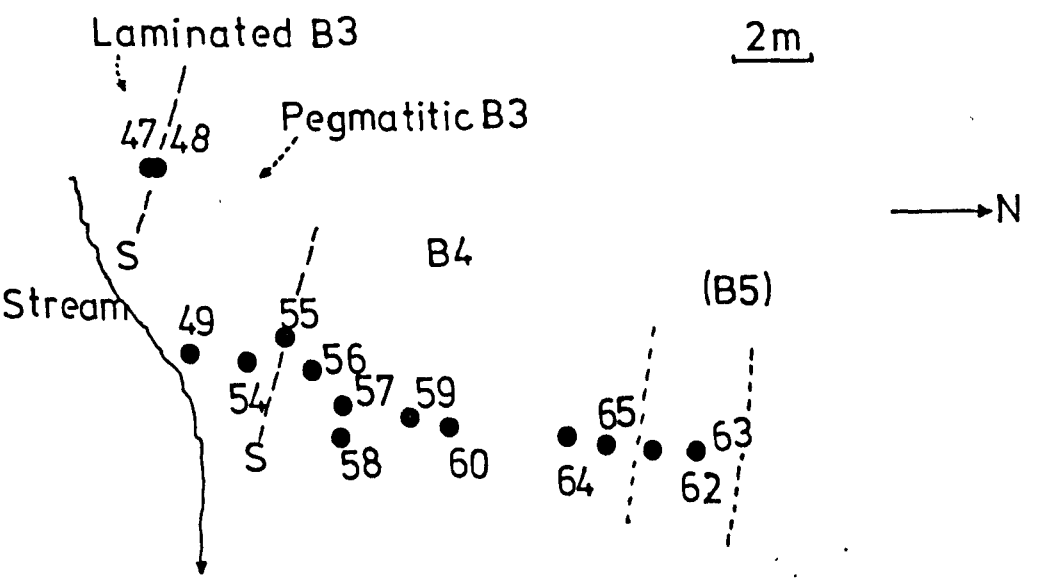

Traverse 6 (3403 3356)

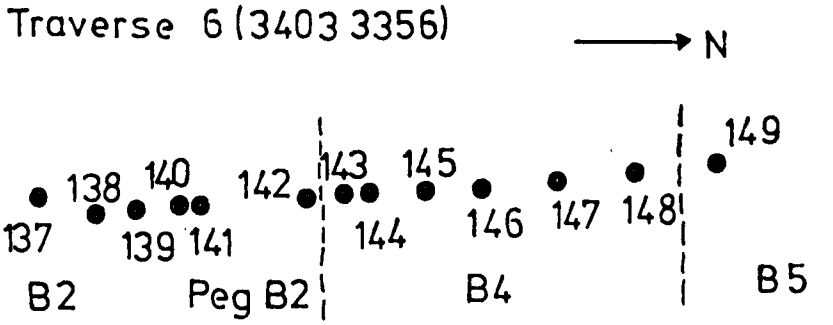

Traverse 5 (3502 3340)

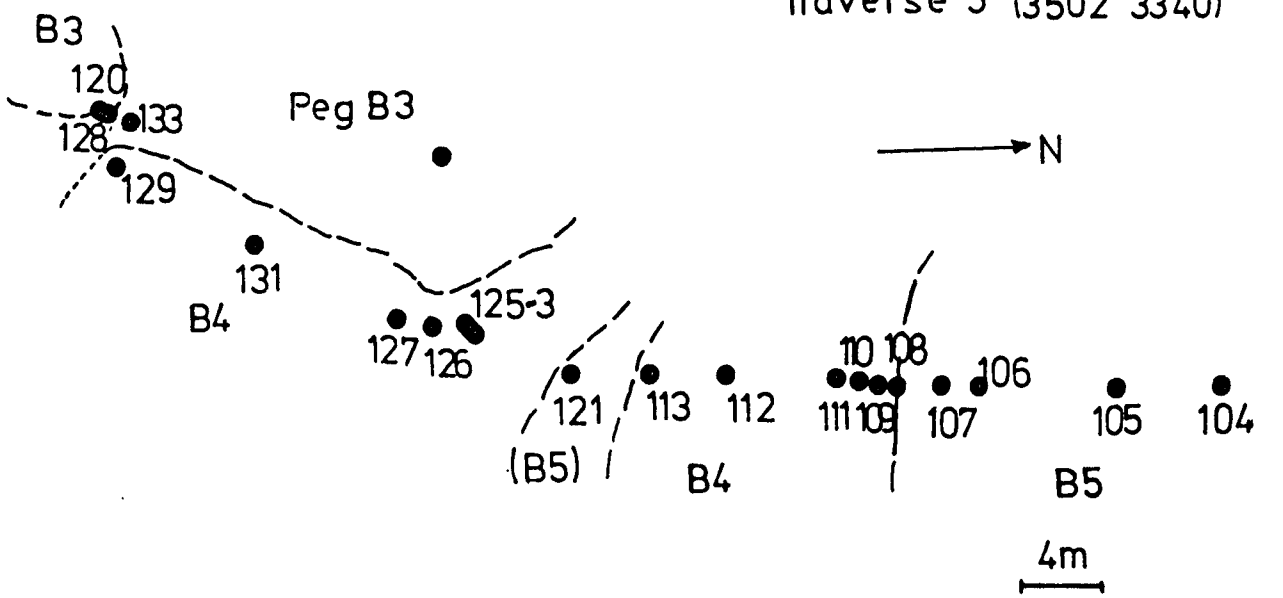

Traverse 4 (3505 3339)

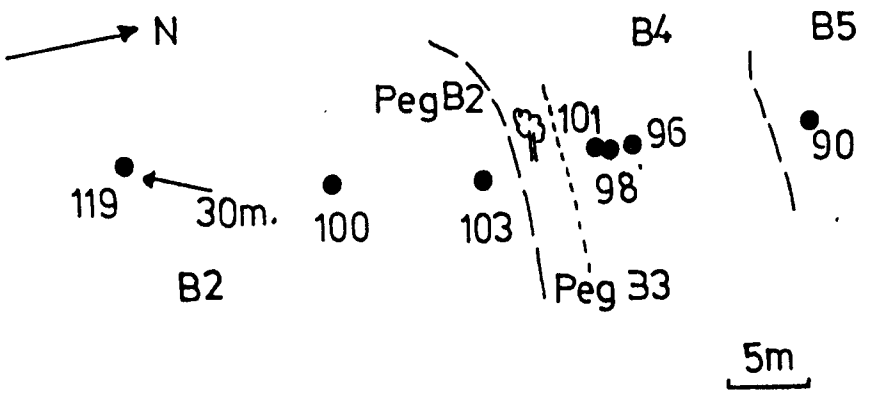

APPENDIX TWO

MINERAL DATA

The mineral analyses listed in this appendix were obtained using a Geoscan Mk II electron probe micro-analyser, operated under a high vacuum, at an accelerating voltage of 15 kv. and a specimen current of 0.04 μA. The electron beam was usually kept focussed, giving a spot analysis diameter of 2-5 μm.

Secondary X-rays were analysed using a wavelength dispersive system, with two crystal spectrometers, which allowed simultaneous analysis of two elements. K.A.P., P.E.T and LIF analysing crystals were used in the analyses. The optimum analysing conditions for the elements determined, and the standards used for each element, are shown in Table A.2.1. Standards and polished thin sections were simultaneously carbon-coated prior to use.

Data from the Geoscan were corrected for the effects of atomic number, mass absorption, and fluorescence (Z.A.F) using an on-line varian 620-100 computer. The Z.A.F. correction procedure was applied using the computer program 'TIM 3', written by A. Peckett.

Standard and unknown peak intensities were measured for each element, and an average of 6 to 10 x 10 second counts was used. Standard and unknown background intensities were measured above and below the peak position and an average 4 to 5 x 10 second counts used. Backgrounds obtained for each phase were used throughout a session, and were not re-analysed for each individual grain.

Calculated detection limits are in the range 200 to 500 ppm (0.02 to 0.05%). The overall accuracy taking into account counting precision and uncertainties in the correction procedure, is probably in the order of $\pm$2% relative (Pinsent, 1974). Precision for SiO_2 may be slightly lower than for other elements because of the effects of thermal expansion and contraction of the P.E.T. crystal. During a session the peak position varied from 109°14' to 108°58'

The probe returns all Fe as FeO. Calculation of Fe^{3+} in amphibole is discussed in Section 4.2.4. The values for Fe_2O_3 in amphibole in the following tables have been re-calculated by the method of Leake (1978). Fe_2O_3 in the oxide phases, has been re-calculated by the method of Carmichael (1967). Both amphibole and biotite are hydrous phases, and the apparent percentage deficiency is taken to be the water + volatile content.

Table A.2.2. shows the phases analysed from each specimen

TABLE A.2.1 Optimum analysing conditions and standards used for Electron probe micro analysis

Atomic Number	Element	Line	Analysing crystal	Counter	Peak 2	Background location	Standard
11	Na	$K\alpha_1$	K.A.P.	Flow	53°08'	±2°	Jadeite
12	Mg	"	"	"	43°33'	"	MgO
13	Al	"	"	"	36°23'	"	Al_2O_3
14	Si	"	P.E.T.	"	109°09'	"	Wollastonite
19	K	"	"	"	50°29'	"	Orthoclase
20	Ca	"	LiF	"	113°13'	"	Wollastonite
22	Ti	"	"	"	86°19'	"	TiO_2
24	Cr	"	"	"	69°20'	"	Cr_2O_3
25	Mn	"	"		62°08'	"	Rhodonite
26	Fe	"	"	"	57°30'	"	Fe

TABLE A2.2 Table of phases probed

SUBUNIT	SAMPLE	Pl	Px	Am	Il	Mt	Bi
A1	2	-	8	-	-	-	2
	46	3	3	-	-	-	-
	87	-	-	-	2	-	-
	88	-	3	1	-	-	-
	115	1	2	1	2	-	-
	136	3	2	-	-	-	-
	150	1	6	-	-	-	-
	151	-	3	1	1	-	1
	158	-	2	-	-	-	-
	159	1	3	1	1	-	-
	160	1	1	-	1	-	-
	170	-	3	-	-	-	-
	E17389	-	10	-	1	-	3
	E15249	-	5	1	-	-	2
	E15242	-	2	-	-	-	-
	E16181	-	3	-	-	-	-
A2	117	5	4	2	2	-	2
	D1536	-	1	-	-	-	-
	D1537	-	5	1	-	-	-
A3	152	7	4	2	1	-	2
B1	14	-	2	-	-	-	-
	18	-	2	-	-	-	-
	20	-	2	-	1	-	-
	32	-	15	-	-	-	-
	33	-	2	-	-	-	-
	34	-	5	-	1	-	-
	35	-	1	3	-	-	-
	114	-	1	-	-	-	-

TABLE A2.2 (Cont.)

SUBUNIT	SAMPLE	Pl	Px	Am	Il	Mt	Bi
B2	50	2	3	-	2	-	-
	69	-	4	2	2	-	-
	100	1	4	1	-	-	-
	119	1	2	-	-	-	-
	135	-	7	2	2	1	-
	137	-	5	-	-	-	-
	138	2	2	-	-	-	-
	139	-	3	-	-	-	-
	140	-	4	-	-	-	-
	141	-	2	-	-	-	-
	142	3	3	-	-	-	-
	163	2	5	-	-	-	-
B3	47	-	2	1	-	1	-
	48	-	4	2	-	-	-
	49	-	2	1	-	-	-
	51	3	2	2	2	1	-
	52	1	2	1	1	1	-
	53	1	3	2	1	1	-
	55	-	3	-	-	-	-
	120	1	2	1	1	-	-
	128	-	3	1	-	-	-
	133	-	2	-	-	-	-
	134	2	-	-	-	-	-
B4	55	-	2	-	-	-	-
	60	2	3	1	-	-	-
	98	-	2	-	-	-	-
	101	-	2	-	-	-	-

TABLE A2.2 (Cont.)

SUBUNIT	SAMPLE	Pl	Px	Am	Il	Mt	Bi
	108b	-	2	2	-	-	-
	127	1	3	-	2	-	-
	143	1	4	3	-	-	-
B5	108a	2	1	-	-	-	-
	121	-	2	-	-	2	-
	D755	2	2	-	-	-	-

TABLE A.2.3

Electron microprobe data

UNIT A pages 259 to 273
UNIT B pages 274 to 297

PLAGIOCLASE ANALYSES. UNIT A. (CORE COMPOSITIONS)

OXIDE Wt.%	136/1a	150	160	117/1	117/2	117/3a	152/1	152/2a	159	46/1a	115
SiO_2	49.48	49.72	53.50	54.08	53.23	53.00	52.82	52.20	53.34	54.43	54.15
Al_2O_3	31.36	31.24	29.27	28.73	28.95	29.53	29.99	30.26	29.53	28.14	28.26
FeO	0.25	0.70	0.12	0.33	0.36	0.39	0.25	0.36	0.17	0.34	0.73
CaO	14.86	14.70	12.23	12.15	12.03	12.70	13.49	13.33	13.46	11.02	11.04
Na_2O	3.00	2.72	4.80	4.55	4.54	4.12	4.11	4.16	4.13	5.03	5.52
K_2O	0.13	0.10	0.13	0.28	0.31	0.26	0.25	0.27	0.30	0.30	0.45
TOTAL	99.08	99.18	100.06	100.13	99.42	99.99	100.92	100.58	100.93	99.26	100.15
ATOMIC PROPORTIONS ON THE BASIS OF 8 OXYGENS											
Si	2.281	2.289	2.422	2.446	2.427	2.405	2.380	2.363	2.402	2.477	2.456
Al	1.705	1.696	1.563	1.533	1.557	1.580	1.594	1.615	1.568	1.510	1.512
Fe	0.010	0.027	0.004	0.012	0.014	0.015	0.009	0.014	0.007	0.013	0.028
Ca	0.734	0.726	0.593	0.589	0.588	0.617	0.515	0.647	0.649	0.538	0.537
Na	0.268	0.243	0.421	0.399	0.402	0.362	0.359	0.365	0.360	0.444	0.485
K	0.008	0.006	0.007	0.016	0.018	0.015	0.014	0.015	0.017	0.018	0.026
END MEMBER COMPOSITIONS											
An	72.7	74.5	58.0	58.6	58.4	62.1	63.6	62.9	63.2	53.8	51.2
Ab	26.5	24.9	41.2	39.8	39.9	36.4	35.0	35.6	35.1	44.4	46.3
Or	0.7	0.6	0.8	1.6	1.7	1.5	1.4	1.5	1.7	1.8	2.5

PLAGIOCLASE ANALYSES. UNIT A. (MARGINAL ANALYSES)

OXIDE Wt.%	136/1b	136/1c	117/3b	117/3c	152/2b	152/2c	152/3	152/2d	152/4	46/1b	46/2
SiO_2	51.98	57.52	54.17	53.44	54.29	55.63	55.00	58.18	62.62	54.97	55.32
Al_2O_3	29.94	26.74	28.10	28.33	28.11	28.45	28.38	25.96	23.64	28.57	27.79
FeO	0.36	0.25	0.40	1.38	0.34	0.27	0.25	0.25	0.41	0.32	0.43
CaO	13.31	9.72	11.49	10.91	11.11	10.93	11.53	8.54	6.04	10.82	10.19
Na_2O	3.77	5.92	5.20	5.32	4.95	5.26	4.57	6.82	7.79	5.58	6.20
K_2O	0.22	0.32	0.32	0.44	0.33	0.24	0.31	0.50	0.78	0.26	0.18
TOTAL	99.59	100.47	99.67	99.82	99.14	100.78	100.05	100.26	101.29	100.51	100.10
ATOMIC PROPORTIONS ON THE BASIS OF 8 OXYGENS											
Si	2.372	2.572	2.463	2.429	2.475	2.489	2.480	2.606	2.754	2.472	2.497
Al	1.612	1.410	1.507	1.525	1.511	1.502	1.509	1.372	1.226	1.515	1.480
Fe	0.014	0.009	0.015	0.053	0.013	0.010	0.009	0.009	0.015	0.012	0.016
Ca	0.651	0.466	0.560	0.534	0.543	0.524	0.557	0.410	0.285	0.521	0.493
Na	0.337	0.513	0.458	0.471	0.438	0.457	0.400	0.592	0.664	0.486	0.543
K	0.013	0.018	0.019	0.025	0.019	0.014	0.018	0.028	0.044	0.015	0.010
END MEMBER COMPOSITIONS											
An	65.3	46.7	54.0	51.8	54.3	52.7	57.1	39.8	28.7	51.0	47.1
Ab	33.4	51.5	44.2	45.7	43.8	45.9	41.0	57.4	66.9	47.6	51.9
Or	1.3	1.8	1.8	2.5	1.9	1.4	1.9	2.8	4.4	1.4	1.0

Pale-mauve CALCIUM RICH CLINOPYROXENE ANALYSES. UNIT A

OXIDE Wt.%	A1 17389/1	17389/2	17389/3	17389/4	17389/5	15242/1	15242/2	46/1	46/2	46/3	115/1	115/2
SiO_2	51.48	50.59	51.25	50.55	50.49	52.39	50.49	50.18	50.05	51.52	51.85	49.28
TiO_2	0.87	0.51	0.89	0.80	0.86	0.50	0.56	0.54	0.49	0.65	0.38	0.67
Al_2O_3	2.11	1.53	2.32	2.04	2.11	1.28	1.27	1.45	1.54	0.39	2.17	2.18
Cr_2O_3	-	-	-	-	-	-	-	-	-	-	-	-
FeO	11.99	12.83	11.01	12.15	11.60	12.57	13.02	17.42	16.20	16.37	16.81	17.45
MnO	0.57	0.38	0.47	0.55	0.43	0.41	0.41	0.48	0.45	0.60	0.59	0.69
MgO	14.30	13.23	14.86	13.57	14.28	13.56	13.16	10.89	11.07	10.78	10.05	9.95
CaO	20.03	19.01	19.36	19.31	20.23	19.39	19.36	18.48	18.43	19.06	18.50	19.68
Na_2O	0.26	0.39	0.28	0.38	0.32	0.33	0.24	0.23	0.26	0.13	0.35	0.39
TOTAL	101.62	98.46	100.44	99.34	100.31	100.41	98.52	99.67	98.49	99.50	100.70	100.28
ATOMIC PROPORTIONS ON THE BASIS OF 6 OXYGENS												
Si	1.912	1.944	1.914	1.922	1.902	1.965	1.943	1.943	1.950	1.988	1.971	1.909
Ti	0.024	0.015	0.025	0.023	0.024	0.014	0.016	0.015	0.014	0.019	0.011	0.020
Al	0.093	0.069	0.102	0.091	0.094	0.057	0.058	0.066	0.071	0.018	0.098	0.100
Cr	-	-	-	-	-	-	-	-	-	-	-	-
Fe	0.372	0.412	0.344	0.386	0.365	0.394	0.419	0.564	0.528	0.528	0.535	0.565
Mn	0.018	0.012	0.015	0.018	0.014	0.013	0.013	0.016	0.015	0.020	0.019	0.023
Mg	0.792	0.758	0.827	0.769	0.801	0.758	0.755	0.629	0.643	0.620	0.570	0.575
Ca	0.797	0.783	0.774	0.787	0.816	0.780	0.798	0.767	0.770	0.788	0.754	0.817
Na	0.018	0.029	0.020	0.028	0.023	0.024	0.018	0.017	0.020	0.010	0.026	0.029
END MEMBER COMPOSITIONS												
Wo	40.3	39.8	39.5	40.2	40.8	40.1	40.2	38.8	39.3	40.3	40.1	41.3
En	40.0	38.5	42.2	39.2	40.2	39.0	38.0	31.8	32.9	31.7	30.4	29.0
Fs	19.7	21.6	18.3	20.6	19.0	20.9	21.8	29.4	27.8	28.0	29.5	29.7

Pale-mauve CALCIUM RICH CLINOPYROXENE ANALYSES. UNIT A

OXIDE	A1								
Wt.%	151/1	151/2	151/3	16181/1	16181/2	16181/3	158/1	158/2	2/1
SiO_2	51.09	50.83	49.42	51.25	50.94	50.96	52.93	51.13	51.92
TiO_2	1.01	0.85	0.10	1.05	0.63	0.68	0.70	1.04	0.86
Al_2O_3	2.28	2.43	1.72	2.18	1.44	0.39	2.01	4.21	1.95
Cr_2O_3	-	-	-	-	-	-	-	-	-
FeO	10.95	13.23	14.70	10.50	15.39	18.53	11.63	11.80	12.23
MnO	0.46	0.45	0.57	0.44	0.79	0.77	0.38	0.36	0.61
MgO	12.78	11.95	10.86	13.13	11.12	8.81	11.96	12.32	13.11
CaO	20.61	19.84	20.45	20.65	19.95	19.65	19.44	19.01	19.71
Na_2O	0.22	0.27	0.24	0.28	0.21	0.25	0.27	0.18	0.31
TOTAL	99.39	99.83	98.05	99.49	100.48	100.06	99.32	100.06	100.72
ATOMIC PROPORTIONS ON THE BASIS OF 6 OXYGENS									
Si	1.933	1.930	1.936	1.933	1.946	1.983	1.992	1.913	1.943
Ti	0.029	0.024	0.003	0.030	0.018	0.020	0.020	0.029	0.024
Al	0.102	0.109	0.079	0.097	0.065	0.018	0.089	0.186	0.086
Cr	-	-	-	-	-	-	-	-	-
Fe	0.346	0.420	0.482	0.331	0.492	0.603	0.366	0.369	0.383
Mn	0.015	0.014	0.019	0.014	0.026	0.026	0.012	0.012	0.019
Mg	0.720	0.676	0.634	0.738	0.633	0.512	0.671	0.687	0.732
Ca	0.836	0.807	0.859	0.835	0.817	0.819	0.784	0.762	0.791
Na	0.016	0.020	0.018	0.020	0.016	0.019	0.019	0.013	0.022
END MEMBER COMPOSITIONS									
Wo	43.6	42.1	43.1	43.5	41.5	41.8	42.8	41.7	41.1
En	37.6	35.2	31.8	38.5	32.2	26.1	36.6	37.5	38.0
Fs	18.8	22.7	25.1	18.0	26.3	32.1	20.6	20.8	20.9

PALE GREEN Ca-RICH CPX ANALYSES. UNIT A.

OXIDE	A1									
Wt.%	170/1	170/2	170/3	159/1	159/2	159/3	15249/1	15249/2	15249/3	15249/4
SiO_2	50.95	52.41	50.44	51.57	50.80	51.59	51.21	51.83	53.03	52.28
TiO_2	0.70	0.15	0.28	0.26	0.27	0.45	0.25	0.84	0.43	0.38
Al_2O_3	1.68	0.45	0.66	0.57	0.73	0.86	0.46	0.46	0.46	1.18
Cr_2O_3	-	-	-	-	-	-	-	-	-	-
FeO	13.34	13.58	16.99	14.76	14.65	13.69	14.02	13.16	13.00	13.30
MnO	0.62	0.57	0.54	0.56	0.59	0.61	0.53	0.53	0.62	0.68
MgO	11.36	10.95	10.17	10.93	11.06	10.94	11.58	11.14	11.95	10.97
CaO	21.16	21.84	20.25	21.01	20.10	20.35	20.78	20.98	20.38	21.13
Na_2O	0.27	0.18	0.25	0.16	0.28	0.18	0.28	0.28	0.25	0.34
TOTAL	100.08	100.13	99.57	99.82	98.48	98.68	99.09	99.22	100.10	100.26
ATOMIC PROPORTIONS ON THE BASIS OF 6 OXYGENS										
Si	1.941	1.996	1.962	1.979	1.975	1.989	1.975	1.987	2.000	1.982
Ti	0.020	0.004	0.008	0.008	0.008	0.013	0.007	0.024	0.012	0.011
Al	0.075	0.020	0.030	0.026	0.033	0.039	0.021	0.021	0.020	0.053
Cr	-	-	-	-	-	-	-	-	-	-
Fe	0.425	0.433	0.553	0.474	0.476	0.441	0.452	0.422	0.411	0.422
Mn	0.020	0.019	0.018	0.018	0.019	0.020	0.017	0.017	0.020	0.022
Mg	0.645	0.621	0.590	0.625	0.641	0.628	0.666	0.637	0.623	0.620
Ca	0.864	0.891	0.844	0.864	0.837	0.841	0.859	0.861	0.825	0.858
Na	0.020	0.013	0.019	0.012	0.021	0.014	0.021	0.021	0.018	0.025
END MEMBER COMPOSITIONS										
Wo	44.2	45.4	42.1	43.6	42.4	43.5	43.1	44.4	42.8	44.6
En	33.0	31.6	29.4	31.6	32.5	32.6	33.4	32.9	34.9	32.3
Fs	22.8	23.0	28.5	24.8	25.1	23.9	23.5	22.7	22.3	23.1

PALE GREEN Ca-RICH CPX ANALYSES. UNIT A

OXIDE	A1									
Wt.%	15249/5	2/2	2/3	2/4	2/5	2/6	2/7	2/8	17389/6	17389/7
SiO_2	50.08	52.01	52.17	52.85	51.71	50.92	50.72	53.40	51.26	52.42
TiO_2	0.73	0.36	0.32	0.31	0.39	0.79	0.80	0.66	0.32	0.18
Al_2O_3	2.03	1.06	1.09	0.95	1.00	2.10	2.43	1.90	1.30	0.57
Cr_2O_3	-	-	-	-	-	-	-	-	-	-
FeO	13.15	11.88	12.95	13.80	11.24	12.15	12.49	10.83	12.38	12.16
MnO	0.58	0.55	0.55	0.58	0.48	0.52	0.49	0.58	0.42	0.59
MgO	10.95	13.27	11.78	11.76	12.46	12.91	11.87	12.94	12.91	11.73
CaO	20.67	21.62	20.89	20.20	21.36	20.95	20.57	20.85	20.79	22.26
Na_2O	0.34	0.28	0.25	0.32	0.53	0.26	0.41	0.27	0.30	0.12
TOTAL	98.53	101.03	100.00	100.76	99.17	100.60	99.78	101.44	99.68	100.02
ATOMIC PROPORTIONS ON THE BASIS OF 6 OXYGENS										
Si	1.937	1.950	1.978	1.990	1.969	1.918	1.927	1.971	1.949	1.988
Ti	0.021	0.010	0.009	0.009	0.011	0.022	0.023	0.018	0.009	0.005
Al	0.093	0.047	0.049	0.042	0.045	0.093	0.109	0.083	0.058	0.026
Cr	-	-	-	-	-	-	-	-	-	-
Fe	0.426	0.373	0.411	0.434	0.358	0.383	0.397	0.334	0.394	0.386
Mn	0.019	0.017	0.018	0.018	0.015	0.017	0.016	0.018	0.014	0.019
Mg	0.631	0.741	0.666	0.660	0.707	0.725	0.672	0.712	0.731	0.663
Ca	0.857	0.869	0.849	0.815	0.872	0.846	0.836	0.824	0.847	0.904
Na	0.026	0.021	0.018	0.023	0.039	0.019	0.030	0.020	0.022	0.009
END MEMBER COMPOSITIONS										
Wo	44.3	43.4	43.7	42.2	44.7	42.9	43.6	43.6	42.7	45.8
En	32.7	37.1	34.3	34.3	36.2	36.8	35.0	37.7	36.8	33.6
Fs	23.0	19.5	22.0	23.5	19.1	20.3	21.4	18.7	20.5	20.6

PALE GREEN Ca-RICH CPX ANALYSES UNIT A.

OXIDE	A1								
Wt.%	17389/8	17389/9	17389/10	150/1	150/2	150/3	150/4	150/5	150/6
SiO_2	50.75	51.34	51.79	52.16	51.31	52.85	53.31	51.92	51.60
TiO_2	0.21	0.36	0.16	0.38	0.68	0.54	0.55	0.60	0.76
Al_2O_3	0.61	0.85	0.54	1.25	1.81	1.53	1.51	1.93	2.18
Cr_2O_3	-	-	-	-	-	-	-	-	-
FeO	13.73	13.36	13.14	11.67	11.68	11.49	11.28	11.95	11.70
MnO	0.39	0.35	0.35	0.52	0.73	0.45	0.58	0.50	0.64
MgO	12.08	11.84	12.18	12.12	12.91	12.30	12.82	12.06	12.80
CaO	21.03	21.58	21.78	20.95	20.74	20.34	19.86	20.44	20.81
Na_2O	0.30	0.32	0.19	0.32	0.33	0.35	0.33	0.17	0.32
TOTAL	99.10	99.60	100.13	99.36	100.20	99.85	100.24	99.56	100.82

ATOMIC PROPORTIONS ON THE BASIS OF 6 OXYGENS

Si	1.958	1.964	1.970	1.979	1.936	1.986	1.990	1.964	1.932
Ti	0.006	0.010	0.004	0.011	0.019	0.015	0.015	0.017	0.021
Al	0.028	0.039	0.024	0.056	0.081	0.068	0.067	0.086	0.096
Cr	-	-	-	-	-	-	-	-	-
Fe	0.443	0.428	0.418	0.370	0.369	0.361	0.352	0.378	0.366
Mn	0.013	0.011	0.011	0.017	0.023	0.014	0.018	0.016	0.020
Mg	0.695	0.675	0.691	0.685	0.726	0.689	0.713	0.680	0.715
Ca	0.869	0.868	0.888	0.852	0.839	0.819	0.794	0.828	0.835
Na	0.022	0.024	0.014	0.023	0.024	0.025	0.024	0.012	0.023

END MEMBER COMPOSITIONS

Wo	43.0	43.6	44.2	44.3	42.9	43.5	42.3	43.5	43.1
En	34.4	34.2	34.4	35.6	37.1	36.6	38.0	35.8	36.9
Fs	22.6	22.2	21.4	20.1	20.0	19.9	19.7	20.7	20.0

Pale-green
CALCIUM RICH CLINOPYROXENE ANALYSES. UNIT A

OXIDE	A1					
Wt.%	88/1	88/2	88/3	136/1	136/2	160
SiO_2	51.61	52.48	52.26	52.32	52.34	51.75
TiO_2	0.90	0.45	0.80	0.77	1.18	0.15
Al_2O_3	2.32	1.45	2.19	1.83	1.20	0.69
Cr_2O_3	-	-	-	-	-	0.08
FeO	9.73	9.47	10.14	10.80	11.06	15.25
MnO	0.42	0.37	0.46	0.54	0.51	0.44
MgO	13.32	14.11	13.76	13.12	12.82	11.68
CaO	20.61	20.65	21.81	20.95	20.68	19.81
Na_2O	0.28	0.34	0.29	0.25	0.33	0.14
TOTAL	99.19	99.32	101.70	100.58	100.13	99.95
ATOMIC PROPORTIONS ON THE BASIS OF 6 OXYGENS						
Si	1.943	1.969	1.928	1.953	1.965	1.978
Ti	0.026	0.013	0.022	0.022	0.033	0.004
Al	0.103	0.064	0.095	0.080	0.053	0.031
Cr	-	-	-	-	-	0.002
Fe	0.306	0.297	0.313	0.337	0.347	0.488
Mn	0.013	0.012	0.014	0.017	0.016	0.014
Mg	0.747	0.789	0.757	0.730	0.717	0.666
Ca	0.831	0.830	0.862	0.838	0.832	0.812
Na	0.020	0.025	0.021	0.018	0.024	0.010
END MEMBER COMPOSITIONS						
Wo	43.8	43.1	44.3	43.6	43.5	41.0
En	39.4	40.9	38.9	38.0	37.5	33.6
Fs	16.8	16.0	16.8	18.4	19.0	25.4

Pale-green

CALCIUM RICH CLINOPYROXENE ANALYSES. UNIT A

OXIDE	A2								A3	
Wt.%	1536/2	117/1	117/2	1537/1	1537/2	1537/3	1537/4	1537/5	152/1	152/2
SiO_2	52.26	51.64	51.97	52.93	51.43	49.87	52.00	51.86	51.14	50.25
TiO_2	0.44	0.64	0.53	0.57	0.39	1.88	0.82	0.39	0.22	0.26
Al_2O_3	1.24	1.39	1.36	1.59	1.20	0.77	1.77	0.79	0.65	0.72
Cr_2O_3	-	0.01	0.08	-	-	-	-	-	0.03	0.04
FeO	12.69	13.32	12.86	12.10	12.44	12.98	12.51	12.34	16.49	17.25
MnO	0.68	0.44	0.54	0.55	0.35	1.72	0.62	0.61	0.49	0.53
MgO	12.62	12.64	12.70	12.83	12.32	12.43	11.86	12.15	10.06	10.51
CaO	19.87	19.90	20.37	19.18	20.14	19.93	19.67	21.00	19.65	19.09
Na_2O	0.22	0.23	0.23	0.35	0.34	0.39	0.34	0.24	0.25	0.27
TOTAL	100.02	100.22	100.64	100.10	98.61	99.97	99.59	99.36	98.99	98.91
ATOMIC PROPORTIONS ON THE BASIS OF 6 OXYGENS										
Si	1.974	1.953	1.956	1.983	1.971	1.912	1.969	1.977	1.987	1.965
Ti	0.013	0.018	0.015	0.016	0.011	0.054	0.023	0.011	0.006	0.008
Al	0.055	0.062	0.060	0.070	0.054	0.035	0.079	0.036	0.030	0.033
Cr	-	0.000	0.002	-	-	-	-	-	0.001	0.001
Fe	0.401	0.421	0.405	0.379	0.399	0.416	0.396	0.393	0.536	0.564
Mn	0.022	0.014	0.017	0.017	0.011	0.056	0.020	0.020	0.016	0.018
Mg	0.710	0.712	0.713	0.716	0.704	0.710	0.670	0.690	0.583	0.612
Ca	0.804	0.807	0.821	0.770	0.827	0.819	0.798	0.858	0.819	0.800
Na	0.016	0.017	0.017	0.026	0.025	0.029	0.025	0.017	0.019	0.021
END MEMBER COMPOSITIONS										
Wo	41.5	41.3	42.0	40.9	42.6	40.9	42.4	43.7	41.9	40.1
En	36.7	36.5	36.4	38.0	36.2	35.5	35.5	35.2	29.8	30.7
Fs	21.8	22.2	21.6	21.1	21.2	23.6	22.1	21.1	28.3	29.2

CALCIUM POOR PYROXENE ANALYSES. UNIT A.

OXIDE Wt.%	117/1	117/2	152/1	152/2	152/3	152/4
SiO_2	49.93	51.77	50.50	50.49	49.40	49.88
TiO_2	0.37	0.41	0.37	0.44	0.41	0.45
Al_2O_3	0.76	0.78	0.86	0.89	0.68	0.24
Cr_2O_3	0.03	0.01	-	-	-	-
FeO	26.12	25.63	28.47	27.49	28.47	28.37
MnO	0.70	0.67	0.82	0.75	0.95	0.91
MgO	17.88	18.17	17.80	17.98	15.97	15.87
CaO	2.17	1.82	1.95	1.75	3.04	3.16
Na_2O	0.01	-	0.03	0.03	0.02	0.08
TOTAL	97.96	99.26	100.80	99.81	98.96	98.94
ATOMIC PROPORTIONS ON THE BASIS OF 6 OXYGENS						
Si	1.955	1.984	1.939	1.948	1.946	1.963
Ti	0.011	0.012	0.011	0.013	0.012	0.013
Al	0.035	0.036	0.039	0.041	0.032	0.011
Cr	0.001	0.000	-	-	-	-
Fe	0.856	0.821	0.914	0.887	0.938	0.934
Mn	0.023	0.022	0.027	0.024	0.032	0.030
Mg	1.044	1.037	1.019	1.034	0.938	0.931
Ca	0.091	0.075	0.080	0.072	0.129	0.133
Na	0.001	-	0.002	0.002	0.002	0.006
END MEMBER COMPOSITIONS						
Wo	4.0	3.8	3.9	3.6	6.3	6.6
En	52.5	53.1	49.9	51.2	46.1	45.9
Fs	43.5	43.1	46.2	45.2	47.6	47.5

ILMENITE ANALYSES UNIT A

	A1								A2		A3
OXIDE Wt%	87/1	87/2	151	159	115/1	115/2	160	173 89	117/1	117/2	152
SiO_2	-	-	-	-	-	0.04	0.08	-	0.11	0.15	0.10
TiO_2	51.8	51.70	52.04	52.06	51.87	51.80	52.23	50.89	49.84	49.77	51.88
Al_2O_3	0.06	0.07	0.06	0.05	0.02	0.06	0.02	0.05	0.01	0.00	0.00
Cr_2O_3	0.07	0.03	0.03	-	-	-	0.13	-	0.07	0.33	0.07
Fe_2O_3	0.74	1.51	0.52	0.03	1.84	2.39	0.44	2.51	5.92	4.85	0.97
FeO	45.12	44.99	44.46	44.75	43.76	43.82	45.38	43.77	42.33	42.44	44.20
MnO	1.30	1.31	2.08	1.76	2.61	2.57	1.39	1.58	2.45	2.25	2.42
MgO	0.12	0.10	0.13	0.16	0.13	0.11	0.16	0.22	0.07	0.12	0.07
TOTAL	99.30	99.72	99.32	98.81	100.23	100.80	99.83	99.02	100.81	99.92	99.71
ATOMIC PROPORTIONS ON THE BASIS OF 6 OXYGENS											
Si	-	-	-	-	-	0.002	0.004	-	0.006	0.008	0.005
Ti	1.983	1.969	1.988	1.998	1.965	1.951	1.984	1.9503	1.881	1.893	1.975
Al	0.004	0.004	0.004	0.003	0.001	0.004	0.001	0.003	0.001	0.000	0.000
Cr	0.003	0.001	0.001	-	-	-	0.005	-	0.003	0.013	0.003
Fe^3	0.028	0.058	0.020	0.001	0.070	0.090	0.017	0.096	0.223	0.185	0.037
Fe^3	1.918	1.905	1.888	1.910	1.843	1.836	1.917	1.865	1.777	1.796	1.871
Mn	0.056	0.056	0.090	0.076	0.111	0.109	0.059	0.068	0.104	0.096	0.104
Mg	0.009	0.008	0.010	0.012	0.010	0.009	0.012	0.017	0.006	0.009	0.005
$\%Ilm_{ss}$	98.5	98.2	98.8	98.9	98.5	98.5	99.3	96.7	94.9	94.8	98.7

BIOTITE ANALYSES. UNIT A

OXIDE Wt.%	17389/ 1	17389/ 2a	17389/ 2b	15249/ 1	15249/ 2	2/1	2/2	151
SiO_2	38.07	38.65	37.10	36.85	36.81	36.22	38.91	37.32
TiO_2	5.84	5.13	5.84	4.74	4.57	5.28	4.65	5.01
Al_2O_3	14.04	13.47	13.76	13.25	12.98	13.17	13.03	13.85
FeO	21.80	20.78	22.41	22.49	26.33	26.01	23.49	25.63
MnO	0.11	0.12	0.09	1.17	0.22	0.26	0.17	0.26
MgO	10.23	11.12	10.49	9.34	6.62	6.93	9.35	7.05
CaO	0.05	0.07	0.09	0.09	0.49	0.07	0.02	0.08
Na_2O	0.17	0.10	0.18	0.18	0.18	0.13	0.13	0.10
K_2O	9.28	9.00	8.74	9.06	8.77	8.86	8.61	9.39
TOTAL	99.57	98.45	98.70	97.17	96.98	96.93	98.36	98.69
ATOMIC PROPORTIONS ON THE BASIS OF 22 OXYGENS								
Si	5.603	5.716	5.529	5.628	5.710	5.618	5.814	5.662
Ti	0.646	0.570	0.655	0.545	0.533	0.616	0.523	0.572
Al	2.437	2.348	2.419	2.387	2.375	2.409	2.296	2.487
Fe	2.684	2.568	2.793	2.873	3.416	3.374	2.936	3.252
Mn	0.014	0.015	0.011	0.151	0.029	0.034	0.022	0.033
Mg	2.244	2.449	2.330	2.126	1.530	1.602	2.082	1.594
Ca	0.008	0.011	0.014	0.015	0.081	0.012	0.003	0.013
Na	0.049	0.029	0.052	0.053	0.054	0.039	0.038	0.029
K	1.743	1.697	1.662	1.765	1.736	1.753	1.641	1.818
$100 \cdot \frac{Mg}{Mg + Fe}$	45.5	48.8	45.5	42.5	30.9	32.2	41.5	32.9

BIOTITE ANALYSES UNIT A

OXIDE Wt.%	152/1	152/2	117/1	117/2
SiO_2	35.41	35.42	36.93	36.76
TiO_2	5.70	5.71	4.89	4.72
Al_2O_3	13.57	13.87	13.53	13.47
FeO	25.72	24.86	21.97	21.58
MnO	0.17	0.11	-	0.14
MgO	7.06	7.26	10.38	11.06
CaO	0.18	0.05	0.07	0.10
Na_2O	0.62	0.27	0.16	0.14
K_2O	8.83	9.03	9.57	8.61
TOTAL	97.26	96.58	97.50	96.58
ATOMIC PROPORTIONS ON THE BASIS OF 22 OXYGENS				
Si	5.486	5.498	5.591	5.584
Ti	0.664	0.666	0.557	0.539
Al	2.480	2.539	2.416	2.413
Fe	3.333	3.227	2.782	2.741
Mn	0.022	0.015	-	0.018
Mg	1.630	1.679	2.342	2.504
Ca	0.030	0.008	0.011	0.016
Na	0.186	0.081	0.047	0.041
K	1.745	1.788	1.848	1.669
$100 \cdot \frac{Mg}{Mg + Fe}$	32.8	34.2	45.7	47.7

AMPHIBOLE ANALYSES. UNIT A

OXIDE Wt.%	88	1537	117/1	117/2	152/1	152/2	15249	159	151	115
SiO_2	46.46	48.12	47.83	47.80	45.10	46.00	48.29	49.41	42.94	45.49
TiO_2	1.96	0.92	1.14	1.13	1.67	1.53	1.03	0.22	0.06	0.95
Al_2O_3	7.82	5.05	5.52	5.65	6.92	6.53	5.11	4.22	7.74	6.70
Cr_2O_3	-	-	0.07	0.07	0.08	0.03	-	-	-	-
FeO	10.13	14.40	18.04	17.95	18.39	18.28	19.72	23.28	25.35	22.78
MnO	0.13	0.20	0.26	0.30	0.21	0.25	0.45	0.16	0.34	0.34
MgO	16.43	14.17	11.86	12.14	10.72	11.21	10.46	8.57	6.27	8.47
CaO	12.11	12.32	11.21	10.57	10.70	10.88	10.57	11.65	10.49	10.54
Na_2O	1.57	0.87	0.99	1.04	1.84	1.68	1.17	0.44	1.66	1.14
K_2O	0.54	0.45	0.33	0.30	0.56	0.52	0.40	0.17	1.04	0.72
TOTAL	97.15	96.49	97.26	96.94	96.20	96.91	97.20	98.12	95.88	97.15
ATOMIC PROPORTIONS ON THE BASIS OF 23 OXYGENS										
Si	6.780	7.176	7.172	7.174	6.906	6.973	7.290	7.476	6.858	7.017
Ti	0.216	0.104	0.129	0.127	0.193	0.174	0.117	0.025	0.007	0.111
Al	1.346	0.888	0.977	1.000	1.250	1.168	0.910	0.752	1.459	1.219
Cr	-	-	0.008	0.008	0.010	0.004	-	-	-	-
Fe	1.237	1.976	2.263	2.254	2.356	2.318	2.490	2.945	3.386	2.939
Mn	0.016	0.025	0.034	0.039	0.028	0.033	0.058	0.020	0.046	0.441
Mg	3.573	3.149	2.649	2.715	2.446	2.533	2.354	1.932	1.491	1.948
Ca	1.893	1.969	1.801	1.699	1.756	1.768	1.709	1.889	1.795	1.742
Ng	0.443	0.253	0.289	0.302	0.548	0.495	0.343	0.130	0.514	0.342
K	0.100	0.086	0.062	0.057	0.109	0.100	0.007	0.033	0.211	0.142

AMPHIBOLE ANALYSES. UNIT A (RECALCULATED $FeO+Fe_2O_3$)

OXIDE Wt.%	88	1537	117/1	117/2	152/1	152/2	15249	159	151	115
Fe_2O_3	5.10	4.20	6.90	9.70	5.70	6.10	6.75	4.70	7.60	8.40
FeO	5.54	10.62	11.82	9.21	13.25	12.78	13.64	19.05	19.04	15.20
TOTAL	97.66	96.92	97.93	97.91	96.75	97.51	97.87	98.59	98.18	97.95

ATOMIC PROPORTIONS ON THE BASIS OF 23 OXYGENS

Si	6.698	7.104	7.053	7.007	6.810	6.870	7.172	7.390	6.637	6.873
Ti	0.212	0.102	0.126	0.125	0.189	0.172	0.115	0.025	0.123	0.108
Al	1.330	0.879	0.960	0.977	1.232	1.150	0.895	0.744	1.411	1.194
Fe^3	0.553	0.467	0.766	1.070	0.648	0.686	0.754	0.529	0.884	0.955
Fe^2	0.668	1.311	1.458	1.129	1.673	1.596	1.694	2.383	2.461	1.921
Mn	0.016	0.025	0.033	0.037	0.027	0.032	0.057	0.020	0.045	0.044
Mg	3.530	3.118	2.606	2.652	2.412	2.495	2.315	1.910	1.444	1.907
Ca	1.871	1.949	1.771	1.660	1.731	1.741	1.682	1.867	1.737	1.706
Na	0.439	0.249	0.283	0.296	0.539	0.487	0.337	0.128	0.498	0.334
K	0.099	0.085	0.062	0.056	0.108	0.099	0.076	0.032	0.205	0.139
Cr	-	-	0.008	0.008	0.010	0.004	-	-	-	-

PLAGIOCLASE ANALYSES. UNIT B (CORE COMPOSITIONS)

OXIDE Wt.%	138/1	138/2	142/1	142/2a	119	100	163a	50/1a	134/1a	120
SiO_2	53.92	52.87	55.76	54.63	54.34	54.67	53.88	54.29	57.26	57.36
Al_2O_3	28.26	28.71	28.02	28.27	28.64	28.26	28.32	28.00	27.09	26.34
FeO	0.55	0.54	0.46	0.41	0.43	0.36	0.35	0.32	0.38	0.29
CaO	11.51	11.48	10.63	11.28	11.60	10.92	11.38	11.14	9.16	8.71
Na_2O	4.88	4.96	5.37	4.82	4.83	4.97	4.88	5.20	5.99	5.81
K_2O	0.22	0.21	0.24	0.19	0.19	0.21	0.20	0.15	0.24	0.31
TOTAL	99.35	98.77	100.48	99.60	100.02	99.38	99.02	99.10	100.11	98.82

ATOMIC PROPORTIONS ON THE BASIS OF 8 OXYGENS

Si	2.458	2.428	2.503	2.476	2.457	2.481	2.460	2.476	2.566	2.597
Al	1.519	1.555	1.483	1.511	1.527	1.513	1.525	1.506	1.432	1.406
Fe	0.021	0.021	0.017	0.016	0.016	0.014	0.014	0.012	0.014	0.011
Ca	0.562	0.565	0.511	0.548	0.562	0.531	0.557	0.544	0.440	0.423
Na	0.432	0.442	0.468	0.424	0.423	0.437	0.432	0.459	0.521	0.510
K	0.013	0.012	0.014	0.011	0.011	0.012	0.012	0.009	0.014	0.018

END MEMBER COMPOSITIONS

An	55.9	55.4	51.5	55.8	56.4	54.2	55.6	53.7	45.1	44.5
Ab	42.8	43.4	47.1	43.1	42.5	44.6	43.2	45.4	53.5	53.6
Or	1.3	1.2	1.4	1.1	1.1	1.2	1.2	0.9	1.4	1.9

PLAGIOCLASE ANALYSES UNIT B (CORE COMPOSITIONS)

OXIDE Wt.%	51/1	51/2a	52	53	127	143	60/1a	163b	108a/1a	755/1a
SiO_2	56.49	57.67	57.24	58.20	61.25	60.38	63.14	59.13	63.04	61.67
Al_2O_3	27.45	26.98	26.60	26.09	24.31	25.36	23.70	25.71	22.75	24.78
FeO	0.82	0.36	0.34	0.37	0.27	0.32	0.39	0.22	0.27	0.17
CaO	9.86	9.37	9.63	8.86	7.04	7.39	5.40	7.13	4.93	5.36
Na_2O	5.83	6.20	5.66	6.13	7.44	7.14	7.48	7.05	8.20	7.86
K_2O	0.17	0.25	0.24	0.23	0.37	0.32	0.46	0.16	0.54	0.59
TOTAL	100.62	100.83	99.70	99.88	100.69	100.91	100.58	99.40	99.72	100.41
ATOMIC PROPORTIONS ON THE BASIS OF 8 OXYGENS										
Si	2.531	2.569	2.576	2.609	2.711	2.670	2.777	2.650	2.800	2.725
Al	1.450	1.418	1.417	1.379	1.269	1.322	1.230	1.359	1.192	1.291
Fe	0.031	0.013	0.013	0.014	0.010	0.012	0.014	0.008	0.010	0.006
Ca	0.473	0.447	0.464	0.426	0.334	0.350	0.255	0.342	0.235	0.254
Na	0.506	0.536	0.494	0.533	0.639	0.612	0.638	0.613	0.706	0.673
K	0.010	0.014	0.014	0.013	0.021	0.018	0.026	0.009	0.031	0.033
END MEMBER COMPOSITIONS										
An	47.8	44.8	47.8	43.8	33.6	35.7	27.7	35.5	24.2	26.4
Ab	51.2	53.7	50.8	54.8	64.3	62.5	69.5	63.6	72.7	70.1
Or	1.0	1.5	1.4	1.4	2.1	1.8	2.8	0.9	3.1	3.5

PLAGIOCLASE ANALYSES UNIT B (MARGINAL COMPOSITIONS)

OXIDE Wt.%	50/1b	142/2b	134/1b	51/2b	108a/1b	755/1b	60/1b
SiO_2	56.41	58.40	65.22	59.44	63.34	61.99	64.32
Al_2O_3	26.68	25.53	21.95	25.03	22.44	22.84	22.25
FeO	0.27	0.31	0.24	0.29	0.38	0.23	0.24
CaO	9.64	7.52	3.52	6.27	4.28	4.38	4.11
Na_2O	6.30	7.11	8.66	7.42	7.74	8.60	9.12
K_2O	0.20	0.38	0.43	0.51	1.83	1.81	0.65
TOTAL	99.49	99.25	100.02	98.97	100.01	99.86	100.68
ATOMIC PROPORTIONS ON THE BASIS OF 8 OXYGENS							
Si	2.552	2.633	2.868	2.677	2.816	2.774	2.830
Al	1.424	1.358	1.138	1.329	1.177	1.206	1.154
Fe	0.010	0.012	0.009	0.011	0.014	0.008	0.009
Ca	0.467	0.364	0.166	0.303	0.204	0.210	0.194
Na	0.553	0.622	0.739	0.648	0.667	0.747	0.776
K	0.011	0.022	0.024	0.029	0.104	0.103	0.036
END MEMBER COMPOSITIONS							
An	45.3	36.1	17.9	30.9	20.9	19.8	19.2
Ab	53.6	61.7	79.5	66.1	68.4	70.4	77.2
Or	1.1	2.2	2.6	3.0	10.7	9.8	3.6

SECTOR ZONED CALCIUM RICH CLINOPYROXENE ANALYSES. UNIT B.

OXIDE	B1											
wt.%	32/1a	32/1b	32/1c	32/1d	32/1e	32/1f	32/1g	32/1h	32/1i	32/1j	32/2a	32/2b
SiO_2	50.11	51.18	50.52	51.08	50.02	49.96	49.79	51.21	50.58	50.65	51.57	51.23
TiO_2	1.11	0.81	0.81	0.75	1.15	1.28	1.05	0.81	0.56	1.37	0.78	0.80
Al_2O_3	3.46	2.01	2.06	2.20	3.48	3.35	3.09	2.14	1.17	2.39	1.80	2.02
Cr_2O_3	-	-	0.24	0.46	0.55	0.26	0.51	0.28	0.04	0.11	0.12	0.28
FeO	8.20	7.75	7.53	6.64	6.79	7.19	7.08	6.58	11.17	8.29	7.59	7.15
MnO	0.27	0.29	0.32	0.33	0.27	0.28	0.28	0.28	0.42	0.40	0.41	0.27
MgO	14.78	16.11	15.95	15.93	15.11	14.80	14.97	15.90	13.37	14.56	16.12	16.59
CaO	22.21	21.72	21.87	21.87	22.55	22.03	22.47	21.85	21.19	22.20	21.80	22.02
Na_2O	0.22	0.20	0.20	0.27	0.25	0.38	0.28	0.23	0.35	0.39	0.20	0.22
TOTAL	100.35	100.06	99.52	99.54	100.18	99.54	99.53	99.27	98.86	100.37	100.40	100.55
ATOMIC PROPORTIONS ON THE BASIS OF 6 OXYGENS												
Si	1.866	1.904	1.896	1.910	1.867	1.873	1.874	1.915	1.936	1.891	1.913	1.898
Ti	0.031	0.023	0.023	0.021	0.032	0.036	0.030	0.023	0.016	0.039	0.022	0.022
Al	0.152	0.088	0.091	0.097	0.153	0.148	0.137	0.094	0.053	0.105	0.079	0.088
Cr												
Fe	0.255	0.241	0.236	0.208	0.212	0.225	0.223	0.206	0.358	0.259	0.236	0.221
Mn	0.008	0.009	0.010	0.011	0.009	0.009	0.009	0.009	0.014	0.013	0.013	0.009
Mg	0.820	0.893	0.892	0.888	0.840	0.827	0.840	0.886	0.763	0.810	0.891	0.916
Ca	0.886	0.865	0.880	0.876	0.902	0.885	0.906	0.875	0.869	0.888	0.866	0.874
Na	0.016	0.015	0.015	0.020	0.018	0.028	0.020	0.017	0.026	0.028	0.015	0.016
END MEMBER COMPOSITIONS												
Wo	45.2	43.3	43.6	44.2	45.9	45.5	45.8	44.3	43.4	45.0	43.2	43.5
En	41.8	44.7	44.2	44.8	42.8	42.5	42.4	44.8	38.1	41.2	44.4	45.5
Fs	13.0	12.0	12.2	11.0	11.3	12.0	11.8	10.9	18.5	13.8	12.4	11.0

CALCIUM RICH CLINOPYROXENE ANALYSES. UNIT B

OXIDE	B1									
Wt.%	32/3	32/4a	32/4b	34/1	34/2a	34/2b	34/2c	34/2d	14/1	14/2
SiO_2	51.23	50.68	50.84	50.79	49.39	50.71	50.05	50.63	50.12	49.42
TiO_2	0.87	0.68	0.94	0.86	1.09	0.69	0.71	0.39	0.79	0.92
Al_2O_3	2.53	3.58	2.69	2.89	4.46	2.97	2.12	0.95	3.14	3.12
Cr_2O_3	-	0.32	0.06	-	-	-	-	-	0.05	0.10
FeO	8.19	7.06	8.94	8.46	8.14	7.41	11.62	17.71	8.13	7.86
MnO	0.35	0.29	0.32	0.35	0.25	0.27	0.70	0.85	0.34	0.28
MgO	14.16	15.15	14.16	14.72	14.51	15.60	13.06	9.64	15.01	14.88
CaO	22.46	21.86	22.30	21.92	21.38	22.13	20.86	18.93	21.73	22.06
Na_2O	0.32	0.23	0.29	0.20	0.34	0.40	0.28	0.33	0.28	0.32
TOTAL	100.12	99.86	100.55	100.20	99.54	100.17	99.40	99.42	99.58	98.95

ATOMIC PROPORTIONS ON THE BASIS OF 6 OXYGENS

Si	1.911	1.883	1.895	1.887	1.850	1.884	1.909	1.972	1.901	1.867
Ti	0.024	0.019	0.026	0.024	0.031	0.019	0.020	0.012	0.023	0.026
Al	0.111	0.157	0.118	0.126	0.197	0.130	0.095	0.044	0.140	0.139
Cr	-	0.009	0.002	-	0.255	-	-	-	0.001	0.003
Fe	0.257	0.219	0.279	0.261	0.255	0.230	0.371	0.577	0.258	0.248
Mn	0.011	0.009	0.010	0.011	0.008	0.009	0.023	0.028	0.011	0.009
Mg	0.787	0.839	0.787	0.808	0.810	0.864	0.742	0.560	0.849	0.838
Ca	0.898	0.870	0.891	0.865	0.858	0.881	0.852	0.790	0.884	0.893
Na	0.023	0.017	0.021	0.014	0.025	0.029	0.021	0.025	0.020	0.024

END MEMBER COMPOSITIONS

Wo	46.0	44.9	45.3	44.5	44.5	44.4	42.9	40.4	44.2	44.9
En	40.3	43.3	40.0	41.6	42.9	43.6	37.3	28.6	42.4	42.2
Fs	13.7	11.8	14.7	13.9	13.6	12.0	19.8	31.0	13.4	12.9

CALCIUM RICH CLINOPYROXENE ANALYSES. UNIT B

OXIDE	B1							
Wt.%	20/1a	20/1b	18/1a	18/1b	33/1	33/2	35	114
SiO_2	51.60	51.67	50.36	51.36	50.49	49.19	51.03	50.27
TiO_2	0.92	0.44	0.83	0.86	0.51	0.47	0.64	1.12
Al_2O_3	2.99	1.93	2.47	1.64	1.19	1.11	2.12	2.93
Cr_2O_3	-	-	-	-	-	-	-	-
FeO	7.74	16.20	12.65	13.49	14.12	I4.50	9.21	8.30
MnO	0.35	0.76	0.53	0.56	0.55	0.65	0.47	0.26
MgO	14.51	10.95	13.17	12.91	12.49	12.81	14.15	14.89
CaO	21.32	18.75	19.37	18.66	20.04	19.87	21.04	21.55
Na_2O	0.27	0.30	0.33	0.45	0.31	0.40	0.27	0.25
TOTAL	99.70	101.00	99.70	99.93	99.70	99.00	98.94	99.57
ATOMIC PROPORTIONS ON THE BASIS OF 6 OXYGENS								
Si	1.918	1.958	1.912	1.946	1.936	1.910	1.928	1.884
Ti	0.026	0.013	0.024	0.025	0.015	0.014	0.018	0.031
Al	0.131	0.086	0.111	0.073	0.054	0.051	0.094	0.130
Cr	-	-	-	-	-	-	-	-
Fe	0.241	0.514	0.401	0.428	0.453	0.471	0.291	0.260
Mn	0.011	0.243	0.017	0.018	0.018	0.021	0.015	0.008
Mg	0.804	0.619	0.745	0.729	0.714	0.741	0.797	0.832
Ca	0.849	0.762	0.788	0.758	0.823	0.827	0.852	0.866
Na	0.019	0.022	0.024	0.033	0.023	0.030	0.020	0.018
END MEMBER COMPOSITIONS								
Wo	44.6	39.7	40.4	39.2	41.0	40.1	43.6	44.2
En	42.2	32.3	38.1	37.7	35.6	36.0	40.8	42.5
Fs	13.2	28.0	21.4	23.1	23.4	23.9	15.7	13.3

CALCIUM RICH CLINOPYROXENE ANALYSES. UNIT B

OXIDE	B2									
wt.%	137/1	137/2	137/3	137/4	137/5	138/1	138/2	139/1	139/2	139/3
SiO_2	49.43	51.29	48.74	50.25	49.76	51.07	50.34	49.62	48.35	48.26
TiO_2	0.85	0.72	0.69	0.74	0.67	0.32	0.69	0.60	0.65	0.45
Al_2O_3	1.39	1.43	2.07	1.38	1.32	1.01	1.37	1.40	1.34	1.20
Cr_2O_3	-	-	-	-	-	-	-	-	-	-
FeO	15.95	16.39	16.64	17.99	19.51	14.67	15.41	18.02	19.84	20.29
MnO	0.68	0.70	0.80	0.77	0.86	0.63	0.61	0.86	0.79	0.82
MgO	11.58	10.60	9.86	9.01	8.14	11.12	11.35	9.52	8.56	8.34
CaO	19.78	19.29	19.22	19.76	19.73	20.62	19.15	19.61	19.80	19.57
Na_2O	0.19	0.22	0.26	0.24	0.33	0.16	0.32	0.29	0.20	0.33
TOTAL	99.85	100.64	98.28	100.13	100.32	99.61	99.23	99.92	99.53	99.27
ATOMIC PROPORTIONS ON THE BASIS OF 6 OXYGENS										
Si	1.912	1.958	1.920	1.951	1.945	1.964	1.945	1.935	1.915	1.921
Ti	0.025	0.021	0.020	0.022	0.020	0.009	0.020	0.018	0.019	0.014
Al	0.063	0.065	0.096	0.063	0.061	0.046	0.062	0.064	0.063	0.056
Cr	-	-	-	-	-	-	-	-	-	-
Fe	0.516	0.523	0.548	0.584	0.638	0.472	0.498	0.588	0.657	0.676
Mn	0.022	0.023	0.027	0.025	0.028	0.021	0.020	0.029	0.027	0.028
Mg	0.668	0.603	0.579	0.521	0.475	0.637	0.654	0.553	0.505	0.495
Ca	0.820	0.789	0.811	0.822	0.826	0.850	0.793	0.819	0.840	0.835
Na	0.015	0.017	0.020	0.018	0.025	0.012	0.024	0.022	0.016	0.026
END MEMBER COMPOSITIONS										
Wo	40.4	40.7	41.3	42.1	42.0	42.9	40.4	41.2	41.4	41.1
En	32.9	31.1	29.5	26.7	24.1	32.2	33.2	27.8	24.9	24.3
Fs	26.7	28.2	29.2	31.2	33.9	24.9	26.4	31.0	33.7	34.6

CALCIUM RICH CLINOPYROXENE ANALYSES UNIT B

OXIDE	B2									
Wt.%	140/1	140/2	140/3	140/4	141/1	141/2	142/1	142/2	142/3	163a/1
SiO_2	49.58	49.83	49.63	48.73	50.13	49.03	47.77	47.82	47.88	49.35
TiO_2	0.69	0.71	0.71	0.63	0.57	0.57	0.71	0.65	0.48	0.79
Al_2O_3	1.36	1.31	1.31	1.30	1.08	1.18	1.11	1.08	0.71	1.45
Cr_2O_3	-	-	-	-	-	-	-	-	-	-
FeO	17.71	17.64	17.81	19.13	21.75	21.89	25.57	25.45	27.34	17.34
MnO	0.75	0.85	0.76	0.85	0.81	0.94	1.09	1.16	1.28	0.76
MgO	9.47	9.17	9.18	8.94	6.43	5.86	3.29	2.83	1.99	9.18
CaO	19.92	19.60	18.95	19.21	20.10	20.49	19.90	20.10	19.46	20.20
Na_2O	0.32	0.21	0.18	0.27	0.27	0.17	0.23	0.25	0.31	0.33
TOTAL	99.80	99.31	98.53	99.06	101.15	100.14	99.65	99.35	99.46	99.41

ATOMIC PROPORTIONS ON THE BASIS OF 6 OXYGENS

Si	1.934	1.949	1.955	1.929	1.962	1.948	1.946	1.954	1.970	1.932
Ti	0.020	0.030	0.021	0.019	0.017	0.017	0.022	0.020	0.015	0.023
Al	0.063	0.060	0.061	0.061	0.050	0.056	0.053	0.052	0.035	0.067
Cr	-	-	-	-	-	-	-	-	-	-
Fe	0.578	0.577	0.587	0.633	0.712	0.728	0.871	0.870	0.941	0.568
Mn	0.025	0.028	0.025	0.029	0.027	0.032	0.038	0.040	0.045	0.025
Mg	0.551	0.534	0.539	0.528	0.375	0.347	0.199	0.173	0.122	0.536
Ca	0.833	0.822	0.800	0.815	0.843	0.873	0.869	0.880	0.858	0.847
Na	0.025	0.016	0.014	0.021	0.021	0.013	0.018	0.020	0.025	0.025

END MEMBER COMPOSITIONS

Wo	41.9	41.9	41.0	40.6	43.0	44.1	44.0	44.8	43.7	42.8
En	27.8	27.2	27.6	26.3	19.2	17.5	10.0	8.8	6.2	27.2
Fs	30.3	30.9	31.4	33.1	37.8	38.4	46.0	46.4	50.1	30.0

CALCIUM RICH CLINOPYROXENE ANALYSES. UNIT B

OXIDE	B2									
Wt.%	163a/2	163a/3	100/1	100/2	100/3	100/4	119/1	119/2	69/1	69/2
SiO_2	50.14	49.65	49.25	49.45	49.77	49.32	50.52	50.73	50.60	51.09
TiO_2	0.67	0.66	0.77	0.64	0.54	0.47	0.71	0.68	0.55	0.61
Al_2O_3	1.33	1.32	1.75	1.40	1.21	1.20	1.43	1.48	1.26	1.24
Cr_2O_3	-	-	-	-	-	-	-	-	-	-
FeO	17.95	17.85	17.85	18.45	19.33	20.22	16.43	16.26	17.99	19.03
MnO	0.84	0.78	0.77	0.72	0.88	0.83	0.71	0.83	0.78	0.72
MgO	9.72	9.38	8.98	8.91	7.89	7.75	10.45	10.09	9.20	8.48
CaO	19.81	20.24	20.06	19.24	19.33	19.43	20.34	19.80	19.41	19.55
Na_2O	0.28	0.23	0.32	0.24	0.26	0.18	0.27	0.24	0.28	0.22
TOTAL	100.74	100.12	99.77	99.06	99.19	99.40	100.87	100.12	100.07	100.94
ATOMIC PROPORTIONS ON THE BASIS OF 6 OXYGENS										
Si	1.937	1.933	1.925	1.946	1.963	1.952	1.935	1.952	1.962	1.970
Ti	0.019	0.019	0.023	0.019	0.016	0.014	0.021	0.020	0.016	0.018
Al	0.061	0.061	0.081	0.065	0.056	0.056	0.065	0.067	0.058	0.056
Cr	-	-	-	-	-	-	-	-	-	-
Fe	0.580	0.581	0.584	0.607	0.638	0.669	0.527	0.524	0.584	0.614
Mn	0.028	0.026	0.026	0.024	0.030	0.028	0.023	0.027	0.026	0.024
Mg	0.559	0.544	0.523	0.522	0.464	0.457	0.597	0.579	0.532	0.487
Ca	0.820	0.845	0.840	0.811	0.817	0.824	0.835	0.817	0.807	0.808
Na	0.021	0.018	0.025	0.018	0.020	0.014	0.020	0.018	0.021	0.017
END MEMBER COMPOSITIONS										
Wo	41.2	42.3	42.6	41.3	41.9	41.7	42.1	41.9	41.4	41.8
En	28.2	27.3	26.5	26.6	23.8	23.1	30.1	29.7	27.3	25.2
Fs	30.6	30.4	30.9	32.1	34.3	35.2	27.8	28.4	31.3	33.0

CALCIUM RICH CLINOPYROXENE ANALYSES. UNIT B

OXIDE	B2									
wt.%	69/3	69/4	50/1	50/2	50/3	135/1	135/2	135/3	135/4	135/5
SiO_2	49.49	49.91	49.80	50.05	49.78	50.09	48.78	49.62	50.24	50.34
TiO_2	0.59	0.24	0.64	0.65	0.61	0.60	0.63	0.64	0.65	0.46
Al_2O_3	1.20	0.73	1.44	1.54	1.54	1.34	1.30	1.51	1.05	1.53
Cr_2O_3	0.04	-	0.01	0.08	0.02	-	-	-	0.01	-
FeO	19.20	21.14	15.22	16.23	16.22	16.41	18.80	18.27	18.18	18.15
MnO	0.75	0.89	0.63	0.57	0.57	0.75	0.85	0.82	0.82	0.92
MgO	7.79	7.19	10.94	10.45	10.36	9.90	9.38	8.80	8.66	8.64
CaO	19.93	18.83	20.26	20.33	20.42	19.60	19.08	19.49	19.49	18.95
Na_2O	0.21	0.47	0.16	0.22	0.33	0.23	0.21	0.43	0.29	0.47
TOTAL	99.20	99.39	99.10	100.12	99.86	98.92	99.04	99.58	99.39	99.06
ATOMIC PROPORTIONS ON THE BASIS OF 6 OXYGENS										
Si	1.955	1.980	1.933	1.931	1.928	1.954	1.927	1.943	1.966	1.975
Ti	0.018	0.007	0.019	0.019	0.018	0.018	0.019	0.019	0.019	0.014
Al	0.056	0.034	0.066	0.070	0.704	0.062	0.061	0.070	0.048	0.052
Cr	0.001	-	0.000	0.002	0.001	-	-	-	0.000	-
Fe	0.634	0.702	0.494	0.524	0.525	0.535	0.621	0.598	0.595	0.595
Mn	0.025	0.030	0.021	0.019	0.019	0.025	0.028	0.027	0.027	0.031
Mg	0.459	0.425	0.633	0.601	0.598	0.575	0.552	0.513	0.505	0.505
Ca	0.844	0.800	0.843	0.840	0.847	0.819	0.807	0.818	0.817	0.797
Na	0.016	0.036	0.012	0.017	0.025	0.017	0.016	0.032	0.022	0.036
END MEMBER COMPOSITIONS										
Wo	43.0	40.9	42.3	42.4	42.6	41.9	40.2	41.8	42.0	41.3
En	23.4	21.7	31.8	30.3	30.1	29.4	27.5	26.2	26.0	26.2
Fs	33.6	37.4	25.9	27.3	27.3	28.7	32.3	32.0	32.0	32.5

CALCIUM RICH CLINOPYROXENE ANALYSES. UNIT B

OXIDE	B2		B3							
Wt.%	135/6	135/7	51/1	51/2	52/1	52/2	53/1	53/2	53/3	47/1
SiO_2	50.15	49.47	48.69	48.67	48.48	48.67	47.62	48.10	47.99	48.52
TiO_2	0.42	0.62	0.32	0.27	0.64	0.49	0.74	0.30	0.40	0.60
Al_2O_3	0.79	1.80	0.89	0.70	1.10	0.94	1.30	0.72	0.77	1.08
Cr_2O_3	-	-	0.02	0.02	0.02	0.03	0.04	0.04	0.06	-
FeO	19.27	18.28	23.23	24.18	24.57	24.92	25.80	26.17	26.78	24.63
MnO	0.91	1.04	0.89	0.87	1.03	1.10	1.10	1.22	1.20	1.05
MgO	8.55	7.59	5.98	5.42	4.23	3.58	3.32	3.36	3.22	4.58
CaO	19.85	20.40	19.37	19.66	19.55	19.40	19.09	19.43	19.45	19.33
Na_2O	0.35	0.44	0.28	0.33	0.29	0.25	0.13	0.23	0.27	0.31
TOTAL	100.28	99.64	99.67	100.12	99.91	99.39	99.15	99.57	100.14	100.11
ATOMIC PROPORTIONS ON THE BASIS OF 6 OXYGENS										
Si	1.959	1.942	1.953	1.954	1.954	1.974	1.947	1.964	1.954	1.952
Ti	0.012	0.018	0.010	0.008	0.020	0.015	0.023	0.009	0.012	0.018
Al	0.037	0.084	0.042	0.033	0.052	0.045	0.063	0.035	0.037	0.051
Cr	-	-	0.001	0.001	0.001	0.001	0.001	0.001	0.002	-
Fe	0.630	0.600	0.780	0.812	0.828	0.846	0.882	0.894	0.912	0.829
Mn	0.030	0.035	0.030	0.029	0.035	0.038	0.038	0.042	0.042	0.036
Mg	0.498	0.444	0.357	0.325	0.254	0.217	0.202	0.205	0.197	0.275
Ca	0.831	0.858	0.833	0.846	0.845	0.843	0.836	0.850	0.849	0.833
Na	0.027	0.034	0.022	0.026	0.023	0.020	0.010	0.018	0.021	0.024
END MEMBER COMPOSITIONS										
Wo	41.8	44.3	41.6	42.0	43.1	43.4	42.7	42.7	42.5	42.3
En	25.0	22.9	17.9	16.2	12.9	11.1	10.3	10.2	9.8	13.9
Fs	33.2	32.8	40.5	41.8	44.0	45.5	47.0	47.1	47.7	43.8

CALCIUM RICH CLINOPYROXENE ANALYSES. UNIT B

OXIDE	B3									
Wt.%	47/2	48/1	48/2	48/3	48/4	49/1	49/2	55/1	55/2	55/3
SiO_2	48.43	48.44	47.65	48.03	48.14	47.34	47.32	47.59	49.06	48.29
TiO_2	0.32	0.60	0.58	0.53	0.34	0.53	0.57	0.69	0.42	0.40
Al_2O_3	0.65	0.71	0.96	1.02	0.72	1.02	1.02	1.31	0.77	0.64
Cr_2O_3	-	-	-	-	0.03	-	-	-	-	-
FeO	24.89	24.35	24.27	24.71	24.59	25.11	25.76	26.49	27.72	27.98
MnO	1.17	0.94	1.02	1.02	1.10	1.04	1.12	1.10	1.35	1.21
MgO	4.59	4.48	4.41	4.27	4.08	3.41	3.20	3.61	1.45	1.00
CaO	19.53	19.29	20.31	19.68	19.39	20.48	20.46	19.95	19.41	19.31
Na_2O	0.41	0.24	0.23	0.21	0.23	0.38	0.36	0.31	0.29	0.29
TOTAL	100.00	99.04	99.43	99.47	98.62	99.32	99.81	101.02	100.47	99.11

ATOMIC PROPORTIONS ON THE BASIS OF 6 OXYGENS

Si	1.957	1.967	1.937	1.949	1.969	1.938	1.934	1.921	1.993	1.996
Ti	0.010	0.018	0.018	0.016	0.011	0.016	0.018	0.021	0.013	0.012
Al	0.031	0.034	0.046	0.049	0.035	0.049	0.049	0.062	0.037	0.031
Cr	-	-	-	-	0.001	-	-	-	-	-
Fe	0.841	0.827	0.825	0.839	0.841	0.860	0.880	0.893	0.942	0.967
Mn	0.040	0.032	0.035	0.035	0.038	0.036	0.039	0.038	0.046	0.042
Mg	0.277	0.271	0.267	0.258	0.249	0.208	0.195	0.217	0.088	0.062
Ca	0.846	0.839	0.885	0.856	0.850	0.898	0.896	0.863	0.845	0.855
Na	0.032	0.019	0.018	0.016	0.019	0.030	0.028	0.024	0.023	0.023

END MEMBER COMPOSITIONS

Wo	42.2	42.6	44.0	43.0	42.9	44.9	44.6	42.9	44.0	44.4
En	13.8	13.8	13.3	13.0	12.6	10.3	9.7	10.8	4.6	3.2
Fs	44.0	43.6	42.7	44.0	44.5	44.8	45.7	46.3	51.4	52.4

CALCIUM RICH CLINOPYROXENE ANALYSES. UNIT B

OXIDE	B3							B4	
Wt.%	120/1	120/2	128/1	128/3	128/3	133/1	133/2	163b/1	163b/2
SiO_2	49.84	50.02	48.39	47.85	47.72	47.51	47.84	49.17	49.55
TiO_2	0.51	0.60	0.68	0.63	0.84	0.88	0.99	0.46	0.66
Al_2O_3	1.08	1.14	0.93	0.91	1.11	1.16	1.33	0.89	1.22
Cr_2O_3	-	-	-	-	-	-	-	-	-
FeO	19.61	21.21	24.69	24.31	24.87	23.21	23.70	19.48	19.04
MnO	0.80	0.99	1.21	1.37	1.18	1.14	1.08	1.03	0.90
MgO	7.50	6.04	3.46	3.55	2.98	4.71	4.82	8.74	8.37
CaO	19.16	19.76	19.76	20.15	20.10	19.90	19.26	19.56	19.72
Na_2O	0.25	0.27	0.33	0.35	0.21	0.32	0.23	0.25	0.33
TOTAL	98.74	100.03	99.44	99.12	99.00	98.90	99.25	99.58	99.79
ATOMIC PROPORTIONS ON THE BASIS OF 6 OXYGENS									
Si	1.976	1.975	1.965	1.954	1.953	1.934	1.936	1.941	1.945
Ti	0.015	0.018	0.021	0.019	0.026	0.027	0.030	0.014	0.020
Al	0.051	0.053	0.044	0.044	0.053	0.056	0.063	0.042	0.057
Cr	-	-	-	-	-	-	-	-	-
Fe	0.650	0.701	0.838	0.830	0.851	0.790	0.802	0.643	0.625
Mn	0.027	0.033	0.042	0.047	0.041	0.039	0.037	0.034	0.030
Mg	0.443	0.356	0.210	0.216	0.182	0.286	0.290	0.514	0.490
Ca	0.814	0.836	0.860	0.882	0.881	0.867	0.835	0.828	0.829
Na	0.019	0.021	0.026	0.028	0.017	0.025	0.018	0.019	0.025
END MEMBER COMPOSITIONS									
Wo	42.1	43.4	45.1	45.7	46.0	43.8	43.3	41.0	42.0
En	22.9	18.5	11.0	11.2	9.5	14.4	15.1	25.5	24.8
Fs	35.0	38.1	43.9	43.1	44.5	41.8	41.6	33.5	33.2

CALCIUM RICH CLINOPYROXENE ANALYSES. UNIT B

OXIDE	B4								
Wt.%	143/1	143/2	143/3	143/4	127/1	127/2	127/3	108b/1	108b/2
SiO_2	50.28	48.95	50.33	48.56	48.02	47.26	48.08	47.61	47.28
TiO_2	0.52	0.50	0.50	0.35	0.61	0.49	0.50	0.66	0.85
Al_2O_3	1.13	1.05	0.99	0.76	0.86	0.77	0.65	0.94	1.02
Cr_2O_3	-	-	-	-	0.02	0.02	0.02	0.02	0.03
FeO	22.20	21.72	22.56	24.19	28.23	29.55	28.65	27.45	27.55
MnO	0.89	0.92	0.94	0.85	1.26	1.36	1.32	1.45	1.41
MgO	5.92	5.80	5.48	4.47	0.94	0.69	0.66	1.40	1.55
CaO	20.32	19.98	19.79	19.59	19.49	19.79	19.89	18.87	19.38
Na_2O	0.39	0.41	0.22	0.35	0.15	0.21	0.23	0.47	0.28
TOTAL	101.63	99.33	100.80	99.12	99.60	100.14	99.99	98.88	99.35
ATOMIC PROPORTIONS ON THE BASIS OF 6 OXYGENS									
Si	1.964	1.959	1.981	1.970	1.978	1.956	1.980	1.972	1.953
Ti	0.015	0.015	0.015	0.011	0.019	0.015	0.015	0.021	0.026
Al	0.052	0.050	0.046	0.037	0.042	0.038	0.032	0.046	0.050
Cr	-	-	-	-	0.001	0.001	0.001	0.001	0.001
Fe	0.725	0.727	0.743	0.821	0.973	1.023	0.987	0.951	0.952
Mn	0.029	0.031	0.031	0.029	0.044	0.048	0.046	0.051	0.049
Mg	0.344	0.346	0.327	0.270	0.058	0.043	0.040	0.087	0.096
Ca	0.850	0.857	0.835	0.852	0.861	0.878	0.878	0.838	0.858
Na	0.029	0.032	0.017	0.028	0.012	0.017	0.018	0.038	0.022
END MEMBER COMPOSITIONS									
Wo	43.6	43.7	43.2	43.2	44.5	44.1	46.1	43.5	43.9
En	17.7	17.6	16.7	13.7	3.0	.2.1	2.1	4.5	4.9
Fs	38.7	38.7	40.1	43.1	52.5	53.8	51.8	52.0	51.2

CALCIUM RICH CLINOPYROXENE ANALYSES. UNIT B

OXIDE	B4									
Wt.%	55/4	55/5	57/1	60/1	60/2	60/3	101/1	101/2	98/1	98/2
SiO_2	47.49	47.39	47.83	47.59	48.04	47.69	46.72	47.73	47.95	48.10
TiO_2	0.55	0.48	0.66	0.49	0.60	0.47	1.77	0.98	0.55	0.69
Al_2O_3	0.83	0.77	0.73	0.65	0.78	0.82	1.22	0.89	0.94	1.02
Cr_2O_3	-	-	-	-	-	-	-	-	-	-
FeO	30.11	30.31	29.56	28.99	29.51	28.18	27.86	28.36	26.56	28.07
MnO	1.34	1.40	1.30	1.42	1.43	1.36	1.36	1.44	1.18	1.19
MgO	0.59	0.51	0.67	0.64	0.85	1.01	0.99	0.95	2.05	2.01
CaO	18.95	19.48	19.33	19.41	19.54	19.40	20.05	19.89	19.35	19.72
Na_2O	0.38	0.31	0.40	0.33	0.31	0.24	0.43	0.38	0.39	0.36
TOTAL	100.25	100.65	100.49	99.52	101.06	99.16	99.80	100.63	98.97	101.17
ATOMIC PROPORTIONS ON THE BASIS OF 6 OXYGENS										
Si	1.963	1.957	1.967	1.975	1.964	1.976	1.931	1.954	1.974	1.950
Ti	0.017	0.015	0.020	0.015	0.019	0.015	0.036	0.030	0.017	0.021
Al	0.041	0.038	0.035	0.032	0.038	0.040	0.059	0.043	0.046	0.049
Cr	-	-	-	-	-	-	-	-	-	-
Fe	1.041	1.047	1.017	1.006	1.009	0.977	0.963	0.971	0.914	0.952
Mn	0.047	0.049	0.045	0.050	0.050	0.048	0.048	0.050	0.413	0.041
Mg	0.037	0.031	0.041	0.040	0.052	0.062	0.061	0.058	0.126	0.122
Ca	0.839	0.862	0.852	0.863	0.856	0.862	0.888	0.873	0.853	0.856
Na	0.031	0.025	0.032	0.027	0.025	0.019	0.035	0.031	0.031	0.029
END MEMBER COMPOSITIONS										
Wo	42.7	43.3	43.6	44.1	43.6	44.2	46.5	45.9	44.1	43.5
En	1.9	1.6	2.1	2.0	2.6	3.2	3.2	3.0	6.5	6.1
Fs	55.4	55.1	54.3	53.9	53.8	52.6	50.3	51.1	49.4	50.4

CALCIUM RICH CLINOPYROXENE ANALYSES. UNIT B

OXIDE	B5				
Wt.%	755/2	121/1	121/2	108a/1	755/1
SiO_2	47.93	47.44	48.23	47.90	48.34
TiO_2	0.39	0.51	0.32	0.42	0.67
Al_2O_3	0.65	0.71	0.58	0.54	0.96
Cr_2O_3	0.03	-	-	-	0.01
FeO	28.53	28.31	28.66	28.55	27.11
MnO	1.37	1.52	1.66	1.46	1.31
MgO	1.00	0.71	0.49	0.97	2.18
CaO	19.08	19.37	19.15	18.85	18.73
Na_2O	0.27	1.65	0.39	0.35	0.45
TOTAL	99.24	100.23	99.48	99.03	99.76
ATOMIC PROPORTIONS ON THE BASIS OF 6 OXYGENS					
Si	1.986	1.959	1.996	1.989	1.974
Ti	0.012	0.016	0.010	0.013	0.021
Al	0.032	0.035	0.028	0.026	0.047
Cr	0.001	-	-	-	0.000
Fe	0.988	0.978	0.992	0.992	0.926
Mn	0.048	0.053	0.058	0.051	0.045
Mg	0.062	0.044	0.030	0.060	0.133
Ca	0.847	0.857	0.849	0.839	0.820
Na	0.022	0.132	0.031	0.029	0.036
END MEMBER COMPOSITIONS					
Wo	43.5	44.4	44.0	43.2	42.6
En	3.2	2.2	1.6	3.1	6.9
Fs	53.3	53.4	54.4	53.7	50.5

AMPHIBOLE ANALYSES. UNIT B

OXIDE				·····recalculated·····		
Wt.%	35/1	35/2	35/3	35/1	35/2	35/3
SiO_2	50.21	49.66	51.04			
TiO_2	0.63	0.96	0.79			
Al_2O_3	3.89	4.01	4.22			
FeO	17.66	17.50	18.35	6.40	9.53	13.76
Fe_2O_3				12.50	8.85	5.10
MnO	0.52	0.73	0.84			
MgO	13.30	12.16	11.22			
CaO	9.97	10.34	10.20			
Na_2O	0.91	0.75	1.56			
K_2O	0.30	0.27	0.36			
TOTAL	97.37	96.38	98.58	98.63	97.26	99.09
ATOMIC PROPORTIONS ON THE BASIS OF 23 OXYGENS						
Si	7.449	7.455	7.516	7.230	7.297	7.425
Ti	0.069	0.108	0.087	0.068	0.106	0.086
Al	0.680	0.710	0.734	0.661	0.695	0.724
Fe^2	2.192	2.197	2.259	0.771	1.171	1.674
Fe^3				1.355	0.978	0.558
Mn	0.065	0.092	0.105	0.063	0.091	0.104
Mg	2.940	2.721	2.463	2.854	2.663	2.433
Ca	1.585	1.663	1.609	1.538	1.628	1.590
Na	0.263	0.217	0.446	0.254	0.214	0.440
K	0.056	0.053	0.067	0.055	0.051	0.067

AMPHIBOLE ANALYSES. UNIT B

OXIDE Wt.%	135/1	135/2	69/1	69/2	100	143/1	143/2	143/3	120	128	51/1
SiO_2	45.50	46.30	42.16	43.87	43.02	43.50	42.75	43.04	44.65	43.03	43.72
TiO_2	1.33	1.19	1.67	1.37	1.49	1.35	1.32	1.33	1.62	1.26	1.16
Al_2O_3	4.87	4.55	6.29	5.52	5.73	6.32	5.35	6.13	5.96	5.86	5.17
Cr_2O_3	0.04	-	0.05	-	-	-	-	-	-	-	-
FeO	25.61	24.77	29.43	29.14	30.62	28.37	29.23	29.21	27.36	30.30	30.16
MnO	0.45	0.59	0.77	0.88	0.94	0.92	0.87	0.95	0.92	1.25	0.80
MgO	7.07	7.06	3.62	3.56	3.66	3.33	4.23	3.49	4.25	3.42	4.20
CaO	10.32	9.90	10.14	9.61	10.03	10.65	9.97	10.62	9.68	9.67	9.77
Na_2O	1.76	1.68	2.21	1.96	2.22	1.90	1.50	1.83	1.33	2.18	1.77
K_2O	0.37	0.48	0.79	0.21	0.95	0.60	0.83	0.70	0.80	0.77	0.69
TOTAL	97.31	96.51	97.13	96.12	98.66	96.93	96.05	97.30	96.57	97.75	97.45
ATOMIC PROPORTIONS ON THE BASIS OF 23 OXYGENS											
Si	7.119	7.259	6.820	7.091	6.882	7.001	6.969	6.947	7.135	6.931	7.026
Ti	0.157	0.140	0.203	0.166	0.179	0.163	0.161	0.161	0.194	0.152	0.141
Al	0.899	0.842	1.201	1.051	1.081	1.200	1.029	1.166	1.123	1.114	0.980
Cr	0.005	-	0.006	-	-	-	-	-	-	-	-
Fe	3.351	3.247	3.982	3.938	4.097	3.818	3.985	3.943	3.656	4.081	4.054
Mn	0.060	0.078	0.106	0.121	0.128	0.126	0.120	0.129	0.125	0.171	0.109
Mg	1.648	1.649	0.873	0.857	0.871	0.798	1.027	0.840	1.012	0.821	1.007
Ca	1.730	1.663	1.757	1.664	1.720	1.836	1.741	1.837	1.658	1.669	1.682
Na	0.534	0.510	0.692	0.615	0.689	0.592	0.475	0.572	0.413	0.682	0.550
K	0.074	0.096	0.163	0.044	0.193	0.122	0.173	0.142	0.160	0.159	0.141

AMPHIBOLE ANALYSES. UNIT B (RECALCULATED FeO + Fe_2O_3)

OXIDE Wt.%	135/1	135/2	69/1	69/2	100	143/1	143/2	143/3	120	128	51/1
Fe_2O_3	7.22	6.40	5.40	6.30	7.00	2.05	8.40	4.00	5.85	7.65	9.10
FeO	19.14	19.00	24.57	23.46	24.31	26.52	21.66	25.61	22.09	23.41	21.96
TOTAL	98.07	97.15	97.67	96.74	99.35	97.14	96.88	97.70	97.15	98.50	98.34
ATOMIC PROPORTIONS ON THE BASIS OF 23 OXYGENS											
Si	6.989	7.141	6.724	6.974	6.758	6.944	6.816	6.852	7.003	6.795	6.863
Ti	0.154	0.138	0.200	0.164	0.176	0.162	0.158	0.159	0.191	0.150	0.137
Al	0.882	0.828	1.183	1.035	1.062	1.190	1.006	1.151	1.103	1.091	0.957
Cr_3	0.005	-	0.006	-	-	-	-	-	-	-	-
Fe^3	0.835	0.743	0.648	0.754	0.828	0.246	1.008	0.479	0.691	0.909	1.075
Fe^2	2.459	2.451	3.277	3.119	3.194	3.541	2.888	3.410	2.898	3.092	2.883
Mn	0.059	0.077	0.104	0.119	0.125	0.124	0.118	0.128	0.122	0.167	0.106
Mg	1.618	1.623	0.860	0.843	0.857	0.792	1.005	0.828	0.993	0.805	0.983
Ca	1.699	1.636	1.733	1.637	1.688	1.822	1.703	1.812	1.627	1.636	1.643
Na	0.524	0.502	0.683	0.604	0.676	0.588	0.464	0.565	0.405	0.668	0.539
K	0.073	0.095	0.161	0.043	0.190	0.122	0.169	0.142	0.160	0.155	0.138

AMPHIBOLE ANALYSES. UNIT B

OXIDE Wt.%	51/2	47	48/1	48/2	52	53/1	53/2	49	60	108b/1	108b/2
SiO_2	42.93	43.78	42.02	42.67	43.21	42.21	41.94	43.72	41.86	44.17	42.97
TiO_2	1.39	1.36	1.40	1.38	1.36	1.46	1.41	1.46	1.73	1.43	1.31
Al_2O_3	5.51	5.62	5.91	6.00	5.80	6.63	6.20	6.01	6.79	4.79	4.53
Cr_2O_3	0.05	0.03	0.06	0.03	0.07	0.02	0.03	-	-	-	0.05
FeO	30.51	30.04	31.93	31.62	30.36	31.66	32.53	30.42	31.99	32.71	33.06
MnO	0.92	0.76	0.98	0.91	1.06	0.86	1.08	1.14	1.05	0.14	1.04
MgO	3.80	3.50	3.42	3.16	3.01	1.50	2.19	1.84	1.02	1.74	1.84
CaO	9.70	10.90	9.59	9.14	9.99	10.23	10.11	10.03	10.19	9.37	8.99
Na_2O	2.03	2.01	2.10	2.04	2.27	2.16	1.90	1.96	2.17	2.46	2.30
K_2O	0.64	0.60	0.80	1.17	0.64	0.93	0.87	1.01	1.10	0.93	0.70
TOTAL	97.48	98.58	98.21	98.12	97.76	97.67	98.28	97.60	97.89	97.74	97.79
ATOMIC PROPORTIONS ON THE BASIS OF 23 OXYGENS											
Si	6.930	6.966	6.800	6.886	6.955	6.862	6.811	7.046	6.818	7.152	7.144
Ti	0.169	0.162	0.170	0.168	0.164	0.179	0.172	0.176	0.212	0.174	0.160
Al	1.049	1.055	1.128	1.142	1.102	1.272	1.188	1.142	1.304	0.915	0.869
Cr	0.006	0.004	0.008	0.004	0.009	0.003	0.004	-	-	-	0.006
Fe	4.119	3.998	4.322	4.268	4.087	4.305	4.418	4.101	4.358	4.429	4.492
Mn	0.126	0.102	0.134	0.124	0.144	0.119	0.149	0.155	0.145	0.019	0.143
Mg	0.914	0.829	0.825	0.761	0.721	0.364	0.530	0.442	0.247	0.420	0.445
Ca	1.678	1.858	1.663	1.580	1.723	1.782	1.759	1.733	1.779	1.626	1.565
Na	0.635	0.619	0.659	0.639	0.708	0.681	0.599	0.613	0.685	0.772	0.725
K	0.132	0.121	0.165	0.242	0.131	0.194	0.180	0.209	0.228	0.192	0.145

AMPHIBOLE ANALYSES. UNIT B (RECALCULATED $FeO+Fe_2O_3$)

OXIDE Wt.%	51/2	47	48/1	48/2	52	53/1	53/2	49	60	108b/1	108b/2
Fe_2O_3	9.20	3.50	11.20	10.20	5.40	3.10	8.00	1.90	2.30	2.88	7.40
FeO	22.20	26.89	21.84	22.42	25.50	28.87	25.32	28.71	29.92	30.12	26.39
TOTAL	98.39	98.95	99.32	99.12	98.31	97.97	99.05	97.78	98.13	98.03	98.52
ATOMIC PROPORTIONS ON THE BASIS OF 23 OXYGENS											
Si	6.766	6.902	6.605	6.707	6.857	6.807	6.670	7.011	6.776	7.098	7.007
Ti	0.165	0.161	0.166	0.163	0.162	0.177	0.169	0.176	0.211	0.173	0.157
Al	1.024	1.045	1.096	1.112	1.086	1.261	1.163	1.137	1.296	0.908	0.851
Cr	0.006	0.004	0.008	0.004	0.009	0.003	0.004	-	-	-	0.006
Fe^3	1.091	0.415	1.325	1.207	0.645	0.376	0.958	0.229	0.280	0.348	0.887
Fe^2	2.929	3.545	2.871	2.947	3.385	3.894	3.368	3.851	4.051	4.048	3.517
Mn	0.123	0.102	0.131	0.121	0.143	0.118	0.146	0.155	0.144	0.019	0.140
Mg	0.893	0.822	0.801	0.740	0.712	0.361	0.519	0.440	0.246	0.417	0.437
Ca	1.638	1.847	1.615	1.539	1.699	1.768	1.723	1.724	1.767	1.613	1.535
Na	0.620	0.614	0.640	0.622	0.699	0.675	0.586	0.610	0.681	0.767	0.711
K	0.129	0.121	0.160	0.235	0.130	0.191	0.177	0.207	0.227	0.191	0.142

ILMENITE ANALYSES UNIT B

OXIDE	B1		B2					
Wt%	34	20	50/1	50/2	135/1	135/2	69/1	69/2
SiO_2	-	0.48	0.23	0.11	0.52	0.12	0.09	0.09
TiO_2	51.27	50.92	51.42	51.65	52.60	52.07	51.81	51.51
Al_2O_3	0.07	0.22	0.04	0.03	0.08	0.04	0.03	0.03
Cr_2O_3	-	-	0.16	-	-	-	0.00	0.05
Fe_2O_3	1.95	1.86	1.74	2.70	0.00	1.50	1.11	3.11
FeO	42.14	42.47	43.48	43.63	44.74	44.05	42.03	41.55
MnO	3.92	3.85	2.89	2.91	3.11	2.75	4.50	4.73
MgO	-	-	0.06	0.00	0.02	0.07	0.06	0.05
TOTAL	99.36	99.83	100.03	101.03	99.50	100.59	99.62	101.13
ATOMIC PROPORTIONS ON THE BASIS OF 6 OXYGENS								
Si	-	0.024	0.012	0.006	0.027	0.006	0.004	0.005
Ti	1.961	1.934	1.951	1.943	2.004	1.965	1.973	1.935
Al	0.004	0.013	0.002	0.002	0.005	0.002	0.002	0.002
Cr	-	-	0.006	-	-	-	0.000	0.002
Fe^3	0.075	0.071	0.066	0.102	0.000	0.057	0.042	0.117
Fe^2	1.792	1.793	1.834	1.825	1.896	1.849	1.780	1.736
Mn	0.169	0.165	0.124	1.232	0.134	0.117	0.193	0.200
Mg	-	-	0.005	0.000	0.002	0.005	0.004	0.004
$\%Ilm_{ss}$	97.4	97.6	98.1	98.3	100.0	99.12	98.5	98.0

ILMENITE ANALYSES UNIT B

	B3				B4		
OXIDE Wt%	51/1	51/2	52/1	53/1	120	127/1	127/2
SiO_2	0.13	0.22	0.37	0.98	0.12	0.16	0.27
TiO_2	52.06	51.50	51.58	51.50	49.88	53.25	52.62
Al_2O_3	0.01	0.03	0.09	0.34	0.08	0.07	-
Cr_2O_3	-	-	-	-	-	-	-
Fe_2O_3	0.58	2.06	0.72	0.00	3.87	0.00	0.00
FeO	42.02	42.37	41.62	43.12	39.21	44.13	43.47
MnO	4.79	4.10	5.14	4.19	5.55	3.90	4.12
MgO	0.06	0.03	-	0.07	0.07	-	-
TOTAL	99.64	100.30	99.52	99.55	98.79	99.38	99.30
ATOMIC PROPORTIONS ON THE BASIS OF 6 OXYGENS							
Si	0.007	0.011	0.019	0.049	0.006	0.008	0.014
Ti	1.982	1.949	1.965	1.953	1.915	2.030	2.009
Al	0.005	0.002	0.005	0.020	0.005	0.005	-
Cr	-	-	-	-	-	-	-
Fe^3	0.022	0.078	0.027	0.000	0.149	0.000	0.000
Fe^2	1.779	1.783	1.763	1.818	1.674	1.871	1.845
Mn	0.205	0.175	0.221	0.179	0.240	0.168	0.177
Mg	0.004	0.002	-	0.005	0.005	-	-
$\%Ilm_{ss}$	99.12	98.32	98.7	100.00	95.0	100.00	100.00

TITANOMAGNETITE ANALYSES UNIT B

OXIDE	B2	B3			B4		
Wt%	135	51	52	53	48	121/1	121/2
SiO_2	0.26	0.43	0.07	0.29	0.26	0.29	0.24
TiO_2	15.71	16.52	17.63	18.02	13.29	18.62	22.49
Al_2O_3	0.97	0.60	0.24	0.43	0.61	0.55	0.62
Cr_2O_3	-	-	-	-	0.06	-	-
Fe_2O_3	36.66	34.86	33.63	33.84	40.96	29.75	26.22
FeO	45.01	45.80	45.64	46.81	42.08	46.29	51.46
MnO	1.04	0.93	1.51	1.79	1.32	1.63	1.76
MgO	0.02	0.07	-	-	-	-	-
TOTAL	99.67	99.21	98.71	101.18	98.57	97.13	102.78
ATOMIC PROPORTIONS ON THE BASIS OF 32 OXYGENS							
Si	0.083	0.132	0.022	0.086	0.081	0.089	0.069
Ti	3.573	3.776	4.060	4.041	3.067	4.341	4.942
Al	0.347	0.214	0.085	0.152	0.220	0.201	0.214
Cr	-	-	-	-	0.014	-	-
Fe^3	8.342	7.972	7.750	7.595	9.466	6.940	5.765
Fe^2	11.383	11.638	11.690	11.675	10.806	12.002	12.576
Mn	0.265	0.239	0.393	0.451	0.344	0.428	0.435
Mg	0.008	0.030	-	-	-	-	-
$\%Usp_{ss}$	44.7	47.4	49.5	51.2	37.9	52.9	63.6

APPENDIX THREE

WHOLE-ROCK ANALYSIS

X-ray fluorescence analysis :

Sample preparation: Samples were split into fragments using a Cutrock Engineering hydraulic splitter. Weathered fragments were removed, and the remainder were broken into a coarse aggregate, using a Sturtevant 2" x 6" Roll Jaw Crusher. An aggregate sample, weighing 200-500 grams, was reduced to about 100 grams by a process of quartering. The sample fraction was ground to a fine powder, using a Tema Laboratory Disc Mill, Model T-100, with tungsten-carbide Widia grinding barrel. Grinding took 3-4 minutes.

A few grams of fine powder were pressed into a briquette, using a hydraulic press, operated at 5-6 tons p.s.i. A few drops of inert P.V.A binding agent ('Mowiol') was added to aid cohesion.

Major element analysis : Sample briquettes were analysed on a Phillips PW1212 automatic spectrometer incorporating a Torrens Industries TE108 automatic sample loader. Details of the routine operating conditions used during x-ray fluorescence analysis are given by Reeves (1971).

The elements Si, Al, Fe, Mg, Ca, Na, K, Ti and P were determined using a Cr target for primary radiation and an evacuated tube. Mn was analysed separately using a W target.

A "fixed counts" operating procedure, employing the use of an internal monitor, was used in order to minimise the effect of electronic instability.

The international standards and U.S. National bureau

standards BR, BCR-1, W-1, SY-1, Na-1, GR, GSP-1, G-1, GH and SI were used to calibrate the data. The compositions of the international standards were taken from Flanagan (1973).

The analytical data were corrected for mass absorption differences between the standards and unknowns using the iterative computer procedure described by Holland and Brindle (1966), and Reeves (1971). Standards were run before and after the analysis run, to check for machine drift. The counts reproduceability was very good, indicating precision is fairly high. Back calculations performed on the calibrated standards suggests the accuracy is in the order of $\pm$2%relative at higher concentrations, but $\pm$5% relative at lower concentrations.

The analyses presented in table A3.2 are Wt% oxides. All fe is expressed as Fe_2O_3, because of the oxidation of the sample during grinding (Fitton and Gill, 1970). The analyses are presented water free and normalised to 100%, because of secondary H_2O in the samples

Trace element analysis : The elements Ba, Nb, Zr, Y, Sr, Rb, Zn, Cr and Ni were determined using a W target and an evacuated x-ray tube. Analytical count data were converted into concentrations, (ppm) using the computer program TRATIO, written by R.C.O. Gill. The program uses the function (peak intensity/background intensity)-1, to compensate for matrix and mass absorption effects, using scattered background radiation as an internal standard. Corrections for blank/contamination and K_β interference (SrK_β on Zr K_α, Rb K_β on Yk_α,and Yk_β on Nb K_α) are included in the program. The nominal detection limits for each element are calculated

from the formula $3(\bar{B}^{\frac{1}{2}})$ where $\bar{B}$ is the mean background - under - peak, in counts. Table A3.1 gives the detection limit and the upper limit of standarisation for each element.

The standards used were synthetic spiked glasses prepared by the Pilkington Research Laboratory (Latham) for use in Lunar investigations (Brown et al, 1971).

Instrumental Neutron Activation Analysis (INAA):

The INAA data was obtained on my behalf by the Open University. General procedures followed are outlined in Gordon et al (1968) and Paul et al (1975).

0.5 gm of rock powder (for preparation see above) was irradiated, together with an OU standard (AC) and the international standard CRRG. BR, at the University of London reactor centre, in a neutron flux of approx. 5×10^{11} n. $cm.^{-2}$. sec^{-1}. for up to 30 hours. After a cooling period of one-week, samples were counted, using a high resolution lithium-drifted germanium detector. (Nuclear Enterprise : resolution at 122 KeV = 630 eV). The 60-180 KeV portion of the gamma spectrum was recorded on a Northern Scientific Econ II analyser.

Data reduction was by the procedure described in Rontti (1969), using the facilities of the London University computer centre.

Corrections were made to resolve peak areas for count-time, half-life decay and neutron-flux variations, which were monitored by means of discs of iron foil, and for interelement interferences.

Reproduceability of counting indicates a precision of the order of $\pm 5\%$.

Table A3.3 lists the INAA data in ppm. for the REE determined, together with selected Trace elements.

TABLE A3.1 Trace element calibration data

	Detection Limit ppm	Upper limit of standards ppm
Ba	8	5000
Nb	3	250
Zr	3	5000
Y	3	500
Sr	3	1100
Rb	3	1000
Zn	2	1000
Cr	2	1000
Ni	2	1000

TABLE A3.2

Whole rock X-Ray Fluorescence Analysis data

UNIT A GABBROS

OXIDE wt.%	A1 150	A1 161	A1 151	A1 158	A1 159	A3 152	A3 157	A1 153	A1 115	A1 156
SiO_2	42.78	50.24	49.01	50.81	51.19	53.71	53.79	54.48	53.68	53.60
Al_2O_3	14.43	15.75	16.26	16.08	16.34	16.36	16.17	17.14	17.54	17.97
Fe_2O_3	18.52	12.02	12.62	11.67	10.61	10.83	10.69	9.45	8.85	9.05
MgO	7.51	8.06	5.19	5.15	4.52	3.50	3.94	3.41	3.33	3.17
CaO	10.23	9.98	9.54	8.32	10.48	8.40	8.96	8.74	9.66	9.87
Na_2O	1.47	1.90	2.89	2.73	2.64	2.74	3.08	3.08	3.46	3.06
K_2O	0.59	0.62	0.98	1.51	0.84	1.86	0.96	1.48	1.36	1.33
TiO_2	4.17	0.93	3.02	3.29	2.94	2.04	1.85	1.68	1.69	1.61
MnO	0.19	0.26	0.24	0.24	0.21	0.21	0.22	0.19	0.17	0.17
P_2O_5	0.10	0.23	0.23	0.17	0.22	0.34	0.32	0.33	0.26	0.26
p.p.m.										
Ba	143	152	207	235	150	317	275	260	233	213
Nb	7	<3	9	7	5	10	8	7	7	5
Zr	59	40	110	148	95	157	486	148	114	92
Y	17	22	29	30	27	37	41	35	30	26
Sr	156	190	204	230	235	171	188	232	228	223
Rb	22	24	30	47	33	72	31	48	51	43
Zn	98	82	87	77	61	88	89	74	58	61
Ni	15	107	17	23	23	20	22	17	21	18
Cr	76	315	83	97	91	74	82	127	70	101

UNIT A GABBROS

OXIDE Wt.%	A1 46	A2 117	A2 154	A2 155	A2 45	A1 136	A1 88	A1 87	A1 118
SiO_2	52.98	49.56	48.62	46.08	44.65	47.26	41.98	34.10	35.21
Al_2O_3	18.08	16.05	14.36	17.90	14.71	16.95	12.40	13.94	14.52
Fe_2O_3	9.19	12.89	12.32	12.23	14.97	10.45	14.07	25.18	25.35
MgO	2.89	6.80	7.22	7.08	8.18	6.36	9.02	12.21	8.94
CaO	10.55	9.37	10.32	11.17	10.09	12.03	12.08	5.83	6.07
Na_2O	3.53	2.21	2.36	2.11	1.75	2.30	1.62	0.22	0.69
K_2O	0.58	0.74	0.50	0.47	0.29	1.41	0.73	0.76	0.98
TiO_2	1.85	1.95	3.71	2.66	4.88	2.96	7.75	7.45	7.93
MnO	0.16	0.23	0.24	0.23	0.27	0.20	0.26	0.25	0.26
P_2O_5	0.17	0.19	0.34	0.06	0.19	0.08	0.07	0.05	0.03
p.p.m.									
Ba	188	139	163	68	111	184	119	176	124
Nb	7	<3	3	3	6	<3	<3	3	7
Zr	77	54	71	20	43	33	43	29	28
Y	30	22	27	25	22	12	16	3	7
Sr	220	171	143	347	146	413	234	155	156
Rb	18	28	17	15	17	38	30	34	35
Zn	80	78	71	51	75	56	49	95	156
Ni	24	45	45	26	78	26	38	96	59
Cr	70	125	55	87	89	96	141	159	143

UNIT A GABBROS. Fitton 1971 Eastwood et al. 1968

OXIDE wt.%	CN7	CN16	CN17	CN64	16180	16181
SiO_2	50.04	54.15	54.11	51.85	41.38	52.25
Al_2O_3	18.36	26.73	21.14	17.75	14.04	18.71
Fe_2O_3	10.18	2.15	7.11	11.16	19.04	9.76
MgO	4.43	0.67	2.46	4.69	5.63	2.84
CaO	8.99	8.88	8.98	7.43	9.73	9.52
Na_2O	3.16	4.35	3.24	3.09	1.56	2.90
K_2O	0.72	2.35	1.06	1.34	0.72	1.18
TiO_2	3.51	0.46	1.40	2.11	5.05	2.18
MnO	0.20	0.03	0.13	0.26	0.37	0.17
P_2O_5	0.18	0.10	0.29	0.25	0.14	0.30
p.p.m.						
Ba	129	234	195	326		
Nb	10	2	6	10		
Zr	107	25	212	134		
Y	22	9	28	35		
Sr	236	578	268	294		
Rb	31	81	43	51		
Zn	74	19	67	103		
Cu	25	13	24	14		
Ni	21	6	16	19		
Cr	49	0	31	74		
V	520	208	222	299		

UNIT B1 GABBROS

OXIDE Wt%	14	18	20	33	34	CNLL	16182
SiO_2	46.58	46.61	52.40	49.97	51.16	46.37	48.51
Al_2O_3	15.45	11.34	14.62	14.72	14.13	20.40	16.83
Fe_2O_3	10.99	19.68	13.74	14.37	14.84	9.34	9.23
MgO	8.58	6.14	4.20	5.31	4.84	7.76	6.78
CaO	14.27	9.90	7.98	8.12	7.90	11.33	10.84
Na_2O	1.75	2.11	3.08	3.05	2.95	2.04	2.36
K_2O	0.93	0.65	1.24	1.38	1.34	1.35	1.25
TiO_2	1.06	2.58	1.75	2.27	1.87	0.98	1.20
MnO	0.18	0.39	0.31	0.29	0.33	0.16	0.15
P_2O_5	0.18	0.58	0.67	0.51	0.63	0.16	0.18
p.p.m.							
Ba	92	183	283	247	279	154	
Nb	4	10	14	14	10	4	
Zr	57	248	263	222	261	76	
Y	17	48	61	49	57	8	
Sr	342	152	245	319	254	480	
Rb	38	23	43	47	47	65	
Zn	63	143	176	138	157	68	
Ni	91	62	23	27	24	63	
Cr	806	100	67	82	44	272	
Cu						141	
V						236	

SUBUNIT B2 FERROGABBROS

OXIDE Wt.%	44	137	138	139	140	141	142	163a
SiO_2	40.66	42.44	42.19	46.61	49.49	54.60	56.24	47.10
Al_2O_3	12.09	11.98	11.65	12.78	13.36	14.30	13.85	14.37
Fe_2O_3	22.29	23.73	22.93	21.42	18.06	18.30	15.36	18.18
MgO	5.36	3.51	4.75	3.02	2.60	1.35	1.96	3.16
CaO	11.15	10.12	10.22	8.64	8.00	4.63	5.50	9.45
Na_2O	1.41	1.73	1.55	2.20	3.31	3.32	2.81	2.68
K_2O	0.69	1.07	1.15	1.36	1.34	1.99	2.48	1.32
TiO_2	3.52	3.24	2.96	2.05	2.30	0.82	0.87	2.00
MnO	0.50	0.59	0.56	0.52	0.40	0.29	0.42	0.41
P_2O_5	2.32	1.57	2.01	1.40	1.13	0.37	0.49	1.36
p.p.m.								
Ba	138	207	197	246	347	351	373	250
Nb	8	6	6	6	10	11	14	6
Zr	60	113	70	97	68	283	101	55
Y	48	57	53	53	63	74	84	53
Sr	159	177	157	179	199	202	191	273
Rb	30	39	46	59	48	72	79	51
Zn		199	165	166	162	158	155	109

SUBUNIT B2 FERROGABBROS

OXIDE Wt.%	50	100	103
SiO_2	50.46	55.46	59.12
Al_2O_3	13.74	15.00	14.30
Fe_2O_3	17.06	12.82	13.40
MgO	3.69	1.78	2.12
CaO	7.24	6.72	3.56
Na_2O	2.48	3.67	3.31
K_2O	1.79	2.13	2.38
TiO_2	1.94	1.31	0.94
MnO	0.38	0.34	0.42
P_2O_5	1.20	0.77	0.43
p.p.m.			
Ba	277	460	363
Nb	7	24	18
Zr	142	255	232
Y	72	73	72
Sr	240	233	153
Rb	100	81	93
Zn	121	159	199

SUBUNIT B3 FERRODIORITES

OXIDE Wt.%	51	52	53	47	49	54	120
SiO_2	54.24	57.07	62.98	57.61	63.87	66.28	62.68
Al_2O_3	13.63	14.46	14.10	13.87	13.65	13.41	14.22
Fe_2O_3	17.01	15.28	10.41	14.56	9.73	8.42	10.79
MgO	1.63	0.95	0.65	0.93	0.70	0.55	0.39
CaO	6.08	4.96	4.15	5.75	3.89	3.05	4.26
Na_2O	3.16	3.54	4.05	3.62	4.30	4.23	4.32
K_2O	1.80	1.92	2.35	1.70	2.63	3.05	2.20
TiO_2	1.37	1.03	0.73	1.08	0.67	0.50	0.62
MnO	0.51	0.45	0.31	0.45	0.32	0.31	0.35
P_2O_5	0.57	0.33	0.25	0.42	0.22	0.20	0.15
p.p.m.							
Ba	265	451	559	434	456	476	477
Nb	23	9	13	10	8	22	17
Zr	192	251	301	328	203	216	355
Y	72	71	82	69	74	89	77
Sr	243	273	281	290	168	129	233
Rb	100	93	87	91	77	83	72
Zn	161	187	158	121	127	145	164

SUBUNIT B4 FERROGRANOPHYRES + PLAGIOFERROGRANOPHYRES

OXIDE Wt.%	163b	143	144	145	146	147	148
SiO_2	60.71	57.87	66.06	68.15	66.74	67.61	67.31
Al_2O_3	19.10	15.67	13.79	13.98	14.13	13.94	14.04
Fe_2O_3	2.84	12.22	8.43	6.80	7.67	7.18	7.26
MgO	1.20	1.24	0.43	0.38	0.45	0.47	0.46
CaO	5.63	5.24	3.37	2.32	2.69	2.48	2.57
Na_2O	6.93	4.06	4.04	4.61	4.65	4.59	4.56
K_2O	2.36	2.22	2.97	3.06	2.83	3.05	2.99
TiO_2	0.40	0.94	0.55	0.39	0.49	0.44	0.46
MnO	0.08	0.31	0.26	0.24	0.28	0.16	0.26
P_2O_5	0.74	0.22	0.10	0.07	0.08	0.08	0.08
p.p.m.							
Ba	383	424	640	578	594	532	645
Nb	3	11	25	27	31	27	29
Zr	122	152	418	504	571	536	614
Y	42	60	89	88	161	97	93
Sr	478	280	147	141	153	153	159
Rb	53	88	95	101	93	108	100
Zn	29	158	217	219	332	218	232

SUBUNIT B4 FERROGRANOPHYRES + PLAGIOFERROGRANOPHYRES

OXIDE wt.%	56	57	59	60	64	65	70	74
SiO_2	64.66	65.12	64.80	62.77	69.43	68.32	65.73	64.96
Al_2O_3	14.50	14.52	14.32	15.47	13.85	13.76	15.23	13.88
Fe_2O_3	8.84	8.41	8.95	8.92	6.06	6.58	7.34	9.15
MgO	0.25	0.29	0.22	0.43	0.22	0.16	0.48	0.23
CaO	3.42	3.29	3.75	3.74	1.88	2.57	2.60	3.70
Na_2O	4.79	4.70	4.47	4.74	4.48	4.55	5.09	4.35
K_2O	2.52	2.73	2.34	2.42	3.39	3.35	2.70	2.79
TiO_2	0.56	0.53	0.77	1.14	0.39	0.38	0.43	0.52
MnO	0.33	0.31	0.28	0.25	0.21	0.24	0.30	0.30
P_2O_5	0.11	0.09	0.09	0.10	0.08	0.07	0.08	0.11
p.p.m.								
Ba	513	517	516	543	598	448	584	480
Nb	23	23	24	26	26	26	21	17
Zr	309	376	304	280	404	341	615	313
Y	98	98	81	73	95	107	84	86
Sr	203	191	219	355	115	129	195	195
Rb	78	85	77	90	124	112	82	86
Zn	231	238	218	205	182	193	200	201

SUBUNIT B4 FERROGRANOPHYRES AND PLAGIOFERROGRANOPHYRES

OXIDE Wt.%	109	110	111	112	113	126	127	131	129
SiO_2	68.40	66.06	67.86	69.05	68.83	64.64	61.68	61.25	58.38
Al_2O_3	14.17	14.42	13.83	13.44	13.71	14.85	14.67	14.32	13.73
Fe_2O_3	6.34	7.14	7.28	6.57	6.31	8.66	10.87	11.40	14.49
MgO	0.53	0.69	0.31	0.19	0.17	0.36	0.37	0.36	0.38
CaO	2.33	3.51	2.53	2.39	2.49	3.27	4.45	4.62	5.60
Na_2O	4.47	4.62	4.50	4.49	4.51	4.55	4.24	4.57	3.93
K_2O	3.08	2.72	2.97	3.23	3.36	2.81	2.57	2.28	2.00
TiO_2	0.47	0.53	0.37	0.31	0.31	0.51	0.61	0.62	0.76
MnO	0.12	0.19	0.26	0.24	0.22	0.27	0.37	0.39	0.50
P_2O_5	0.08	0.08	0.08	0.07	0.08	0.08	0.15	0.17	0.22
p.p.m.									
Ba	575	545	601	577	529	564	500	517	466
Nb	35	29	27	22	23	17	17	17	18
Zr	574	620	529	395	384	323	152	178	168
Y	91	95	94	104	92	75	69	63	78
Sr	119	82	141	135	129	311	306	304	234
Rb	107	83	108	124	129	107	108	79	74
Zn	42	76	208	190	172	185	220	191	283

SUBUNIT B4 FERROGRANOPHYRES

OXIDE Wt%	96	98	101
SiO_2	63.14	61.90	61.19
Al_2O_3	13.20	13.90	14.57
Fe_2O_3	11.30	11.69	12.14
MgO	0.76	0.64	0.61
CaO	4.30	4.12	3.43
Na_2O	3.62	3.85	4.11
K_2O	2.48	2.60	2.69
TiO_2	0.61	0.72	0.70
MnO	0.27	0.36	0.36
P_2O_5	0.22	0.21	0.17
p.p.m			
Ba	421	447	462
Nb	17	20	13
Zr	250	247	295
Y	84	81	75
Sr	151	150	158
Rb	102	96	111
Zn	83	176	203

SUBUNIT B5 GRANOPHYRES

OXIDE Wt.%	9	12	13	30	31	40	42	43	36	37
SiO_2	70.49	71.19	71.03	72.23	72.40	72.44	73.61	73.27	72.43	72.98
Al_2O_3	13.45	13.20	13.38	13.06	13.34	12.95	13.41	13.48	13.14	13.44
Fe_2O_3	5.40	5.09	5.13	3.72	3.69	4.09	3.07	2.99	3.84	3.51
MgO	0.63	0.57	0.41	0.17	0.18	0.23	0.14	0.29	0.26	0.24
CaO	1.34	1.74	1.53	2.27	1.59	2.19	1.09	1.30	1.90	1.10
Na_2O	4.66	4.57	4.51	4.95	4.95	3.95	4.65	4.54	4.71	4.82
K_2O	3.39	3.07	3.47	3.12	3.38	3.64	3.65	3.68	3.24	3.52
TiO_2	0.43	0.37	0.36	0.29	0.29	0.31	0.24	0.30	0.29	0.24
MnO	0.14	0.14	0.14	0.14	0.12	0.14	0.10	0.09	0.12	0.12
P_2O_5	0.05	0.05	0.02	0.04	0.05	0.04	0.04	0.05	0.05	0.02
p.p.m.										
Ba	556	590	528	577	595	661	549	607	574	591
Nb	31	28	30	31	29	33	32	31	30	32
Zr	534	538	537	545	538	540	527	520	535	531
Y	127	98	97	114	117	120	108	115	118	116
Sr	53	69	63	51	54	49	58	48	52	76
Rb	127	116	134	131	140	142	144	141	137	129
Zn	128	93	109	63	39	240	90	28	77	144
U	2	5	5		7		2	2		5
Th	17	20	14		13		22	21		18

SUBUNIT B5 GRANOPHYRES

OXIDE Wt.%.	38	39	19	15	66	90	104	105	106	107	149
SiO_2	73.68	72.84	73.11	72.85	72.86	72.41	72.95	73.36	72.72	72.32	72.49
Al_2O_3	13.35	13.35	13.23	13.49	13.49	13.31	13.32	13.07	13.57	13.24	13.25
Fe_2O_3	3.17	3.71	3.51	3.65	3.70	3.37	3.65	2.93	3.77	3.87	3.79
MgO	0.16	0.21	0.18	0.31	0.11	0.38	0.18	0.29	0.29	0.19	0.24
CaO	1.05	1.26	1.29	1.02	1.26	2.08	1.31	1.95	1.12	1.80	1.25
Na_2O	4.67	4.77	4.87	4.61	5.05	4.51	4.51	4.45	4.40	4.55	4.82
K_2O	3.52	3.40	3.37	3.63	3.07	3.46	3.62	3.51	3.69	3.57	3.57
TiO_2	0.23	0.26	0.26	0.25	0.25	0.32	0.28	0.30	0.28	0.27	0.26
MnO	0.11	0.12	0.12	0.11	0.13	0.10	0.12	0.11	0.10	0.12	0.27
P_2O_5	0.04	0.08	0.05	0.05	0.07	0.04	0.03	0.03	0.04	0.04	0.04
p.p.m.											
Ba	554	610	548	627	586	515	645	599	605	563	678
Nb	31	32	34	34	33	33	33	35	31	30	32
Zr	518	529	536	549	538	542	550	535	474	499	518
Y	113	112	117	116	119	108	109	109	109	117	109
Sr	66	66	65	69	82	46	72	75	56	50	75
Rb	141	133	140	118	90	108	115	103	133	125	131
Zn	138	134	170	129	142	41	121	161	166	184	187
U		3		5				4		5	
Th		14		17				18		21	

SUBUNIT B5 GRANOPHYRES

OXIDE Wt.%	62	63	82	121	CN10	CN71	16184
SiO_2	71.78	72.69	72.73	72.19	72.94	72.93	73.17
Al_2O_3	13.73	13.54	13.39	13.67	12.88	12.69	12.95
Fe_2O_3	4.04	3.55	3.75	3.55	4.00	5.07	3.51
MgO	0.11	0.15	0.14	0.14	0.51	0.78	0.08
CaO	1.52	1.19	1.36	1.66	0.68	0.06	1.30
Na_2O	4.85	4.75	4.69	4.88	4.78	4.60	4.37
K_2O	3.51	3.74	3.53	3.50	3.72	3.28	3.67
TiO_2	0.25	0.21	0.22	0.22	0.27	0.40	0.39
MnO	0.14	0.12	0.14	0.13	0.13	0.10	0.11
P_2O_5	0.05	0.05	0.02	0.05	0.01	0.02	0.07
p.p.m.							
Ba	522	500	550	605	591	574	-
Nb	28	33	30	28	28	26	-
Zr	538	563	513	509	505	597	-
Y	111	118	104	106	120	111	-
Sr	91	75	78	88	69	59	-
Rb	108	137	125	133	162	123	-
Zn	155	120	148	102	161	167	-

UNIT B R.N. THOMPSON DATA (personal communication)

OXIDE Wt.%	ME2	ME4	ME8	ME9	ME10a	ME10b	ME12	ME14
SiO_2	40.58	54.23	60.99	62.09	59.81	62.98	65.68	71.99
Al_2O_3	12.08	13.48	14.13	13.60	12.63	14.18	14.27	13.75
Fe_2O_3	4.76	3.23	3.63	3.51	5.13	3.30	3.73	1.97
FeO	16.52	11.01	6.62	6.27	7.72	6.10	3.43	1.86
MnO	0.51	0.44	0.37	0.36	0.53	0.39	0.32	0.15
MgO	4.68	2.05	1.23	0.86	1.33	0.60	0.39	0.20
CaO	9.90	5.75	4.54	3.81	4.48	3.87	2.88	1.45
Na_2O	1.85	3.63	4.14	4.13	3.65	4.54	4.88	4.48
K_2O	0.96	1.53	2.25	2.67	2.41	1.98	2.66	3.45
TiO_2	3.65	1.67	0.72	0.57	0.56	0.60	0.45	0.28
P_2O_5	2.29	0.72	0.38	0.23	0.30	0.19	0.08	0.02
H_2O^+	2.39	2.29	1.28	1.61	1.74	1.44	0.86	0.80
CO_2	0.10	0.16	0.02	0.08	0.00	0.01	0.02	0.04
TOTAL	100.27	100.19	100.30	99.79	100.29	100.18	99.65	100.44
SUBUNIT	B2	B3	B3	B3	B3	B3	B4	B5

TABLE A3.3

Whole rock Instrumental Neutron Activation Analysis data

RARE EARTH ELEMENT AND SELECTED TRACE ELEMENT ANALYSES

p.p.m.	44	163a	142	148	39	150	152
La	19.5	24.6	36.7	53.1	61.9	9.1	23.0
Ce	50.4	57.8	76.4	113.9	128.3	20.4	47.7
Nd	39.6	40.1	50.5	63.7	67.4	11.8	26.2
Sm	10.3	10.1	12.4	13.9	14.8	2.8	6.0
Eu	3.31	3.27	3.88	4.60	2.79	1.16	1.85
Gd	11.7	11.6	14.2	15.5	16.8	3.2	6.4
Tb	1.55	1.62	2.06	2.29	2.48	0.51	1.00
Tm	0.66	0.78	1.14	1.44	1.48	0.27	0.60
Yb	3.27	4.14	6.70	9.92	10.32	1.96	3.62
Lu	0.55	0.68	1.13	1.69	1.68	0.31	0.58
Th	1.67	2.06	7.01	11.62	15.23	1.57	5.14
Ta	0.99	0.84	1.63	2.62	3.03	0.84	1.15
Hf	1.70	1.96	3.75	13.53	11.74	1.73	3.89
Sc	85.8	91.2	52.0	16.8	6.4	68.8	44.6
Co	128.4	30.6	23.2	24.9	38.6	68.3	37.3
SUBUNIT	B2	B2	B2	B4	B5	A1	A3

TABLE A3.4

CIPW Norms.

The norms in the following table were calculated by computer, using the program NORMCAL, written by R.C.O. Gill. A fixed Fe_2O_3/FeO ratio of 0.21 was used. The differentiation index shown is the Thorton-Tuttle index (Thorton and Tuttle, 1960).

UNIT A GABBROS

NORMCAL .. R.C.O.GILL

SUMMARY NORM TABLE

	150	151	151	158	159	160	152	157	153	115	156	46
QUARTZ	0.0	1.7	3.7	3.3	5.1	0.0	7.0	7.0	7.1	3.9	5.6	4.6
ORTHOCLASE	2.2	13.3	15.6	20.3	15.5	4.4	11.1	5.6	8.8	3.8	5.9	3.5
ALBITE	12.1	16.5	24.8	22.7	23.6	22.3	22.7	22.7	22.6	22.5	26.1	30.1
ANORTHITE	13.1	13.2	21.4	22.1	23.1	23.3	22.0	22.1	22.1	22.8	31.6	32.0
DIOPSIDE	1.1	1.6	1.5	1.6	1.1	1.7	1.2	1.2	1.1	2.1	1.2	1.6
HYPERSTHENE	1	2	1	1	1	1	1	1	1	1	0	0
OLIVINE	0.0	0.0	0.0	0.0	0.0	0.0	0.0	0.0	0.0	0.0	0.0	0.0
MAGNETITE	0.0	0.0	0.0	0.0	0.0	0.0	0.0	0.0	0.0	0.0	0.0	0.0
ILMENITE	0.0	0.0	0.0	0.0	0.0	0.0	0.0	0.0	0.0	0.0	0.0	0.0
APATITE	0.0	0.0	0.0	0.0	0.0	0.0	0.0	0.0	0.0	0.0	0.0	0.0
DIFF. INDEX	16.4	31.7	50.8	45.6	43.6	27.4	41.4	39.0	42.1	41.5	39.6	38.1
AB/(NA+K)	1.000	1.000	1.000	1.000	1.000	1.000	1.000	1.000	1.000	1.000	1.000	1.000
(NA+K)/AL	0.21	0.24	0.21	0.21	0.21	0.21	0.21	0.21	0.21	0.21	0.21	0.21
F3/(F2+F3)	0.21	0.21	0.21	0.21	0.21	0.21	0.21	0.21	0.21	0.21	0.21	0.21

UNIT A GABBROS

NORMCAL .. R.C.O.GILL

SUMMARY NORM TABLE

	117	154	155	45	134	88	119	87	CN7	CN64	CN16	CN17
QUARTZ	1.0	1.0	0.0	0.0	0.0	0.0	0.0	0.0	9.0	2.0	0.0	7.0
CORUNDUM	1.0	1.0	0.0	0.0	0.0	0.0	0.0	0.0	2.0	3.0	0.0	6.0
ORTHOCLASE	12	12	13	12	13	12	3	2	(3)	(3)	13	24
ALBITE	12	11	14	12	2	2	1	1	1	1	4	1
ANORTHITE	1.0	1.0	1.0	1.0	0.2	0.2	0.1	0.1	0.4	0.6	0.0	0.7
HYPERSTHENE	0.0	0.0	0.0	0.0	0.0	0.0	0.0	0.0	0.0	0.0	0.0	0.0
DIOPSIDE	0.0	0.0	0.0	0.0	0.0	0.0	0.0	0.0	0.0	0.0	0.0	0.0
OLIVINE	0.0	0.0	0.0	0.0	0.0	0.0	0.0	0.0	0.0	0.0	0.0	0.0
MAGNETITE	0.0	0.0	0.0	0.0	0.0	0.0	0.0	0.0	0.0	0.0	0.0	0.0
ILMENITE	0.0	0.0	0.0	0.0	0.0	0.0	0.0	0.0	0.0	0.0	0.0	0.0
APATITE	0.0	0.0	0.0	0.0	0.0	0.0	0.0	0.0	0.0	0.0	0.0	0.0
DIFF. INDEX	25.1	25.2	20.8	16.7	27.5	18.2	11.9	6.5	34.2	77.6	50.8	40.9
NA/(NA+K)	0.5	0.6	0.2	0.9	0.7	0.7	0.5	0.7	0.8	0.7	0.7	0.8
(NA+K)/AL	0.6	0.6	0.2	0.2	0.3	0.2	0.5	0.8	0.3	0.3	0.3	0.3
F3/(F2+F3)	0.2	0.1	0.2	0.2	0.2	0.2	0.2	0.2	0.2	0.2	0.2	0.2

UNIT A GAPEROS

SUMMARY NORM TABLE

	16180	16191
QUARTZ	0.0	0.0
CORUNDUM	0.0	0.0
ORTHOCLASE	0.0	0.0
ALBITE	0.0	0.0
ANORTHITE	0.0	0.0
SODIUM METASILICATE	0.0	0.0
POTASSIUM METASILICATE	0.0	0.0
LEUCITE	0.0	0.0
KALSILITE	0.0	0.0
ACMITE	0.0	0.0
DIOPSIDE	0.0	0.0
WOLLASTONITE	0.0	0.0
HYPERSTHENE	0.0	0.0
OLIVINE	0.0	0.0
MAGNETITE	0.0	0.0
ILMENITE	0.0	0.0
HEMATITE	0.0	0.0
APATITE	0.0	0.0
FLUORITE	0.0	0.0
CALCITE	0.0	0.0
SALT	0.0	0.0
GYPSUM	0.0	0.0
WATER	0.0	0.0
DIFF. INDEX	0.0	0.0
(SA+KO)/AL	0.0	0.0
(SA+KO)/AL	0.0	0.0
FM/(FM+FE)	0.0	0.0

SUBUNIT B1 GABBROS

SUMMARY NORM TABLE

	14	18	20	33	34	16192	CN11
QUARTZ	0.00	2.19	1.46	3.22	0.00	0.00	0.00
CLASE	0.00	0.00	0.00	0.00	0.00	0.67	0.00
	14.31	14.20	12.66	9.90	12.21	20.70	15.41
	0.00	0.00	0.00	0.00	0.00	0.00	0.00
	0.00	0.00	0.00	0.00	0.00	0.00	0.00
	2.00	2.00	2.00	2.00	2.00	2.00	2.00
	0.00	0.00	0.00	0.00	0.00	0.00	0

SUBUNIT 82 FERROGABBROS

NORMCAL .. P.C.O.GILL

SUMMARY NORM TABLE

	44	137	138	139	163A	140	141	142	50	100	103
QUARTZ	0.0	0.0	0.0	2.5	0.4	2.6	8.4	11.0	5.6	7.5	14.8
CORUNDUM	0.4	0.6	0.6	0.0	0.0	0.3	0.0	0.0	0.7	0.7	0.0
ORTHOCLASE	12.2	14.2	12.6	11.1	25.1	17.8	11.1	14.1	10.7	12.2	14.4
ALBITE	12.2	13.2	12.2	11.1	12.2	17.8	12.2	24.1	21.1	13.8	21.1
ANORTHITE	2.4	2.1	2.4	1.1	1.2	12.7	1.2	1.5	2.1	1.1	1.5
DIOPSIDE	0.0	0.0	0.0	0.0	0.0	0.0	0.0	0.0	0.0	0.0	0.0
HYPERSTHENE	17.6	17.6	17.6	17.6	17.6	17.6	17.6	19.1	17.6	17.6	19.1
OLIVINE	0.0	0.0	0.0	0.0	0.0	0.0	0.0	0.0	0.0	0.0	0.0
MAGNETITE	2.7	2.7	2.7	2.7	2.7	2.7	2.7	1.2	2.9	1.3	1.0
APATITE	0.0	0.0	0.0	0.0	0.0	0.0	0.0	0.0	0.0	0.0	0.0
DIFF. INDEX	16.3	21.3	21.1	29.5	31.2	39.0	42.8	49.3	37.4	51.3	57.8
NA/(NA+K)	0.7	0.7	0.6	0.7	0.7	0.7	0.7	0.6	0.6	0.7	0.6
(NA+K)/AL	0.2	0.2	0.2	0.4	0.4	0.5	0.5	0.5	0.4	0.5	0.5
F3/(F2+F3)	0.21	0.21	0.21	0.21	0.21	0.21	0.21	0.21	0.21	0.21	0.2

SUBUNIT B3 PERPRODIORITES

NORMCAL .. P.C.O.GILL

SUMMARY NORM TABLE

	51	52	53	47	49	54	120
[illegible]	[illegible]	11.7	17.6	12.6	17.1	20.3	14.2
[illegible]	[illegible]	11.5	14.0	11.[illegible]	15.7	14.[illegible]	13.[illegible]
[illegible]	[illegible]	16.[illegible]	14.[illegible]	14.[illegible]	14.[illegible]	10.7	14.[illegible]
[illegible]	[illegible]	[illegible]	[illegible]	[illegible]	[illegible]	[illegible]	[

SUBUNIT B4 PLAGIC-FERROGRANOPHYRES

NORMCAL .. R.C.O.GILL

SUMMARY NORM TABLE

	163B	143	144	145	146	147	148	56	57	59	60	64
QUARTZ	0.30	9.02	20.89	21.62	19.78	20.88	20.66	16.74	17.22	18.94	14.62	23.62
ORTHOCLASE	14.08	13.02	17.74	13.92	16.82	18.11	17.68	15.08	16.20	13.91	14.44	20.11
ALBITE	54.15	34.27	34.48	29.62	30.64	29.11	32.81	40.87	40.05	32.12	40.49	38.11	
ANORTHITE	14.15	16.27	10.87	9.44	8.59	8.91	10.71	10.57	12.23	12.93	7.71	
DIOPSIDE	7.00	0.77	4.77	3.19	2.93	2.18	2.75	4.75	5.32	3.69	1.06	
HYPERSTHENE	1.13	13.18	7.76	7.32	7.32	7.63	7.56	7.28	7.98	6.69		
MAGNETITE	2.66	2.11	2.49	2.88	2.69	2.77	2.60	2.85	2.82	1.97		
ILMENITE	1.70	1.80	2.00	2.00	2.00	2.00	2.00	1.13	2.00	2.00	2.00	0.72
APATITE	1.00	0.85	0.12	0.12	0.12	0.12	0.12	0.13	0.02	0.12	0.12	0.12
DIFF. INDEX	77.12	56.96	72.99	79.00	74.11	75.00	77.26	72.55	73.50	70.94	69.44	81.92
NA/(NA+K)	0.67	0.46	0.67	0.70	0.71	0.70	0.70	0.74	0.72	0.74	0.75	0.67
(NA+K)/AL	0.73	0.58	0.72	0.78	0.74	0.79	0.76	0.73	0.74	0.69	0.67	0.80
FE/(FE+FE)	0.21	0.21	0.21	0.21	0.21	0.21	0.21	0.21	0.21	0.21	0.21	0.21

SUBUNIT B4 PLAGIO-FERROGRANOPHYRES

NORMCAL .. P.C.O.GILL

SUMMARY NORM TABLE

	65	70	74	109	110	111	112	113	126	127	131	129
QUARTZ	21.4	16.5	18.2	22.5	18.5	21.8	23.1	22.3	16.8	13.9	12.5	11.5
ORTHOCLASE	19.7	15.1	16.6	13.3	16.5	17.7	19.2	20.4	16.7	15.3	13.6	12.0
ALBITE	33.7	41.3	37.1	39.6	39.3	33.3	33.2	28.4	33.8	36.2	39.9	33.6
ANORTHITE	10.7	10.8	10.2	9.6	10.6	8.9	7.0	7.3	11.9	13.5	11.9	14.1
DIOPSIDE	4.0	1.4	4.7	1.5	4.5	2.9	3.9	4.1	3.5	6.8	8.9	11.1
HYPERSTHENE	7.0	8.6	7.1	7.2	6.4	7.4	5.2	5.2	8.7	9.4	8.3	11.3
MAGNETITE	2.0	2.6	2.6	2.0	2.2	2.6	2.0	2.0	2.7	3.4	3.5	4.5
ILMENITE	0.0	0.0	1.0	0.0	1.0	0.0	0.0	0.0	1.0	1.2	1.2	1.5
APATITE	0.0	0.0	0.0	0.0	0.0	0.0	0.0	0.0	0.0	0.4	0.4	0.5
DIFF. INDEX	80.0	75.9	71.9	78.8	74.0	77.6	80.5	80.6	72.3	65.4	65.2	57.0
NA/(NA+K)	0.81	0.74	0.70	0.69	0.72	0.70	0.68	0.67	0.71	0.71	0.75	0.75
(NA+K)/AL	0.81	0.74	0.73	0.75	0.73	0.77	0.81	0.81	0.71	0.67	0.70	0.63
FE/(FE+MG)	0.21	0.21	0.21	0.21	0.21	0.21	0.21	0.21	0.21	0.21	0.21	0.21

SUBUNIT B4 PLAGIO-FERROGRANOPHYRES

NORMCAL .. R.C.O.GILL

SUMMARY NORM TABLE

	96	99	101
QUARTZ	19.0	16.1	13.9
ORTHOCLASE	14.0	15.5	16.1
ALBITE	30.9	32.9	35.1
ANORTHITE	12.2	13.1	13.5
DIOPSIDE	6.4	5.4	2.3
HYPERSTHENE	10.9	11.5	13.7
MAGNETITE	1.5	3.6	3.8
ILMENITE	1.5	1.4	1.2
APATITE	0.5	0.5	0.4
DIFF. INDEX	64.7	64.5	65.1
NA/(NA+K)	0.69	0.69	0.70
(NA+K)/AL	0.65	0.66	0.66
F3/(F2+F3)	0.21	0.21	0.21

SUBUNIT B5 GRANOPHYRES

NORMCAL .. R.C.O.GILL

SUMMARY NORM TABLE

	9	12	13	30	31	40	42	43	36	37	38	39
QUARTZ	24.4	26.5	25.6	26.2	26.2	29.5	28.8	28.5	27.4	27.3	29.2	27.7
CORUNDUM	0.0	0.0	0.0	0.0	0.0	0.0	0.0	0.0	0.0	0.0	0.0	0.0
ORTHOCLASE	23.9	14.8	23.8	14.8	24.0	23.3	23.1	23.5	14.0	20.9	20.9	20.5
ALBITE	14.0	18.8	14.8	18.8	16.8	16.6	19.5	18.5	19.2	24.7	30.6	40.5
ANORTHITE	10.5	16.1	11.1	12.4	10.2	6.3	6.4	5.5	5.3	4.6	5.0	5.0
DIOPSIDE	0.0	0.0	0.0	0.0	0.0	0.0	0.0	0.0	0.0	0.0	0.0	0.7
HYPERSTHENE	10.0	10.0	10.0	11.0	11.4	11.1	10.5	10.5	10.2	10.6	10.8	10.2
MAGNETITE	1.0	1.0	1.0	1.0	1.0	1.0	1.0	1.0	1.0	1.1	1.0	1.1
ILMENITE	0.1	0.1	0.1	0.1	0.1	0.1	0.1	0.1	0.1	0.0	0.1	0.2
APATITE	0.1	0.1	0.0	0.1	0.1	0.1	0.1	0.1	0.1	0.0	0.1	0.2
DIFF. INDEX	84.1	83.5	84.5	83.7	88.2	84.7	80.6	88.8	36.6	89.1	89.7	88.4
NA/(NA+K)	0.68	0.68	0.68	0.71	0.68	0.68	0.67	0.65	0.69	0.68	0.67	0.68
(NA+K)/AL	0.84	0.82	0.84	0.81	0.81	0.82	0.82	0.85	0.86	0.87	0.86	0.86
F3/(F2+F3)	0.21	0.21	0.21	0.21	0.21	0.21	0.21	0.21	0.21	0.21	0.21	0.21

SUBUNIT B5 GRANOPHYRES

NORMCAL .. P.C.O.GILL

SUMMARY NORM TABLE

	19	15	90	104	105	106	107	149	62	63	82	121
QUARTZ	27.7	27.3	27.4	28.4	29.1	28.6	27.1	26.4	25.3	26.6	27.4	25.7
CORUNDUM	0.0	0.0	0.0	0.0	0.0	0.4	0.0	0.0	0.0	0.0	0.0	0.0
ORTHOCLASE	24	23	23	21	23	21	23	24	24	24	23	24
ALBITE	41	40	40	40	37	37	38	40	41	40	39	41
ANORTHITE	1.1	0.7	0.4	0.5	0.7	0.5	0.2	0.0	0.2	0.6	0.1	0.5
DIOPSIDE	1.6	1.7	1.6	1.5	1.6	2.1	1.6	2.9	1.7	0.9	1.4	1.9
HYPERSTHENE	0.4	0.7	0.5	0.3	0.9	0.7	1.0	1.1	1.3	0.8	1.3	2.1
MAGNETITE	1.5	1.5	1.5	1.5	1.4	1.2	1.5	1.2	1.5	1.4	1.5	1.4
ILMENITE	0.1	0.1	0.1	0.1	0.1	0.1	0.1	0.1	0.1	0.1	0.0	0.1
DIFF. INDEX	89.2	88.6	86.2	88.1	87.6	87.8	86.0	88.5	87.3	89.1	89.2	87.9
NA/(NA+K)	0.68	0.68	0.66	0.68	0.66	0.68	0.66	0.67	0.68	0.66	0.67	0.68
(NA+K)/AL	0.21	0.21	0.21	0.21	0.21	0.21	0.21	0.21	0.21	0.21	0.21	0.21
F3/(F2+F3)	0.21	0.21	0.21	0.21	0.21	0.21	0.21	0.21	0.21	0.21	0.21	0.21

SUBUNIT 55 GRANOPHYRES

NORMCAL .. R.C.O.GILL

SUMMARY NORM TABLE

	16184
QUARTZ	29.8
ORTHOCLASE	21.8
ALBITE	37.6
ANORTHITE	4.9
DIOPSIDE	1.0
HYPERSTHENE	3.2
MAGNETITE	1.1
ILMENITE	0.7
APATITE	0.2
DIFF. INDEX	88.9
NA/(NA+K)	.64
(NA+K)/AL	.86
F3/(F2+F3)	0.21

UNIT B RN.THOMPSON DATA

NORMCAL .. R.C.O.GILL

SUMMARY NORM TABLE

	ME2	ME4	ME8	ME9	ME10A	ME10B	ME12	ME14
QUARTZ	0.0	9.5	14.4	16.0	14.4	17.2	18.3	27.7
CORUNDUM	0.0	0.0	0.0	0.0	0.0	0.0	0.0	0.1
ORTHOCLASE	5.0	9.4	13.5	16.2	14.6	11.9	16.0	20.5
ALBITE	16.3	31.8	35.6	35.9	31.7	39.2	42.0	38.2
ANORTHITE	23.7	16.5	13.6	11.0	11.2	12.7	9.3	7.1
DIOPSIDE	10.8	6.9	5.9	6.0	8.3	4.9	4.1	0.0
HYPERSTHENE	20.1	16.3	11.4	10.1	14.0	9.5	6.9	4.7
OLIVINE	4.6	0.0	0.0	0.0	0.0	0.0	0.0	0.0
MAGNETITE	6.8	4.5	3.2	3.1	4.1	3.0	2.3	1.2
ILMENITE	7.2	4.3	1.4	1.1	1.1	1.2	0.9	0.5
APATITE	5.6	1.8	0.9	0.6	0.7	0.5	0.2	0.0
DIFF. INDEX	22.2	50.6	63.6	68.1	60.6	68.3	76.4	86.4
NA/(NA+K)	0.75	0.78	0.74	0.70	0.70	0.78	0.74	0.66
(NA+K)/AL	0.34	0.57	0.65	0.71	0.68	0.68	0.76	0.81
F3/(F2+F3)	0.21	0.21	0.21	0.21	0.21	0.21	0.21	0.21

Durham University SCIENCE 30 OCT 1980 SECTION Library

Plate 1.2 A GEOLOGICAL MAP OF THE EASTERN PART OF THE CARROCK FELL IGNEOUS COMPLEX

Unit A: A1, A2, A3 — Unit B: B1, B2, B3, B4, B5

× Xenolith

SS Skiddaw Slates

EVG Eycott Volcanic Group

●56 Sample locality

T1-6 Sample traverses (see App. One)

Dip of lamination

600 Contours in meters

SCALE 1:5000 0 100 metres

NORTH

Miton Hill
Rae Crags
Round Knott
CARROCK FELL (660m.)
Pike
Iron Crags
Scurith
Further Gill Sike
White Crags
Crag Fast
Buck Kirk
Snailshell Crags
Black Crag
Kelt Crags
Round-house
Swineside
River Caldew
MOSEDALE
Mosedale Moss
Black Dub
Fault
Black Moss
Black Beck
Stone Ends
Linewath
Linewath Steps
EVG
? EVG/SS ?
SS